

1 **Response to reviewers for the paper “In situ secondary organic aerosol formation from ambient pine**  
2 **forest air using an oxidation flow reactor.”**

3 **B. B. Palm, J. L. Jimenez, et al.**

4 We thank the reviewers for their comments on our paper. To guide the review process we have copied  
5 the reviewer comments in black text. Our responses are in regular blue font. We have responded to all  
6 the referee comments and made alterations to our paper (**in bold text**).

7 **Anonymous Referee #1**

8 Overview

9 R1.0. The paper summarizes observations of SOA formation and evolution in the ambient air and  
10 oxidized ambient air in a flow tube reactor at a forested site in Colorado. The paper is well thought  
11 (especially the extent of corrections performed for possible losses in the sampling lines, etc.) and results  
12 are clearly presented. The main conclusion of the paper is that oxidation of the measured VOCs is not  
13 enough to explain the formation of SOA upon aging. This is not a new finding, but the value of the paper  
14 in my opinion is to attempt a mass closure and determine the necessary SOA formation yields for the  
15 measured S/IVOCs to explain the observed increase in OA mass after photochemical aging. The analysis  
16 for relevant time scales for a typical OFR operation is also valuable for the community. I suggest  
17 publishing the manuscript after my comments below are addressed.

18 We thank the reviewer for his/her input. However, we disagree that showing that oxidation of the  
19 measured VOCs is not enough to explain the formation of SOA *formed in-situ from ambient air in a*  
20 *forest* is not a new finding. We believe that it is a new finding in at least two ways: (1) To our knowledge  
21 that has only been shown before through more complex analyses that join together VOCs and SOA  
22 measured at different points in time, and not when comparing SOA formation and VOCs measured  
23 simultaneously in ambient air in a forest. (2) The underestimation of SOA has only been consistently  
24 observed for urban air, and not in biogenically-dominated air.

25 We have modified the text in the abstract at P30411 L25 to read:

26 **“Approximately 4.4 times more SOA was formed in the reactor from OH oxidation than could be**  
27 **explained by the VOCs measured in ambient air. To our knowledge this is the first time that this has**  
28 **been shown when comparing VOCs and SOA formation measured at the same time, rather than**  
29 **comparing measurements made at different times.”**

30 We have also modified the introduction at P30413 L5 to read:

31 **“Aerosol models using traditional (pre-2007) aerosol yields for volatile organic compounds (VOCs)**  
32 **from chamber studies generally underpredict SOA mass by a factor of 10 in urban areas (Volkamer et**  
33 **al., 2006; Hodzic et al., 2010; Hayes et al., 2015). More recent models are able to better predict SOA**  
34 **mass in urban areas by using higher VOC yields and adding previously ignored semivolatile and**  
35 **intermediate volatility organic compounds (S/IVOCs; Hodzic et al., 2010; Hayes et al., 2015). Model**  
36 **comparisons for biogenically-dominated areas have not shown such systematic underpredictions even**  
37 **when using older models (e.g., Tunved et al., 2006; Chen et al., 2009; Hodzic et al., 2009; Slowik et al.,**  
38 **2010).”**

39 We added the following sentence to the conclusions at P30444 L5:

40 **“To our knowledge, this is the first time this has been demonstrated by comparing simultaneous VOC**  
41 **measurements with in situ SOA formation, particularly in a biogenic environment.”**

42 R1.1. P 30412, L20: consider changing to “. . .functionalized products” and “. . . fragmented products.”

43 We have modified the text at P30412, L20 as suggested.

44 R1.2. P 30422, L25: Max SOA is observed over night when in reality oxidation by OH in the ambient air  
45 would be low and oxidation by O<sub>3</sub> would be high, but OFR185 doesn't include much of an oxidation by  
46 O<sub>3</sub>, so how relevant are these observations to understanding the ambient SOA formation at the site?

47 The reviewer raises a good question that we have discussed at various points during analysis of this  
48 dataset and others using the OFR, but may have not made clear enough in the manuscript. We did not  
49 mean to suggest that SOA formation from OH oxidation is actually producing more SOA in the forest at  
50 night. Rather we are reporting the observation that the SOA formation potential from OH oxidation of  
51 nighttime air is larger and quantifiable. In fact the lack of much OH in nighttime air is likely an important  
52 factor to explain why the potential for OH-produced SOA is higher at night: the longer lifetime of  
53 monoterpenes and their oxidation products allows building up higher concentrations in nighttime air.  
54 During this study we also investigated O<sub>3</sub>-produced and NO<sub>3</sub>-produced SOA in the OFR which, together  
55 with these OH oxidation results, can provide a more complete picture of the complex interplay between  
56 different oxidant-driven SOA formation processes. The O<sub>3</sub> and NO<sub>3</sub> oxidation results will be the subject  
57 of an upcoming manuscript, as it was too much material to attempt to cover in one manuscript. We  
58 have modified the text in several places to clarify how OFR measurements can be related to ambient  
59 SOA formation:

60 **P30411 L2: “An oxidation flow reactor (OFR) is a vessel inside which the concentration of a chosen**  
61 **oxidant can be increased for the purpose of studying SOA formation and aging by that oxidant. During**  
62 **the BEACHON-RoMBAS field campaign, ambient pine forest air was oxidized by OH radicals in an OFR**  
63 **to measure the amount of SOA that could be formed from the real mix of ambient SOA-precursor**  
64 **gases, and how that amount changed with time as precursors changed.”**

65 **P30411 L28: “An SOA yield of 18-58% from those compounds can explain the observed SOA formation.**  
66 **This work suggests that these typically unmeasured gases play a substantial role in ambient SOA**  
67 **formation.”**

68 **P30412 L3: “These measurements help clarify the magnitude of potential SOA formation from OH**  
69 **oxidation in forested environments, and demonstrate methods for interpretation of ambient OFR**  
70 **measurements.”**

71 **P30419 L2: “This allows the potential of SOA formation from OH oxidation to be studied over the**  
72 **whole range of exposures as functions of time of day and the concentration of precursors that change**  
73 **on that time scale.”**

74 **P30424 L3: “Under typical operation, an OFR is used to study oxidation dominated by a single oxidant,**  
75 **similar to typical large chamber experiments. In the case of a field application (as in this study) the**  
76 **sample is a complex and time-varying mixture of ambient precursors that enter the OFR. Importantly,**  
77 **the OH:O<sub>3</sub>:NO<sub>3</sub> oxidant ratios produced within the OFR are generally not the same as the changing**

ambient ratios. Therefore SOA formation in the OFR does not, and is not meant to, reproduce in situ ambient SOA formation at each point in time. In other words, the OFR can be used as a tool to determine the amount of SOA from a single oxidant that would form upon oxidation of ambient gases (both identified and unidentified) at any time of day.

Typical OFR operation of OH oxidation using the OFR185 method is illustrated..."

**P30433 L22: "SOA will be formed in the OFR from these changing VOC mixtures and any other gases present in the ambient air that enters the reactor, so it might be expected that different amounts of SOA production would be observed during daytime vs. nighttime."**

**P30434 L10: "In other words, this OH oxidation in the OFR is not meant to reproduce true ambient nighttime chemistry, rather it allows us to measure SOA formation from OH oxidation of the true mix of ambient gases as it evolves with time of day, including nighttime. In fact, the lack of ambient nighttime OH oxidation may help explain the increased SOA formation potential when nighttime air is oxidized by OH in the OFR."**

R1.3. P. 30435, L15-20: authors suggest that OFR185 is more suitable for forested environments. I don't agree with this statement since comparisons could not be carried out for short aging times and since OFR185 does not allow for significant O<sub>3</sub> oxidation whereas MTs have a high reactivity with O<sub>3</sub>. Plus, for some long aging times, there is a non-negligible difference between OA enhancements observed in OFR185 and OFR254.

Please see our response to R1.2 for an explanation that the OFR is used to study oxidation by a single oxidant at a time. In our opinion, it is more informative to perform O<sub>3</sub>-only oxidation and OH-dominated oxidation separately and compare the results than to try to perform simultaneous oxidation by several oxidants, which is more complex to interpret.

We have modified P30435, L18-19 to read:

**"... we recommend the OFR185 mode of operation for future OFR studies of OH oxidation in forested areas."**

The reviewer is correct that a comparison of OH oxidation between the two methods could not be made for short aging times, but this is because of limitations of the OFR254 method, which are discussed starting on P30421 L3. The OFR185 method allowed for studying OH oxidation at ages <1 eq. day, whereas the OFR254 method did not during this study. Therefore, the OFR185 mode was more useful for a forested environment where many of the ambient SOA-forming gases will react during these short aging times.

For completeness, we have also added the following text to P30421 L13:

**"Measuring the decay of a compound that reacts relatively quickly with OH but does not react with O<sub>3</sub> could allow for better OH<sub>exp</sub> quantification at low ages for OFR254-70."**

Regarding the "non-negligible differences between OA enhancements observed in OFR185 and OFR254" at high ages, please see the response to R3.20 below.

R1.4. P. 30432, L24: It's unclear to me why SO<sub>4</sub> mass should be scaled by Faer? Is this the correction that's referenced in line 27? Similarly, I don't understand why a correction for LVOC condensation needs

to be applied. Is the idea to account for the max possible amount of SOA formed beyond the time scales of residence in the flow tube?

The reasoning for including an LVOC fate correction is discussed in the first paragraph of Sect. 3.3.1, starting on P30426 L25. To clarify, we have changed the text starting at P30427 L11 to read:

**“However, if they are subject to one of the other three fates, then the AMS + SMPS measurements would underestimate the amount of SOA that would form in the atmosphere at the same level of OH exposure. Similar to loss of gases to large Teflon chamber walls (e.g., Matsunaga and Ziemann, 2010), these other three fates are experimental limitations of the OFR technique that need to be corrected in order to relate OFR measurements to real atmospheric SOA formation processes.”**

To clarify why SO<sub>4</sub> mass also needs to be corrected by  $F_{aer}$ , we have replaced the first sentence of Sect 3.3.2 at P30432 L11 to read:

**“In addition to LVOCs, H<sub>2</sub>SO<sub>4</sub> can also be produced in the OFR from OH oxidation of SO<sub>2</sub>. H<sub>2</sub>SO<sub>4</sub> molecules can also condense onto OFR or sampling line walls (but not be lost to further reaction with OH). These limitations of the OFR technique need to be corrected in order to relate OFR measurements to real atmospheric processes. H<sub>2</sub>SO<sub>4</sub> formation is an analogous yet much simpler system compared to LVOC formation, so it can be used to validate the LVOC fate model.”**

This is indeed the correction referenced in P30432 L27, and we have clarified the text at that line to read:

**“After applying the correction for H<sub>2</sub>SO<sub>4</sub> wall and sampling line losses as described in the previous paragraph, the measured ...”**

R1.5. P. 30437, L 20: Are the mentioned SOA yield values the chamber-derived yield values, just scaled accordingly for ~5 ug/m<sup>3</sup> of OA? If so, what formulation was used to scale down the yields?

To clarify the manuscript, we have added a new table (Table 2) and modified the text starting at P30437 L12 to read:

**“SOA formation was predicted by applying low-NO<sub>x</sub>, OA-concentration-dependent, chamber derived aerosol yields to the ambient VOC concentrations predicted to react in the OFR based on OH<sub>exp</sub>. Estimated fractions reacted were >99% of ambient MT, SQT, and isoprene, and ~45% of toluene+*p*-cymene in the age range of 0.4–1.5 eq. days. The yields used to predict SOA formation were calculated for each individual data point as a function of the OA mass concentration measured after oxidation in the OFR, using the two- or four-product basis set parameterizations listed in Table 2 (Henze and Seinfeld, 2006; Tsimpidi et al., 2010). With an average post-oxidation OA concentration of 4.1 g m<sup>-3</sup> when the LVOC fate correction was applied, this resulted in campaign-average SOA yields of 12.5, 13.2, 13.8, and 3.2% for MT, SQT, toluene, and isoprene, respectively. Previous experiments have shown SOA yields from various precursor gases oxidized in the OFR to be of the same order as yields from large environmental chambers (Kang et al., 2007, 2011; Lambe et al., 2011, 2015).”**

See also the response to R2.1 discussing the new table of SOA yield parameters.

R1.6. P. 30443, L11-12: Please add the aging times when OFR185 and 254 were compared (comparison wasn't possible at short photochemical times and so a general statement on the similarity of the results is not warranted).

We have modified the text starting at P30443 L12 to read:

**“Similar amounts of SOA formation were observed from both the OFR185 and OFR254-70 methods for the overlapping range of eq. ages (~1-30 days). Comparison at shorter ages was not possible because the OFR254-70 method, especially as it was employed during this campaign, was not suitable for measuring <1 eq. day of OH aging.”**

Please see the response to comment R1.3 for an explanation of why comparison between OFR185 and OFR254-70 was not possible at short photochemical ages for this study.

R1.7. Section S1: Particle loss correction: Adding in particle mass to what the AMS measured based on the volume fraction of different species is valid only if there is no size dependent composition differences. Is that a valid assumption in this data set?

To address this comment, we have modified Fig. S1 and its caption to read:

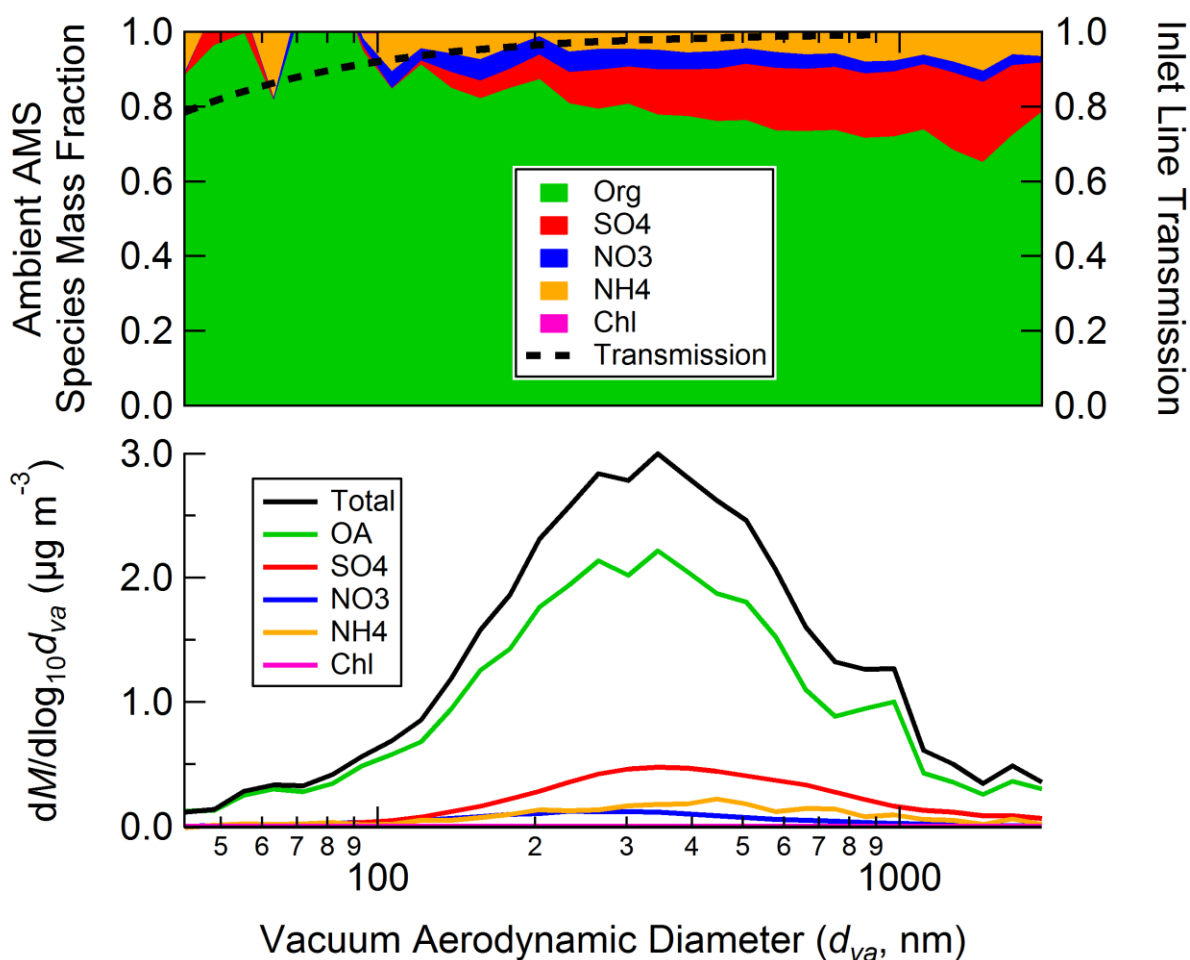


Fig. S1. Top: Average species mass fraction of ambient aerosol measured by the AMS, and inlet sampling line particle transmission efficiency. The transmission efficiency was estimated using the Max Planck Institute for Chemistry Particle Loss Calculator (von der Weiden et al., 2009). This transmission curve was used to correct SMPS size distributions for particle losses in the ambient and OFR sampling lines. Particle losses to surfaces inside the OFR are discussed in Sect. S3. Bottom: Average species mass size distribution of ambient aerosol measured by the AMS.

We have also added the following text to L29 of Sect. S1:

“As seen in Fig. S1, there was on average only a slight size dependence to the species mass fractions of ambient aerosol. The mass fractions are also particularly noisy at smaller particle sizes due to small mass concentrations. Ideally, the species size distributions measured at each point in time could be used to allocate the sampling line particle losses to each species. In practice, the AMS size-distribution measurement mode is not sensitive data point. Thus, we have applied the best correction possible and expect that it should improve quantification. Regardless, the small size dependence of species mass fractions would have a minimal impact on this analysis since the correction is at most 20% at the smallest sizes.”

R1.8. Figure S3 and S6. I’m confused as to why the right panels that plot AMS or SMPS volume added after oxidation show negative values. Please clarify.

Figures S3 and S6 include all OFR185 data, over the entire range of eq. OH ages. To clarify the negative values in these figures, we have added the following text to the captions of Figs. S3 and S6:

“At the highest ages, heterogeneous oxidation led to fragmentation/volatilization of preexisting OA, resulting in a net loss of OA.”

We have also modified the text to say “change in volume” throughout the manuscript.

## Anonymous Referee #2

### Overview

R2.0. This study is focused on using an oxidation flow reactor to study secondary organic aerosol formation in a forest environment. During the BEACHON-RoMBAS field study multiple VOC species and organic aerosol concentrations were measured. The authors predicted the SOA concentrations by using the measured VOCs and known SOA yields. The predicted SOA concentrations show that still there are unmeasured SOA precursors in the forest environment. The findings of this study could help to better understand and model the SOA formation in an environment dominated by biogenic VOCs. The study demonstrates that the oxidation flow reactor is a powerful tool to study the contribution of different unidentified species to SOA formation. The paper is well written. I have some minor comments on the paper.

R2.1. Show all the SOA yields used in the calculations in a separate table. In SOA calculations do you take into account BVOC oxidation by ozone?

For typical yields under the conditions of our study, see the response to comment R1.5.

To document the full details, we have added Table 2 (reproduced below) to the revised paper. Note that the SOA yield values used for isoprene have been updated compared to the ACPD version, leading to slightly larger yields. This change has no consequence for the conclusions drawn in this analysis, as isoprene is a very minor contribution to the predicted SOA amounts.

**Table 2. Low-NO<sub>x</sub> SOA yield parameters using basis sets, used to estimate SOA yields from VOCs in the OFR (Sect. 3.6.1).**

SOA precursor	C* saturation vapor concentrations at 298K ( $\mu\text{g m}^{-3}$ )			
	1	10	100	1000
MT <sup>a</sup>	0.107	0.092	0.359	0.600
SQT <sup>a</sup>	0.075	0.150	0.750	0.900
Toluene <sup>a</sup>	0.075	0.225	0.375	0.525
	C* saturation vapor concentrations at 295K ( $\mu\text{g m}^{-3}$ )			
	0.6		116	
Isoprene <sup>b</sup>	0.0288		0.232	

<sup>a</sup>(Tsimpidi et al., 2010), not including the chemical “aging” parameterization

<sup>b</sup>(Henze and Seinfeld, 2006)

Regarding BVOC oxidation by ozone, please see our response to R3.4 below.

R2.2. You use a number of abbreviations, please put them in one table so it’s easier to follow. For example, what is “CS”?

We have added a Glossary after the main text:

OFR	Oxidation flow reactor
SOA	Secondary organic aerosol
LVOC	Low volatility organic compound
OA	Organic aerosol
VOC	Volatile organic compound

<b>S/IVOC</b>	<b>Semi- and intermediate-volatility organic compound</b>
<b>PTR-TOF-MS</b>	<b>Proton transfer reaction time-of-flight mass spectrometer</b>
<b>OH</b>	<b>Hydroxyl radical</b>
<b>O<sub>3</sub></b>	<b>Ozone</b>
<b>NO<sub>3</sub></b>	<b>Nitrate radical</b>
<b>MBO</b>	<b>2-methyl-3-buten-2-ol</b>
<b>MT</b>	<b>Monoterpenes</b>
<b>SQT</b>	<b>Sesquiterpenes</b>
<b>OHR<sub>ext</sub></b>	<b>External OH reactivity</b>
<b>OHR<sub>int</sub></b>	<b>Internal OH reactivity</b>
<b>OH<sub>exp</sub></b>	<b>OH exposure</b>
<b>eq.</b>	<b>Equivalent</b>
<b>SMPS</b>	<b>Scanning mobility particle sizer</b>
<b>AMS</b>	<b>Aerodyne High-Resolution Time-of-Flight Aerosol Mass Spectrometer (HR-ToF-AMS)</b>
<b>k<sub>OH</sub></b>	<b>Rate constant for reaction with OH</b>
<b>k<sub>O3</sub></b>	<b>Rate constant for reaction with O<sub>3</sub></b>
<b>TD-EIMS</b>	<b>Thermal desorption electron impact mass spectrometer</b>
<b>C*</b>	<b>Effective saturation vapor concentration</b>
<b>τ<sub>aer</sub></b>	<b>Lifetime of LVOCs (or H<sub>2</sub>SO<sub>4</sub>) for condensation onto aerosols</b>
<b>τ<sub>wall</sub></b>	<b>Lifetime of LVOCs (or H<sub>2</sub>SO<sub>4</sub>) for loss to OFR walls</b>
<b>τ<sub>OH</sub></b>	<b>Lifetime of LVOCs for reaction with OH</b>
<b>τ<sub>total</sub></b>	<b>Total lifetime for loss of LVOCs (or H<sub>2</sub>SO<sub>4</sub>)</b>
<b>CS</b>	<b>Condensational sink</b>
<b>D</b>	<b>Gas diffusion coefficient</b>
<b>r</b>	<b>Particle radius</b>
<b>N(r)</b>	<b>Particle number size distribution</b>
<b>α</b>	<b>Sticking coefficient</b>
<b>Kn</b>	<b>Knudsen number</b>
<b>λ<sub>g</sub></b>	<b>Mean free path of gas molecules</b>
<b>A/V</b>	<b>Surface-area-to-volume ratio of OFR</b>
<b>k<sub>e</sub></b>	<b>Coefficient of eddy diffusion</b>
<b>F<sub>x</sub></b>	<b>Fraction of LVOCs (or H<sub>2</sub>SO<sub>4</sub>) lost to pathway x</b>
<b>SO<sub>4</sub></b>	<b>Sulfate aerosol</b>

216

217 R2.3. Section 3.6.2: You didn't use any aging in calculation of SOA formation from measured VOCs. Here  
218 you state that "At night, O<sub>3</sub> and NO<sub>3</sub> may react with the C=C-containing MT and SQT emissions leading  
219 to a buildup of S/IVOC oxidation products that lack C=C double bonds, molecules with which O<sub>3</sub> and  
220 NO<sub>3</sub> generally do not react". Doesn't this imply that these first generation oxidation products of  
221 monoterpenes will produce more SOA by further oxidation? Therefore, applying aging in the calculations  
222 would reduce the gap between predicted and measured SOA. I'm aware that there are some  
223 uncertainties related to using aging in the SOA predictions. Nevertheless, there are several papers based  
224 on laboratory studies, which show multi-generational SOA production from alpha-pinene.

225 To address this point we have added the following text at P30437 L22:



226 “These yield values reflect the amount of SOA that forms after several generations of gas-phase  
227 oxidation of precursor gases. We do not include additional “aging” of the precursors through  
228 additional oxidation steps, as such parameterizations are not well-supported experimentally.”

229 This comment is also addressed as part of the restructuring of Sect. 3.6.2 as part of the response to  
230 R3.24 below.

231 We agree that additional oxidation by OH of products of e.g. terpene oxidation by NO<sub>3</sub> or O<sub>3</sub> may be part  
232 of the missing SOA precursors observed at night (see last paragraph of Sect. 3.6.2).

233

234 **Short Comment: “Relevant Reference”, C.N. Hewitt, 9 Nov 2015**

235 The authors of this interesting manuscript may wish to refer to a paper we published in ACP in 2014 in  
236 which we studied the formation of aerosol particles in a reaction chamber into which gas-phase  
237 emissions from trees were fed:

238 Emissions of biogenic volatile organic compounds and subsequent photochemical production of  
239 secondary organic aerosol in mesocosm studies of temperate and tropical plant species (2014) K.P.  
240 Wyche, A.C. Ryan, C. N. Hewitt, M. R. Alfarra, G. McFiggans, T. Carr, P.S. Monks, K.L. Smallbone, G.  
241 Capes, J.F. Hamilton, T.A.M. Pugh, and A. R. MacKenzie, Atmospheric Chemistry and Physics, 14, 12781 –  
242 12801

243 [We have modified the text at P30413 L26:](#)

244 **[“Also, while chamber experiments have been performed using emissions from mesocosm \(e.g., whole](#)  
245 **[tree\) systems in the laboratory \(e.g., Wyche et al., 2014\), it is difficult to perform field experiments](#)  
246 **[with ambient air in chambers \(Tanaka et al., 2003\).”](#)******

247

248 **Anonymous Referee #3**

249 Overview

250 The authors present results from measurements of SOA formation made using an oxidation flow reactor  
251 in a forested environment. They provide a detailed discussion of the physical mechanisms at play, and  
252 find some interesting relationships between the SOA formation potential and the ambient  
253 concentrations of monoterpenes, in particular. They find that the SOA that they would predict to form  
254 based on the observed MT concentrations is lower than the observed formation. They use this, along  
255 with some direct measurements of the concentrations of S/IVOCs, to estimate effective yields for these  
256 species and to explain the observation-prediction gap. I find this section to be a bit weaker than it could  
257 be, I think because the authors are working to not show data that is under review elsewhere (Hunter et  
258 al., Submitted to Nat. Geosci.). I suggest that the authors be more direct in this section. Overall I think  
259 that this study is well done, provides interesting results and should be publishable once the authors  
260 address the comments below.

261 R3.1. P30414, L13: Although it seems very likely that S/IVOCs are contributors to SOA formation from  
262 biomass burning and vehicle exhaust, some of the difference between the observed and predicted SOA  
263 formation from VOCs in the two cited studies (Ortega et al., 2013; Tkacik et al., 2014) could potentially  
264 be explained by the assumed SOA yields used to make the predictions being too low, a consequence of  
265 the losses of semivolatile gases alluded to on the previous page. It seem appropriate to also mention  
266 this here.

267 We have modified the text at P30414 L 13 to clarify this point as:

268 **“Bruns et al. (2015) found that for a wood combustion system, the amount of SOA formed in an OFR**  
269 **compared to a large chamber agreed reasonably well. Tkacik et al. (2014) and Ortega et al. (2013)**  
270 **showed substantially more SOA formation than could be explained from speciated VOCs. Despite**  
271 **relying on SOA yields measured in large chambers, which can be affected by the aforementioned wall**  
272 **losses of semivolatile gases, these results suggest that S/IVOCs contribute to SOA formation in**  
273 **biomass burning plumes and vehicle exhaust.”**

274 R3.2. P30415, L25: I find the statement here regarding the NO<sup>+</sup> ion to be a bit unclear how specifically  
275 this links to the first part of the sentence. Do the authors mean whole air samples analyzed using a CIMS  
276 technique with NO<sup>+</sup> as the reagent ion?

277 For clarification, we have modified the text at P30415 L25 to clarify this point as:

278 **“The relative ratio of isoprene/(MBO + isoprene) at this field site was estimated using a combination**  
279 **of GC-MS, PTR-TOF-MS, and whole air sample measurements during summer 2010 (Kaser et al., 2013)**  
280 **and using NO<sup>+</sup> ionization mass spectrometry during the BEACHON-RoMBAS campaign (Karl et al.,**  
281 **2012) to be approximately 20%.”**

282 R3.3. P30416, L13: Is the mesh smaller than the ID of the OFR body (14 vs. 19.7 cm)? This makes it  
283 difficult to understand how this really acted as a screen (not that this really matters to the results of this  
284 study, but it could be clarified in case someone else wants to apply this methodology).

285 The text at P30416 L10 has been modified to clarify this point as:

**“The 14 cm diameter inlet plate was removed from the intake end of the OFR to reduce possible losses of semivolatile SOA precursors to the inlet plate inferred in a previous study (Ortega et al., 2013) and to reduce the width of the residence time distribution in the reactor (Ortega et al., 2015). Air was sampled into the reactor through this 14 cm diameter opening, which was covered with a coarse-grid mesh screen to reduce turbulence in the reactor and prevent insects and debris from entering the reactor.”**

It is correct that that inlet plate is of smaller diameter than the diameter of the body of the OFR. There is a solid ring on the front face of the reactor that seals the region between the inlet plate (or mess screen) and the outer diameter of the reactor. This can roughly be seen in Fig. 2 (solid black line) and more clearly in the photo in Fig. 1b in Ortega et al. (2015). The reason for this difference in diameters is that the UV lamps and mounting hardware are located the other diameter of the reactor.

R3.4. P30417, L22: It would be useful if the authors were to elaborate as to what “a small number means.” If, for example, the number of compounds influenced is small but they are the most abundant, then the influence on the system would not be small.

We have modified the text at P30417 L16 to address this point as:

**“According to Fig. 5 of Peng et al. (2015b), O<sub>3</sub> in the OFR185 method during this study likely contributed only a minor (< 20%) role in the oxidation of a few biogenic VOCs with the largest  $k_{O_3}/k_{OH}$  ratios (e.g.,  $\beta$ -caryophyllene,  $\alpha$ -terpinene,  $\alpha$ -humulene), and only at the lowest OH exposures (OH<sub>exp</sub>) equivalent to several hours of aging. With the OFR254-70 method though, the ratio of O<sub>3</sub> exposure to OH<sub>exp</sub> was as high as 10<sup>6</sup> for the lowest OH<sub>exp</sub> in this study. Under these conditions, O<sub>3</sub> may have played a substantial role in the initial oxidation of a larger number of species of biogenic VOCs (e.g., reacting with ~100% of  $\beta$ -caryophyllene and  $\alpha$ -terpinene, ~60% of  $\alpha$ -pinene and limonene, ~20% of 3-carene and  $\beta$ -pinene, 10% of isoprene).”**

R3.5. P30418, L2: It would be useful if the authors were to define “external OH reactivity” further here, so the reader doesn’t have to look this up in the Li et al. paper. Additionally, the authors could elaborate as to how this was estimated.

The text starting at P30417 L28 was modified to:

**“OH<sub>exp</sub> for the OFR185 method was estimated in part based on a model-derived equation, which uses measurements of ambient water vapor concentration, O<sub>3</sub> produced in the reactor, and estimated external OH reactivity (OHR<sub>ext</sub>) as equation parameters (Li et al., 2015). OHR<sub>ext</sub> is the OH reactivity from ambient gases such as VOCs, CO, SO<sub>2</sub>, and is accounted for separately from the “internal OH reactivity (OHR<sub>int</sub>)” from species such as HO<sub>x</sub>/H<sub>2</sub>O<sub>2</sub>/O<sub>3</sub> that are greatly enhanced by the reactor. For this study, OH<sub>exp</sub> was calculated using an estimated OHR<sub>ext</sub> = 10 s<sup>-1</sup>, based on measurements at the same field site and season during previous campaigns (Kim et al., 2013; Nakashima et al., 2014).”**

R3.6. I suggest the authors just write out “equivalent” rather than using the abbreviation “eq.”, which I find awkward.

We thank the reviewer for this suggestion, but prefer to keep using the abbreviation “eq.” This term has been defined on first use, is included in Table 2 as part of the response to R2.2, and is used consistently throughout the manuscript.

R3.7. Line 30420, L24 and elsewhere: Given that the net change in the amount of particle volume observed can either increase or decrease, I suggest that the authors move away from using the terminology “volume added,” which to me implies that things only increase, to something like  $\Delta V$  (where  $\Delta$  is the delta symbol) to capture that this is not unidirectional.

Please refer to the response to R1.8.

R3.8. P30421: Although I understand the arguments as to why the OFR185 and OFR254 measurements are different, given that they apparently “give consistent results” I do not see why the OFR254 measurements would be excluded from the bulk of the analysis. Why not merge the data sets, which should be straight forward if they are “consistent”.

To clarify why we have chosen to not merge the OFR254-70 measurements into the analysis, we have added this sentence to P30421 L5 to read:

**“The analysis of SOA mass formed vs. predicted in Sect. 3.6 was done using the age range that produced the maximum SOA formation (0.4–1.5 eq. days). However, determination of ages below approximately 1 eq. day using the OFR254-70 method was limited by the ability to accurately measure the amount of injected  $O_3$  that was consumed in the reactor.”**

We have also modified the text at P30421 L18 to read:

**“This short time period of OFR254-70 measurements combined with the difficulty of sampling at short eq. ages with this particular experimental setup meant that there were few OFR254-70 measurements relative to OFR185 measurements for the analysis in Sect. 3.6. Also, there were no concurrent measurements of S/IVOC concentrations and SOA formation using OFR254-70 available for the analysis in Sect. 3.6.2. If these analyses would have been performed on a combined dataset using both OH production methods, the results would be driven almost completely by OFR185 measurements. For these reasons, the analyses were performed and conclusions reached using only OFR185 measurements. Regardless, we document below that both OH oxidation methods gave consistent results for SOA production over the range of overlapping ages (~1-30 eq. days) used during this campaign (Sect. 3.4).”**

R3.9. P30424, L14: The authors note that as the OH exposure is increased the  $SO_4$  mass formed continued to increase. However, in looking at Fig. 2 it appears that the  $SO_4$  mass increases to a point, but plateaus at high OH exposure. Is this generally true? If so, it should be mentioned.

At P30424 L12, the text has been modified as follows:

**“As the eq. age continued to increase, OA mass enhancement decreased, eventually resulting in net OA loss. These high ages led to a lack of formation of  $SO_4$  as well as heterogeneous oxidation of the preexisting OA, leading to fragmentation and evaporation (Ortega et al., 2015). The amount of  $SO_4$  aerosol production increased with eq. age, and plateaued with no further production at ages above ~10 days. This behavior is consistent with theory, since  $SO_2$  has a lifetime of ~8 days with respect to oxidation by OH (Sander et al., 2011). Also, as expected,  $SO_4$  aerosol (and  $H_2SO_4$  gas) was not consumed by excess  $OH_{exp}$  in the same way as OA (and SOA precursor gases).”**

R3.10. P30426, L5: The authors here note that the accuracy of the model-derived OH exposures could be assessed by comparing the measured vs. predicted depletion curves. However, since the factor of 2

364 scaling was determined by comparing the model results with the observations, I don't really think that  
365 this is an assessment of the accuracy of the "model-derived OHexp". I realize the authors have the  
366 caveat "(including the factor of two decrease)", but I don't find this sufficient. I suggest that the authors  
367 very simply replace "accuracy" with "reasonableness".

368 We have replaced the word "accuracy" with "**reasonableness**" in P30426 L5 as suggested.

369 R3.11. P30427, L2: I think that here the authors are more specifically defining LVOCs as species that  
370 "irreversibly" condense, not just condense. I suggest they add this word.

371 The words "**(effectively) irreversibly**" have been added to P30427 L2.

372 R3.12. P30427: Regarding the fates of the LVOCs relative to their fate in the atmosphere, given that this  
373 study focuses on a forested area where the available surface area may be low, do they think that  
374 (perhaps) the LVOCs may condense onto things like leaves, trees, rather than onto particles? If this were  
375 to occur, then some of the loss processes discussed here might actually be relevant to this particular  
376 environment. I am speculating here, but perhaps something to consider adding a note about? Of course,  
377 such high exposures as considered here would not be relevant for the particles within the canopy, in  
378 general, but for those transported far downwind and so perhaps this line of thinking on my part is  
379 generally irrelevant.

380 We have changed P30427 L4 to:

381 **"In the atmosphere, the dominant fate of these LVOCs is to condense onto aerosols (lifetime of**  
382 **~minutes), as dry and wet deposition of even fast-depositing species are generally slower sinks**  
383 **(lifetime of ~hours; Farmer and Cohen, 2008; Knote et al., 2015; Nguyen et al., 2015)."**

384 We have also added the following sentence to P30427 L14:

385 **"As mentioned above, this correction takes into account that dry deposition of such LVOCs is not**  
386 **competitive with condensation onto particles in the atmosphere (Knote et al., 2015; Nguyen et al.,**  
387 **2015)."**

388 R3.13. P30427, L20: The authors here seem to be implying that the low volatility of SOA results solely  
389 from the condensing species being low volatility. However, this neglects that some of the low volatility  
390 nature of SOA may result from condensed phase reactions involving SVOCs. If such condensed phase  
391 reactions are fast, then distinguishing between SVOC and LVOC condensation may not be important.

392 We have modified the text at P30427 L20 to:

393 **"Some semivolatile species (SVOC) will likely also be produced. However, we focus on irreversibly**  
394 **condensing LVOCs, both for simplicity and based on the observation that most of the OA has low**  
395 **volatility at this site, according to thermal denuder measurements (Hunter et al., 2016), and**  
396 **consistent with measurements at other locations (Cappa and Jimenez, 2010; Lopez-Hilfiker et al.,**  
397 **2016). If the low volatility of OA is a result of condensation of SVOC followed by fast particle-phase**  
398 **reactions to produce low-volatility species, then the distinction between LVOC and SVOC would be**  
399 **irrelevant for this analysis."**

400 R3.14. P30427, L25: I find this to be an odd way to start a sentence.

401 We have added the following text to the end of P30427 L24:

402 **“The lifetimes of LVOCs against different processes are estimated as follows:”**

403 R3.15. P30429, L13: I think the units are incorrect on the surface area concentration.

404 Thanks for the catch. The units have been changed from “ $\mu\text{m cm}^{-3}$ ” to “ $\mu\text{m}^2 \text{cm}^{-3}$ ” in three places:  
405 P30429 L13, P30429 L15, and P30467, L5 of Fig. 9 caption.

406 R3.16. P30432, L24: Do the authors mean by dividing the newly produced  $\text{SO}_4$  mass, and not the total  
407  $\text{SO}_4$  mass, which would include pre-existing  $\text{SO}_4$  that is not influenced by the loss to walls or exiting the  
408 OFR?

409 The sentence starting at P30432 L22 has been changed as follows to clarify this point:

410 **“Using the model results, the fraction of  $\text{H}_2\text{SO}_4$  that does not condense onto aerosol was corrected for**  
411 **by dividing the newly produced  $\text{SO}_4$  mass measured with the AMS by  $F_{\text{aer}}$ .”**

412 R3.17. Figure 6: There does not appear to be a blue curve, as indicated in the legend. Do the authors  
413 mean black?

414 The word “blue” has been changed to “**black**” in L5 of the Fig. 6 caption on P30464.

415 R3.18. P30433: I agree that the  $\text{H}_2\text{SO}_4$  results suggest a strong potential for the LVOC correction method  
416 to help/work, however I think that the authors should also note that there is a great deal of scatter at  
417 low enhancements, when the corrections are particularly large, meaning that these values are  
418 particularly uncertain.

419 The following detail has been added to the captions of Fig. 6 and Fig. S10:

420 **“Ambient  $\text{SO}_2$  concentrations  $<0.2$  ppb have been excluded from this analysis.”**

421 We have also modified the text starting at P30433 L5 to read:

422 **“Generally, the amount of  $\text{SO}_4$  formed after applying the  $\text{H}_2\text{SO}_4$  wall and sampling line loss correction**  
423 **was consistent with the expected amount within the uncertainties. The amount of scatter introduced**  
424 **by applying the correction was larger when the amount of  $\text{SO}_4$  produced (and predicted) was close to**  
425 **zero, when the  $F_{\text{aer}}$  correction factor was less than  $\sim 0.3$ . This suggests that the LVOC fate model**  
426 **becomes more uncertain when the correction factors are large and  $F_{\text{aer}}$  is close to zero. However, this**  
427 **analysis demonstrates that a correction can be successfully applied for  $\text{H}_2\text{SO}_4$  condensation, and that a**  
428 **similar correction should also be applied for LVOC condensation to more accurately interpret the**  
429 **results of SOA formation in an OFR.”**

430 R3.19. P30435, L5: I suggest a reference to (Lambe et al., 2015) would be good here, as they compare  
431 OFR to chamber experiments for isoprene SOA.

432 We have modified the text at P30435 L2 to read:

433 **“This includes the IEPOX pathway from isoprene (Paulot et al., 2009) and the similar pathway**  
434 **proposed for MBO (Zhang et al., 2012). While SOA formation from isoprene in an OFR has been**

demonstrated (Lambe et al., 2015), the total SOA formation potential from MBO + isoprene may be underestimated in our study.”

R3.20. P30435, L14: In Fig. 7, comparing the daytime points, the difference between OFR185 and OFR254 at the lowest OH exposure was fairly large. Although I agree that there are no major differences between the OFR185 and OFR254, I am not entirely convinced that “significant” is justified here.

We have modified the text at P30435 L 13 to read:

“From Fig. 7, we conclude that there were no major differences in the amount of SOA formation between the OFR185 and OFR254-70 methods over the range of ages measured in this campaign. Minor differences in SOA formation between the two methods are likely a result of limits on the ability to determine the proper eq. age (especially for low ages in OFR254-70 as discussed in Sect. 2.3) or due to real changes in ambient SOA precursor gases, since the measurements using each method were not simultaneous. Additional comparisons of both methods sampling the same air, carefully designed and controlled to more accurately determine low ages in OFR254-70, would be useful to further explore this issue. Since the OFR185 mode is experimentally simpler and does not require addition of O<sub>3</sub> (with associated issues of mixing, dilution, possible contamination, etc.), and since the OFR185 mode more faithfully simulates OH chemistry due to reduced O<sub>3</sub> concentrations (Peng et al., 2015b), we recommend the OFR185 mode of operation for future OFR studies of OH oxidation in forested areas.”

R3.21. P30439, L7: Given the authors acknowledgement on the previous page that the yields of SOA in chamber experiments due to losses of S/IVOCs to chamber walls might be low, I think that the authors should change their language to indicate that other S/IVOCs “contribute” to the discrepancy, don’t “cause” the discrepancy.

The text has been modified at P30439 L6 to:

“The gases that enter the OFR as S/IVOCs are the most likely source of SOA formation contributing to the factor of 6 discrepancy in Sect. 3.6.1.”

We have also changed the word “explained” to “completely explained” in P30444 L6.

R3.22. Section 3.6.2: Given that the Hunter et al. manuscript is not yet published and not available for consideration, I find it difficult to really assess this section. For example, the authors report here measurements of MT concentrations that are typically around 0.5-1 ppb, which corresponds to 2.5-5 ug/3m. The logC\* of MTs is around 6 or 7. Either way, they should fall in one of the TD-EIMS bins shown in Fig. 12. However, the max concentration in those bins is only 0.5 ug/m<sup>3</sup>. Where are the MTs? I see the argument that “the TD-EIMS instrument experiences a loss of sampling efficiency in that bin and MT are not expected to be measured,” but without being able to read the Hunter paper I do not understand how one specific class within a bin would be missed (which is implied by the statement). If the authors simply mean that the overall efficiency in this bin is low, that I can understand.

We have modified the sentence at P30440 L13 to read:

“While MT are in the C\* = 10<sup>7</sup> µg m<sup>-3</sup> volatility bin, that bin is at the upper volatility limit of the TD-EIMS measurement capability. Some gases in that bin were sampled, but MT were expected to be too volatile to be measured (Hunter et al., 2016). This was supported by the fact that the campaign-



average mass in the  $C^* = 10^7 \mu\text{g m}^{-3}$  bin was only  $0.43 \mu\text{g m}^{-3}$ , which would correspond to only approximately 0.1 ppbv MT, if there were no other gases in that bin. The campaign-average in-canopy MT concentration measured by the PTR-TOF-MS was approximately 0.8 ppbv.”

R3.23. S/IVOCs Diurnal Dependence? The authors note a substantial difference in day/night SOA formation. This correlates really well with the day/night variation in MT concentrations. What about for S/IVOCs?

We have added the diurnal trace of S/IVOCs measured by the TD-EIMS instrument to Fig. 11, shown below.

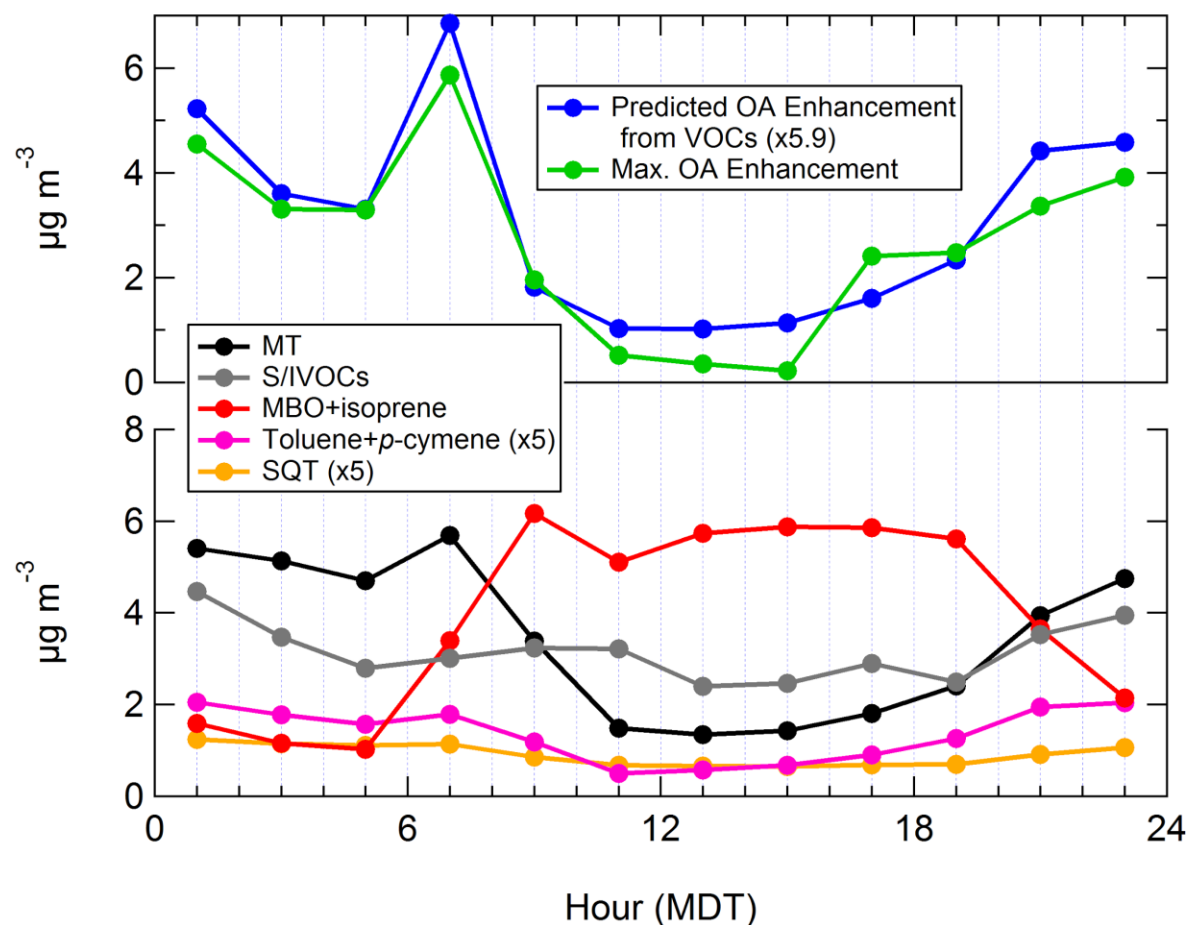


**Fig. 11. Top: diurnal maximum measured OA enhancement (all data from 0.4–1.5 eq. days aging, LVOC fate corrected) in the OFR from OH oxidation using the OFR185 method, and predicted OA formation from measured VOCs (x4.4). Bottom: ambient MT, SQT (x5), toluene+p-cymene (x5), MBO+isoprene, and S/IVOC mass concentrations vs. time of day.**

We also added or modified the following text:

P30438 L11: “A diurnal plot of the measured maximum (0.4–1.5 eq. days age) and predicted SOA formation is shown in Fig. 11, along with ambient MT, SQT, toluene+*p*-cymene, and MBO+isoprene concentrations (and S/IVOC concentrations, discussed in Sect. 3.6.2).”

See also the response to R3.24 for discussion of the diurnal S/IVOC concentrations.

R3.24. P30440/L28: I don’t fully follow what is being compared here. I thought that the SOA yields from S/IVOCs were just derived by comparing the S/IVOCs to the SOA. But then here they are comparing the SOA predicted from S/IVOCs (and VOCs) to the observed SOA. Isn’t this circular? Is the point here only the R2 value since the slope was effectively forced to one? This should be clarified. But given that the authors seem to use campaign-average values, not time-dependent values, for the S/IVOC concentrations it is not especially surprising to me that the R2 decreases from when compared to just the SOA predicted from VOCs. Or am I missing that, in fact, time dependent S/IVOC concentrations were used here? I think I am confused because of the statements on the previous page that a “full time series analysis” was not possible. I suggest that this section could be somewhat clearer regarding what specifically is being done with the S/IVOC measurements. (I suspect the authors are trying to not show too much of this data given the other pending publication. If the Hunter paper has been published by the time this is revised, I strongly encourage the authors to use a figure to help facilitate understanding here.)

We have restructured Sect. 3.6.2 as follows to clarify these topics:

P30439 L15-16: this last sentence of the paragraph has been removed.

Starting at P30439 L23: “With the substantial temporal overlap between OFR185 operation and TD-EIMS measurements, it is feasible to perform a point-by-point analysis using the full TD-EIMS time series (shown in Fig. S7) to determine what the SOA yield of the lower limit S/IVOC mass would need to be in order to fully explain the amount of SOA formed from OH oxidation in the OFR.

Ideally, the total mass of S/IVOCs at each data point that would be converted into SOA by oxidation would be determined by multiplying the mass in each volatility bin by the SOA yields of each bin. Since experimental measurements of the aerosol yields of such gases are generally not available and the ambient mixture of S/IVOCs was not fully speciated, we instead proceed under the assumption that all of the SOA formation that was not due to the previously discussed PTR-TOF-MS-measured VOCs came instead from the mass measured in the  $C^* = 10^1\text{--}10^7 \mu\text{g m}^{-3}$  volatility bins, with one correction. Since SQT are typically in the  $C^* = 10^5 \mu\text{g m}^{-3}$  range, we subtracted the SQT mass measured by the PTR-TOF-MS from the bulk S/IVOC mass (a subtraction of 6% of the total TD-EIMS measurement), to avoid double-counting due to this expected measurement overlap. While MT are in the  $C^* = 10^7 \mu\text{g m}^{-3}$  volatility bin, that bin is at the upper volatility limit of the TD-EIMS measurement capability. Some gases in that bin were sampled, but MT were expected to be too volatile to be measured (Hunter et al., 2016). This was supported by the fact that the campaign-average mass in the  $C^* = 10^7 \mu\text{g m}^{-3}$  bin was only  $0.43 \mu\text{g m}^{-3}$ , which would correspond to only approximately 0.1 ppbv MT, if there were no other gases in that bin. The campaign-average in-canopy MT concentration measured by the PTR-TOF-MS was approximately 0.8 ppbv.

For the lower limit S/IVOC mass case, the average SOA yield of the total S/IVOCs was determined by finding the yield value that made the slope of SOA measured vs. predicted from VOCs + S/IVOCs equal to one. As shown in Fig. 12, an average SOA yield of 58% for the bulk S/IVOC mass was required in order to bring the measured vs. predicted SOA formation into optimal agreement in this time series analysis. The correlation between measured and predicted SOA formation including the S/IVOCs and VOCs was  $R^2=0.66$ . Attempts were made to optimize the correlation between measured and predicted SOA formation by applying arbitrary  $C^*$ -dependent yields, but this did not result in significantly better correlations. Since speciated S/IVOC measurements as well as yields for each volatility bin (which may have varied with diurnal changes in the composition of each bin) were not available, we concluded that further detailed interpretation of SOA production from the measured S/IVOCs would be under-constrained.

As mentioned above, this average SOA yield for S/IVOCs of 58% was estimated by assuming the lower limit case where the total ambient S/IVOC mass was sampled using only the TD-EIMS. The upper limit mass case in Hunter et al. (2016) assumed that the several instruments that measured S/IVOCs were measuring different subsets of total S/IVOCs, so the measurements needed to be summed in order to determine the total mass concentration. Due to limited temporal overlap between all instruments, the analysis in Hunter et al. (2016) was performed on campaign average measurements. For this reason, the average SOA yield of S/IVOCs for the upper limit case is also done using the campaign average values instead of the time series analysis that was possible for the lower limit case. The average upper and lower limit S/IVOC mass concentrations were 10 and  $3.1 \mu\text{g m}^{-3}$ . To estimate the SOA yield of S/IVOCs in the upper limit case, the TD-EIMS time series data was multiplied by 3.2, so that it reflected a campaign average of  $10 \mu\text{g m}^{-3}$ . Using this upper limit mass time series, an average SOA yield for S/IVOCs of 18% was needed to bring measured vs. predicted SOA formation in the OFR into agreement. This makes the assumption that the ratio of S/IVOC mass measured by each technique was constant.

While measurements of SOA yields for speciated S/IVOCs are limited, especially for the relatively low OA concentrations in this study, previous work suggests that this range of 18-58% yield is reasonable. A yield of 51% was measured for n-heptadecane ( $C^* = 10^4 \mu\text{g/m}^3$ ) with OA =  $15.4 \mu\text{g/m}^3$  under high- $\text{NO}_x$  conditions (Presto et al., 2010). Yields can be even higher from cyclic compounds (Lim and Ziemann, 2009; Tkacik et al., 2012) and under low- $\text{NO}_x$  conditions (Ng et al., 2007; Lane et al., 2008). SOA yields from several other IVOCs (naphthalene and alkylnaphthalenes) under low- $\text{NO}_x$  conditions were determined to be 58-73% with OA concentrations of  $10\text{--}40 \mu\text{g/m}^3$  (Chan et al., 2009).

This analysis suggests that OH oxidation of organic gases in a parcel of ambient pine forest air will produce approximately 3.4 times more SOA from S/IVOC gases than from VOCs. This does not provide information about the sources of the lower volatility organic gases. They may be directly emitted, formed as oxidation products of VOCs that were emitted upwind of this parcel, or some combination of these two options. Ambient MT measured by the PTR-TOF-MS and S/IVOC concentrations measured by the TD-EIMS exhibit a modest correlation ( $R^2 = 0.43$ , shown in Fig. S13), suggesting that the S/IVOCs may at least partially come from a biogenic source related to the emission of MT. For

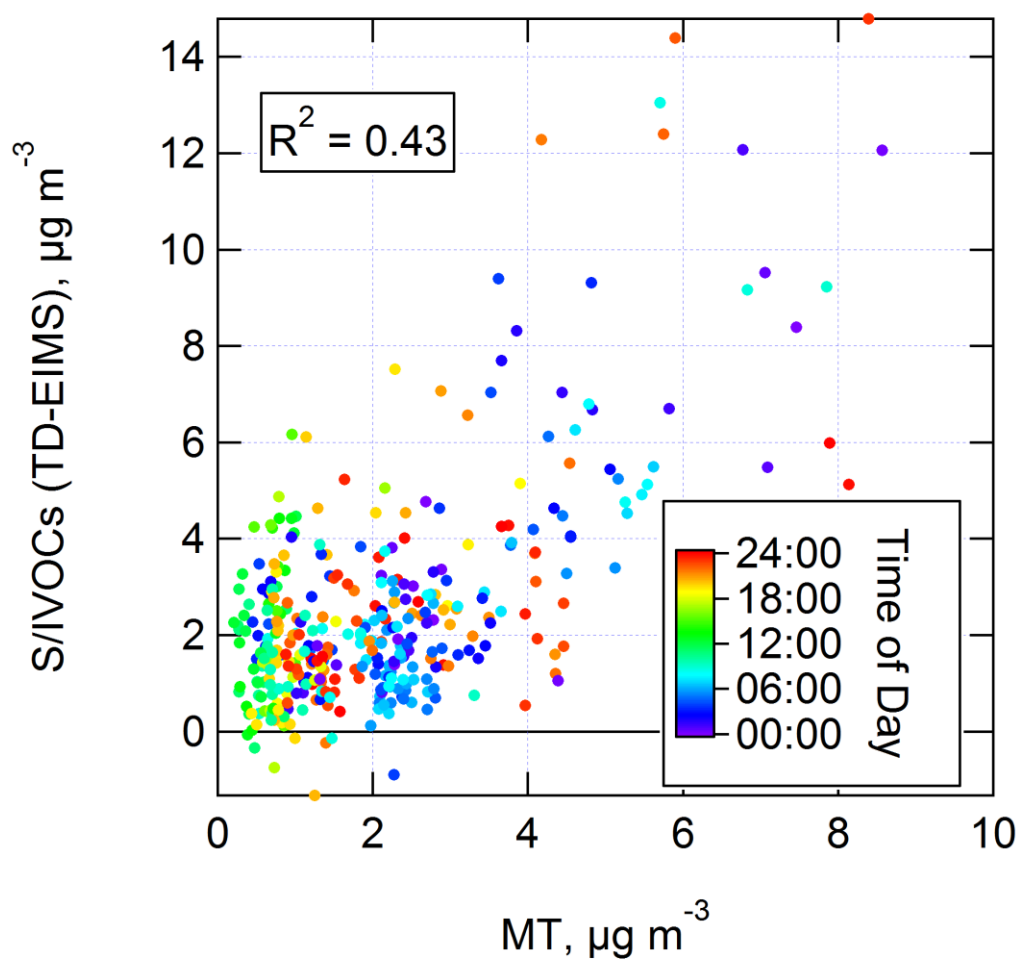
example,  $O_3$  and  $NO_3$  may react with the C=C-containing MT and SQT emissions during nighttime, leading to a buildup of oxidation product S/IVOCs that lack C=C double bonds and would generally not react further with  $O_3$  and  $NO_3$  (Atkinson, 1997). If this occurs, then OFR oxidation is merely starting with precursors that are partway through the “aging” process from VOC emission to SOA formation. Variations in the ratio of measured to predicted SOA formation in Figs. 10 and 12 could be due partly to variations in the ratio of the concentrations of S/IVOCs to VOCs due to changes in the meteorological or chemical conditions of the atmosphere, or from periodic changes in the biogenic and/or anthropogenic sources of S/IVOCs. However, as shown in Fig. 11, the diurnal profile of S/IVOC concentrations showed a relatively smaller increase in concentrations at night compared to MT or measured SOA formation. Since emissions and losses (e.g. OH oxidation) generally change with time of day, it would not be unreasonable to expect the speciation and SOA formation potential of ambient S/IVOCs to also change with time of day. Until the S/IVOCs in a dataset such as this can be better speciated and quantified, these conclusions remain speculative.”

R3.25. P30441, L8: I think the authors need to change “will produce” to “can potentially produce.” As I see what the authors have done, it is simply a matching exercise that does not definitively indicate that S/IVOCs form this much more SOA compared to VOCs in this environment because the authors have not addressed the issue of potential yield underestimates for VOCs in a quantitative manner.

We have changed the words “will produce” to “can potentially produce” in P30441 L8, as suggested.

R3.26. P30441/L12: The authors here discuss how the correlation between SOA and MT concentrations indicates that S/IVOCs come from biogenic sources related to MTs. I believe it would be much more straight forward to compare the SOA formation to the S/IVOC concentrations or the MT concentrations to S/IVOC concentrations directly to make this point. As written, this conclusion seems one step removed from the desired actual comparison.

We have modified the text as part of the response to R3.24, and have included the following Fig. S13 in the supplemental information:



590

591 **Fig. S13.** Scatterplot of mass concentration of ambient S/IVOCs (lower limit measured by TD-EIMS) vs.  
 592 ambient MT measured by PTR-TOF-MS. Data are shown colored by local time of day.

Other Changes:

In order to conform with the terminology introduced by Peng et al. (2015a), we have changed from “OFR254” to **“OFR254-70”** at all relevant references, signifying the typical injection of 70 ppm of O<sub>3</sub> during this campaign. This detail is relevant for understanding the oxidant chemistry in the OFR, which will assist with any future comparisons that are made with this dataset. To this end, we have modified the text at P30417 L9 to read:

**“In the OFR254 method, the mercury lamps were mounted inside Teflon-coated quartz sheaths, which blocked transmission of 185 nm light into the OFR, and only (R4-5) produced OH by photolysis of injected O<sub>3</sub>. Following the terminology introduced by Peng et al. (2015a), the method used in this work can be referred to as OFR254-70, signifying that typically 70 ppm of O<sub>3</sub> was injected when using the OFR254 method.”**

We have also introduced an additional correction to the LVOC fate modeling. Previously, the condensational sink (CS) was calculated using the dry SMPS measurements. However since oxidation in the OFR took place under ambient RH, the CS would be larger due to hygroscopic growth of particles in the atmosphere. We have now accounted for the added CS due to particle water, and the details were added starting at P30427 L25, which now reads:

**“-  $\tau_{aer}$ : Following Pirjola et al. (1999), the lifetime for LVOC condensation onto aerosols was calculated as**

$$\tau_{aer} = \frac{1}{4\pi \cdot CS \cdot D} \quad (1)$$

**with a diffusion coefficient  $D = 7 \times 10^{-6} \text{ m}^2 \text{ s}^{-1}$  representative of an oxidized organic molecule with a molecular weight of approximately 200 g mol<sup>-1</sup> at the field site ambient pressure (Tang et al., 2015). CS is the “condensational sink”**

$$CS = \int_0^\infty r \beta(r) N(r) dr \quad (2)$$

**which is the integral of the first moment of the particle size distribution, where  $r$  is the wet particle radius,  $N(r)$  is the particle number size distribution, and**

$$\beta(r) = \frac{Kn+1}{0.377Kn+1+\frac{4}{3}\alpha^{-1}Kn^2+\frac{4}{3}\alpha^{-1}Kn} \quad (3)$$

**is the Fuchs-Sutugin correction for gas diffusion to a particle surface in the transition regime, calculated using the sticking coefficient  $\alpha$  of the condensing species (Seinfeld and Pandis, 2006). CS was calculated using the average of the size distributions of ambient air entering the OFR and of air exiting the OFR after oxidation, as a best approximation of the actual CS experienced by LVOCs in the OFR. Since LVOC condensation in the OFR took place under ambient RH, the dried SMPS particle size**

distribution measurement was corrected to account for the increase in CS from hygroscopic particle growth as a function of RH. For each data point, a growth factor ( $gf$ ) was calculated from the equation

$$\kappa = \sum \varepsilon_i \kappa_i = (gf^3 - 1)(1 - a_w)a_w^{-1} \quad (4)$$

from Petters and Kreidenweis (2007) and Nguyen et al. (2015), where  $\varepsilon_i$  is the volume fraction of aerosol species  $i$ ,  $\kappa_i$  is the hygroscopicity parameter of aerosol species  $i$ ,  $\kappa$  is the hygroscopicity parameter of the total aerosol, and  $a_w$  is water activity. We approximate  $a_w$  as being equal to RH, between 0 and 1. Total  $\kappa$  was estimated using  $\kappa_{OA} = 0.13$  as previously reported for this site and campaign (Levin et al., 2014) and  $\kappa_{inorganic} = 0.6$ , using the volume mixing rule (Petters and Kreidenweis, 2007). The volume fractions were calculated from AMS measurements in ambient air or after OFR oxidation, using estimated component densities (Salcedo et al., 2006; Kuwata et al., 2012). The  $gf$  ranged between 1 and 2.3 with an average of 1.2. It was applied to the dry SMPS particle diameter before calculating CS.”

This correction to CS for hygroscopic growth of particles resulted in minor updates to values quoted throughout the manuscript, as well as Figs. 5–8, 10–13, S10, and S12. None of these updates resulted in substantial changes to the interpretation of our results.

## 641 **References**

- 642 Atkinson, R.: Gas-Phase Tropospheric Chemistry of Volatile Organic Compounds: 1. Alkanes and Alkenes,  
643 J. Phys. Chem. Ref. Data, 26, 215, doi:10.1063/1.556012, 1997.
- 644 Bruns, E. A., El Haddad, I., Keller, A., Klein, F., Kumar, N. K., Pieber, S. M., Corbin, J. C., Slowik, J. G.,  
645 Brune, W. H., Baltensperger, U. and Prévôt, A. S. H.: Inter-comparison of laboratory smog chamber and  
646 flow reactor systems on organic aerosol yield and composition, Atmos. Meas. Tech., 8, 2315–2332,  
647 doi:10.5194/amt-8-2315-2015, 2015.
- 648 Cappa, C. D. and Jimenez, J. L.: Quantitative estimates of the volatility of ambient organic aerosol,  
649 Atmos. Chem. Phys., 10, 5409–5424, doi:10.5194/acp-10-5409-2010, 2010.
- 650 Chan, A. W. H., Kautzman, K. E., Chhabra, P. S., Surratt, J. D., Chan, M. N., Crounse, J. D., Kürten, A.,  
651 Wennberg, P. O., Flagan, R. C. and Seinfeld, J. H.: Secondary organic aerosol formation from  
652 photooxidation of naphthalene and alkylnaphthalenes: implications for oxidation of intermediate  
653 volatility organic compounds (IVOCs), Atmos. Chem. Phys., 9, 3049–3060, doi:10.5194/acp-9-3049-2009,  
654 2009.
- 655 Chen, Q., Farmer, D. K., Schneider, J., Zorn, S. R., Heald, C. L., Karl, T. G., Guenther, A., Allan, J. D.,  
656 Robinson, N., Coe, H., Kimmel, J. R., Pauliquevis, T., Borrmann, S., Pöschl, U., Andreae, M. O., Artaxo, P.,  
657 Jimenez, J. L. and Martin, S. T.: Mass spectral characterization of submicron biogenic organic particles in  
658 the Amazon Basin, Geophys. Res. Lett., 36, L20806, doi:10.1029/2009GL039880, 2009.
- 659 Farmer, D. K. and Cohen, R. C.: Observations of HNO<sub>3</sub>, ΣAN, ΣPN and NO<sub>2</sub> fluxes: evidence for rapid HO<sub>x</sub>  
660 chemistry within a pine forest canopy, Atmos. Chem. Phys., 8, 3899–3917, doi:10.5194/acp-8-3899-  
661 2008, 2008.
- 662 Hayes, P. L., Carlton, A. G., Baker, K. R., Ahmadov, R., Washenfelder, R. A., Alvarez, S., Rappenglück, B.,  
663 Gilman, J. B., Kuster, W. C., de Gouw, J. A., Zotter, P., Prévôt, A. S. H., Szidat, S., Kleindienst, T. E.,  
664 Offenberg, J. H., Ma, P. K. and Jimenez, J. L.: Modeling the formation and aging of secondary organic  
665 aerosols in Los Angeles during CalNex 2010, Atmos. Chem. Phys., 15, 5773–5801, doi:10.5194/acp-15-  
666 5773-2015, 2015.
- 667 Henze, D. K. and Seinfeld, J. H.: Global secondary organic aerosol from isoprene oxidation, Geophys. Res.  
668 Lett., 33, L09812, doi:10.1029/2006GL025976, 2006.
- 669 Hodzic, A., Jimenez, J. L., Madronich, S., Aiken, A. C., Bessagnet, B., Curci, G., Fast, J., Lamarque, J. F.,  
670 Onasch, T. B., Roux, G., Schauer, J. J., Stone, E. A. and Ulbrich, I. M.: Modeling organic aerosols during  
671 MILAGRO: importance of biogenic secondary organic aerosols, Atmos. Chem. Phys., 9, 6949–6981, 2009.
- 672 Hodzic, A., Jimenez, J. L., Madronich, S., Canagaratna, M. R., DeCarlo, P. F., Kleinman, L. and Fast, J.:  
673 Modeling organic aerosols in a megacity: potential contribution of semi-volatile and intermediate  
674 volatility primary organic compounds to secondary organic aerosol formation, Atmos. Chem. Phys., 10,  
675 5491–5514, doi:doi:10.5194/acp-10-5491-2010, 2010.
- 676 Hunter, J. F., Day, D. A., Yatavelli, R. N., Chan, A., Kaser, L., Cappellin, L., Hayes, P. L., Palm, B. B., Cross, E.  
677 B., Carrasquillo, A., Campuzano-Jost, P., Stark, H., Zhao, Y., Hohaus, T., Smith, J. N., Hansel, A., Karl, T.,  
678 Goldstein, A. H., Guenther, A., Worsnop, D. R., Thornton, J. A., Heald, C. L., Jimenez, J. L. and Kroll, J. H.:



679 Comprehensive characterization of atmospheric organic carbon at a forested site, submitted, 2016.

680 Kang, E., Root, M. J., Toohey, D. W. and Brune, W. H.: Introducing the concept of Potential Aerosol Mass  
681 (PAM), *Atmos. Chem. Phys.*, 7, 5727–5744, doi:10.5194/acp-7-5727-2007, 2007.

682 Kang, E., Toohey, D. W. and Brune, W. H.: Dependence of SOA oxidation on organic aerosol mass  
683 concentration and OH exposure: experimental PAM chamber studies, *Atmos. Chem. Phys.*, 11, 1837–  
684 1852, doi:10.5194/acp-11-1837-2011, 2011.

685 Karl, T., Hansel, A., Cappellin, L., Kaser, L., Herdlinger-Blatt, I. and Jud, W.: Selective measurements of  
686 isoprene and 2-methyl-3-buten-2-ol based on  $\text{NO}^+$  ionization mass spectrometry, *Atmos. Chem. Phys.*,  
687 12, 11877–11884, doi:10.5194/acp-12-11877-2012, 2012.

688 Kaser, L., Karl, T., Schnitzhofer, R., Graus, M., Herdlinger-Blatt, I. S., DiGangi, J. P., Sive, B., Turnipseed, A.,  
689 Hornbrook, R. S., Zheng, W., Flocke, F. M., Guenther, A., Keutsch, F. N., Apel, E. and Hansel, A.:  
690 Comparison of different real time VOC measurement techniques in a ponderosa pine forest, *Atmos.*  
691 *Chem. Phys.*, 13, 2893–2906, doi:10.5194/acp-13-2893-2013, 2013.

692 Kim, S., Wolfe, G. M., Mauldin, L., Cantrell, C., Guenther, A., Karl, T., Turnipseed, A., Greenberg, J., Hall,  
693 S. R., Ullmann, K., Apel, E., Hornbrook, R., Kajii, Y., Nakashima, Y., Keutsch, F. N., DiGangi, J. P., Henry, S.  
694 B., Kaser, L., Schnitzhofer, R., Graus, M., Hansel, A., Zheng, W. and Flocke, F. F.: Evaluation of  $\text{HO}_x$   
695 sources and cycling using measurement-constrained model calculations in a 2-methyl-3-butene-2-ol  
696 (MBO) and monoterpene (MT) dominated ecosystem, *Atmos. Chem. Phys.*, 13, 2031–2044,  
697 doi:10.5194/acp-13-2031-2013, 2013.

698 Knote, C., Hodzic, A. and Jimenez, J. L.: The effect of dry and wet deposition of condensable vapors on  
699 secondary organic aerosols concentrations over the continental US, *Atmos. Chem. Phys.*, 15, 1–18,  
700 doi:10.5194/acp-15-1-2015, 2015.

701 Kuwata, M., Zorn, S. R. and Martin, S. T.: Using elemental ratios to predict the density of organic  
702 material composed of carbon, hydrogen, and oxygen., *Environ. Sci. Technol.*, 46, 787–94,  
703 doi:10.1021/es202525q, 2012.

704 Lambe, A. T., Onasch, T. B., Massoli, P., Croasdale, D. R., Wright, J. P., Ahern, A. T., Williams, L. R.,  
705 Worsnop, D. R., Brune, W. H. and Davidovits, P.: Laboratory studies of the chemical composition and  
706 cloud condensation nuclei (CCN) activity of secondary organic aerosol (SOA) and oxidized primary  
707 organic aerosol (OPOA), *Atmos. Chem. Phys.*, 11, 8913–8928, doi:10.5194/acp-11-8913-2011, 2011.

708 Lambe, A. T., Chhabra, P. S., Onasch, T. B., Brune, W. H., Hunter, J. F., Kroll, J. H., Cummings, M. J.,  
709 Brogan, J. F., Parmar, Y., Worsnop, D. R., Kolb, C. E. and Davidovits, P.: Effect of oxidant concentration,  
710 exposure time, and seed particles on secondary organic aerosol chemical composition and yield, *Atmos.*  
711 *Chem. Phys.*, 15, 3063–3075, doi:10.5194/acp-15-3063-2015, 2015.

712 Lane, T. E., Donahue, N. M. and Pandis, S. N.: Effect of  $\text{NO}_x$  on secondary organic aerosol concentrations,  
713 *Environ. Sci. Technol.*, 42, 6022–6027, doi:Doi 10.1021/Es703225a, 2008.

714 Levin, E. J. T., Prenni, A. J., Palm, B. B., Day, D. A., Campuzano-Jost, P., Winkler, P. M., Kreidenweis, S. M.,  
715 Demott, P. J., Jimenez, J. L. and Smith, J. N.: Size-resolved aerosol composition and its link to  
716 hygroscopicity at a forested site in Colorado, *Atmos. Chem. Phys.*, 14, 2657–2667, 2014.

Li, R., Palm, B. B., Ortega, A. M., Hlywiak, J., Hu, W., Peng, Z., Day, D. A., Knote, C., Brune, W. H., de Gouw, J. A. and Jimenez, J. L.: Modeling the Radical Chemistry in an Oxidation Flow Reactor: Radical Formation and Recycling, Sensitivities, and the OH Exposure Estimation Equation, *J. Phys. Chem. A*, 119, 4418–4432, doi:10.1021/jp509534k, 2015.

Lim, Y. B. and Ziemann, P. J.: Effects of Molecular Structure on Aerosol Yields from OH Radical-Initiated Reactions of Linear, Branched, and Cyclic Alkanes in the Presence of NO<sub>x</sub>, *Environ. Sci. Technol.*, 43, 2328–2334, doi:10.1021/es803389s, 2009.

Lopez-Hilfiker, F. D., Mohr, C., D'Ambro, E. L., Lutz, A., Riedel, T. P., Gaston, C. J., Iyer, S., Zhang, Z., Gold, A., Surratt, J. D., Lee, B. H., Kurten, T., Hu, W. W., Jimenez, J., Hallquist, M. and Thornton, J. A.: Molecular Composition and Volatility of Organic Aerosol in the Southeastern U.S.: Implications for IEPOX Derived SOA, *Environ. Sci. Technol.*, accepted, acs.est.5b04769, doi:10.1021/acs.est.5b04769, 2016.

Matsunaga, A. and Ziemann, P. J.: Gas-Wall Partitioning of Organic Compounds in a Teflon Film Chamber and Potential Effects on Reaction Product and Aerosol Yield Measurements, *Aerosol Sci. Technol.*, 44, 881–892, doi:10.1080/02786826.2010.501044, 2010.

Nakashima, Y., Kato, S., Greenberg, J., Harley, P., Karl, T., Turnipseed, A., Apel, E., Guenther, A., Smith, J. and Kajii, Y.: Total OH reactivity measurements in ambient air in a southern Rocky mountain ponderosa pine forest during BEACHON-SRM08 summer campaign, *Atmos. Environ.*, 85, 1–8, doi:10.1016/j.atmosenv.2013.11.042, 2014.

Ng, N. L., Chhabra, P. S., Chan, A. W. H., Surratt, J. D., Kroll, J. H., Kwan, A. J., McCabe, D. C., Wennberg, P. O., Sorooshian, A., Murphy, S. M., Dalleska, N. F., Flagan, R. C. and Seinfeld, J. H.: Effect of NO<sub>x</sub> level on secondary organic aerosol (SOA) formation from the photooxidation of terpenes, *Atmos. Chem. Phys.*, 7, 5159–5174, doi:10.5194/acp-7-5159-2007, 2007.

Nguyen, T. B., Crounse, J. D., Teng, A. P., St. Clair, J. M., Paulot, F., Wolfe, G. M. and Wennberg, P. O.: Rapid deposition of oxidized biogenic compounds to a temperate forest, *P. Natl. Acad. Sci. USA*, 112, E392–E401, doi:10.1073/pnas.1418702112, 2015.

Ortega, A. M., Day, D. A., Cubison, M. J., Brune, W. H., Bon, D., de Gouw, J. A. and Jimenez, J. L.: Secondary organic aerosol formation and primary organic aerosol oxidation from biomass-burning smoke in a flow reactor during FLAME-3, *Atmos. Chem. Phys.*, 13, 11551–11571, doi:10.5194/acp-13-11551-2013, 2013.

Ortega, A. M., Hayes, P. L., Peng, Z., Palm, B. B., Hu, W., Day, D. A., Li, R., Cubison, M. J., Brune, W. H., Graus, M., Warneke, C., Gilman, J. B., Kuster, W. C., de Gouw, J. A. and Jimenez, J. L.: Real-time measurements of secondary organic aerosol formation and aging from ambient air in an oxidation flow reactor in the Los Angeles area, *Atmos. Chem. Phys. Discuss.*, 15, 21907–21958, doi:10.5194/acpd-15-21907-2015, 2015.

Paulot, F., Crounse, J. D., Kjaergaard, H. G., Kürten, A., St Clair, J. M., Seinfeld, J. H., Wennberg, P. O., Kurten, A., St Clair, J. M., Seinfeld, J. H., Wennberg, P. O., Kürten, A., St Clair, J. M., Seinfeld, J. H. and Wennberg, P. O.: Unexpected epoxide formation in the gas-phase photooxidation of isoprene., *Science*, 325, 730–3, doi:10.1126/science.1172910, 2009.

Peng, Z., Day, D. A., Stark, H., Li, R., Lee-Taylor, J., Palm, B. B., Brune, W. H. and Jimenez, J. L.: HO<sub>x</sub> radical

756 chemistry in oxidation flow reactors with low-pressure mercury lamps systematically examined by  
 757 modeling, *Atmos. Meas. Tech.*, 8, 4863–4890, doi:10.5194/amt-8-4863-2015, 2015a.

758 Peng, Z., Day, D. A., Ortega, A. M., Palm, B. B., Hu, W. W., Stark, H., Li, R., Tsigaridis, K., Brune, W. H. and  
 759 Jimenez, J. L.: Non-OH chemistry in oxidation flow reactors for the study of atmospheric chemistry  
 760 systematically examined by modeling, *Atmos. Chem. Phys. Discuss.*, 15, 23543–23586,  
 761 doi:10.5194/acpd-15-23543-2015, 2015b.

762 Petters, M. D. and Kreidenweis, S. M.: A single parameter representation of hygroscopic growth and  
 763 cloud condensation nucleus activity, *Atmos. Chem. Phys.*, 7, 1961–1971, doi:10.5194/acp-7-1961-2007,  
 764 2007.

765 Pirjola, L., Kulmala, M., Wilck, M., Bischoff, A., Stratmann, F. and Otto, E.: Formation Of Sulphuric Acid  
 766 Aerosols And Cloud Condensation Nuclei: An Expression For Significant Nucleation And Model  
 767 Comparison, *J. Aerosol Sci.*, 30, 1079–1094, doi:10.1016/S0021-8502(98)00776-9, 1999.

768 Presto, A. A., Miracolo, M. A., Donahue, N. M. and Robinson, A. L.: Secondary Organic Aerosol Formation  
 769 from High-NO<sub>x</sub> Photo-Oxidation of Low Volatility Precursors: N-Alkanes, *Environ. Sci. Technol.*, 44, 2029–  
 770 2034, doi:10.1021/es903712r, 2010.

771 Salcedo, D., Onasch, T. B., Dzepina, K., Canagaratna, M. R., Zhang, Q., Huffman, J. A., DeCarlo, P. F.,  
 772 Jayne, J. T., Mortimer, P., Worsnop, D. R., Kolb, C. E., Johnson, K. S., Zuberi, B., Marr, L. C., Volkamer, R.,  
 773 Molina, L. T., Molina, M. J., Cardenas, B., Bernabé, R. M., Márquez, C., Gaffney, J. S., Marley, N. A.,  
 774 Laskin, A., Shutthanandan, V., Xie, Y., Brune, W., Leshner, R., Shirley, T. and Jimenez, J. L.: Characterization  
 775 of ambient aerosols in Mexico City during the MCMA-2003 campaign with Aerosol Mass Spectrometry:  
 776 results from the CENICA Supersite, *Atmos. Chem. Phys.*, 6, 925–946, doi:10.5194/acp-6-925-2006, 2006.

777 Sander, S. P., Abbatt, J. P. D., Barker, J. R., Burkholder, J. B., Friedl, R. R., Golden, D. M., Huie, R. E., Kolb,  
 778 C. E., Kurylo, M. J., Moortgat, G. K., Orkin, V. L. and Wine, P. H.: Chemical Kinetics and Photochemical  
 779 Data for Use in Atmospheric Studies Evaluation Number 17, JPL Publ. 10-6, 2011.

780 Seinfeld, J. H. and Pandis, S. N.: Atmospheric chemistry and physics: from air pollution to climate change,  
 781 2nd ed., John Wiley & Sons, Inc., Hoboken, New Jersey, USA., 2006.

782 Slowik, J. G., Stroud, C., Bottenheim, J. W., Brickell, P. C., Chang, R. Y.-W., Liggio, J., Makar, P. A., Martin,  
 783 R. V., Moran, M. D., Shantz, N. C., Sjostedt, S. J., van Donkelaar, A., Vlasenko, A., Wiebe, H. A., Xia, A. G.,  
 784 Zhang, J., Leaitch, W. R. and Abbatt, J. P. D.: Characterization of a large biogenic secondary organic  
 785 aerosol event from eastern Canadian forests, *Atmos. Chem. Phys.*, 10, 2825–2845, doi:10.5194/acp-10-  
 786 2825-2010, 2010.

787 Tanaka, P. L., Allen, D. T. and Mullins, C. B.: An environmental chamber investigation of chlorine-  
 788 enhanced ozone formation in Houston, Texas, *J. Geophys. Res.*, 108, 4576, doi:10.1029/2002JD003314,  
 789 2003.

790 Tang, M. J., Shiraiwa, M., Pöschl, U., Cox, R. A. and Kalberer, M.: Compilation and evaluation of gas  
 791 phase diffusion coefficients of reactive trace gases in the atmosphere: Volume 2. Diffusivities of organic  
 792 compounds, pressure-normalised mean free paths, and average Knudsen numbers for gas uptake  
 793 calculations, *Atmos. Chem. Phys.*, 15, 5585–5598, doi:10.5194/acp-15-5585-2015, 2015.

794 Tkacik, D. S., Presto, A. A., Donahue, N. M. and Robinson, A. L.: Secondary organic aerosol formation  
 795 from intermediate-volatility organic compounds: cyclic, linear, and branched alkanes., *Environ. Sci.*  
 796 *Technol.*, 46, 8773–81, doi:10.1021/es301112c, 2012.

797 Tkacik, D. S., Lambe, A. T., Jathar, S., Li, X., Presto, A. A., Zhao, Y., Blake, D., Meinardi, S., Jayne, J. T.,  
 798 Croteau, P. L. and Robinson, A. L.: Secondary Organic Aerosol Formation from in-Use Motor Vehicle  
 799 Emissions Using a Potential Aerosol Mass Reactor, *Environ. Sci. Technol.*, 48, 11235–11242,  
 800 doi:10.1021/es502239v, 2014.

801 Tsimpidi, A. P., Karydis, V. A., Zavala, M., Lei, W., Molina, L., Ulbrich, I. M., Jimenez, J. L. and Pandis, S. N.:  
 802 Evaluation of the volatility basis-set approach for the simulation of organic aerosol formation in the  
 803 Mexico City metropolitan area, *Atmos. Chem. Phys.*, 10, 525–546, doi:10.5194/acp-10-525-2010, 2010.

804 Tunved, P., Hansson, H.-C., Kerminen, V.-M., Ström, J., Maso, M. D., Lihavainen, H., Viisanen, Y., Aalto, P.  
 805 P., Komppula, M. and Kulmala, M.: High natural aerosol loading over boreal forests., *Science*, 312, 261–  
 806 3, doi:10.1126/science.1123052, 2006.

807 Volkamer, R., Jimenez, J. L., San Martini, F., Dzepina, K., Zhang, Q., Salcedo, D., Molina, L. T., Worsnop, D.  
 808 R. and Molina, M. J.: Secondary organic aerosol formation from anthropogenic air pollution: Rapid and  
 809 higher than expected, *Geophys. Res. Lett.*, 33, L17811, doi:doi:10.1029/2006gl026899, 2006.

810 von der Weiden, S.-L., Drewnick, F. and Borrmann, S.: Particle Loss Calculator – a new software tool for  
 811 the assessment of the performance of aerosol inlet systems, *Atmos. Meas. Tech.*, 2, 479–494,  
 812 doi:10.5194/amt-2-479-2009, 2009.

813 Wyche, K. P., Ryan, A. C., Hewitt, C. N., Alfarra, M. R., McFiggans, G., Carr, T., Monks, P. S., Smallbone, K.  
 814 L., Capes, G., Hamilton, J. F., Pugh, T. A. M. and MacKenzie, A. R.: Emissions of biogenic volatile organic  
 815 compounds and subsequent photochemical production of secondary organic aerosol in mesocosm  
 816 studies of temperate and tropical plant species, *Atmos. Chem. Phys.*, 14, 12781–12801,  
 817 doi:10.5194/acp-14-12781-2014, 2014.

818 Zhang, H., Worton, D. R., Lewandowski, M., Ortega, J., Rubitschun, C. L., Park, J.-H., Kristensen, K.,  
 819 Campuzano-Jost, P., Day, D. A., Jimenez, J. L., Jaoui, M., Offenberg, J. H., Kleindienst, T. E., Gilman, J.,  
 820 Kuster, W. C., de Gouw, J., Park, C., Schade, G. W., Frossard, A. A., Russell, L., Kaser, L., Jud, W., Hansel,  
 821 A., Cappellin, L., Karl, T., Glasius, M., Guenther, A., Goldstein, A. H., Seinfeld, J. H., Gold, A., Kamens, R.  
 822 M. and Surratt, J. D.: Organosulfates as Tracers for Secondary Organic Aerosol (SOA) Formation from 2-  
 823 Methyl-3-Buten-2-ol (MBO) in the Atmosphere, *Environ. Sci. Technol.*, 46, 9437–9446,  
 824 doi:10.1021/es301648z, 2012.

825

# In situ secondary organic aerosol formation from ambient pine forest air using an oxidation flow reactor

Brett B. Palm<sup>1,2</sup>, Pedro Campuzano-Jost<sup>1,2</sup>, Amber M. Ortega<sup>1,3</sup>, Douglas A. Day<sup>1,2</sup>, Lisa Kaser<sup>4,5</sup>, Werner Jud<sup>5</sup>, Thomas Karl<sup>6</sup>, Armin Hansel<sup>5</sup>, James F. Hunter<sup>7</sup>, Eben S. Cross<sup>7</sup>, Jesse H. Kroll<sup>7,8</sup>, Zhe Peng<sup>1,2</sup>, William H. Brune<sup>9</sup>, and Jose L. Jimenez<sup>1,2</sup>

<sup>1</sup>Cooperative Institute for Research in Environmental Sciences, University of Colorado, Boulder, USA;

<sup>2</sup>Department of Chemistry and Biochemistry, University of Colorado, Boulder, USA;

<sup>3</sup>Department of Atmospheric and Oceanic Science, University of Colorado, Boulder, USA;

<sup>4</sup>National Center for Atmospheric Research, Boulder, CO, USA;

<sup>5</sup>Institute of Ion Physics and Applied Physics, University of Innsbruck, Innsbruck, Austria;

<sup>6</sup>Institute of Meteorology and Geophysics, University of Innsbruck, Innsbruck, Austria;

<sup>7</sup>Department of Civil and Environmental Engineering, Massachusetts Institute of Technology, Cambridge, MA, USA

<sup>8</sup>Department of Chemical Engineering, Massachusetts Institute of Technology, Cambridge, MA, USA

<sup>9</sup>Department of Meteorology, Pennsylvania State University, State College, PA, USA

Correspondence to: J.L. Jimenez (jose.jimenez@colorado.edu)

## Abstract

Ambient air was oxidized by OH radicals in an oxidation flow reactor (OFR) located in a montane pine forest during the BEACHON-RoMBAS campaign to study biogenic secondary organic aerosol (SOA) formation and aging. An oxidation flow reactor (OFR) is a vessel inside which the concentration of a chosen oxidant can be increased for the purpose of studying SOA formation and aging by that oxidant. During the BEACHON-RoMBAS field campaign, ambient pine forest air was oxidized by OH radicals in an OFR to measure the amount of SOA that could be formed from the real mix of ambient SOA-precursor gases, and how that amount changed with time as precursors changed. High OH concentrations and short residence times allowed for semi-continuous cycling through a large range of OH exposures ranging from hours to weeks of equivalent (eq.) atmospheric aging. A simple model is derived and used to account for the relative time scales of condensation of low volatility organic compounds (LVOCs) onto particles, condensational loss to the walls, and further reaction to produce volatile, non-condensing fragmentation products. More SOA production was observed in the OFR at nighttime (average  $43 \mu\text{g m}^{-3}$  when LVOC fate corrected) compared to daytime (average  $40.9 \mu\text{g m}^{-3}$  when LVOC fate corrected), with maximum formation observed at 0.4–1.5 eq. days of photochemical aging. SOA formation followed a similar diurnal pattern to monoterpenes, sesquiterpenes, and toluene+*p*-cymene concentrations, including a substantial increase just after sunrise at 7 AM local time. Higher photochemical aging (>10 eq. days) led to a decrease in new SOA formation and a loss of preexisting OA due to heterogeneous oxidation followed by fragmentation and volatilization. When comparing two different commonly used methods of OH production in OFRs (OFR185 and OFR254-70), similar amounts of SOA formation were observed. We recommend the OFR185 mode for future forest studies. Concurrent gas-phase measurements of air after OH oxidation illustrate the decay of primary VOCs, production of small oxidized organic compounds, and net production at lower ages followed by net consumption of terpenoid oxidation products as photochemical age increased. New particle formation was observed in the reactor after oxidation, especially during times when precursor gas concentrations and SOA formation were largest. Approximately 64.4 times more SOA was formed in the reactor from OH oxidation than could be explained by the VOCs measured in ambient air. To our knowledge this is the first time that this has been shown when comparing VOCs and SOA formation measured at the same time, rather than comparing measurements made at different times. Several recently-developed instruments quantified ambient semi- and intermediate-volatility organic compounds (S/IVOCs) that were not detected by a PTR-TOF-MS. An SOA yield of 24–80% from those compounds can explain the observed SOA, suggesting formation. This work suggests that these typically unmeasured S/IVOCs play a substantial role in ambient SOA formation. Our results allow ruling out

Formatted: Space Before: 0 pt, Line spacing: single

Formatted: Font: 10 pt

Formatted: Line spacing: single

Formatted: Space Before: 0 pt

Formatted: Font: Italic

Formatted: Font: Italic

condensation sticking coefficients much lower than 1. ~~Our~~These measurements help clarify the magnitude of potential SOA formation from OH oxidation in forested environments, and demonstrate methods for interpretation of ambient OFR measurements.

## 1 Introduction

Atmospheric aerosols play a complex and important role in air pollution, human health, and global climate. Exposure to fine particles has adverse effects on cardiopulmonary health (Pope and Dockery, 2006). Aerosols affect climate forcing by directly scattering or absorbing incoming solar radiation. They also act as cloud condensation nuclei (CCN), affecting the reflectivity, lifetime, and precipitation of clouds (~~IPCC, 2013~~)(IPCC, 2013). Among all radiative forcings, the estimates for aerosols represent the largest uncertainty (Myhre et al., 2013).

Organic aerosols (OA) make up a substantial fraction of submicron aerosols (Murphy et al., 2006; Zhang et al., 2007; Jimenez et al., 2009). OA is composed of thousands of different molecules, of which only a small fraction has been speciated (Goldstein and Galbally, 2007). OA can be emitted directly in the particle phase as primary OA (POA), or it can be formed as secondary OA (SOA) through gas-to-particle conversion. During gas-phase SOA formation, an oxidant (mainly OH, O<sub>3</sub>, or NO<sub>3</sub>) reacts with organic gases to produce either less-volatile functionalization products (e.g., reacting to add a hydroxyl group) or more-volatile fragmentation products (e.g., breaking C-C bonds to produce smaller molecules). If the reaction products have sufficiently lower volatility, they can then partition into the particle phase to form SOA (Pankow, 1994; Donahue et al., 2006). In addition to gas-phase oxidation pathways, SOA formation can result from aqueous chemistry within aerosol water or in cloud droplets (e.g., Lim et al., 2010; Ervens et al., 2011; Ervens, 2015) or heterogeneous uptake reactions (e.g., Surratt et al., 2010). Oxidative aging of gases and particles continues until deposition occurs (or CO<sub>2</sub> is produced). The complexity of OA chemistry arises from this intricate mix of multiphase-multigenerational reaction pathways and physicochemical processes involving thousands of molecules.

Much progress has been made in the past decade towards identifying and quantifying the sources, formation, and aging mechanisms of SOA. Aerosol models using traditional (pre-2007) aerosol yields for volatile organic compounds (VOCs) from chamber studies generally underpredict SOA mass by a factor of 10 in urban areas (Volkamer et al., 2006; Hodzic et al., 2010; Hayes et al., 2015). More recent models are able to better predict SOA mass in urban areas by adding previously ignored semivolatile and intermediate-volatility organic compounds (S/IVOCs; Hodzic et al., 2010; Hayes et al., 2015). Recent measurements of the oxidation of biomass burning emissions, vehicle exhaust, and urban air have also

Field Code Changed

found S/IVOCs to be important contributors to SOA formation (Grieshop et al., 2009; Miracolo et al., 2010; Zhao et al., 2014), building on the ideas of Robinson, et al. (2007). However, model parameterizations of SOA formation from S/IVOCs are based on large extrapolations and are still uncertain. The recent AeroCom intercomparison of 31 global OA models showed large variability between models and low temporal correlations between models and measurements (Tsigaridis et al., 2014). Their work suggests that current model parameterizations of SOA formation, transport, and removal processes are inadequate.

SOA formation has traditionally been studied in large environmental “smog” chambers. These chamber experiments have provided the SOA yields for models, but recent evidence shows that chamber experiments are affected by large losses of semivolatile gases to chamber walls (Matsunaga and Ziemann, 2010; Zhang et al., 2014; Krechmer et al., 2015) in addition to well-known particle wall losses (Pierce et al., 2008). This is especially true at long (>1 day) residence times, making it difficult to study SOA formation and aging on longer time scales. It is also difficult to perform field experiments with ambient air in smog chambers (Tanaka et al., 2003). To explore the sources of SOA on a rapid time scale and with a wide range of oxidant exposures, a variety of oxidation flow reactors (OFR) have been developed (Kang et al., 2007; George et al., 2008; Smith et al., 2009; Keller and Bertscher, 2012). OFRs employ higher oxidant concentrations than chambers while having a short residence time with reduced wall contact. This allows hours to months of equivalent (eq.) atmospheric aging, and the same experimental system can be used in both laboratory and field experiments.

Previous experiments have shown SOA yields from various precursor gases oxidized in an OFR to be similar to yields from large environmental chambers (Kang et al., 2007, 2011; Lambe et al., 2011b, 2015). OFRs have also been used to investigate SOA formation from pollution source emissions containing complex mixtures of precursors such as controlled biomass burning (Ortega et al., 2013; Bruns et al., 2015) and vehicular emissions in a tunnel (Tkacik et al., 2014). Ortega et al. (2015) pioneered the use of an OFR to study SOA formation from ambient air in an urban study in the Los Angeles area. Tkacik et al. (2014) and Ortega et al. (2013) showed substantially more SOA formation than could be explained from speciated VOCs, suggesting that S/IVOCs contribute to SOA formation in biomass burning plumes and vehicle exhaust.

In this study, we used an OFR to expose ambient air to variable levels of OH in a ponderosa pine forest during the BEACHON-RoMBAS campaign. We extensively characterized both the gas and particle phase

to investigate the formation and aging of SOA. Changes in aerosol formation with gas-precursor concentrations, time of day, and OH exposure were explored. The fate of condensable organic gases in the OFR was modeled. This model was used to estimate how much SOA formation was missed in the OFR due to gas-phase wall losses, excessive OH reaction that led to gas-phase fragmentation prior to condensation, and inadequate time/particle surface area for condensation. The SOA mass produced via oxidation was compared to the amount of SOA predicted based on literature yields of measured VOCs. The role of S/IVOCs in SOA formation in a forest was also explored. These results are discussed in the context of improving our knowledge of SOA sources and formation processes in a biogenic-dominated environment.

## **2 Experimental Methods**

### **2.1 BEACHON RoMBAS Campaign**

The BEACHON RoMBAS field campaign (Bio-hydro-atmosphere interactions of Energy, Aerosols, Carbon, H<sub>2</sub>O, Organics & Nitrogen – Rocky Mountain Biogenic Aerosol Study; <http://cires.colorado.edu/iimenez-group/wiki/index.php/BEACHON-RoMBAS>) took place at the Manitou Experimental Forest Observatory near Woodland Park, Colorado, in July–August 2011 (39.10° N, 105.10° W; 2370 m elevation). It was a collaboration of 27 institutions from the United States and Europe, focused on understanding primary and secondary biogenic aerosol emissions, formation and processing. An overview of atmospheric chemistry research at the Manitou Experimental Forest Observatory, including the BEACHON RoMBAS campaign, has been previously published (Ortega et al., 2014).

The sampling site was located in a ponderosa-pine forest in a mountain valley. VOC concentrations were characterized by high 2-methyl-3-buten-2-ol (MBO) during the daytime and monoterpenes (MT) during the nighttime. VOCs at this site have been described in detail for previous campaigns during July–September 2008 (Kim et al., 2010) and August–September 2010 (Kaser et al., 2013a, b), while Fry et al. (Fry et al., 2013) discussed diurnal cycles of select biogenic and anthropogenic VOCs during this campaign. The diurnal cycle of the concentration of MBO+isoprene (detected as the same product ion in the proton transfer reaction time-of-flight mass spectrometer; PTR-TOF-MS) measured at an above-canopy 25-m inlet ranged from about 1.5 ppb during the day to 0.3 ppb at night, while MT concentrations were on average 0.1 ppb during the day and 0.5 ppb at night. The relative ratio of isoprene/(MBO+isoprene) at this field site was estimated using GC-MS, PTR-TOF-MS, and whole air samples during summer 2010 (Kaser et al., 2013b) and using NO<sup>+</sup> as a reagent ion during this campaign.



(Karl et al., 2012) to be approximately 20%. Isoprene concentrations are calculated in this study using that approximation, which gives values typically <200 ppt. While largely dominated by biogenic emissions, the site receives some airflow from the front range urban areas (Denver metropolitan area and Colorado Springs) on most days, as evidenced by moderate increases in  $\text{NO}_x$ , CO, and anthropogenic VOCs during late afternoon and into the evening (Fry et al., 2013; Ortega et al., 2014; Chan et al., 2015).

## 2.2 Oxidation flow reactor

The Potential Aerosol Mass (PAM) oxidation flow reactor (hereafter flow reactor or OFR) is a cylindrical tube 45.7 cm long and 19.7 cm ID with a volume of approximately 13 liters, previously described elsewhere (Kang et al., 2007, 2011; Lambe et al., 2011a; Ortega et al., 2013, 2015). Ambient air was sampled through the reactor with a residence time of 2–4 min (3.5–6.5 lpm total flow rate), achieving oxidant exposures of hours to months of eq. atmospheric aging. The inlet plate of the OFR was removed to reduce possible losses of semivolatile SOA precursors to the inlet plate inferred in a previous study (Ortega et al., 2013) and to reduce the width of the residence time distribution in the reactor. Air was sampled into the reactor through a 14 cm diameter coarse grid mesh screen to reduce turbulence in the reactor and prevent insects and debris from entering the reactor. The mesh was coated with an inert silicon coating (Sulfinert by SilcoTek, Bellefonte, PA) to minimize gas and particle losses. OH radicals in the OFR were produced inside the reactor through one of two methods: OH production from photolysis of ambient  $\text{H}_2\text{O}$ ,  $\text{O}_2$ , and concurrently produced  $\text{O}_3$  using 185 and 254 nm light (referred to as the OFR185 method), or OH production from photolysis of injected (externally produced)  $\text{O}_3$  using 254 nm light (referred to as the OFR254 method; Peng et al., 2015a).  $\text{O}_3$  and  $\text{NO}_3$  oxidation were also investigated and will be the subject of a future manuscript.

For both methods, UV light was produced using two low-pressure mercury lamps (BHK, Inc., model no. 82-9304-03) mounted inside and on the upper part of the flow reactor. The lamps have discrete emission wavelengths of 185 and 254 nm. The following reactions produce the OH radicals:



In the OFR185 method, OH was produced by H<sub>2</sub>O photolysis (R1) and also by O<sub>3</sub> photolysis (R4-5), as O<sub>3</sub> was formed in the reactor from O<sub>2</sub> photolysis (R2-3). In the OFR254 method, the mercury lamps were mounted inside Teflon-coated quartz sheaths, which blocked transmission of 185 nm light into the OFR, and only (R4-5) produced OH. Note that both wavelengths (185 and 254 nm) may initiate chemistry not normally occurring in the troposphere, and O(<sup>2</sup>P) and O(<sup>4</sup>D) are also present in the reactor at elevated concentrations. However, under the OFR conditions of our study neither of those non-OH reactants is a competitive reaction pathway (Peng et al., 2015b). O<sub>3</sub> oxidation, on the other hand, can be competitive in the OH oxidation experiments under certain conditions. According to Fig. 5 of Peng et al. (Peng et al., 2015b), O<sub>3</sub> in the OFR185 method during this study likely contributed only a minor (<20%) role in the oxidation of a few biogenic VOCs with largest k<sub>O<sub>3</sub></sub>/k<sub>OH</sub> ratios, and only at the lowest OH exposures (OH<sub>exp</sub>) equivalent to several hours of aging. With the OFR254 method though, the ratio of O<sub>3</sub> exposure to OH<sub>exp</sub> was as high as 10<sup>6</sup> for the lowest OH<sub>exp</sub> in this study, meaning O<sub>3</sub> may have played a substantial role in the initial oxidation of a small number of biogenic VOCs under those conditions. Still, the relative importance of O<sub>3</sub> vs. OH oxidation in the OFR was over an order of magnitude lower than under typical daily average atmospheric conditions (Peng et al., 2015b).

The OH exposure was stepped over a range of exposures by adjusting the mercury lamp intensities using programmable computer controls. A key parameter for interpreting the flow reactor aging was the total oxidant exposure, or oxidant concentration integrated over time, experienced by the sampled air. OH<sub>exp</sub> for the OFR185 method was estimated in part based on a model-derived equation, which uses measurements of ambient water vapor concentration, O<sub>3</sub> produced in the reactor, and estimated external OH reactivity (OHR<sub>ext</sub>) as equation parameters (Li et al., 2015). To provide the best estimate of OH<sub>exp</sub> for this study, the output OH<sub>exp</sub> from the model was divided by a factor of two (which is within the estimated model uncertainty of a factor of three) in order to bring it into better agreement with VOC decay rates measured during this campaign (Sect. 3.2). OH<sub>exp</sub> for the OFR254 method was calculated from a different model-derived equation, using OHR<sub>ext</sub> and a measurement of the amount of O<sub>3</sub> consumed as equation parameters (Peng et al., 2015a), and was also divided by a factor of two. For both methods, OH<sub>exp</sub> was converted to eq. days of atmospheric aging by dividing by a 24 h average atmospheric concentration of 1.5 × 10<sup>6</sup> molec cm<sup>-3</sup> OH (Mao et al., 2009). All usage of hours/days of aging in this work refers to eq. ages calculated in this manner.

Oxidant exposure is not the only factor that determines aerosol chemistry. NO<sub>x</sub> concentrations have been shown to affect oxidation products and aerosol yields in chamber studies, especially due to the

competition of NO and HO<sub>2</sub>/RO<sub>2</sub> to react with the RO<sub>2</sub> radicals formed during oxidation (e.g., Ng et al., 2007; Lim and Ziemann, 2009). In all OH oxidation experiments in the reactor, ambient NO<sub>x</sub> was rapidly oxidized to HNO<sub>2</sub> in as little as a couple of seconds at the highest OH concentrations, while photolysis of HNO<sub>2</sub> back to NO<sub>x</sub> was too slow to compete with oxidation (Li et al., 2015). Thus, the OH flow reactor experiments were assumed to occur under RO<sub>2</sub>+HO<sub>2</sub> conditions.

### 2.3 Sampling Strategy and Measurements

An important advantage of the OFR technique is that the oxidant concentration inside the reactor can be rapidly and consistently controlled to achieve any desired amount of oxidation from hours up to many weeks of eq. atmospheric age. Stepping through a repeating cycle of several oxidant concentrations from no added OH to several weeks of eq. aging allowed continuous investigation of SOA formation as a function of this age. The time needed to complete one cycle was kept as short as possible (~2 h), limited by the number of steps and reactor residence time). This allows SOA formation. Organic aerosols (OA) make up a substantial fraction of submicron aerosols (Murphy et al., 2006; Zhang et al., 2007; Jimenez et al., 2009). OA is composed of thousands of different molecules, of which only a small fraction has been speciated (Goldstein and Galbally, 2007). OA can be emitted directly in the particle phase as primary OA (POA), or it can be formed as secondary OA (SOA) through gas-to-particle conversion. During gas-phase SOA formation, an oxidant (mainly OH, O<sub>3</sub>, or NO<sub>3</sub>) reacts with organic gases to produce either less-volatile functionalized products (e.g., reacting to add a hydroxyl group) or more-volatile fragmented products (e.g., breaking C-C bonds to produce smaller molecules). If the reaction products have sufficiently lower volatility, they can then partition into the particle phase to form SOA (Pankow, 1994; Donahue et al., 2006). In addition to gas-phase oxidation pathways, SOA formation can result from aqueous chemistry within aerosol water or in cloud droplets (e.g., Lim et al., 2010; Ervens et al., 2011; Ervens, 2015) or heterogeneous uptake reactions (e.g., Surratt et al., 2010). Oxidative aging of gases and particles continues until deposition occurs (or CO<sub>2</sub> is produced). The complexity of OA chemistry arises from this intricate mix of multiphase-multigenerational reaction pathways and physicochemical processes involving thousands of molecules.

Much progress has been made in the past decade towards identifying and quantifying the sources, formation, and aging mechanisms of SOA. Aerosol models using traditional (pre-2007) aerosol yields for volatile organic compounds (VOCs) from chamber studies generally underpredict SOA mass by a factor of 10 in urban areas (Volkamer et al., 2006; Hodzic et al., 2010; Hayes et al., 2015). More recent models

are able to better predict SOA mass in urban areas by using higher VOC yields and adding previously ignored semivolatile and intermediate volatility organic compounds (S/IVOCs; Hodzic et al., 2010; Hayes et al., 2015). Model comparisons for biogenically-dominated areas have not shown such systematic underpredictions even when using older models (e.g., Tunved et al., 2006; Chen et al., 2009; Hodzic et al., 2009; Slowik et al., 2010). Recent measurements of the oxidation of biomass burning emissions, vehicle exhaust, and urban air have also found S/IVOCs to be important contributors to SOA formation (Grieshop et al., 2009; Miracolo et al., 2010; Zhao et al., 2014), building on the ideas of Robinson, et al. (2007). However, model parameterizations of SOA formation from S/IVOCs are based on large extrapolations and are still uncertain. The recent AeroCom intercomparison of 31 global OA models showed large variability between models and low temporal correlations between models and measurements (Tsigaridis et al., 2014). Their work suggests that current model parameterizations of SOA formation, transport, and removal processes are inadequate.

SOA formation has traditionally been studied in large environmental “smog” chambers. These chamber experiments have provided the SOA yields for models, but recent evidence shows that chamber experiments are affected by large losses of semivolatile gases to chamber walls (Matsunaga and Ziemann, 2010; Zhang et al., 2014; Krechmer et al., 2015) in addition to well-known particle wall losses (Pierce et al., 2008). This is especially true at long (>1 day) residence times, making it difficult to study SOA formation and aging on longer time scales. Also, while chamber experiments have been performed using emissions from mesocosm (e.g., whole tree) systems in the laboratory (e.g., Wyche et al., 2014), it is difficult to perform field experiments with ambient air in chambers (Tanaka et al., 2003). To explore the sources of SOA on a rapid time scale and with a wide range of oxidant exposures, a variety of oxidation flow reactors (OFR) have been developed (Kang et al., 2007; George et al., 2008; Smith et al., 2009; Keller and Bartsch, 2012). OFRs employ higher oxidant concentrations than chambers while having a short residence time with reduced wall contact. This allows hours to months of equivalent (eq.) atmospheric aging, and the same experimental system can be used in both laboratory and field experiments.

Previous experiments have shown SOA yields from various precursor gases oxidized in an OFR to be similar to yields from large environmental chambers (Kang et al., 2007, 2011; Lambe et al., 2011b, 2015). OFRs have also been used to investigate SOA formation from pollution source emissions containing complex mixtures of precursors such as controlled biomass burning (Ortega et al., 2013; Bruns et al., 2015) and vehicular emissions in a tunnel (Tkacik et al., 2014). Ortega et al. (2015) pioneered the use of

an OFR to study SOA formation from ambient air in an urban study in the Los Angeles area. Bruns et al. (2015) found that for a wood combustion system, the amount of SOA formed in an OFR compared to a large chamber agreed reasonably well. Tkacik et al. (2014) and Ortega et al. (2013) showed substantially more SOA formation than could be explained from speciated VOCs. Despite relying on SOA yields measured in large chambers, which can be affected by the aforementioned wall losses of semivolatile gases, these results suggest that S/IVOCs contribute to SOA formation in biomass burning plumes and vehicle exhaust.

In this study, we used an OFR to expose ambient air to variable levels of OH in a ponderosa pine forest during the BEACHON-RoMBAS campaign. We extensively characterized both the gas and particle phase to investigate the formation and aging of SOA. Changes in aerosol formation with gas precursor concentrations, time of day, and OH exposure were explored. The fate of condensable organic gases in the OFR was modeled. This model was used to estimate how much SOA formation was missed in the OFR due to gas-phase wall losses, excessive OH reaction that led to gas-phase fragmentation prior to condensation, and inadequate time/particle surface area for condensation. The SOA mass produced via oxidation was compared to the amount of SOA predicted based on literature yields of measured VOCs. The role of S/IVOCs in SOA formation in a forest was also explored. These results are discussed in the context of improving our knowledge of SOA sources and formation processes in a biogenic-dominated environment.

## **2 Experimental Methods**

### **2.1 BEACHON-RoMBAS Campaign**

The BEACHON-RoMBAS field campaign (Bio-hydro-atmosphere interactions of Energy, Aerosols, Carbon, H<sub>2</sub>O, Organics & Nitrogen – Rocky Mountain Biogenic Aerosol Study; <http://cires.colorado.edu/jimenez-group/wiki/index.php/BEACHON-RoMBAS>) took place at the Manitou Experimental Forest Observatory near Woodland Park, Colorado, in July–August 2011 (39.10° N, 105.10° W; 2370 m elevation). It was a collaboration of 27 institutions from the United States and Europe, focused on understanding primary and secondary biogenic aerosol emissions, formation and processing. An overview of atmospheric chemistry research at the Manitou Experimental Forest Observatory, including the BEACHON-RoMBAS campaign, has been previously published (Ortega et al., 2014).

The sampling site was located in a ponderosa pine forest in a mountain valley. VOC concentrations were characterized by high 2-methyl-3-buten-2-ol (MBO) during the daytime and monoterpenes (MT) during the nighttime. VOCs at this site have been described in detail for previous campaigns during July–September 2008 (Kim et al., 2010) and August–September 2010 (Kaser et al., 2013a, 2013b), while Fry et al. (2013) discussed diurnal cycles of select biogenic and anthropogenic VOCs during this campaign. The diurnal cycle of the concentration of MBO+isoprene (detected as the same product ion in the proton transfer reaction time-of-flight mass spectrometer; PTR-TOF-MS) measured at an above-canopy 25 m inlet ranged from about 1.5 ppb during the day to 0.3 ppb at night, while MT concentrations were on average 0.1 ppb during the day and 0.5 ppb at night. The relative ratio of isoprene/(MBO + isoprene) at this field site was estimated using a combination of GC-MS, PTR-TOF-MS, and whole air sample measurements during summer 2010 (Kaser et al., 2013a) and using NO<sup>+</sup> ionization mass spectrometry during the BEACHON-RoMBAS campaign (Karl et al., 2012) to be approximately 20%. Isoprene concentrations are calculated in this study using that approximation, which gives values typically <300 ppt. While largely dominated by biogenic emissions, the site receives some airflow from the front range urban areas (Denver metropolitan area and Colorado Springs) on most days, as evidenced by moderate increases in NO<sub>x</sub>, CO, and anthropogenic VOCs during late afternoon and into the evening (Fry et al., 2013; Ortega et al., 2014; Chan et al., 2016).

## **2.2 Oxidation flow reactor**

The Potential Aerosol Mass (PAM) oxidation flow reactor (hereafter flow reactor or OFR) is a cylindrical tube 45.7 cm long and 19.7 cm ID with a volume of approximately 13 liters, previously described elsewhere (Kang et al., 2007, 2011; Lambe et al., 2011a; Ortega et al., 2013, 2015). Ambient air was sampled through the reactor with a residence time of 2–4 min (3.5–6.5 lpm total flow rate), achieving oxidant exposures of hours to months of eq. atmospheric aging. The 14 cm diameter inlet plate was removed from the intake end of the OFR to reduce possible losses of semivolatile SOA precursors to the inlet plate inferred in a previous study (Ortega et al., 2013) and to reduce the width of the residence time distribution in the reactor (Ortega et al., 2015). Air was sampled into the reactor through this 14 cm diameter opening, which was covered with a coarse-grid mesh screen to reduce turbulence in the reactor and prevent insects and debris from entering the reactor. The mesh was coated with an inert silicon coating (Sulfinert by SilcoTek, Bellefonte, PA) to minimize gas and particle losses. OH radicals in the OFR were produced inside the reactor through one of two methods: OH production from photolysis of ambient H<sub>2</sub>O, O<sub>2</sub>, and concurrently produced O<sub>3</sub> using 185 and 254 nm light (referred to as the

OFR185 method), or OH production from photolysis of injected (externally produced) O<sub>3</sub> using 254 nm light (referred to as the OFR254 method; Peng et al., 2015a). O<sub>3</sub> and NO<sub>3</sub> oxidation were also investigated and will be the subject of a future manuscript.

For both methods, UV light was produced using two low-pressure mercury lamps (BHK, Inc., model no. 82-9304-03) mounted inside and on the upper part of the flow reactor. The lamps have discrete emission wavelengths of 185 and 254 nm. The following reactions produce the OH radicals:



In the OFR185 method, OH was produced by H<sub>2</sub>O photolysis (R1) and also by O<sub>3</sub> photolysis (R4-5), as O<sub>3</sub> was formed in the reactor from O<sub>2</sub> photolysis (R2-3). In the OFR254 method, the mercury lamps were mounted inside Teflon-coated quartz sheaths, which blocked transmission of 185 nm light into the OFR, and only (R4-5) produced OH by photolysis of injected O<sub>3</sub>. Following the terminology introduced by Peng et al. (2015a), the method used in this work can be referred to as OFR254-70, signifying that typically 70 ppm of O<sub>3</sub> was injected when using the OFR254 method. Note that both wavelengths (185 and 254 nm) may initiate chemistry not normally occurring in the troposphere, and O(^3P) and O(^1D) are also present in the reactor at elevated concentrations. However, under the OFR conditions of our study neither of those non-OH reactants is a competitive reaction pathway (Peng et al., 2015b). O<sub>3</sub> oxidation, on the other hand, can be competitive in the OH oxidation experiments under certain conditions. According to Fig. 5 of Peng et al. (2015b), O<sub>3</sub> in the OFR185 method during this study likely contributed only a minor (< 20%) role in the oxidation of a few biogenic VOCs with the largest  $k_{\text{O}_3}/k_{\text{OH}}$  ratios (e.g.,  $\beta$ -caryophyllene,  $\alpha$ -terpinene,  $\alpha$ -humulene), and only at the lowest OH exposures (OH<sub>exp</sub>) equivalent to several hours of aging. With the OFR254-70 method though, the ratio of O<sub>3</sub> exposure to OH<sub>exp</sub> was as high as 10<sup>6</sup> for the lowest OH<sub>exp</sub> in this study. Under these conditions, O<sub>3</sub> may have played a substantial role in the initial oxidation of a larger number of species of biogenic VOCs (e.g., reacting with ~100% of  $\beta$ -caryophyllene and  $\alpha$ -terpinene, ~60% of  $\alpha$ -pinene and limonene, ~20% of 3-carene and  $\beta$ -pinene, 10% of isoprene). Still, the relative importance of O<sub>3</sub> vs. OH oxidation in the OFR was over an order-of-magnitude lower than under typical daily-average atmospheric conditions (Peng et al., 2015b).

The OH exposure was stepped over a range of exposures by adjusting the mercury lamp intensities using programmable computer controls. A key parameter for interpreting the flow reactor aging was the total oxidant exposure, or oxidant concentration integrated over time, experienced by the sampled air.  $OH_{exp}$  for the OFR185 method was estimated in part based on a model-derived equation, which uses measurements of ambient water vapor concentration,  $O_3$  produced in the reactor, and estimated external OH reactivity ( $OHR_{ext}$ ) as equation parameters (Li et al., 2015).  $OHR_{ext}$  is the OH reactivity from ambient gases such as VOCs, CO,  $SO_2$ , and is accounted for separately from the “internal OH reactivity ( $OHR_{int}$ )” from species such as  $HO_x/H_2O_2/O_3$  that are greatly enhanced by this reactor. For this study,  $OH_{exp}$  was calculated using an estimated  $OHR_{ext} = 10\ s^{-1}$ , based on measurements at the same field site and season during previous campaigns (Kim et al., 2013; Nakashima et al., 2014). To provide the best estimate of  $OH_{exp}$  for this study, the output  $OH_{exp}$  from the model was divided by a factor of two (which is within the estimated model uncertainty of a factor of three) in order to bring it into better agreement with VOC decay rates measured during this campaign (Sect. 3.2).  $OH_{exp}$  for the OFR254-70 method was calculated from a different model-derived equation, using  $OHR_{ext}$  and a measurement of the amount of  $O_3$  consumed as equation parameters (Peng et al., 2015a), and was also divided by a factor of two. For both methods,  $OH_{exp}$  was converted to eq. days of atmospheric aging by dividing by a 24-h-average atmospheric concentration of  $1.5 \times 10^6\ molec\ cm^{-3}\ OH$  (Mao et al., 2009). All usage of hours/days of aging in this work refers to eq. ages calculated in this manner.

Oxidant exposure is not the only factor that determines aerosol chemistry.  $NO_x$  concentrations have been shown to affect oxidation products and aerosol yields in chamber studies, especially due to the competition of NO and  $HO_2/RO_2$  to react with the  $RO_2$  radicals formed during oxidation (e.g., Ng et al., 2007; Lim and Ziemann, 2009). In all OH oxidation experiments in the reactor, ambient  $NO_x$  was rapidly oxidized to  $HNO_3$  in as little as a couple of seconds at the highest OH concentrations, while photolysis of  $HNO_3$  back to  $NO_x$  was too slow to compete with oxidation (Li et al., 2015). Thus, the OH flow reactor experiments were assumed to occur under  $RO_2+HO_2$  conditions.

### **2.3 Sampling Strategy and Measurements**

An important advantage of the OFR technique is that the oxidant concentration inside the reactor can be rapidly and consistently controlled to achieve any desired amount of oxidation from hours up to many weeks of eq. atmospheric age. Stepping through a repeating cycle of several oxidant concentrations from no added OH to several weeks of eq. aging allowed continuous investigation of SOA



formation as a function of this age. The time needed to complete one cycle was kept as short as possible (~2 h), limited by the number of steps and reactor residence time). This allows the potential of SOA formation from OH oxidation to be studied over the whole range of exposures as functions of time of day and the concentration of precursors that change on that time scale.

In typical OFR185 and OFR254 exposure cycles during BEACHON-RoMBAS, the UV lamps inside the reactor were stepped through six 20-min-long settings of varying lamp intensities for a combined cycle length of 2 h, from both lamps off to both lamps at full intensity. Oxidant and product concentrations in the reactor were allowed 15 min (~4–7 reactor residence times) to reach a steady state at each light setting (mainly to allow the OFR to flush, as the lamp UV intensity stabilizes within seconds) before being sampled for the last 5 min of each cycle. Immediately after this 5 min sampling period, the lamp intensity was changed to prepare for the next oxidant concentration in the cycle. During the 15 min in which the OFR was not being sampled, ambient aerosols were sampled directly, through a thermodenuder (Huffman et al., 2008), and directly again, for 5 min each. In this method, all perturbation measurements (OFR or thermodenuder) are bracketed by unperturbed ambient measurements. The ambient AMS sampling has also been described in Fry et al. (Fry et al., 2013).

In typical OFR185 and OFR254-70 exposure cycles during BEACHON-RoMBAS, the UV lamps inside the reactor were stepped through six 20-min-long settings of varying lamp intensities for a combined cycle length of 2 h, from both lamps off to both lamps at full intensity. Oxidant and product concentrations in the reactor were allowed 15 min (~4–7 reactor residence times) to reach a steady state at each light setting (mainly to allow the OFR to flush, as the lamp UV intensity stabilizes within seconds) before being sampled for the last 5 min of each cycle. Immediately after this 5 min sampling period, the lamp intensity was changed to prepare for the next oxidant concentration in the cycle. During the 15 min in which the OFR was not being sampled, ambient aerosols were sampled directly, through a thermodenuder (Huffman et al., 2008), and directly again, for 5 min each. In this method, all perturbation measurements (OFR or thermodenuder) are bracketed by unperturbed ambient measurements. The ambient AMS sampling has also been described in Fry et al. (2013).

Ambient aerosols and those after oxidation in the OFR were measured using a TSI 3936 Scanning Mobility Particle Sizer (SMPS) and an Aerodyne High-Resolution Time-of-Flight Aerosol Mass Spectrometer (HR-ToF-AMS, hereafter AMS; DeCarlo et al., 2006) (HR-ToF-AMS, hereafter AMS; DeCarlo et al., 2006). A system of automated valves (Aerodyne AutoValve), controlled by a custom

410 automation program written in Labview (National Instruments, Inc.), was used to multiplex the AMS and  
411 SMPS to alternate between measuring ambient air and air oxidized in the OFR (or heated by the  
412 thermodenuder). The flow rate through the OFR and all sampling lines was kept constant at all times by  
413 using make-up flows when not sampling from each of the inlet lines or reactors. The same custom  
414 software was used to control and schedule the UV lamp cycling as well as record [relative humidity \(RH<sub>r</sub>\)](#),  
415 temperature and output O<sub>3</sub> concentrations in the OFR. Sampled air was dried to <30% relative humidity  
416 upstream of the SMPS and AMS using a Nafion membrane drier (Perma Pure, LLC; MD-110-24S-4). For  
417 OH<sub>exp</sub> calculations in the OFR, O<sub>3</sub> was measured using a 2B Technologies Model 205 Monitor and  
418 ambient water vapor was measured using a Vaisala HM70 probe. A schematic of the experimental setup  
419 is shown in Fig. 1. The SMPS consisted of a TSI 3080 Electrostatic Classifier, a 3081 long Differential  
420 Mobility Analyzer (DMA) column, and a 3010 Condensation Particle Counter (CPC). It was operated with  
421 sheath and aerosol flow rates of 3.0 and 0.3 lpm, respectively, with a TSI Kr-85 neutralizer and no  
422 impactor. The SMPS sampled the range of 14–626 nm mobility diameters, with one 4 min scan every five  
423 minutes, and synchronized with OFR and AMS sampling.

424 The AMS data used in this analysis was recorded as 2.5 min average mass spectra in “V-mode”.  
425 Instrument sensitivity was calibrated every 3 days with 400 nm monodisperse, dried, ammonium nitrate  
426 particles. The gas-phase N<sub>2</sub> signal, commonly referred to as the airbeam, was used to track changes in  
427 sensitivity between calibrations. The flow rate of air into the AMS was calibrated in the field before  
428 measurements began. A fluorocarbon standard was leaked into the ionization chamber in order to  
429 provide high *m/z* background peaks for improved *m/z* calibration up to approximately *m/z* 300 (~~DeCarlo~~  
430 [et al., 2006](#))([DeCarlo et al., 2006](#)). Corrections were applied to account for gas-phase CO<sub>2</sub> interference  
431 and water fragmentation patterns using daily aerosol-free background filters and continuous ambient  
432 CO<sub>2</sub> measurements. AMS and SMPS concentrations and SMPS size distributions were corrected to  
433 account for diffusion losses to the walls of the inlet sampling lines, described in Sect. S1. AMS data was  
434 processed using a collection efficiency (CE) of 1, detailed in Sect. S2 and based on a comparison of the  
435 AMS and SMPS measurements of ambient aerosol volume (Fig. S2), OFR-oxidized aerosol volume and  
436 [change in volume added](#)(Fig. S3), and total volume enhancement as a function of photochemical age  
437 (Fig. S4). AMS concentrations were also corrected for losses of small particles through the aerodynamic  
438 lens and to the OFR walls. Details for these corrections can be found in the Sect. S3. AMS data is  
439 reported at 293 K and 0.76 atm (typical ambient values at this research site). The time series, diurnal

cycles, and average size distributions of ambient OA, sulfate (SO<sub>4</sub>), nitrate (NO<sub>3</sub>), and ammonium (NH<sub>4</sub>) aerosol mass concentrations have been previously published (Ortega et al., 2014).

Field Code Changed

While both OH generation methods detailed above were used during the campaign, the analysis in this paper will mainly focus on the OFR185 mode for several reasons. ~~Determination~~The analysis of SOA mass formed vs. predicted in Sect. 3.6 was done using the age range that produced the maximum SOA formation (0.4–1.5 eq. days). However, determination of ages below approximately 1 eq. day using the OFR254-70 method was limited by the ability to accurately measure the amount of injected O<sub>3</sub> that was consumed in the reactor. The variability of the measurement of the initial concentration of O<sub>3</sub> inside the reactor was approximately ±2 ppm (when reaching a total of about 70 ppm of O<sub>3</sub>) due to variations in the mixing of injected O<sub>3</sub> with ambient air sampled into the OFR, especially when sampling in windy conditions. The model used to estimate eq. age for the OFR254-70 method estimated that 2 ppm of photolyzed O<sub>3</sub> produced an age of 0.5 eq. days, so that was the effective lower limit of detection of age with the OFR254-70 method under the experimental conditions used during this campaign. Measuring the decay of a compound that reacts relatively quickly with OH but does not react with O<sub>3</sub> could allow for better OH<sub>exp</sub> quantification at low ages for OFR254-70. Also, the OFR254 method requires high concentrations of O<sub>3</sub> (up to 70 ppm in this study) to be injected in order to reach high ages. As discussed above, O<sub>3</sub> may play a role in the oxidation of some VOCs in the OFR254-70 method, while the role of O<sub>3</sub> oxidation in OFR185 is minor. This could further complicate the interpretation of the results of OH oxidation for the lower measurable ages (hours–days) when using OFR254-70. In addition, the temporal data coverage of OFR185 oxidation (23 July–4 August, 9–14 and 24–26 August) was much greater than OFR254 ~~(17–20 and 28–30 August)~~(17–20 and 28–30 August). This short time period of OFR254-70 measurements combined with the difficulty of sampling at short eq. ages with this particular experimental setup meant that there were few OFR254-70 measurements relative to OFR185 measurements for the analysis in Sect. 3.6. Also, there were no concurrent measurements of S/IVOC concentrations and SOA formation using OFR254-70 available for the analysis in Sect. 3.6.2. If these analyses would have been performed on a combined dataset using both OH production methods, the results would be driven almost completely by OFR185 measurements. For these reasons, the analyses were performed and conclusions reached using only OFR185 measurements. Regardless, we document below that both OH oxidation methods gave consistent results for SOA production over the range of overlapping ages (~1–30 eq. days) used during this campaign (Sect. 3.4). ~~For these reasons OFR254 data~~

Formatted: Font: Bold, Font color: Blue

was not included in the rest of the analyses. The time series of OFR185 and OFR254-70 OA measurements are shown compared to ambient OA, MT, and MTS/IVOCs in Fig. S7.

This work focuses on the changes in OA mass due to SOA formation and OA aging as a result of exposure of ambient air to OH. OA enhancement is defined here as the difference between OA mass measured by the AMS after oxidation in the OFR and the average of the two ambient OA concentrations measured just before and after the oxidation data point. If SOA was produced in the reactor, the OA enhancement was positive; if oxidation led to a net loss of OA mass, then the OA enhancement was negative. As discussed in the results below, SOA formation in the OFR correlated with ambient precursor gas concentrations. If the ambient concentration of those gases was close to zero, then no SOA formation was observed (e.g., Fig 8). Therefore, any SOA formation from, e.g., gases desorbing from the OFR walls, was negligible.

Measurements of VOCs in ambient air and after OFR oxidation were made using a high-resolution PTR-TOF-MS (Kaser et al., 2013b). This technique can separate and identify isobaric compounds with a mass resolution ( $m/\Delta m$ ) of up to  $\sim 4000$ . This allowed for tracking of the depletion of primary biogenic species in the OFR as well as the production of more oxygenated products. Signals from isotopes, internal standards, and possible artifacts (e.g., saturated hydrocarbons that correlate with  $O_3$  concentration in the reactor) were removed from the analysis. When calculating predicted depletion for  $\alpha$ -pinene,  $\beta$ -pinene, 3-carene, toluene, *p*-cymene, methanol, and sesquiterpenes (SQT; using longifolene as a representative compound) in the following analysis, the rate constants used were:  $k_{OH} = 5.3 \times 10^{-11}$ ,  $7.7 \times 10^{-11}$ ,  $8.7 \times 10^{-11}$ ,  $5.5 \times 10^{-12}$ ,  $1.5 \times 10^{-11}$ ,  $9.1 \times 10^{-13}$ , and  $4.8 \times 10^{-11} \text{ cm}^3 \text{ molec}^{-1} \text{ s}^{-1}$ , respectively (Calvert et al., 2002; Atkinson and Arey, 2003; Alarcón et al., 2014). As an approximation of previous measurements at this site, MT are assumed to be an equal mix of  $\alpha$ -pinene,  $\beta$ -pinene, and 3-carene for this analysis (Kim et al., 2010; Ortega et al., 2014). Likewise, the ratio of toluene:*p*-cymene used in calculations was taken from Kaser et al. (2013b) to be 74:26 (Kaser et al., 2013a). This technique can separate and identify isobaric compounds with a mass resolution ( $m/\Delta m$ ) of up to  $\sim 4000$ . This allowed for tracking of the depletion of primary biogenic species in the OFR as well as the production of more oxygenated products. Signals from isotopes, internal standards, and possible artifacts (e.g., saturated hydrocarbons that correlate with  $O_3$  concentration in the reactor) were removed from the analysis. When calculating predicted depletion for  $\alpha$ -pinene,  $\beta$ -pinene, 3-carene, toluene, *p*-cymene, methanol, and sesquiterpenes (SQT; using longifolene as a representative compound) in the following analysis, the rate constants used were:  $k_{OH} = 5.3 \times 10^{-11}$ ,  $7.7 \times 10^{-11}$ ,  $8.7 \times 10^{-11}$ ,  $5.5 \times 10^{-12}$ ,  $1.5 \times 10^{-11}$ ,  $9.1 \times 10^{-13}$ , and  $4.8 \times 10^{-11} \text{ cm}^3 \text{ molec}^{-1}$

s<sup>-1</sup>, respectively (Calvert et al., 2002; Atkinson and Arey, 2003; Alarcón et al., 2014). As an approximation of previous measurements at this site, MT are assumed to be an equal mix of  $\alpha$ -pinene,  $\beta$ -pinene, and 3-carene for this analysis (Kim et al., 2010; Ortega et al., 2014). Likewise, the ratio of toluene:*p*-cymene used in calculations was taken from Kaser et al. (2013a) to be 74:26. Similar to the multiplexing scheme described above for particle sampling, a system of automated Teflon valves was used to alternate between measuring ambient air and air through the OFR, sampling from the OFR concurrently with the AMS+SMPS. PTR-TOF-MS measurements from the OFR were performed during 1-4 and 24-25 August, 2011, while using the OFR185 method. The analysis here focuses on two consecutive sampling cycles from 00:00–04:00 MDT (local time) on 3 August, 2011, when the concentration of MT was relatively high (0.8 ppbv) and the concentration of MBO+isoprene was relatively low (0.1 ppbv).

Ambient PTR-TOF-MS measurements are also used in this work to estimate how much SOA could form in the OFR. The continuous PTR-TOF-MS measurements during BEACHON-RoMBAS were made from an inlet at the top of a tower above the canopy at 25 m height, while the OFR was located on top of an instrument trailer within the canopy at approximately 4 m height. In-canopy gradients were accounted for by comparing the PTR-TOF-MS measurements at 25 m with measurements made through the OFR in the absence of oxidant and with measurements from a different nearby inlet at 1 m height. It was observed that the concentrations of MT, SQT, MBO+isoprene, and toluene+*p*-cymene were approximately 1.9, 5.9, 1.4, and 1.2 times higher in the canopy than at 25 m, respectively (discussed in Sect. S4). All analyses in this work were done using estimated in-canopy concentrations, which were inferred by applying these empirical relationships to the continuous 25 m inlet measurements. This scaling technique has been used before, producing similar results when applied to measurements during the summer 2010 BEACHON-ROCS campaign at the same field location (Kim et al., 2013; Wolfe et al., 2014). Ambient PTR-TOF-MS measurements are also used in this work to estimate how much SOA could form in the OFR. The continuous PTR-TOF-MS measurements during BEACHON-RoMBAS were made from an inlet at the top of a tower above the canopy at 25 m height, while the OFR was located on top of an instrument trailer within the canopy at approximately 4 m height. In-canopy gradients were accounted for by comparing the PTR-TOF-MS measurements at 25 m with measurements made through the OFR in the absence of oxidant and with measurements from a different nearby inlet at 1 m height. It was observed that the concentrations of MT, SQT, MBO+isoprene, and toluene+*p*-cymene were approximately 1.9, 5.9, 1.4, and 1.2 times higher in the canopy than at 25 m, respectively (discussed in Sect. S4). All analyses in this work were done using estimated in-canopy concentrations, which were

inferred by applying these empirical relationships to the continuous 25 m inlet measurements. This scaling technique has been used before, producing similar results when applied to measurements during the summer 2010 BEACHON-ROCS campaign at the same field location (Kim et al., 2013; Wolfe et al., 2014).

Ambient SO<sub>2</sub> concentrations were measured using a Thermo Environmental Model 43C-TLE analyzer. Data were reported as 5 min averages from 6 different heights on a tower up to 25.1 m. We used only data measured at the 5 m height, to best match the height of the OFR on top of the trailer. The SO<sub>2</sub> instrument was automatically zeroed every 6 h, using scrubbed zero grade air. It was calibrated by a standard addition of 3 sccm of a 14 ppmv SO<sub>2</sub> in N<sub>2</sub> standard (Scott-Marrin) into the 3 slpm sample flow.

A novel thermal desorption electron impact mass spectrometer (TD-EIMS) was used to measure ambient concentrations of ensemble S/IVOCs with volatilities in the range of effective saturation vapor concentrations (C\*) of 10<sup>-1</sup>-10<sup>7</sup> μg/m<sup>3</sup>. This method involved cryogenic collection of organic gases, temperature-programmed desorption into ultra-high-purity (UHP) helium, and measurement with a high-resolution time-of-flight mass spectrometer (Cross et al., 2013; Hunter et al., 2015). (Cross et al., 2013; Hunter et al., 2016). The TD-EIMS provided a time series of the gas-phase organic mass and composition in each volatility bin.

Formatted: Font: Italic

### 3 Results and Discussion

#### 3.1 OFR operation

Typical OFR operation using the OFR185 method is illustrated in Fig. 2, by an example of the evolution of OA and SO<sub>4</sub> aerosol mass concentrations as OH concentration was cycled through the range of eq. ages. As age increased over the first few lamp settings, OA mass increased due to production and condensation of low volatility species from the oxidation of gas-phase SOA precursors. SO<sub>4</sub> mass remained nearly the same as in ambient air for these lower ages. The increase of SOA mass at lower ages compared to SO<sub>4</sub> is thought to be due to the different rate constants for reaction of OH. The rates with biogenic VOCs, e.g.,  $k_{OH} = 5.3 \times 10^{-11} \text{ cm}^3 \text{ molec}^{-1} \text{ s}^{-1}$  for  $\alpha$ -pinene (Atkinson and Arey, 2003), are generally much faster than the reaction of OH with SO<sub>2</sub>, where  $k_{OH} = 9.49 \times 10^{-13} \text{ cm}^3 \text{ molec}^{-1} \text{ s}^{-1}$  (Sander et al., 2011). As the eq. age continued to increase, OA mass enhancement decreased, eventually resulting in net OA loss, while SO<sub>4</sub> mass continued to increase. This high eq. age led to lack of formation of SOA as well as heterogeneous oxidation of the preexisting OA, leading to fragmentation and

evaporation (Ortega et al., 2015). As expected,  $\text{SO}_4$  aerosol was not consumed in this way by excess

$\text{OH}_{\text{exp}}$

### 3.2 VOC enhancement/depletion vs eq. age

VOCs were measured before (in ambient air) and after OH oxidation in the OFR using a PTR-TOF MS. This showed which VOCs were being depleted, potentially to form SOA, as well as which products were being formed. Also, the decay of VOCs after oxidation provided a direct measurement for validation of the model-derived age estimates. Under typical operation, an OFR is used to study oxidation dominated by a single oxidant, similar to typical large chamber experiments. In the case of a field application (as in this study) the sample is a complex and time-varying mixture of ambient precursors that enter the OFR. Importantly, the  $\text{OH}:\text{O}_3:\text{NO}_3$  oxidant ratios produced within the OFR are generally not the same as the changing ambient ratios. Therefore SOA formation in the OFR does not, and is not meant to, reproduce in situ ambient SOA formation at each point in time. In other words, the OFR can be used as a tool to determine the amount of SOA from a single oxidant that would form upon oxidation of ambient gases (both identified and unidentified) at any time of day.

Typical OFR operation of OH oxidation using the OFR185 method is illustrated in Fig. 2, by an example of the evolution of OA and  $\text{SO}_4$  aerosol mass concentrations as OH concentration was cycled through the range of eq. ages. As age increased over the first few lamp settings, OA mass increased due to production and condensation of low volatility species from the oxidation of gas-phase SOA precursors.  $\text{SO}_4$  mass remained nearly the same as in ambient air for these lower ages. The increase of SOA mass at lower ages compared to  $\text{SO}_4$  is thought to be due to the different rate constants for reaction of OH. The rates with biogenic VOCs, e.g.,  $k_{\text{OH}} = 5.3 \times 10^{-11} \text{ cm}^3 \text{ molec}^{-1} \text{ s}^{-1}$  for  $\alpha$ -pinene (Atkinson and Arey, 2003), are generally much faster than the reaction of OH with  $\text{SO}_2$ , where  $k_{\text{OH}} = 9.49 \times 10^{-13} \text{ cm}^3 \text{ molec}^{-1} \text{ s}^{-1}$  (Sander et al., 2011). As the eq. age continued to increase, OA mass enhancement decreased, eventually resulting in net OA loss. These high ages led to a lack of formation of SOA as well as heterogeneous oxidation of the preexisting OA, leading to fragmentation and evaporation (Ortega et al., 2015). The amount of  $\text{SO}_4$  aerosol production increased with eq. age, and plateaued with no further production at ages above ~10 days. This behavior is consistent with theory, since  $\text{SO}_2$  has a lifetime of ~8 days with respect to oxidation by OH (Sander et al., 2011). Also, as expected,  $\text{SO}_4$  aerosol (and  $\text{H}_2\text{SO}_4$  gas) was not consumed by excess  $\text{OH}_{\text{exp}}$  in the same way as OA (and SOA precursor gases).

### 3.2 VOC enhancement/depletion vs eq. age

VOCs were measured before (in ambient air) and after OH oxidation in the OFR using a PTR-TOF-MS. This showed which VOCs were being depleted, potentially to form SOA, as well as which products were being formed. Also, the decay of VOCs after oxidation provided a direct measurement for validation of the model-derived age estimates. A number of likely compounds have been identified based on measurements from previous campaigns at the Manitou Experimental Forest Observatory site (Kim et al., 2010; Kaser et al., 2013a), as listed in Table 1. (Kim et al., 2010; Kaser et al., 2013b), as listed in Table 1.

For an overview of PTR-TOF-MS measurements, the difference mass spectrum and mass defect (exact mass minus nominal mass) plots for 4 eq. hours of aging during nighttime are shown in Fig. 3. The greatest absolute magnitude of depletion in oxidized air compared to ambient nighttime air was observed for MT. Depletion was also observed for toluene+*p*-cymene, MBO+isoprene, SQT, pinonaldehyde+caronaldehyde, and camphor+ $\alpha$ -pinene oxide. Notably, formation of nopinone was observed after 4 eq. hours of aging. OH oxidation also led to substantial production of several relatively small oxidation product molecules, including formaldehyde, acetaldehyde, formic acid, acetone, and acetic acid, which have been commonly observed in similar photooxidation experiments (e.g., Lee et al., 2006; Ortega et al., 2013)(e.g., Lee et al., 2006; Ortega et al., 2013). Many other unidentified molecules were observed to be produced in smaller concentrations as a result of OH oxidation in the flow reactor. A similar plot is shown for higher eq. age (7 days) in Fig. S9, for comparison to Fig. 3. At such a high age, species such as MT, SQT, and toluene+*p*-cymene were completely depleted, while many small oxidation products increased as much as 5-fold.

In general for all degrees of oxidation, molecules with higher positive mass defects (corresponding to more chemically reduced species such as hydrocarbons) were depleted. Conversely, molecules with lower mass defect (more oxygenated compounds) were formed. This trend is consistent with what would be expected from gas-phase or heterogeneous OH oxidation chemistry. Also, Fig. 3 shows that monoterpenes constituted the majority of VOCs measured by the PTR-TOF-MS that were depleted after oxidation, while other compounds associated with terpenoid emissions and/or oxidation products were consumed or produced in smaller concentrations.

The relative changes of each of the compounds discussed above are shown as a function of OH<sub>exp</sub> in Fig. 4. As previously discussed, nopinone is an example of a compound that increased in concentration at 4 hours eq. age, indicating that it was an oxidation product in the OFR. This signal showed net formation



at low ages (earlier than the peak of maximum SOA formation in the OFR) and eventually decreased to net loss at high exposures, as expected due to its reactivity with OH. Fig. 4 also shows the net decay of several other terpene-related species and the formation of smaller, more volatile oxidation products as OH<sub>exp</sub> increased. While the MBO+isoprene signal showed a substantial increase with increasing age, this is likely due to production of an isomeric interference, e.g., a fragment of an oxidation product.

An assessment of the ~~accuracy~~reasonableness of the model-derived OH<sub>exp</sub> (including the factor of two decrease discussed in Sect. 2.2) can be made by comparing the measured depletion of gases vs. expected depletion using published reaction rates with OH. This comparison is shown for an average speciated MT mixture, toluene+*p*-cymene, and methanol in Fig. 4. The MT and methanol signals decay slower than predicted, while the toluene+*p*-cymene signal decays slightly faster. ~~These results are consistent with the previous evaluation of the model-predicted OH<sub>exp</sub> for laboratory and field studies (Li et al., 2015). Determination of OH<sub>exp</sub> in the OFR is limited by many factors, including model uncertainties (Peng et al., 2015a)~~These results are consistent with the previous evaluation of the model-predicted OH<sub>exp</sub> for laboratory and field studies (Li et al., 2015). Determination of OH<sub>exp</sub> in the OFR is limited by many factors, including model uncertainties (Peng et al., 2015a), the true non-plug-flow residence time distribution in the OFR, the difficulty of measuring a difference of signals using the PTR-TOF-MS in a perturbed environment, the possibility of competing production of the measured compounds (e.g., methanol), interferences and/or false identification of measured signal (e.g., fragments or different species with the same elemental composition interfering with the measured ions), and uncertainty in the relative composition of the MT and toluene+*p*-cymene mixtures. Despite these uncertainties, the PTR-TOF-MS is clearly measuring formation and decay of compounds that react with OH on the time scale of several hours of photochemical age. This is strong evidence that the OFR can be used to study a wide range of atmospherically-relevant time scales.

### 3.3 Fate of condensable gases in an OFR

#### 3.3.1 Modeled Low-volatility organic compound (LVOC) Fate

In order to properly interpret SOA formation as a function of age in an OFR, the time scales of various competing processes need to be carefully considered in the context of the relative importance of those processes in the OFR vs the atmosphere. When organic gases are oxidized in the OFR, they can form LVOCs, a term used here to describe organic gases with volatilities that are low enough to (~~effectively~~) irreversibly condense onto particles or surfaces. In the atmosphere, the dominant fate of these LVOCs is

to condense onto aerosols, (lifetime of ~minutes), as dry and wet deposition of even fast-depositing species are generally slower sinks (Knote et al., 2015; Nguyen et al., 2015)(lifetime of ~hours; Farmer and Cohen, 2008; Knote et al., 2015; Nguyen et al., 2015). However, due to the different time scales, the LVOCs formed in the OFR can have other fates besides condensation onto aerosols. These include condensational loss to the walls of the OFR, further reaction with OH to produce either condensable or non-condensable gas-phase products, or exiting the reactor in the gas-phase (where they will almost entirely condense on the sampling tube walls, due to the large surface-area-to-volume ratio). If the LVOCs condense onto aerosols, then they are measured by the AMS+SMPS. However, if they are subject to one of the other three fates, then the AMS+SMPS measurements would underestimate the amount of SOA that would form in the atmosphere at the same level of OH exposure, and a. Similar to loss of gases to large Teflon chamber walls (e.g., Matsunaga and Ziemann, 2010), these other three fates are experimental limitations of the OFR technique that need to be corrected in order to relate OFR measurements to real atmospheric SOA formation processes. As mentioned above, this correction is needed-takes into account that dry deposition of such LVOCs is not competitive with condensation onto particles in the atmosphere (Knote et al., 2015; Nguyen et al., 2015). Note that this section pertains to gas-phase losses, while a correction for particle losses to the OFR walls was also included as described in Sect. S3. The need for an LVOC correction to OFR measurements has been suggested before (Lambe et al., 2011a, 2015), but to our knowledge this work is the first attempt to apply one.

Field Code Changed

In this analysis, we calculate approximate lifetimes of LVOCs for condensation onto aerosols ( $\tau_{aer}$ ), loss to the walls of the OFR ( $\tau_{wall}$ ), and reaction with OH ( $\tau_{OH}$ ) as a function of  $OH_{exp}$ . Some semivolatile species (SVOC) will also be produced. However, we focus on LVOCs for simplicity, and also based on the observation that most of the OA has low volatility at this site, according to thermal denuder measurements (Hunter et al., 2015), and consistent with measurements at other locations (Cappa and Jimenez, 2010; Lopez-Hilfiker et al., 2015).

Following Pirjola et al. (1999), the lifetime for LVOC condensation onto aerosols was calculated as

$$\tau_{aer} = \frac{1}{4\pi \cdot CS \cdot D} \quad (1)$$

with a diffusion coefficient  $D = 7 \times 10^{-6} \text{ m}^2 \text{ s}^{-1}$  representative of an oxidized organic molecule with a molecular weight of approximately  $200 \text{ g mol}^{-1}$  at the field site ambient pressure (Tang et al., 2015). CS is the “condensational sink”

$$CS = \int_0^{\infty} r \beta(r) N(r) dr \quad (2)$$

which is the integral of the first moment of the particle size distribution, where  $r$  is the particle radius. In this analysis, we calculate approximate lifetimes of LVOCs for condensation onto aerosols ( $\tau_{aer}$ ), loss to the walls of the OFR ( $\tau_{wall}$ ), and reaction with OH ( $\tau_{OH}$ ) as a function of  $OH_{exp}$ . Some semivolatile species (SVOC) will likely also be produced. However, we focus on irreversibly condensing LVOCs, both for simplicity and based on the observation that most of the OA has low volatility at this site, according to thermal denuder measurements (Hunter et al., 2016), and consistent with measurements at other locations (Cappa and Jimenez, 2010; Lopez-Hilfiker et al., 2016). If the low volatility of OA is a result of condensation of SVOC followed by fast particle-phase reactions to produce low-volatility species, then the distinction between LVOC and SVOC would be irrelevant for this analysis. The lifetimes of LVOCs against different processes are estimated as follows:

–  $\tau_{aer}$ : Following Pirjola et al. (1999), the lifetime for LVOC condensation onto aerosols was calculated as

$$\tau_{aer} = \frac{1}{4\pi \cdot CS \cdot D} \quad (1)$$

with a diffusion coefficient  $D = 7 \times 10^{-6} \text{ m}^2 \text{ s}^{-1}$  representative of an oxidized organic molecule with a molecular weight of approximately  $200 \text{ g mol}^{-1}$  at the field site ambient pressure (Tang et al., 2015).  $CS$  is the “condensational sink”

$$CS = \int_0^\infty r \beta(r) N(r) dr \quad (2)$$

which is the integral of the first moment of the particle size distribution, where  $r$  is the wet particle radius,  $N(r)$  is the particle number size distribution, and

$$\beta(r) = \frac{Kn+1}{0.377Kn+1+\frac{4}{3}\alpha^{-1}Kn^2+\frac{4}{3}\alpha^{-1}Kn} \quad (3)$$

is the Fuchs-Sutugin correction for gas diffusion to a particle surface in the transition regime, calculated using the sticking coefficient  $\alpha$  of the condensing species (Seinfeld and Pandis, 2006).  $CS$  was calculated using the average of the SMPS size distributions of ambient air entering the OFR and of air exiting the OFR after oxidation, as a best approximation of the actual  $CS$  experienced by LVOCs in the OFR. The correction  $\beta(r)$  is a function of the Knudsen number

$$Kn = \frac{\lambda_g}{r} \quad (4)$$

where  $\lambda_g$  is the mean free path of the condensing gas. Based on previous modeling and measurements, we assume  $\alpha = 1$  for LVOCs (Kulmala and Wagner, 2001; Julin et al., 2014; Krechmer et al., 2015). A sensitivity study on the values of  $D$ , the impact of deviations from  $\alpha = 1$ , and the choice of SMPS size distribution used to calculate  $CS$  is discussed below in Sect. 3.6.3.

–  $\tau_{wall}$ : Following McMurtry and Grosjean (1985), we estimate the first-order rate of LVOC loss to the walls of the OFR limited by eddy diffusion as

$$k_{wall} = \frac{1}{\tau_{wall}} = \frac{A}{V} \cdot \frac{2}{\pi} \cdot \sqrt{k_e D} \quad (5)$$

is the Fuchs-Sutugin correction for gas diffusion to a particle surface in the transition regime, calculated using the sticking coefficient  $\alpha$  of the condensing species (Seinfeld and Pandis, 2006). CS was calculated using the average of the size distributions of ambient air entering the OFR and of air exiting the OFR after oxidation, as a best approximation of the actual CS experienced by LVOCs in the OFR. Since LVOC condensation in the OFR took place under ambient RH, the dried SMPS particle size distribution measurement was corrected to account for the increase in CS from hygroscopic particle growth as a function of RH. For each data point, a growth factor ( $gf$ ) was calculated from the equation

$$\kappa = \sum \varepsilon_i \kappa_i = (gf^3 - 1)(1 - a_w) a_w^{-1} \quad (4)$$

from Petters and Kreidenweis (2007) and Nguyen et al. (2015), where  $\varepsilon_i$  is the volume fraction of aerosol species  $i$ ,  $\kappa_i$  is the hygroscopicity parameter of aerosol species  $i$ ,  $\kappa$  is the hygroscopicity parameter of the total aerosol, and  $a_w$  is water activity. We approximate  $a_w$  as being equal to RH, between 0 and 1. Total  $\kappa$  was estimated using  $\kappa_{OA} = 0.13$  as previously reported for this site and campaign (Levin et al., 2014) and  $\kappa_{inorganic} = 0.6$ , using the volume mixing rule (Petters and Kreidenweis, 2007). The volume fractions were calculated from AMS measurements in ambient air or after OFR oxidation, using estimated component densities (Salcedo et al., 2006; Kuwata et al., 2012). The  $gf$  ranged between 1 and 2.3 with an average of 1.2. It was applied to the dry SMPS particle diameter before calculating CS. The correction  $\beta(r)$  is a function of the Knudsen number

$$Kn = \frac{\lambda_g}{r} \quad (5)$$

where  $\lambda_g$  is the mean free path of the condensing gas. Based on previous modeling and measurements, we assume  $\alpha = 1$  for LVOCs (Kulmala and Wagner, 2001; Julin et al., 2014; Krechmer et al., 2015). A sensitivity study on the values of  $D$ , the impact of deviations from  $\alpha = 1$ , and the choice of SMPS size distribution used to calculate CS is discussed below in Sect. 3.6.3.

-  $\tau_{wall}$ : Following McMurry and Grosjean (1985), we estimate the first-order rate of LVOC loss to the walls of the OFR limited by eddy diffusion as

$$k_{wall} = \frac{1}{\tau_{wall}} = \frac{A}{V} \cdot \frac{2}{\pi} \cdot \sqrt{k_e D} \quad (6)$$

which is the version of this equation that is valid when  $\alpha$  is sufficiently large (i.e., greater than  $\sim 10^{-5}$ ). We used the measured OFR surface-area-to-volume ratio of  $A/V = 25 \text{ m}^{-1}$  and a coefficient of eddy diffusion  $k_e = 0.0036 \text{ s}^{-1}$  (much faster than the coefficient  $D$  estimated above), estimated by extrapolating values given in McMurry and Grosjean (1985). The choice of  $k_e$  is included in the sensitivity analysis in Sect. 3.6.3. Equation (56) results in an estimated wall loss rate of  $0.0025 \text{ s}^{-1}$  ( $\tau_{wall} = 400 \text{ s}$ ), similar to the

Formatted: Space Before: 0 pt

lifetime of ~600 s estimated for this type of OFR in Lambe et al. (2011a),(2011a). In the absence of any CS and oxidant, an upper limit of approximately 30% of LVOCs would be lost to the walls and the balance would exit the reactor and be lost to the tubing walls. When including this campaign's average integrated dry particle surface area of  $63 \mu\text{m}^2 \text{cm}^{-3}$  (with number mode at ~50 nm) in the calculation, the percentage lost to the walls decreases by only a few percent to 26%. If using an integrated particle surface area of  $500 \mu\text{m}^2 \text{cm}^{-3}$  that might be found in an urban, pollution source, or lab study, the percentage drops to 15%.

-  $\tau_{OH}$ : To estimate the loss of LVOCs to non-condensable products due to continued reaction with OH,  $\tau_{OH}$ , we make the assumption that LVOCs will remain available to condense on aerosols, walls, or exit the reactor for up to 5 generations of OH reaction. After they have reacted 5 times with OH, they are deemed lost by fragmentation into small oxidized molecules that are too volatile to condense. Further, we assume a rate constant for reaction with OH (of the order of that for an oxygenated molecule with ten carbon atoms and no C=C double bonds) of  $k_{OH} = 1 \times 10^{-11} \text{ cm}^3 \text{ molec}^{-1} \text{ s}^{-1}$  (Ziemann and Atkinson, 2012), so

$$\tau_{OH} = \frac{5}{k_{OH}[\text{OH}]} \quad (67)$$

Sensitivity studies for variations in parameters  $k_{OH}$  and the number of reactions with OH before LVOCs fragment to non-condensable products are also discussed in Sect. 3.6.3.

These three lifetimes are combined to determine the total lifetime of loss of LVOCs to these three combined pathways,

$$\tau_{total} = \left( \frac{1}{\tau_{aer}} + \frac{1}{\tau_{wall}} + \frac{1}{\tau_{OH}} \right)^{-1} \quad (78)$$

This total lifetime is compared to the average OFR residence time  $\tau_{OFR}$  (OFR volume divided by flow rate) to determine the fraction of LVOCs that exits the OFR without reaching one of the three other fates (and thus condenses onto sampling line walls),

$$F_{exit} = e^{\frac{-\tau_{OFR}}{\tau_{total}}} \quad (89)$$

The fraction of LVOCs that is lost to each pathway inside the OFR is then

$$F_x = (1 - F_{exit}) \cdot \left( \frac{k_x}{k_{total}} \right) \quad (910)$$

where the rate constant  $k_x = \tau_x^{-1}$  and x = wall, OH, or aerosol (aer).

Figure 5c compares all of the LVOC lifetimes and fractional fates as a function of age and  $\text{OH}_{\text{exp}}$ , with a typical OFR residence time of 140 s shown for comparison. The fractional fates are shown using high

Field Code Changed

(Fig. 5a) and low (Fig. 5b) rates of condensation to aerosol, based on typical higher and lower aerosol surface areas during this particular campaign. As discussed below (Sect. 3.5), OH oxidation leads to a substantial increase in the number of small particles when gas-phase precursors are available. This in turn increases the surface area available for condensation of LVOCs, and therefore  $\tau_{aer}$  depends on the amount of SOA formed from OH oxidation in the OFR in addition to the ambient particle surface area. During times of low SOA formation ( $<0.3 \mu\text{g m}^{-3}$ ), total dry surface area concentrations after oxidation are similar to ambient concentrations in the range of  $30\text{--}100 \mu\text{m}^2 \text{cm}^{-3}$ , and  $\tau_{aer}$  is estimated to be approximately 400 s or longer. However, during times with  $>1.5 \mu\text{g m}^{-3}$  SOA formation, total dry surface area concentrations increase to  $100\text{--}400 \mu\text{m}^2 \text{cm}^{-3}$  or larger and  $\tau_{aer}$  becomes  $<100$  s.

Formatted: Font: Italic

Formatted: Font: Italic

Formatted: Font: Italic

Formatted: Font: Italic

For an eq. age of 0.1 day, as little as 20% of the LVOCs formed in the OFR are predicted to condense onto aerosols, with the rest being lost to the walls in or after the OFR. However, the majority of LVOCs are likely not produced until higher  $\text{OH}_{\text{exp}}$ , concurrent with the highest SOA production. As eq. age increases into the 0.2–3 day range, condensation onto aerosols can account for as much as ~~60~~75% of LVOC fate, provided there is enough SOA formation to sufficiently increase the total particle surface area. In this case, shown in Fig. 5a, the remaining ~~40~~25% of LVOCs are approximately equally split between loss to the walls, exiting the OFR, and reacting with OH  $>5$  times. However if sufficient particle surface area is not formed, as in Fig. 5b, then still only 20% of LVOCs will condense onto aerosols.

For the conditions analyzed here from the BEACHON-RoMBAS campaign, these calculations suggest that when there were enough gas-phase precursors to produce  $>1.5 \mu\text{g m}^{-3}$  SOA, it is likely that the majority of this aerosol (up to ~~60~~75%) would be produced and measured in the OFR despite the perturbed time scales. When there were relatively few gas-phase precursors and little SOA was formed, it is likely that a majority of the LVOCs were not able to condense into SOA during the reactor residence time. However, if there were few precursors to begin with, the absolute amount of potential SOA mass that would not have time to condense would still be relatively small, limiting the effect of this correction on the objectives of this study.

Formatted: Font: Italic

~~Another important conclusion from this analysis is that for high eq. ages  $>10$  days, a very small fraction of the LVOC formed ( $<10\%$ ) will condense to form new SOA. The remainder will react many times with OH before having a chance to condense, likely leading to smaller fragmentation products that are too volatile to condense into SOA. This is, of course, different from what occurs in the atmosphere, where LVOCs would typically have sufficient time for condensation to aerosols under most conditions. Since~~

this rapid oxidation will remove any semi-volatile vapors from the gas phase, semi-volatile OA molecules will begin to evaporate to reestablish equilibrium partitioning. However, measurements of evaporation kinetics for ambient and lab-generated SOA suggest that evaporation is too slow to account for the changes measured during the short OFR residence time (Vaden et al., 2011). Furthermore, thermodenuder measurements have shown that only a small fraction (~20%) of ambient OA would be susceptible to evaporation due to removal of the gas-phase molecules (Cappa and Jimenez, 2010; Ortega et al., 2015). Therefore, heterogeneous oxidation of the preexisting OA by OH likely dominates the measured OA depletion at very high eq. ages (DeCarlo et al., 2008; Ortega et al., 2015).

### 3.3.2 Model validation: sulfuric acid ( $\text{H}_2\text{SO}_4$ ) condensation

To validate this LVOC fate model, we use the analogous and simpler system of oxidation of  $\text{SO}_2$  by OH to form  $\text{H}_2\text{SO}_4$ . If the  $\text{H}_2\text{SO}_4$  condenses onto aerosols, it will be measured as  $\text{SO}_4$  aerosol by the AMS.  $\text{SO}_4$  aerosol formation in the OFR was predicted by using estimated  $\text{OH}_{\text{exp}}$  to calculate how much ambient  $\text{SO}_2$  would be oxidized into  $\text{H}_2\text{SO}_4$ . The LVOC fate model was then used to determine  $F_{\text{aer},T}$ ,  $F_{\text{wall},T}$  and  $F_{\text{exit}}$  for  $\text{H}_2\text{SO}_4$ , while  $F_{\text{OH},T}$  was set equal to zero since gas-phase  $\text{H}_2\text{SO}_4$  will not continue to react with OH to produce volatile fragments. We used  $D = 1 \times 10^{-5} \text{ m}^2 \text{ s}^{-1}$  for an  $\text{H}_2\text{SO}_4$  molecule hydrated by  $\text{H}_2\text{O}$  molecules in the gas phase at the relevant ambient pressure and humidity (Hanson and Eisele, 2000), and the best-fit value of  $\alpha = 0.65$  from Pöschl et al. (1998). An additional minor correction was applied to account for the fact that the  $\text{SO}_2 + \text{OH}$  reaction is relatively slow, so the effective  $\tau_{\text{OFR}}$  for  $\text{H}_2\text{SO}_4$  molecules in the reactor can be less than the full OFR residence time depending on  $\text{OH}_{\text{exp}}$ . Using the model results, the fraction of  $\text{H}_2\text{SO}_4$  that does not condense onto aerosol was corrected for by dividing the  $\text{SO}_4$  mass measured with the AMS by  $F_{\text{aer},T}$ .

Another important conclusion from this analysis is that for high eq. ages >10 days, a very small fraction of the LVOC formed (<10%) will condense to form new SOA. The remainder will react many times with OH before having a chance to condense, likely leading to smaller fragmentation products that are too volatile to condense into SOA. This is, of course, different from what occurs in the atmosphere, where LVOCs would typically have sufficient time for condensation to aerosols under most conditions. Since this rapid oxidation will remove any semi-volatile vapors from the gas phase, semi-volatile OA molecules will begin to evaporate to reestablish equilibrium partitioning. However, measurements of evaporation kinetics for ambient and lab-generated SOA suggest that evaporation is too slow to account for the changes measured during the short OFR residence time (Vaden et al., 2011). Furthermore,

thermodenuder measurements have shown that only a small fraction (~20%) of ambient OA would be susceptible to evaporation due to removal of the gas phase molecules (Cappa and Jimenez, 2010; Ortega et al., 2015). Therefore, heterogeneous oxidation of the preexisting OA by OH likely dominates the measured OA depletion at very high eq. ages (DeCarlo et al., 2008; Ortega et al., 2015).

### 3.3.2 Model validation: sulfuric acid (H<sub>2</sub>SO<sub>4</sub>) condensation

In addition to LVOCs, H<sub>2</sub>SO<sub>4</sub> can also be produced in the OFR from OH oxidation of SO<sub>2</sub>. H<sub>2</sub>SO<sub>4</sub> molecules can also condense onto OFR or sampling line walls (but not be lost to further reaction with OH). These limitations of the OFR technique need to be corrected in order to relate OFR measurements to real atmospheric processes. H<sub>2</sub>SO<sub>4</sub> formation is an analogous yet much simpler system compared to LVOC formation, so it can be used to validate the LVOC fate model. If the H<sub>2</sub>SO<sub>4</sub> condenses onto aerosols, it will be measured as SO<sub>4</sub> aerosol by the AMS. SO<sub>4</sub> aerosol formation in the OFR was predicted by using estimated OH<sub>exp</sub> to calculate how much ambient SO<sub>2</sub> would be oxidized into H<sub>2</sub>SO<sub>4</sub>. The LVOC fate model was then used to determine  $F_{aer}$ ,  $F_{wall}$ , and  $F_{exit}$  for H<sub>2</sub>SO<sub>4</sub>, while  $F_{OH}$  was set equal to zero since gas-phase H<sub>2</sub>SO<sub>4</sub> will not continue to react with OH to produce volatile fragments. We used  $D = 1 \times 10^{-5} \text{ m}^2 \text{ s}^{-1}$  for an H<sub>2</sub>SO<sub>4</sub> molecule hydrated by H<sub>2</sub>O molecules in the gas phase at the relevant ambient pressure and humidity (Hanson and Eisele, 2000), and the best-fit value of  $\alpha = 0.65$  from Pöschl et al. (1998). An additional minor correction was applied to account for the fact that the SO<sub>2</sub>+OH reaction is relatively slow, so the effective  $\tau_{OFR}$  for H<sub>2</sub>SO<sub>4</sub> molecules in the reactor can be less than the full OFR residence time depending on OH<sub>exp</sub>. Using the model results, the fraction of H<sub>2</sub>SO<sub>4</sub> that does not condense onto aerosol was corrected for by dividing the newly produced SO<sub>4</sub> mass measured with the AMS by  $F_{aer}$ .

The measured vs. predicted SO<sub>4</sub> enhancement after OH oxidation in the OFR using the OFR185 method is shown in Fig. 6. The AMS measured 61% of the predicted SO<sub>4</sub> enhancement. After applying the correction for H<sub>2</sub>SO<sub>4</sub> wall and sampling line losses as described in the previous paragraph, the measured and predicted SO<sub>4</sub> enhancements agreed well with a slope of 0.8981, and R<sup>2</sup> slightly increased from 0.80 to 0.8485. To illustrate the sensitivities of this model to key uncertain parameters, namely the effects of using the range of  $\alpha = 0.43$ -1 given in Pöschl et al. (1998)(1998) and using the SMPS-size distributions measured before or after oxidation in the OFR (as lower and upper bounds of CS) are illustrated in Fig. S10. Generally, the amount of SO<sub>4</sub> formed after applying the H<sub>2</sub>SO<sub>4</sub> wall and sampling line loss correction was consistent with the expected amount within the uncertainties. The amount of scatter introduced by applying the correction was larger when the amount of SO<sub>4</sub> produced (and predicted) was



close to zero, when the  $F_{aer}$  correction factor was less than ~0.3. This suggests that the LVOC fate model becomes more uncertain when the correction factors are large and  $F_{aer}$  is close to zero. However, this analysis demonstrates that a correction can be successfully applied for  $H_2SO_4$  condensation, and that a similar correction should also be applied for LVOC condensation to accurately interpret the results of SOA formation in an OFR.

In the subsequent analyses, SOA formation is presented both with and without applying a correction to account for incomplete LVOC condensation to aerosol in the reactor. The correction, hereafter referred to as the “LVOC fate correction,” is applied by dividing the amount of SOA mass formed by  $F_{aer}$ . The correction is only applied for data with eq. age < 5 days. At higher exposures, it becomes unfeasible to apply the correction, because dividing small SOA mass formation by small fractions of condensation on aerosol results in large uncertainties. Instead, only uncorrected data is shown for eq. age > 5 days, and it is interpreted as being dominated by heterogeneous oxidation.

#### 3.4 SOA mass enhancement vs. $OH_{exp}$

Both the concentrations and relative fractions of ambient SOA precursor gases changed between day and night. They were dominated by MBO+isoprene (under ambient OH chemistry) during the day, and by MT+SQT (under ambient  $O_3/NO_3$  chemistry) at night (Fry et al., 2013)(Fry et al., 2013). Thus we SOA will be formed in the OFR from these changing VOC mixtures and any other gases present in the ambient air that enters the reactor, so it might expect to see be expected that different OA amounts of SOA production ~~is~~ would be observed during daytime vs. nighttime vs. daytime. Fig. 7 shows daytime and nighttime OA enhancement as a function of eq. age and  $OH_{exp}$ . During all times of the day, OA enhancement was largest in the range of 0.4–1.5 eq. days of photochemical aging, hereafter referred to as the age range of maximum OA enhancement. The diurnal profile of the OA enhancement in this range (inset of Fig. 7) shows that the maximum OA enhancement follows a pattern that is more nuanced than strictly daytime vs. nighttime, with a peak of SOA production in the early morning. Net loss of OA was observed above 10 eq. days of aging, consistent with the LVOC fate model and the interpretation that heterogeneous oxidation dominates at high eq. ages. This is also consistent with previous studies of heterogeneous OH oxidation of OA in a flow tube (George et al., 2008)(George et al., 2008) and with results with the OFR in the Los Angeles urban area (Ortega et al., 2015).

As shown in Fig. 7, OA enhancement shows a strong difference between daytime and nighttime. However, SOA formation potential in the OFR should not be a function of time of day itself. Rather, this

Field Code Changed

is thought to be a coincidental dependence based on the SOA precursor gas concentrations that change in a diurnal manner. In other words, this OH oxidation in the OFR is not ~~reproducing~~ meant to reproduce true ambient nighttime chemistry, rather it allows us to measure SOA formation from OH oxidation of the true mix of ambient gases ~~during all times as it evolves with time~~ of day, including nighttime. In fact, the lack of ambient nighttime OH oxidation may help explain the increased SOA formation potential when nighttime air is oxidized by OH in the OFR.

These measurements were made in a pine forest dominated by MT ~~(Ortega et al., 2014)~~ Ortega et al., 2014. As an alternative to separating by time of day, the data are separated by ambient MT concentrations in Fig. 8. The magnitude of SOA formation increased with ambient MT concentrations, ranging from no formation up to greater than ~~96~~  $\mu\text{g m}^{-3}$  OA enhancement (up to  $3 \mu\text{g m}^{-3}$  enhancement without the LVOC fate correction). For the range of ages with maximum OA enhancement (0.4–1.5 eq. days), a correlation is observed between OA enhancement and MT concentrations ( $R^2=0.4756$ ). Of course, MT may not be the only important precursors driving this correlation. Other gases that are correlated with MT, e.g. sesquiterpenes ( $R^2=0.70$  with MT shown in Fig. S11) or MT reaction products, may also contribute to the observed correlations. Although MT emissions are strongest during daytime due to their positive temperature dependence, their concentrations are higher at night due to the shallower nighttime boundary layer and reduced oxidation rate (Kim et al., 2010).

Field Code Changed

~~We observed much less SOA formation during the daytime, when concentrations of MBO+isoprene peaked but MT concentrations were lower. We note that SOA formation mechanisms that involve heterogeneous uptake followed by multiphase reactions are not efficiently simulated by the OFR, as their time scales are not shortened proportionally to increased OH concentrations (Hu et al., 2015). We observed much less SOA formation during the daytime, when concentrations of MBO+isoprene peaked but MT concentrations were lower. We note that SOA formation mechanisms that involve heterogeneous uptake followed by multiphase reactions are not efficiently simulated by the OFR, as their time scales are not shortened proportionally to increased OH concentrations (Hu et al., 2016).~~ This includes the IEPOX pathway from isoprene (Paulot et al., 2009) and the similar pathway proposed for MBO (Zhang et al., 2012), and thus ~~SOA formation potential from MBO+(Zhang et al., 2012).~~ While SOA formation from isoprene in an OFR has been demonstrated (Lambe et al., 2015), the total SOA formation potential from MBO + isoprene may be underestimated in our study.

OA enhancement from the OFR185 and OFR254-70 modes of operation are compared in Fig. 7. Because these were performed with the same physical reactor, we could only perform one of them at a time (see Fig. S7). Since ambient MT concentrations changed over the course of the campaign and they correlated with the amount of SOA formed in the reactor, this effect needed to be corrected before the results of the two reactor modes could be compared. The positive OA enhancement for the OFR254-70 data was multiplied by the ratio of average MT concentrations between the OFR185 and OFR254-70 periods (a factor of 1.8). From Fig. 7, we conclude that there were no ~~significant~~major differences in the amount of SOA formation between the OFR185 and OFR254-70 methods over the range of ages measured in this campaign. Minor differences in SOA formation between the two methods are likely a result of limits on the ability to determine the proper eq. age (especially for low ages in OFR254-70 as discussed in Sect. 2.3) or due to real changes in ambient SOA precursor gases, since the measurements using each method were not simultaneous. Additional comparisons of both methods sampling the same air, carefully designed and controlled to more accurately determine low ages in OFR254-70, would be useful to further explore this issue. Since the OFR185 mode is experimentally simpler and does not require addition of O<sub>3</sub> (with associated issues of mixing, dilution, possible contamination, etc.), and since the OFR185 mode more faithfully simulates OH chemistry due to reduced O<sub>3</sub> concentrations (~~Peng et al., 2015b~~)(Peng et al., 2015b), we recommend ~~this~~the OFR185 mode of operation for future OFR studies of OH oxidation in forested areas. ~~Additional comparisons of both modes at other locations are also desirable.~~

### 3.5 — Condensation vs. Nucleation in the OFR

~~When gas-phase molecules are oxidized and achieve a low enough volatility, they can condense onto existing particles (or other surfaces) or nucleate/grow new particles. The difference can be important experimentally because nucleation may produce some particles too small for the size range of the AMS, and it also increases surface area more efficiently than condensation to preexisting particles. Changes in the size distributions measured by the SMPS are used here to investigate the relative importance of these processes.~~

~~Particle volume size distributions of air oxidized over the full range of eq. photochemical ages in the flow reactor are shown in Fig. 9, during a period with relatively large OA enhancement in order to clearly demonstrate the behavior. OH oxidation in the reactor resulted in substantial new particle formation and growth, as well as growth of the preexisting ambient particles. The maximum enhancement in both~~

particle modes occurred at an eq. age of  $\sim 1$  day, consistent with AMS measurements of total mass enhancement. At higher ages, the new particle mode decreased in magnitude and diameter and eventually was not present at the highest ages. This is consistent with the results of the LVOC fate model, where at high eq. ages organic gases are rapidly oxidized into smaller volatile products that do not condense. The accumulation mode was also depleted at higher eq. ages, consistent with heterogeneous oxidation leading to fragmentation and evaporation of OA. The observed nucleation at lower eq. ages likely results from some combination of  $\text{H}_2\text{SO}_4$  and extremely low volatility organic compounds (ELVOCs; Kirkby et al., 2011; Ehn et al., 2014).

For the data shown in Fig. 9, a larger fraction of SOA molecules condensed onto the freshly nucleated particle mode than onto the preexisting particles. This behavior likely depends on the availability and position of the CS in the size distribution. With the small aerosol concentrations during this campaign, the CS from the new small particles sometimes competed with the CS from ambient particles. During periods when the CS entering the OFR in ambient air was larger, it reduced the condensation of SOA onto new particles, consistent with the lower importance of this mode for an OFR study in the Los Angeles area (Ortega et al., 2015). These results support the possibility of using flow reactors to study the potential for new particle formation and growth in different ambient airmasses and sources (Ezell et al., 2014; Chen et al., 2015).

### **3.6—Sources of SOA in ambient air**

#### **3.6.1—SOA mass formed vs. mass predicted from VOCs**

Many previous studies have measured the yields of SOA from oxidation of VOCs in chambers. Those experiments were generally performed under controlled conditions, with detailed information about the type and amount of VOCs available to form SOA at the beginning of the experiment. In this study, we also measured the yield of SOA from oxidation of organic gases, but in this case we started with a complex mixture of ambient organic gases, with some species not being directly measured or speciated. Therefore, the method used here provided a measure of the total SOA formation (or destruction) as a function of oxidant exposure from *all* ambient gases present, measured and unmeasured. The total SOA formation in the OFR was compared to the amount predicted from measured VOCs. SOA formation was predicted by applying low- $\text{NO}_x$  OA concentration dependent, chamber-derived aerosol yields (not including the chemical “aging” parameterization; Tsimpidi et al., 2010) to the percentage of ambient VOC concentrations predicted to react in the OFR based on  $\text{OH}_{\text{exp}}$  (>99% of ambient MT, SQT, and

isoprene, and ~45% of toluene+*p*-cymene in the age range of 0.4–1.5 eq. days). Previous experiments have shown SOA yields from various precursor gases oxidized in an OFR to be similar to yields from large environmental chambers (Kang et al., 2007, 2011, Lambe et al., 2011b, 2015). With an average post-oxidation OA concentration of  $5.1 \mu\text{g m}^{-3}$  with the correction applied, this resulted in campaign average SOA yields of 13.3%, 14.9%, 15.9%, and 1.8% for MT, SQT, toluene+*p*-cymene, and isoprene, respectively.

### 3.5 Condensation vs. Nucleation in the OFR

When gas-phase molecules are oxidized and achieve a low enough volatility, they can condense onto existing particles (or other surfaces) or nucleate/grow new particles. The difference can be important experimentally because nucleation may produce some particles too small for the size range of the AMS, and it also increases surface area more efficiently than condensation to preexisting particles. Changes in the size distributions measured by the SMPS are used here to investigate the relative importance of these processes.

Particle volume size distributions of air oxidized over the full range of eq. photochemical ages in the flow reactor are shown in Fig. 9, during a period with relatively large OA enhancement in order to clearly demonstrate the behavior. OH oxidation in the reactor resulted in substantial new particle formation and growth, as well as growth of the preexisting ambient particles. The maximum enhancement in both particle modes occurred at an eq. age of ~1 day, consistent with AMS measurements of total mass enhancement. At higher ages, the new particle mode decreased in magnitude and diameter and eventually was not present at the highest ages. This is consistent with the results of the LVOC fate model, where at high eq. ages organic gases are rapidly oxidized into smaller volatile products that do not condense. The accumulation mode was also depleted at higher eq. ages, consistent with heterogeneous oxidation leading to fragmentation and evaporation of OA. The observed nucleation at lower eq. ages likely results from some combination of  $\text{H}_2\text{SO}_4$  and extremely low-volatility organic compounds (ELVOCs; Kirkby et al., 2011; Ehn et al., 2014).

For the data shown in Fig. 9, a larger fraction of SOA molecules condensed onto the freshly nucleated particle mode than onto the preexisting particles. This behavior likely depends on the availability and position of the CS in the size distribution. With the small aerosol concentrations during this campaign, the CS from the new small particles sometimes competed with the CS from ambient particles. During periods when the CS entering the OFR in ambient air was larger, it reduced the condensation of SOA

1011 onto new particles, consistent with the lower importance of this mode for an OFR study in the Los  
1012 Angeles area (Ortega et al., 2015). These results support the possibility of using flow reactors to study  
1013 the potential for new particle formation and growth in different ambient airmasses and sources (Ezell et  
1014 al., 2014; Chen et al., 2015).

### 1015 **3.6 Sources of SOA in ambient air**

#### 1016 **3.6.1 SOA mass formed vs. mass predicted from VOCs**

1017 Many previous studies have measured the yields of SOA from oxidation of VOCs in chambers. Those  
1018 experiments were generally performed under controlled conditions, with detailed information about the  
1019 type and amount of VOCs available to form SOA at the beginning of the experiment. In this study, we  
1020 also measured the yield of SOA from oxidation of organic gases, but in this case we started with a  
1021 complex mixture of ambient organic gases, with some species not being directly measured or speciated.  
1022 Therefore, the method used here provided a measure of the total SOA formation (or destruction) as a  
1023 function of oxidant exposure from all ambient gases present, measured and unmeasured. The total SOA  
1024 formation in the OFR was compared to the amount predicted from measured VOCs. SOA formation was  
1025 predicted by applying low-NO<sub>x</sub> OA-concentration-dependent, chamber derived aerosol yields to the  
1026 ambient VOC concentrations predicted to react in the OFR based on OH<sub>exp</sub>. Estimated fractions reacted  
1027 were >99% of ambient MT, SQT, and isoprene, and ~45% of toluene+*p*-cymene in the age range of 0.4–  
1028 1.5 eq. days. The yields used to predict SOA formation were calculated for each individual data point as  
1029 a function of the OA mass concentration measured after oxidation in the OFR, using the two- or four-  
1030 product basis set parameterizations listed in Table 2 (Henze and Seinfeld, 2006; Tsimpidi et al., 2010).  
1031 With an average post-oxidation OA concentration of 4.1 g m<sup>-3</sup> with the LVOC fate correction applied, this  
1032 resulted in campaign-average SOA yields of 12.5, 13.2, 13.8, and 3.2% for MT, SQT, toluene, and  
1033 isoprene, respectively. Previous experiments have shown SOA yields from various precursor gases  
1034 oxidized in the OFR to be of the same order as yields from large environmental chambers (Kang et al.,  
1035 2007, 2011; Lambe et al., 2011b, 2015). These yield values reflect the amount of SOA that forms after  
1036 several generations of gas-phase oxidation of precursor gases. We do not include additional “aging” of  
1037 the precursors through additional oxidation steps, as such parameterizations are not well-supported  
1038 experimentally.

1039 The comparison of maximum measured vs. predicted SOA formation in Fig. 10 shows that approximately  
1040 **64.4** times more SOA was formed than predicted from MT, SQT, toluene+*p*-cymene, and isoprene. If the

1041 LVOC fate correction is not applied, still 3.1 times more SOA was measured than predicted (Fig. S12).  
1042 Note that while the LVOC fate correction led to a factor of ~32.5 increase in OA enhancement (seen in  
1043 Figs. 7-8), it causes only a factor of 21.4 increase in the slope in Fig. 10. This is because the higher OA  
1044 concentrations also lead to higher predicted SOA formation due to increased SOA yields (resulting from  
1045 increased partitioning to the particle phase).

1046 MT were the dominant SOA precursors, contributing an average of 88.7% to predicted SOA formation,  
1047 with SQT, toluene+*p*-cymene, and isoprene contributing 5%, 4.3%, and 2.5%, respectively. Other known  
1048 VOCs that form SOA, such as benzene or xylenes, were present in such low concentrations that they  
1049 would contribute even smaller percentages to predicted SOA formation, so they were not included in  
1050 this analysis.

1051 The correlation between measured and predicted SOA was  $R^2 = 0.5865$ , indicating that SOA formation  
1052 potential was controlled mainly by MT and other biogenic gases with similar concentration diurnal  
1053 patterns, including SQT. Toluene also likely originated at least partially from biogenic sources at this site  
1054 (~~Misztal et al., 2015~~)(Misztal et al., 2015). A diurnal plot of the measured maximum (0.4–1.5 eq. days  
1055 age) and predicted SOA formation is shown in Fig. 11, along with ambient MT, SQT, toluene+*p*-cymene,  
1056 and MBO+isoprene concentrations: (and S/IVOC concentrations, discussed in Sect. 3.6.2). SOA formation  
1057 followed a similar diurnal pattern to MT, SQT, and toluene+*p*-cymene, including a substantial increase  
1058 just after sunrise at 7 AM local time. SOA formation in the OFR followed a very different diurnal pattern  
1059 than ambient MBO+isoprene, supporting the conclusion that MBO+isoprene was an insignificant  
1060 contributor to SOA formation in the OFR for the ambient conditions of this campaign.

1061 In order for SOA formation in the OFR to be fully explained by the ambient VOCs, the SOA yields would  
1062 have needed to be approximately a factor of 64.4 larger than the values used in this analysis. This would  
1063 mean, e.g., a 78.5% yield from MT with the OA concentrations of only  $54.1 \mu\text{g m}^{-3}$  (33%34% at  $2.9 \mu\text{g m}^{-3}$   
1064 <sup>3</sup> if the LVOC fate correction is not applied), which is inconsistent with previous OFR and chamber  
1065 studies that have only achieved such high SOA yields in experiments with over an order of magnitude  
1066 higher OA concentrations (~~Kang et al., 2007, 2011; Tsimpidi et al., 2010; Lambe et al., 2011b,~~  
1067 ~~2015~~)(Kang et al., 2007, 2011; Tsimpidi et al., 2010; Lambe et al., 2011b, 2015). Accounting for S/IVOC  
1068 wall losses in such experiments (~~Matsunaga and Ziemann, 2010; Zhang et al., 2014~~)(Matsunaga and  
1069 Ziemann, 2010; Zhang et al., 2014) or including aging parameterizations (~~e.g.,~~ Tsimpidi et al., 2010)  
1070 might lessen this discrepancy, but is unlikely to be the entire answer. Therefore, this analysis strongly

Formatted: Font: Italic

Field Code Changed

suggests that there are other gases in ambient air than the VOCs measured by the PTR-TOF-MS that make important contributions to SOA formation.

### **3.6.2 SOA mass formed vs. predicted from S/IVOCs**

While the lowest volatility organic matter (i.e., OA) is measured by the AMS and the highest volatility range (VOCs and some IVOCs) is sampled by the PTR-TOF-MS, there is a substantial range of S/IVOCs between them. The gases that enter the OFR as S/IVOCs are the most likely source of SOA formation causing the factor of 6 discrepancy in Sect. 3.6.1. During the BEACHON-RoMBAS campaign, measurements were made using the TD-EIMS instrument to quantify the bulk (volatility resolved) ambient S/IVOC mass (Hunter et al., 2015). Other techniques at the site identified and quantified various subsets of the S/IVOCs (Yatavelli et al., 2014; Chan et al., 2015). All of the measurements are compiled in Hunter et al. (2015) to determine the total average organic volatility distribution during the campaign, which shows that S/IVOCs were the only pool of gas-phase species that could possibly produce as much SOA mass as observed in our study. Thus we estimate the in situ SOA yield of S/IVOCs needed to explain SOA formation in the OFR.

The average bulk S/IVOC mass concentrations measured with the TD-EIMS are shown as a function of  $\log(C^*)$  in the inset of Fig. 12. In Hunter et al. (2015), this mass was interpreted as being an approximate lower limit to S/IVOC mass, assuming the S/IVOCs measured by Yatavelli et al. (2014), Chan et al. (2015), and by the PTR-TOF-MS were subsets of the TD-EIMS measurement. The upper limit is to assume that each instrument measured a different set of S/IVOCs with no overlap, and would be  $\sim 3.2$  times larger than the mass shown in the inset of Fig. 12. With the substantial temporal overlap between OFR operation and TD-EIMS measurements, it is feasible here to determine the SOA yield of S/IVOCs assuming the lower limit case using the full time series, rather than the average concentrations. However, the overlap between OFR operation and all of the measurements of S/IVOCs included in the upper limit case was not sufficient to allow a full time series analysis. Therefore, we use the campaign-average ratio of upper limit to lower limit S/IVOC mass ( $10 \mu\text{g m}^{-3}$  vs.  $3.1 \mu\text{g m}^{-3}$ ) to estimate the SOA yield from S/IVOCs for the upper limit case.

### **3.6.2 SOA mass formed vs. predicted from S/IVOCs**

While the lowest volatility organic matter (i.e., OA) is measured by the AMS and the highest volatility range (VOCs and some IVOCs) is sampled by the PTR-TOF-MS, there is a substantial range of S/IVOCs



1100 between them. The gases that enter the OFR as S/IVOCs are the most likely source of SOA formation  
 1101 contributing to the factor of 4.4 discrepancy in Sect. 3.6.1. During the BEACHON-RoMBAS campaign,  
 1102 measurements were made using the TD-EIMS instrument to quantify the bulk (volatility-resolved)  
 1103 ambient S/IVOC mass (Hunter et al., 2016). Other techniques at the site identified and quantified various  
 1104 subsets of the S/IVOCs (Yatavelli et al., 2014; Chan et al., 2016). All of the measurements are compiled in  
 1105 Hunter et al. (2016) to determine the total average organic volatility distribution during the campaign,  
 1106 which shows that S/IVOCs were the only pool of gas-phase species that could possibly produce as much  
 1107 SOA mass as observed in our study.  
 1108 The average bulk S/IVOC mass concentrations measured with the TD-EIMS are shown as a function of  
 1109  $\log(C^*)$  in the inset of Fig. 12. In Hunter et al. (2016), this mass was interpreted as being an approximate  
 1110 lower limit to S/IVOC mass, assuming the S/IVOCs measured by Yatavelli et al. (2014), Chan et al. (2016),  
 1111 and by the PTR-TOF-MS were subsets of the TD-EIMS measurement. The upper limit is to assume that  
 1112 each instrument measured a different set of S/IVOCs with no overlap, and would be ~3.2 times larger  
 1113 than the mass shown in the inset of Fig. 12. With the substantial temporal overlap between OFR185  
 1114 operation and TD-EIMS measurements, it is feasible to perform a point-by-point analysis using the full  
 1115 TD-EIMS time series (shown in Fig. S7) to determine what the SOA yield of the lower limit S/IVOC mass  
 1116 would need to be in order to fully explain the amount of SOA formed from OH oxidation in the OFR.

1117 Ideally, the total mass of S/IVOCs at each data point that would be converted into SOA by oxidation of  
 1118 ~~these gases~~ would be determined by multiplying the mass in each volatility bin by the SOA yields of each  
 1119 bin. Since experimental measurements of the aerosol yields of such gases are generally not available  
 1120 and the ambient mixture of S/IVOCs was not fully speciated, we instead proceed under the assumption  
 1121 that all of the SOA formation that was not due to the previously discussed PTR-TOF-MS-measured VOCs  
 1122 came instead from the mass measured in the  $C^* = 10^1 - 10^7 \mu\text{g}/\text{m}^3 \text{ m}^{-3}$  volatility bins, with one  
 1123 correction. Since SQT are typically in the  $C^* = 10^5 \mu\text{g}/\text{m}^3 \text{ m}^{-3}$  range, we subtracted the SQT mass  
 1124 measured by the PTR-TOF-MS from the bulk S/IVOC mass (a subtraction of 6% of the total TD-EIMS  
 1125 measurement), to avoid double-counting due to this expected measurement overlap. While MT are in  
 1126 the  $C^* = 10^7 \mu\text{g}/\text{m}^3$  range, ~~the TD-EIMS instrument experiences a loss of sampling efficiency in  $\text{m}^{-3}$~~   
 1127 volatility bin, that bin is at the upper volatility limit of the TD-EIMS measurement capability. Some  
 1128 gases in that bin were sampled, but MT are not ~~are not~~ expected to be too volatile to be measured (Hunter  
 1129 et al., 2015)-(Hunter et al., 2016). This was supported by the fact that the campaign-average mass in the  
 1130  $C^* = 10^7 \mu\text{g}/\text{m}^3$  bin was only  $0.43 \mu\text{g}/\text{m}^3$ , which would correspond to only approximately 0.1 ppbv MT, if

Formatted: Space Before: 0 pt, After: 10 pt

Formatted: Font: Italic

Formatted: Font: Italic

Formatted: Font: Not Italic

Formatted: Font: Italic

there were no other gases in that bin. The campaign-average in-canopy MT concentration measured by the PTR-TOF-MS was approximately 0.8 ppbv.

For the lower limit S/IVOC mass case, the average SOA yield of the total S/IVOCs was determined by finding the yield value that made the slope of SOA measured vs. predicted from VOCs + S/IVOCs equal to one. As shown in Fig. 12, an average SOA yield of 58% for the bulk S/IVOC mass was required in order to bring the measured vs. predicted SOA formation into agreement in the lower limit S/IVOC mass case. Using the upper limit, an average SOA yield of 24% is needed. While measurements of SOA yields for speciated S/IVOCs are limited, especially for the relatively low OA concentrations in this study, previous work suggests that this range of 24–80% yield is reasonable. A yield of 51% was measured for n-heptadecane ( $C^* = 10^4 \mu\text{g}/\text{m}^3$ ) with  $\text{OA} = 15.4 \mu\text{g}/\text{m}^3$  under high- $\text{NO}_x$  conditions (Presto et al., 2010). Yields can be even higher from cyclic compounds (Lim and Ziemann, 2009; Tkacik et al., 2012), and under low- $\text{NO}_x$  conditions (Ng et al., 2007; Lane et al., 2008). SOA yields from several other IVOCs (naphthalene and alkyl naphthalenes) under low- $\text{NO}_x$  conditions were determined to be 58–73% with OA concentrations of 10–40  $\mu\text{g}/\text{m}^3$  (Chan et al., 2009).

When including SOA produced from S/IVOC oxidation in Fig. 12, the correlation between measured and predicted SOA formation was  $R^2=0.68$ . Attempts were made to optimize the correlation between measured and predicted SOA formation by applying  $C^*$ -dependent yields, but this did not result in significantly better correlations. Since speciated S/IVOC measurements as well as yields for each volatility bin (which may have varied with diurnal changes in the composition of each bin) were not available, we concluded that further detailed interpretation of SOA production from the measured S/IVOCs would be under-constrained.

% for the bulk S/IVOC mass was required in order to bring the measured vs. predicted SOA formation into optimal agreement in this time series analysis. The correlation between measured and predicted SOA formation was  $R^2=0.66$ . Attempts were made to optimize the correlation between measured and predicted SOA formation by applying arbitrary  $C^*$ -dependent yields, but this did not result in significantly better correlations. Since speciated S/IVOC measurements as well as yields for each volatility bin (which may have varied with diurnal changes in the composition of each bin) were not available, we concluded that further detailed interpretation of SOA production from the measured S/IVOCs would be under-constrained.

As mentioned above, this average SOA yield for S/IVOCs of 58% was estimated by assuming the lower limit case where the total ambient S/IVOC mass was sampled by the TD-EIMS. The upper limit mass case in Hunter et al. (2016) assumed that the several instruments that measured S/IVOCs were measuring different subsets of total S/IVOCs, so the measurements needed to be summed in order to determine the total mass concentration. Due to limited temporal overlap between all instruments, the analysis in Hunter et al. (2016) was performed on campaign average measurements. For this reason, the average SOA yield of S/IVOCs for the upper limit case is also done using the campaign average values instead of the time series analysis that was possible for the lower limit case. The average upper and lower limit S/IVOC mass concentrations were 10 and  $3.1 \mu\text{g m}^{-3}$ . To estimate the SOA yield of S/IVOCs in the upper limit case, the TD-EIMS time series data was multiplied by 3.2, so that it reflected a campaign average of  $10 \mu\text{g m}^{-3}$ . Using this upper limit mass time series, an average SOA yield for S/IVOCs of 18% was needed to bring measured vs. predicted SOA formation in the OFR into agreement. This makes the assumption that the ratio of S/IVOC mass measured by each technique was always constant.

While measurements of SOA yields for speciated S/IVOCs are limited, especially for the relatively low OA concentrations in this study, previous work suggests that this range of 18-58% yield is reasonable. A yield of 51% was measured for n-heptadecane ( $C^* = 10^4 \mu\text{g/m}^3$ ) with OA =  $15.4 \mu\text{g/m}^3$  under high- $\text{NO}_x$  conditions (Presto et al., 2010). Yields can be even higher from cyclic compounds (Lim and Ziemann, 2009; Tkacik et al., 2012) and under low- $\text{NO}_x$  conditions (Ng et al., 2007; Lane et al., 2008). SOA yields from several other IVOCs (naphthalene and alkylnaphthalenes) under low- $\text{NO}_x$  conditions were determined to be 58-73% with OA concentrations of  $10\text{--}40 \mu\text{g/m}^3$  (Chan et al., 2009).

This analysis suggests that OH oxidation of organic gases in a parcel of ambient pine forest air ~~will~~can potentially produce approximately 53.4 times more SOA from S/IVOC gases than from VOCs. This does not provide information about the sources of the lower volatility organic gases in this parcel. They may be directly emitted, formed as oxidation products of VOCs that were emitted upwind of this parcel, or some combination of these two options. ~~The high correlation between SOA formation and ambient MT and ambient MTS/IVOC concentrations suggests~~measured by the TD-EIMS exhibit a modest correlation ( $R^2 = 0.43$ , shown in Fig. S13), suggesting that the S/IVOCs ~~likely came~~may at least partially come from a biogenic source related to the emission of MT. ~~At night~~For example,  $\text{O}_3$  and  $\text{NO}_3$  may react with the C=C-containing MT and SQT emissions ~~during nighttime~~, leading to a buildup of S/IVOC-oxidation ~~products~~product S/IVOCs that lack C=C double bonds, ~~molecules with which  $\text{O}_3$  and  $\text{NO}_3$  would~~generally do not react ~~further with  $\text{O}_3$  and  $\text{NO}_3$  (Atkinson, 1997)~~(Atkinson, 1997). If this occurs, then OFR

oxidation is merely starting with precursors that are partway through the “aging” process from VOC emission to SOA formation. Variations in the ratio of measured to predicted SOA formation in Figs. 10 and 12 could be due partly to variations in the ratio of the concentrations of S/IVOCs to VOCs due to changes in the meteorological or chemical conditions of the atmosphere, or from periodic changes in the biogenic and/or anthropogenic sources of S/IVOCs. However, as shown in Fig. 11, the diurnal profile of S/IVOC concentrations showed a relatively smaller increase in concentrations at night compared to MT or measured SOA formation. Since emissions generally change with time of day, it would not be unreasonable to expect the speciation and SOA formation potential of ambient S/IVOCs to also change with time of day. Until the S/IVOCs in a dataset such as this can be better speciated and quantified, these conclusions remain speculative.

### 3.6.3 Sensitivity to LVOC fate model parameters

The LVOC fate correction in this analysis led to a relatively large factor of 32.5 increase in OA enhancement and factor of 21.4 increase in measured vs. predicted SOA formation. As the values of several of the model parameters are not well constrained, in this section we investigate the sensitivity of the LVOC fate correction to these parameters. Fig. 13 shows the sensitivity of the slope of measured vs. predicted SOA formation from VOCs, as well as how that affected the range of SOA yields needed from S/IVOCs in order to explain the total SOA formation in the OFR. Sensitivity was tested for  $k_{OH}$ , the number of reactions with OH before LVOCs are lost to volatile, non-condensable products, the SMPS size distribution used to calculate  $CS$ ,  $\alpha$ ,  $k_e$ , and  $D$ .

The least-well-defined parameters in the model were likely  $k_{OH}$  and the number of reactions with OH, especially since the analysis of  $H_2SO_4$  condensation in Sect. 3.3.2 did not use them. However, the LVOC fate correction was relatively insensitive to these parameters, specifically for values of  $k_{OH}$  less than  $3 \times 10^{-11} \text{ cm}^3 \text{ molec}^{-1} \text{ s}^{-1}$  or when assuming 2+ reactions with OH. If we assume LVOCs always remain available to condense and never fragment, the slope reaches a lower asymptote of 5.64.1. The model also showed a relatively low sensitivity to  $k_e$  and  $D$  over several orders of magnitude.

The slope of measured vs. predicted SOA formation was more sensitive to the choice of  $CS$  and  $\alpha$ . The slope is mainly sensitive to  $CS$  when approaching the ambient (smaller) value. Since using the average value of  $CS$  worked well for the  $H_2SO_4$  analysis (and the ambient  $CS$  gave poor results there), it is likely that the average  $CS$  is at least close enough to the proper value as not to cause systematic biases. Using values of  $\alpha$  less than 1 led to a rapid increase in the magnitude of the LVOC fate correction. Values less

1221 than approximately  $\alpha = 0.31$  would require the SOA yield from S/IVOCs to approach 100% as a lower  
1222 limit, which is unlikely to be the case. In other words, if the sticking coefficient was very low (e.g.  $\alpha < 0.1$ )  
1223 it would be impossible to explain the amount of SOA formed from the carbon present in the gas-phase.  
1224 This suggests that  $\alpha = 1$  or close to 1 is a good approximation for the conditions in the OFR at this  
1225 campaign, and allows us to rule out values much lower than 1.

1226 It is noteworthy that none of the changes to these four parameters led to a substantial *decrease* in the  
1227 slope of measured vs. predicted SOA formation. The parameters that can lead to a considerable increase  
1228 in  $F_{aer}$  are the CS and residence time of the OFR (i.e., time allowed for condensation onto particles,  
1229 which is controlled by flow rate). However, these values were among the best constrained parameters,  
1230 since we had direct measurements of both during the campaign. This suggests that while the LVOC fate  
1231 correction was relatively large, it was unlikely to be much smaller.

#### 1232 4 Conclusions

1233 During the BEACHON-RoMBAS campaign, ambient air was oxidized by OH in an OFR to study in situ SOA  
1234 formation from the ambient mixture of SOA precursors as they exist in a forest environment. SOA  
1235 formation was measured semi-continuously, and the changes in both gas and particle phases were  
1236 documented as a function of photochemical age. The amount of SOA formation increased with age to a  
1237 maximum at 0.4–1.5 days of eq. photochemical aging, coinciding with depletion of known SOA  
1238 precursors measured with the PTR-TOF-MS. SOA formation in the OFR correlated with MT  
1239 concentrations, both of which were typically larger during nighttime. ~~The~~ Net SOA loss was observed at  
1240 >10 days eq. age, consistent with heterogeneous oxidation processes being important only for the  
1241 longest lived aerosol (e.g., free tropospheric aerosol). Similar amounts of SOA formation were observed  
1242 from both the OFR185 and OFR254-70 methods ~~everfor~~ the overlapping range of eq. ages ~~used~~ (~1-30  
1243 days). Comparison at shorter ages was not possible because the OFR254-70 method, especially as it was  
1244 employed during this campaign, was not suitable for measuring <1 eq. day of OH aging. Condensation  
1245 onto preexisting ambient particles and nucleation and growth of small particles were both observed.

1246 A modeling analysis of the fate of LVOCs in the OFR was presented. The validity of this model was  
1247 evaluated using the simpler process of SO<sub>2</sub> gas conversion to SO<sub>4</sub> aerosol. The fraction of LVOCs that  
1248 condense onto aerosols, versus the other fates of LVOCs including condensing on the reactor walls,  
1249 exiting the reactor to condense on sampling lines, or reacting with OH to produce volatile fragmentation  
1250 products, depends strongly on the aerosol surface area available for condensation. Our measurements

rule out sticking coefficients much lower than 1. For ambient experiments in rural areas with low CS, laboratory experiments without seed aerosol, or when sampling with a relatively short residence time, a large correction may be required. Addition of an aerosol seed to sample air with low aerosol CS (such as this study) would reduce the uncertainties associated with the LVOC fate correction. In urban areas or in laboratory studies with large seed aerosol surface area, the correction can be much smaller (<20%). In either case, the relative time scales of key processes in the OFR need to be carefully considered in order to properly interpret the results of measured SOA formation.

The amount of SOA that could be produced from OH oxidation of the major VOC species measured at this site (MT, SQT, toluene+*p*-cymene, and isoprene) was insufficient to explain the measured SOA formation in the reactor by a factor of ~~6-4.4~~. To our knowledge, this is the first time this has been demonstrated by comparing simultaneous VOC measurements with in situ SOA formation, particularly in a biogenic environment. A discrepancy this large is unlikely to be completely explained by incorrect yields for the speciated VOCs or by experimental uncertainties. The correlation between measured and predicted SOA formation suggests that the unidentified SOA precursors were of biogenic origin with a similar diurnal pattern to MT, SQT, and toluene +*p*-cymene. Novel TD-EIMS measurements quantified the reservoir of S/IVOCs, which are not measured efficiently by a PTR-TOF-MS and represent the only pool of gas-phase carbon at the site that could possibly explain the observed SOA. An SOA yield of ~~24-80~~ 18-58% for the total mass of S/IVOCs measured was required to account for all of the SOA formation from OH oxidation in the OFR. This research points to a need to improve our understanding and measurement capabilities of S/IVOCs.

We have demonstrated how an OFR can be used in combination with a variety of aerosol and gas instruments to provide information about the net SOA formation potential of forest air. The OFR technique allows investigating the quantity and variability of SOA precursor gases that are present in ambient air. These results could be used to inform the treatment of S/IVOCs, such as VOC oxidation products, in SOA models. Future OFR experiments could be designed with additional specialized instrumentation to determine the molecular identities of S/IVOCs and investigate their specific SOA yields.

#### Acknowledgements

We thank US NSF grants AGS-1243354 and AGS-1360834, NOAA grants NA13OAR4310063 and NA10OAR4310106, U.S. DOE ASR Program (Office of Science, BER, DE-SC0011105), Austrian Science

1281 Fund (FWF) project number L518-N20, and the US EPA (STAR 83587701-0) for partial support for this  
 1282 research. BBP acknowledges support from a CIRES Graduate Student Research Fellowship and a US EPA  
 1283 STAR Graduate Fellowship (FP-91761701-0). LK acknowledges support from DOC-fORTE-fellowship of  
 1284 the Austrian Academy of Science. This work has not been formally reviewed by the US EPA. The views  
 1285 expressed are solely those of the authors, and the US EPA does not endorse any products or commercial  
 1286 services mentioned in this work. AMO acknowledges a fellowship from the DOE SCGP Fellowship  
 1287 Program (ORAU, ORISE). We are grateful to Alex Guenther and Jim Smith of NCAR for co-organizing the  
 1288 BEACHON-RoMBAS field campaign, to Andrew Turnipseed for SO<sub>2</sub> measurements, and to the USFS  
 1289 Manitou Experimental Forest Observatory for site support.

## 1290 Glossary

<u>OFR</u>	<u>Oxidation flow reactor</u>
<u>SOA</u>	<u>Secondary organic aerosol</u>
<u>LVO</u>	<u>Low volatility organic compound</u>
<u>OA</u>	<u>Organic aerosol</u>
<u>VOC</u>	<u>Volatile organic compound</u>
<u>S/IVOC</u>	<u>Semi- and intermediate-volatility organic compound</u>
<u>PTR-TOF-MS</u>	<u>Proton transfer reaction time-of-flight mass spectrometer</u>
<u>OH</u>	<u>Hydroxyl radical</u>
<u>O<sub>3</sub></u>	<u>Ozone</u>
<u>NO<sub>3</sub></u>	<u>Nitrate radical</u>
<u>MBO</u>	<u>2-methyl-3-buten-2-ol</u>
<u>MT</u>	<u>Monoterpenes</u>
<u>SQT</u>	<u>Sesquiterpenes</u>
<u>OHR<sub>ext</sub></u>	<u>External OH reactivity</u>
<u>OHR<sub>int</sub></u>	<u>Internal OH reactivity</u>
<u>OH<sub>exp</sub></u>	<u>OH exposure</u>
<u>eq.</u>	<u>Equivalent</u>
<u>SMPS</u>	<u>Scanning mobility particle sizer</u>
<u>AMS</u>	<u>Aerodyne High-Resolution Time-of-Flight Aerosol Mass Spectrometer</u>
<u>k<sub>OH</sub></u>	<u>Rate constant for reaction with OH</u>
<u>k<sub>O<sub>3</sub></sub></u>	<u>Rate constant for reaction with O<sub>3</sub></u>
<u>TD-EIMS</u>	<u>Thermal desorption electron impact mass spectrometer</u>
<u>C*</u>	<u>Effective saturation vapor concentration</u>
<u>τ<sub>aer</sub></u>	<u>Lifetime of LVOs (or H<sub>2</sub>SO<sub>4</sub>) for condensation onto aerosols</u>
<u>τ<sub>wall</sub></u>	<u>Lifetime of LVOs (or H<sub>2</sub>SO<sub>4</sub>) for loss to OFR walls</u>
<u>τ<sub>OH</sub></u>	<u>Lifetime of LVOs for reaction with OH</u>
<u>τ<sub>total</sub></u>	<u>Total lifetime for loss of LVOs (or H<sub>2</sub>SO<sub>4</sub>)</u>
<u>CS</u>	<u>Condensational sink</u>
<u>D</u>	<u>Gas diffusion coefficient</u>
<u>r</u>	<u>Particle radius</u>
<u>N(r)</u>	<u>Particle number size distribution</u>

$\alpha$	<u>Sticking coefficient</u>
$Kn$	<u>Knudsen number</u>
$\lambda_g$	<u>Mean free path of gas molecules</u>
$A/V$	<u>Surface-area-to-volume ratio of OFR</u>
$k_e$	<u>Coefficient of eddy diffusion</u>
$F_x$	<u>Fraction of LVOCs (or <math>H_2SO_4</math>) lost to pathway <math>x</math></u>
$SO_4$	<u>Sulfate aerosol</u>



## 1292 References

- 1293 Alarcón, P., Bohn, B., Zetzsch, C., Rayez, M.-T. and Rayez, J.-C.: Reversible addition of the OH  
1294 radical to *p*-cymene in the gas phase: multiple adduct formation. Part 2., Phys. Chem. Chem.  
1295 Phys., 16, 17315–26, doi:10.1039/c4cp02073a, 2014.
- 1296 Atkinson, R.: Gas-Phase Tropospheric Chemistry of Volatile Organic Compounds: 1. Alkanes  
1297 and Alkenes, J. Phys. Chem. Ref. Data, 26, 215, doi:10.1063/1.556012, 1997.
- 1298 Atkinson, R. and Arey, J.: Gas-phase tropospheric chemistry of biogenic volatile organic  
1299 compounds: a review, Atmos. Environ., 37, 197–219, doi:10.1016/S1352-2310(03)00391-1,  
1300 2003.
- 1301 Bruns, E. ~~aA~~, El Haddad, I., Keller, A., Klein, F., Kumar, N. K., Pieber, S. M., Corbin, J. C.,  
1302 Slowik, J. G., Brune, W. H., Baltensperger, U. and Prévôt, ~~aA~~ S. H.: Inter-comparison of  
1303 laboratory smog chamber and flow reactor systems on organic aerosol yield and composition,  
1304 Atmos. Meas. Tech., 8, 2315–2332, doi:10.5194/amt-8-2315-2015, 2015.
- 1305 Calvert, J. G., Atkinson, R., Becker, K. H., Kamens, R. M., Seinfeld, J. H., Wallington, T. H. and  
1306 Yarwood, G.: The Mechanisms of Atmospheric Oxidation of the Aromatic Hydrocarbons,  
1307 Oxford University Press, New York, ~~USA~~, 2002.
- 1308 Cappa, C. D. and Jimenez, J. L.: Quantitative estimates of the volatility of ambient organic  
1309 aerosol, Atmos. Chem. Phys., 10, 5409–5424, doi:10.5194/acp-10-5409-2010, 2010.
- 1310 Chan, A. W. H., Kautzman, K. E., Chhabra, P. S., Surratt, J. D., Chan, M. N., Crounse, J. D.,  
1311 ~~Kurten~~Kürten, A., Wennberg, P. O., Flagan, R. C. ~~7~~, and Seinfeld, J. H. ~~and Sciences, P.~~: Secondary  
1312 organic aerosol formation from photooxidation of naphthalene and alkylnaphthalenes-~~2~~,  
1313 implications for oxidation of intermediate volatility organic compounds (IVOCs-), Atmos.  
1314 Chem. Phys., 9, 3049–3060, doi:10.5194/acp-9-3049-2009, 2009.
- 1315 Chan, A. W. H., Kreisberg, N. M., Hohaus, T., Campuzano-Jost, P., Zhao, Y., Day, D. A., Kaser,  
1316 L., Karl, T., Hansel, A., Teng, A. P., Ruehl, C. R., Sueper, D. T., Jayne, J. T., Worsnop, D. R.,  
1317 Jimenez, J. L., Hering, S. V. and Goldstein, A. H.: Speciated measurements of semivolatile and  
1318 intermediate volatility organic compounds (S/IVOCs) in a pine forest during BEACHON-  
1319 RoMBAS 2011, Atmos. Chem. Phys. ~~Discuss.~~, ~~15~~, ~~22331–22377~~, ~~16~~, 1187–1205,  
1320 doi:10.5194/~~acpd~~ ~~15-22331-2015~~, ~~2015~~ ~~acp~~ ~~16-1187-2016~~, 2016.
- 1321 Chen, H., Ezell, M. J., Arquero, K. D., Varner, M. E., Dawson, M. L., Gerber, R. B. and  
1322 Finlayson-Pitts, B. J.: New particle formation and growth from methanesulfonic acid,  
1323 trimethylamine and water, Phys. Chem. Chem. Phys., 17, 13699–13709,  
1324 doi:10.1039/C5CP00838G, 2015.
- 1325 Chen, Q., Farmer, D. K., Schneider, J., Zorn, S. R., Heald, C. L., Karl, T. G., Guenther, A.,  
1326 Allan, J. D., Robinson, N., Coe, H., Kimmel, J. R., Pauliquevis, T., Borrmann, S., Pöschl, U.,  
1327 Andreae, M. O., Artaxo, P., Jimenez, J. L. and Martin, S. T.: Mass spectral characterization of  
1328 submicron biogenic organic particles in the Amazon Basin, Geophys. Res. Lett., 36, L20806,  
1329 doi:10.1029/2009GL039880, 2009.

Formatted: Line spacing: single

Formatted: Font: Times New Roman, 12 pt

Formatted: Normal, Space Before: 12 pt, No widow/orphan control, Don't adjust space between Latin and Asian text, Don't adjust space between Asian text and numbers

Formatted: Font: Times New Roman, 12 pt, Italic

Formatted: Font: Times New Roman, 12 pt

Formatted: Font: Times New Roman, 12 pt

Formatted: Font: Times New Roman, 12 pt

Formatted: Font: Times New Roman, 12 pt

Formatted: Font: Times New Roman, 12 pt

Formatted: Font: Times New Roman, 12 pt

Formatted: Font: Times New Roman, 12 pt

Formatted: Font: Times New Roman, 12 pt

Formatted: Font: Times New Roman, 12 pt

Formatted: Font: Times New Roman, 12 pt

Formatted: Font: Times New Roman, 12 pt

Formatted: Font: Times New Roman, 12 pt

Formatted: Font: Times New Roman, 12 pt

Formatted: Font: Times New Roman, 12 pt

1330 Cross, E. S., Hunter, J. F., Carrasquillo, A. J., Franklin, J. P., Herndon, S. C., Jayne, J. T.,  
 1331 Worsnop, D. R., Miake-Lye, R. C. and Kroll, J. H.: Online measurements of the emissions of  
 1332 intermediate-volatility and semi-volatile organic compounds from aircraft, *Atmos. Chem. Phys.*,  
 1333 13, 7845–7858, doi:10.5194/acp-13-7845-2013, 2013.

1334 DeCarlo, P. F., Kimmel, J. R., Trimborn, A., Northway, M. J., Jayne, J. T., Aiken, A. C., Gonin,  
 1335 M., Fuhrer, K., Horvath, T., Docherty, K. S., Worsnop, D. R. and Jimenez, J. L.: Field-  
 1336 Deployable, High-Resolution, Time-of-Flight Aerosol Mass Spectrometer, *Anal. Chem.*, 78,  
 1337 8281–8289, doi:10.1021/ac061249n, 2006.

1338 DeCarlo, P. F., Dunlea, E. J., Kimmel, J. R., Aiken, A. C., Sueper, D., Crounse, J., Wennberg, P.  
 1339 O., Emmons, L., Shinozuka, Y., Clarke, A., Zhou, J., Tomlinson, J., Collins, D. R., Knapp, D.,  
 1340 Weinheimer, A. J., Montzka, D. D., Campos, T. and Jimenez, J. L.: Fast airborne aerosol size  
 1341 and chemistry measurements above Mexico City and Central Mexico during the MILAGRO  
 1342 campaign, *Atmos. Chem. Phys.*, 8, 4027–4048, doi:10.5194/acp-8-4027-2008, 2008.

1343 DeCarlo, P. F., Kimmel, J. R., Trimborn, A., Northway, M. J., Jayne, J. T., Aiken, A. C., Gonin,  
 1344 M., Fuhrer, K., Horvath, T., Docherty, K. S., Worsnop, D. R. and Jimenez, J. L.: Field-  
 1345 Deployable, High-Resolution, Time-of-Flight Aerosol Mass Spectrometer, *Anal. Chem.*, 78,  
 1346 8281–8289, doi:10.1021/ac061249n, 2006.

1347 Donahue, N. M., Robinson, A. L., Stanier, C. O. and Pandis, S. N.: Coupled Partitioning,  
 1348 Dilution, and Chemical Aging of Semivolatile Organics, *Environ. Sci. Technol.*, 40, 2635–2643,  
 1349 doi:10.1021/es052297c, 2006.

1350 Ehn, M., Thornton, J. A., Kleist, E., Sipilä, M., Junninen, H., Pullinen, I., Springer, M.,  
 1351 Rubach, F., Tillmann, R., Lee, B., Lopez-Hilfiker, F., Andres, S., Acir, I.-H., Rissanen, M.,  
 1352 Jokinen, T., Schobesberger, S., Kangasluoma, J., Kontkanen, J., Nieminen, T., Kurtén, T.,  
 1353 Nielsen, L. B., Jørgensen, S., Kjaergaard, H. G., Canagaratna, M., Maso, M. D., Berndt, T.,  
 1354 Petäjä, T., Wahner, A., Kerminen, V.-M., Kulmala, M., Worsnop, D. R., Wildt, J. and Mentel, T.  
 1355 F.: A large source of low-volatility secondary organic aerosol, *Nature*, 506, 476–479,  
 1356 doi:10.1038/nature13032, 2014.

1357 Ervens, B.: Modeling the Processing of Aerosol and Trace Gases in Clouds and Fogs, *Chem.*  
 1358 *Rev.*, 115, 4157–4198, doi:10.1021/cr5005887, 2015.

1359 Ervens, B., Turpin, B. J. and Weber, R. J.: Secondary organic aerosol formation in cloud droplets  
 1360 and aqueous particles (aqSOA): a review of laboratory, field and model studies, *Atmos. Chem.*  
 1361 *Phys.*, 11, 11069–11102, doi:10.5194/acp-11-11069-2011, 2011.

1362 Ezell, M. J., Chen, H., Arquero, K. D. and Finlayson-pitts, B. J.: Aerosol fast flow reactor  
 1363 for laboratory studies of new particle formation, *J. Aerosol Sci.*, 78, 30–40,  
 1364 doi:10.1016/j.jaerosci.2014.08.009, 2014.

1365 Farmer, D. K. and Cohen, R. C.: Observations of HNO<sub>3</sub>, ΣAN, ΣPN and NO<sub>2</sub> fluxes: evidence  
 1366 for rapid HO<sub>x</sub> chemistry within a pine forest canopy, *Atmos. Chem. Phys.*, 8, 3899–3917,  
 1367 doi:10.5194/acp-8-3899-2008, 2008.

Formatted: Font: Times New Roman, 12 pt

Formatted: Normal, Space Before: 12 pt, No widow/orphan control, Don't adjust space between Latin and Asian text, Don't adjust space between Asian text and numbers

Formatted: Font: Times New Roman, 12 pt

Formatted: Font: Times New Roman, 12 pt

Formatted: Font: Times New Roman, 12 pt

Formatted: Font: Times New Roman, 12 pt

Formatted: Font: Times New Roman, 12 pt

Formatted: Font: Times New Roman, 12 pt

Formatted: Font: Times New Roman, 12 pt

Formatted: Font: Times New Roman, 12 pt

Formatted: Font: Times New Roman, 12 pt

1368 Fry, J. L., Draper, D. C., Zarzana, K. J., Campuzano-Jost, P., Day, D. A., Jimenez, J. L., Brown,  
1369 S. S., Cohen, R. C., Kaser, L., Hansel, A., Cappellin, L., Karl, T., Hodzic Roux, A., Turnipseed,  
1370 A., Cantrell, C., Lefer, B. L. and Grossberg, N.: Observations of gas- and aerosol-phase organic  
1371 nitrates at BEACHON-RoMBAS 2011, Atmos. Chem. Phys., 13, 8585–8605, doi:10.5194/acp-  
1372 13-8585-2013, 2013.

1373 George, I. J., Slowik, J. and Abbatt, J. P. D.: Chemical aging of ambient organic aerosol from  
1374 heterogeneous reaction with hydroxyl radicals, Geophys. Res. Lett., 35, L13811,  
1375 doi:10.1029/2008GL033884, 2008.

1376 Goldstein, A. H. and Galbally, I. E.: Known and ~~unexplored organic constituents~~Unexplored  
1377 Organic Constituents in the ~~earth's atmosphere~~Earth's Atmosphere, Environ. Sci. Technol., 41,  
1378 1514–1521, doi:10.1021/es072476p, 2007.

1379 Grieshop, A. P., Logue, J. M., Donahue, N. M. and Robinson, A. L.: Laboratory investigation of  
1380 photochemical oxidation of organic aerosol from wood fires 1: measurement and simulation of  
1381 organic aerosol evolution, Atmos. Chem. Phys., 9, 1263–1277, doi:10.5194/acp-9-1263-2009,  
1382 2009.

1383 Hanson, D. R. and Eisele, F.: Diffusion of ~~H<sub>2</sub>SO<sub>4</sub>~~H<sub>2</sub>SO<sub>4</sub> in Humidified Nitrogen: Hydrated ~~H<sub>2</sub>~~  
1384 ~~SO<sub>4</sub>H<sub>2</sub>SO<sub>4</sub>~~, J. Phys. Chem. A, 104, 1715–1719, doi:10.1021/jp993622j, 2000.

1385 Hayes, P. L., Carlton, A. G., Baker, K. R., Ahmadov, R., Washenfelder, R. ~~a~~A., Alvarez, S.,  
1386 Rappenglück, B., Gilman, J. B., Kuster, W. C., de Gouw, J. ~~a~~A., Zotter, P., Prévôt, ~~a~~A. S. H.,  
1387 Szidat, S., Kleindienst, T. E., Offenberg, J. ~~H.~~, Jimenez, J. ~~L.H.~~, Ma, P. K. and Jimenez, J. L.:  
1388 Modeling the formation and aging of secondary organic aerosols in Los Angeles during CalNex  
1389 2010, Atmos. Chem. Phys., 15, 5773–5801, doi:10.5194/acp-15-5773-2015, 2015.

1390 Henze, D. K. and Seinfeld, J. H.: Global secondary organic aerosol from isoprene oxidation,  
1391 Geophys. Res. Lett., 33, L09812, doi:10.1029/2006GL025976, 2006.

1392 Hodzic, A., Jimenez, J. L., Madronich, S., Aiken, A. C., Bessagnet, B., Curci, G., Fast, J.,  
1393 Lamarque, J. F., Onasch, T. B., Roux, G., Schauer, J. J., Stone, E. A. and Ulbrich, I. M.:  
1394 Modeling organic aerosols during MILAGRO: importance of biogenic secondary organic  
1395 aerosols, Atmos. Chem. Phys., 9, 6949–6981, 2009.

1396 Hodzic, A., Jimenez, J. L., Madronich, S., Canagaratna, M. R., DeCarlo, P. F., Kleinman, L. and  
1397 Fast, J.: Modeling organic aerosols in a megacity: potential contribution of semi-volatile and  
1398 intermediate volatility primary organic compounds to secondary organic aerosol formation,  
1399 Atmos. Chem. Phys., 10, 5491–5514, doi:doi:10.5194/acp-10-5491-2010, 2010.

1400 Hu, W., Palm, B. B., Day, D. A., Campuzano-Jost, P., Krechmer, J. E., de Sá, S. S., Martin, S.  
1401 T., Alexander, M. L., Canonaco, F., Prevot, A. S. H., Brune, W. H. and Jimenez, J.-L.: The aging  
1402 and low-volatility of Isoprene Epoxidiols-Derived Secondary Organic Aerosol (IEPOX-SOA) in  
1403 real ambient environment: determination of reactive uptake coefficient ( $\gamma$ ), in prep., 20152016.

1404 Huffman, J. A., Ziemann, P. J., Jayne, J. T., Worsnop, D. R. and Jimenez, J. L.: Development  
1405 and Characterization of a Fast-Stepping/Scanning Thermodenuder for Chemically-Resolved

Formatted: Font: Times New Roman, 12 pt

Formatted: Normal, Space Before: 12 pt, No widow/orphan control, Don't adjust space between Latin and Asian text, Don't adjust space between Asian text and numbers

Formatted: Font: Times New Roman, 12 pt

Formatted: Font: Times New Roman, 12 pt

Formatted: Font: Times New Roman, 12 pt

Formatted: Font: Times New Roman, 12 pt

Formatted: Font: Times New Roman, 12 pt

Formatted: Font: Times New Roman, 12 pt

Formatted: Font: Times New Roman, 12 pt

Formatted: Font: Times New Roman, 12 pt

Formatted: Font: Times New Roman, 12 pt

Formatted: Font: Times New Roman, 12 pt

Formatted: Font: Times New Roman, 12 pt

Formatted: Font: Times New Roman, 12 pt

Formatted: Font: Times New Roman, 12 pt

Formatted: Normal, Space Before: 12 pt, No widow/orphan control, Don't adjust space between Latin and Asian text, Don't adjust space between Asian text and numbers

Formatted: Font: Times New Roman, 12 pt

Formatted: Font: Times New Roman, 12 pt

1406 Aerosol Volatility Measurements, *Aerosol Sci. Technol.*, 42, 395–407,  
 1407 doi:10.1080/02786820802104981, 2008.

1408 Hunter, J. F., Day, D. A., ~~Cappellin, L., Chan, A.,~~ Yataavelli, R. N., ~~Chan, A., Kaser, L., Cappellin,~~  
 1409 ~~L., Hayes, P. L., Palm, B. B.,~~ Cross, E. B., Carrasquillo, A., ~~Hayes, P. L.,~~ Campuzano-Jost, P.,  
 1410 ~~Palm, B. B., Stark, H., Thompson, S., Kaser, L., Karl,~~ Zhao, Y., Hohaus, T., Smith, J. N., Hansel, A.,  
 1411 ~~Jimenez, J. L., Karl, T.,~~ Goldstein, A. H., ~~Guenther, A.,~~ Worsnop, D. R., Thornton, J. A., Heald, C.  
 1412 ~~L., Jimenez, J. L.~~ and Kroll, J. H.: Comprehensive characterization of atmospheric organic  
 1413 carbon, *in prep.*, 2015 at a forested site, submitted, 2016.

1414 IPCC: IPCC 2013: Climate Change 2013: The Physical Science Basis. Contribution of Working  
 1415 Group I to the Fifth Assessment Report of the Intergovernmental Panel on Climate Change,  
 1416 edited by T. F. Stocker, D. Qin, G. Plattner, M. Tignor, S. K. Allen, V. Bex, and P. M. Midgley,  
 1417 Cambridge University Press, Cambridge, United Kingdom and New York, NY, USA, 2013.

1418 Jimenez, J. L., Canagaratna, M. R., Donahue, N. M., Prevot, ~~a~~A., S. H., Zhang, Q., Kroll, J. H.,  
 1419 DeCarlo, P. F., Allan, J. D., Coe, H., Ng, N. L., Aiken, ~~a~~A., C., Docherty, K. S., Ulbrich, I. M.,  
 1420 Grieshop, ~~a~~A., P., Robinson, ~~a~~A., L., Duplissy, J., Smith, J. D., Wilson, K. R., Lanz, V. A.,  
 1421 Hueglin, C., Sun, Y. L., Tian, J., Laaksonen, A., Raatikainen, T., Rautiainen, J., Vaattovaara, P.,  
 1422 Ehn, M., Kulmala, M., Tomlinson, J. M., Collins, D. R., Cubison, M. J., Dunlea, J., Huffman, J.  
 1423 ~~a~~, Onasch, T. B., Alfarra, M. R., Williams, P. I., Bower, K., Kondo, Y., Schneider, J., Drewnick, F., Borrmann,  
 1424 S., Weimer, S., Demerjian, K., Salcedo, D., Cottrell, L., Griffin, R., Takami, ~~a~~, Miyoshi, T., Hatakeyama, S.,  
 1425 Shimono, ~~a~~, Sun, J. Y., Zhang, Y. M., Dzepina, K., Kimmel, J. R., Sueper, D., Jayne, J. T., Herndon, S. C.,  
 1426 Trimborn, ~~a~~ M., Williams, L. R., Wood, E. C., Middlebrook, A. M., Kolb, C. E., Baltensperger, U., Worsnop,  
 1427 ~~D. R., Dunlea, E. J., Huffman, J. ~~a~~, A.~~ Onasch, T. B., Alfarra, M. R., Williams, P. I., Bower, K.,  
 1428 Kondo, Y., Schneider, J., Drewnick, F., Borrmann, S., Weimer, S., Demerjian, K., Salcedo, D.,  
 1429 Cottrell, L., Griffin, R., Takami, ~~a~~, A., Miyoshi, T., Hatakeyama, S., Shimono, ~~a~~, A., Sun, J. Y.,  
 1430 Zhang, Y. M., Dzepina, K., Kimmel, J. R., Sueper, D., Jayne, J. T., Herndon, S. C., Trimborn,  
 1431 ~~a~~A., M., Williams, L. R., Wood, E. C., Middlebrook, A. M., Kolb, C. E., Baltensperger, U. and  
 1432 Worsnop, D. R.: Evolution of ~~organic aerosols~~ **Organic Aerosols** in the ~~atmosphere,~~ **Atmosphere**,  
 1433 *Science*, 326, 1525–~~91529~~, doi:10.1126/science.1180353, 2009.

1434 Julin, J., Winkler, P. M. P., Donahue, N. M., Wagner, P. E. and Riipinen, I.: Near-unity mass  
 1435 accommodation coefficient of organic molecules of varying structure., *Environ. Sci. Technol.*,  
 1436 48, 12083–9, doi:10.1021/es501816h, 2014.

1437 Kang, E., Root, M. J., Toohey, D. W. and Brune, W. H.: Introducing the concept of Potential  
 1438 Aerosol Mass (PAM), *Atmos. Chem. Phys.*, 7, 5727–5744, doi:10.5194/acp-7-5727-2007, 2007.

1439 Kang, E., Toohey, D. W. and Brune, W. H.: Dependence of SOA oxidation on organic aerosol  
 1440 mass concentration and OH exposure: experimental PAM chamber studies, *Atmos. Chem. Phys.*,  
 1441 11, 1837–1852, doi:10.5194/acp-11-1837-2011, 2011.

1442 Karl, T., Hansel, A., Cappellin, L., Kaser, L., Herdinger-Blatt, I. and Jud, W.: Selective  
 1443 measurements of isoprene and 2-methyl-3-buten-2-ol based on NO<sup>+</sup><sub>3</sub> ionization mass  
 1444 spectrometry, *Atmos. Chem. Phys.*, 12, 11877–11884, doi:10.5194/acp-12-11877-2012, 2012.

Formatted: Font: Times New Roman, 12 pt

Formatted: Font: Times New Roman, 12 pt

Formatted: Font: Times New Roman, 12 pt

Formatted: Font: Times New Roman, 12 pt

Formatted: Font: Times New Roman, 12 pt

Formatted: Font: Times New Roman, 12 pt

Formatted: Font: Times New Roman, 12 pt

Formatted: Font: Times New Roman, 12 pt

Formatted: Font: Times New Roman, 12 pt

Formatted: Font: Times New Roman, 12 pt

Formatted: Font: Times New Roman, 12 pt

Formatted: Font: Times New Roman, 12 pt

Formatted: Font: Times New Roman, 12 pt

Formatted: Font: Times New Roman, 12 pt

Formatted: Font: Times New Roman, 12 pt

Formatted: Font: Times New Roman, 12 pt

Formatted: Font: Times New Roman, 12 pt

Formatted: Font: Times New Roman, 12 pt

Formatted: Font: Times New Roman, 12 pt

Formatted: Font: Times New Roman, 12 pt

Formatted: Font: Times New Roman, 12 pt

Formatted: Font: Times New Roman, 12 pt

Formatted: Font: Times New Roman, 12 pt, Superscript

Formatted: Font: Times New Roman, 12 pt

1445 Kaser, L., Karl, T., Schnitzhofer, R., Graus, M., Herdinger-Blatt, I. S., DiGangi, J. P., Sive, B.,  
 1446 Turnipseed, A., Hornbrook, R. S., Zheng, W., Flocke, F. M., Guenther, A., Keutsch, F. N., Apel,  
 1447 E. and Hansel, A.: Comparison of different real time VOC measurement techniques in a  
 1448 ponderosa pine forest, *Atmos. Chem. Phys.*, 13, 2893–2906, doi:10.5194/acp-13-2893-2013,  
 1449 2013a.

1450 Kaser, L., Karl, T., Guenther, A., Graus, M., Schnitzhofer, R., Turnipseed, A., Fischer, L.,  
 1451 Harley, P., Madronich, M., Gochis, D., Keutsch, F. N. and Hansel, A.: Undisturbed and disturbed  
 1452 above canopy ponderosa pine emissions: PTR-TOF-MS measurements and MEGAN 2.1 model  
 1453 results, *Atmos. Chem. Phys.*, 13, 11935–11947, doi:10.5194/acp-13-11935-2013, 2013a, 2013b.

1454 Kaser, L., Karl, T., Schnitzhofer, R., Graus, M., Herdinger-Blatt, I. S., DiGangi, J. P., Sive, B.,  
 1455 Turnipseed, A., Hornbrook, R. S., Zheng, W., Flocke, F. M., Guenther, A., Keutsch, F. N., Apel, E. and  
 1456 Hansel, A.: Comparison of different real time VOC measurement techniques in a ponderosa pine  
 1457 forest, *Atmos. Chem. Phys.*, 13, 2893–2906, doi:10.5194/acp-13-2893-2013, 2013b.

1458 Keller, A. and Bartscher, H.: A continuous photo-oxidation flow reactor for a defined  
 1459 measurement of the SOA formation potential of wood burning emissions, *J. Aerosol Sci.*, 49, 9–  
 1460 20, doi:10.1016/j.jaerosci.2012.02.007, 2012.

1461 Kim, S., Karl, T., Guenther, A., Tyndall, G., Orlando, J., Harley, P., Rasmussen, R. and Apel, E.:  
 1462 Emissions and ambient distributions of Biogenic Volatile Organic Compounds (BVOC) in a  
 1463 ponderosa pine ecosystem: interpretation of PTR-MS mass spectra, *Atmos. Chem. Phys.*, 10,  
 1464 1759–1771, doi:10.5194/acp-10-1759-2010, 2010.

1465 Kim, S., Wolfe, G. M., Mauldin, L., Cantrell, C., Guenther, A., Karl, T., Turnipseed, A.,  
 1466 Greenberg, J., Hall, S. R., Ullmann, K., Apel, E., Hornbrook, R., Kajii, Y., Nakashima, Y.,  
 1467 Keutsch, F. N., DiGangi, J. P., Henry, S. B., Kaser, L., Schnitzhofer, R., Graus, M., Hansel, A.,  
 1468 Zheng, W. and Flocke, F. F.: Evaluation of HO<sub>x</sub> sources and cycling using measurement-  
 1469 constrained model calculations in a 2-methyl-3-butene-2-ol (MBO) and monoterpene (MT)  
 1470 dominated ecosystem, *Atmos. Chem. Phys.*, 13, 2031–2044, doi:10.5194/acp-13-2031-2013,  
 1471 2013.

1472 Kirkby, J., Curtius, J., Almeida, J., Dunne, E., Duplissy, J., Ehrhart, S., Franchin, A., Gagné, S.,  
 1473 Ickes, L., Kürten, A., Kupc, A., Metzger, A., Riccobono, F., Rondo, L., Schobesberger, S.,  
 1474 Tsagkogeorgas, G., Wimmer, D., Amorim, A., Bianchi, F., Breitenlechner, M., David, A.,  
 1475 Dommen, J., Downard, A., Ehn, M., Flagan, R. C., Haider, S., Hansel, A., Hauser, D., Jud, W.,  
 1476 Junninen, H., Kreissl, F., Kvashin, A., Laaksonen, A., Lehtipalo, K., Lima, J., Lovejoy, E. R.,  
 1477 Makhmutov, V., Mathot, S., Mikkilä, J., Minginette, P., Mogo, S., Nieminen, T., Onnela, A.,  
 1478 Pereira, P., Petäjä, T., Schnitzhofer, R., Seinfeld, J. H., Sipilä, M., Stozhkov, Y., Stratmann, F.,  
 1479 Tomé, A., Vanhanen, J., Viisanen, Y., Vrtala, A., Wagner, P. E., Walther, H., Weingartner, E.,  
 1480 Wex, H., Winkler, P. M., Carslaw, K. S., Worsnop, D. R., Baltensperger, U., and Kulmala, M.,  
 1481 Gagne, S., Ickes, L., Kurten, A., Kupc, A., Metzger, A., Riccobono, F., Rondo, L., Schobesberger, S.,  
 1482 Tsagkogeorgas, G., Wimmer, D., Amorim, A., Bianchi, F., Breitenlechner, M., David, A., Dommen, J.,  
 1483 Downard, A., Ehn, M., Flagan, R. C., Haider, S., Hansel, A., Hauser, D., Jud, W., Junninen, H., Kreissl, F.,  
 1484 Kvashin, A., Laaksonen, A., Lehtipalo, K., Lima, J., Lovejoy, E. R., Makhmutov, V., Mathot, S., Mikkilä, J.,  
 1485 Minginette, P., Mogo, S., Nieminen, T., Onnela, A., et al.: Role of sulphuric acid, ammonia and

Formatted: Font: Times New Roman, 12 pt

Formatted: Normal, Space Before: 12 pt, No widow/orphan control, Don't adjust space between Latin and Asian text, Don't adjust space between Asian text and numbers

Formatted: Font: Times New Roman, 12 pt

Formatted: Font: Times New Roman, 12 pt

Formatted: Font: Times New Roman, 12 pt

Formatted: Font: Times New Roman, 12 pt

Formatted: Font: Times New Roman, 12 pt

Formatted: Normal, Space Before: 12 pt, No widow/orphan control, Don't adjust space between Latin and Asian text, Don't adjust space between Asian text and numbers

Formatted: Font: Times New Roman, 12 pt

Formatted: Font: Times New Roman, 12 pt

Formatted: Font: Times New Roman, 12 pt

Formatted: Font: Times New Roman, 12 pt



galactic cosmic rays in atmospheric aerosol nucleation, Nature, 476, 429–433, doi:10.1038/nature10343, 2011.

Knote, C., Hodzic, A. and Jimenez, J. L.: The effect of dry and wet deposition of condensable vapors on secondary organic aerosols concentrations over the continental US, Atmos. Chem. Phys., 15, 1–18, doi:10.5194/acp-15-1-2015, 2015.

Krechmer, J. E., Coggon, M. M., Massoli, P., Nguyen, T. B., Crounse, J. D., Hu, W., Day, D. A., Tyndall, G. S., Henze, D. K., Rivera-Rios, J. C., Nowak, J. B., Kimmel, J. R., Mauldin, R. L., Stark, H., Jayne, J. T., Sipilä, M., Junninen, H., Clair, J. M. St., Zhang, X., Feiner, P. A., Zhang, L., Miller, D. O., Brune, W. H., Keutsch, F. N., Wennberg, P. O., Seinfeld, J. H., Worsnop, D. R., Jimenez, J. L. and Canagaratna, M. R.: Formation of Low Volatility Organic Compounds and Secondary Organic Aerosol from Isoprene Hydroxyhydroperoxide Low-NO Oxidation, Environ. Sci. Technol., 49, 10330–10339, doi:10.1021/acs.est.5b02031, 2015.

Kulmala, M. and Wagner, P. E.: Mass accommodation and uptake coefficients — a quantitative comparison, J. Aerosol Sci., 32, 833–841, doi:10.1016/S0021-8502(00)00116-6, 2001.

Kuwata, M., Zorn, S. R. and Martin, S. T.: Using elemental ratios to predict the density of organic material composed of carbon, hydrogen, and oxygen, Environ. Sci. Technol., 46, 787–794, doi:10.1021/es202525q, 2012.

Lambe, A. T., Ahern, A. T., Williams, L. R., Slowik, J. G., Wong, J. P. S., Abbatt, J. P. D., Brune, W. H., Ng, N. L., Wright, J. P., Croasdale, D. R., Worsnop, D. R., Davidovits, P. and Onasch, T. B.: Characterization of aerosol photooxidation flow reactors: heterogeneous oxidation, secondary organic aerosol formation and cloud condensation nuclei activity measurements, Atmos. Meas. Tech., 4, 445–461, doi:10.5194/amt-4-445-2011, 2011a.

Lambe, A. T., Chhabra, P. S., Onasch, T. B., Brune, W. H., Hunter, J. F., Kroll, J. H., Cummings, M. J., Brogan, J. F., Parmar, Y., Worsnop, D. R., Kolb, C. E. and Davidovits, P.: Effect of oxidant concentration, exposure time, and seed particles on secondary organic aerosol chemical composition and yield, Atmos. Chem. Phys., 15, 3063–3075, doi:10.5194/acp-15-3063-2015, 2015.

Lambe, A. T., Onasch, T. B., Massoli, P., Croasdale, D. R., Wright, J. P., Ahern, A. T., Williams, L. R., Worsnop, D. R., Brune, W. H. and Davidovits, P.: Laboratory studies of the chemical composition and cloud condensation nuclei (CCN) activity of secondary organic aerosol (SOA) and oxidized primary organic aerosol (OPOA), Atmos. Chem. Phys., 11, 8913–8928, doi:10.5194/acp-11-8913-2011, 2011b.

Lambe, A. T., Chhabra, P. S., Onasch, T. B., Brune, W. H., Hunter, J. F., Kroll, J. H., Cummings, M. J., Brogan, J. F., Parmar, Y., Worsnop, D. R., Kolb, C. E. and Davidovits, P.: Effect of oxidant concentration, exposure time, and seed particles on secondary organic aerosol chemical composition and yield, Atmos. Chem. Phys., 15, 3063–3075, doi:10.5194/acp-15-3063-2015, 2015.

Lane, T. E., Donahue, N. M. and Pandis, S. N.: Effect of NO<sub>x</sub> on secondary organic aerosol concentrations, Environ. Sci. Technol., 42, 6022–6027, doi:10.1021/Es703225a, 2008.

Formatted: Font: Times New Roman, 12 pt

Formatted: Font: Times New Roman, 12 pt

Formatted: Font: Times New Roman, 12 pt

Formatted: Font: Times New Roman, 12 pt

Formatted: Normal, Space Before: 12 pt, No widow/orphan control, Don't adjust space between Latin and Asian text, Don't adjust space between Asian text and numbers

Formatted: Font: Times New Roman, 12 pt

Formatted: Font: Times New Roman, 12 pt

Formatted: Font: Times New Roman, 12 pt, Subscript

Formatted: Font: Times New Roman, 12 pt

1525 Lee, A., Goldstein, A. H., Kroll, J. H., Ng, N. L., Varutbangkul, V., Flagan, R. C. and Seinfeld,  
1526 J. H.: Gas-phase products and secondary aerosol yields from the photooxidation of 16 different  
1527 terpenes, *J. Geophys. Res.*, 111, D17305, doi:10.1029/2006JD007050, 2006.

1528 Levin, E. J. T., Prenni, A. J., Palm, B. B., Day, D. A., Campuzano-Jost, P., Winkler, P. M.,  
1529 Kreidenweis, S. M., Demott, P. J., Jimenez, J. L. and Smith, J. N.: Size-resolved aerosol  
1530 composition and its link to hygroscopicity at a forested site in Colorado, *Atmos. Chem. Phys.*,  
1531 14, 2657–2667, 2014.

1532 Li, R., Palm, B. B., Ortega, A. M., Hlywiak, J., Hu, W., Peng, Z., Day, D. A., Knote, C., Brune,  
1533 W. H., de Gouw, J. A. and Jimenez, J. L.: Modeling the Radical Chemistry in an Oxidation Flow  
1534 Reactor: Radical Formation and Recycling, Sensitivities, and the OH Exposure Estimation  
1535 Equation, *J. Phys. Chem. A*, 119, 4418–4432, doi:10.1021/jp509534k, 2015.

1536 Lim, Y. B. and Ziemann, P. J.: Effects of Molecular Structure on Aerosol Yields from OH  
1537 Radical-Initiated Reactions of Linear, Branched, and Cyclic Alkanes in the Presence of NO<sub>x</sub>,  
1538 *Environ. Sci. Technol.*, 43, 2328–2334, doi:10.1021/es803389s, 2009.

1539 Lim, Y. B., Tan, Y., Perri, M. J., Seitzinger, S. P. and Turpin, B. J.: Aqueous chemistry and its  
1540 role in secondary organic aerosol (SOA) formation, *Atmos. Chem. Phys.*, 10, 10521–10539,  
1541 doi:doi:10.5194/acp-10-10521-2010, 2010.

1542 Lim, Y. B. and Ziemann, P. J.: Effects of Molecular Structure on Aerosol Yields from OH  
1543 Radical-Initiated Reactions of Linear, Branched, and Cyclic Alkanes in the Presence of NO<sub>x</sub>,  
1544 *Environ. Sci. Technol.*, 43, 2328–2334, doi:10.1021/es803389s, 2009.

1545 Lopez-Hilfiker, F. D., Mohr, C., D'Ambro, E. L., Lutz, A., ~~Iyer, S.~~, Riedel, T. P., ~~Gaston, C. J.,~~  
1546 ~~Iyer, S., Zhang, Z., Gold, A.,~~ Surratt, J. D., Lee, B. H., Kurten, T., Hu, W. W., Jimenez, J. L.,  
1547 ~~Carlton, A. G., Baumann, K., Edgerton, E.,~~ Hallquist, M. and Thornton, J. A.: Molecular  
1548 ~~composition~~ Composition and ~~volatility~~ Volatility of ~~organic aerosol formed~~ Organic Aerosol in a  
1549 ~~polluted isoprene-rich region, Environmental~~ the Southeastern U.S.: Implications for IEPOX Derived  
1550 SOA, *Environ. Sci. Technol.*, submitted, 2015 accepted, acs.est.5b04769,  
1551 doi:10.1021/acs.est.5b04769, 2016.

1552 Mao, J., Ren, X., Brune, W. H., Olson, J. R., Crawford, J. H., Fried, ~~a~~, Huey, L. G., Cohen, R.  
1553 C., Heikes, B., Singh, H. B., Blake, D. R., Sachse, G. W., Diskin, G. S., Hall, S. R. and Shetter,  
1554 R. E.: Airborne measurement of OH reactivity during INTEX-B, *Atmos. Chem. Phys.*, 9, 163–  
1555 173, doi:10.5194/acp-9-163-2009, 2009.

1556 Matsunaga, A. and Ziemann, P. J.: Gas-Wall Partitioning of Organic Compounds in a Teflon  
1557 Film Chamber and Potential Effects on Reaction Product and Aerosol Yield Measurements,  
1558 *Aerosol Sci. Technol.*, 44, 881–892, doi:10.1080/02786826.2010.501044, 2010.

1559 McMurry, P. H. and Grosjean, D.: Gas and aerosol wall losses in Teflon film smog chambers,  
1560 *Environ. Sci. Technol.*, 19, 1176–82, doi:10.1021/es00142a006, 1985.

1561 Miracolo, M. A., Presto, A. A., Lambe, A. T., Hennigan, C. J., Donahue, N. M., Kroll, J. H.,

Formatted: Font: Times New Roman, 12 pt

Formatted: Normal, Space Before: 12 pt, No widow/orphan control, Don't adjust space between Latin and Asian text, Don't adjust space between Asian text and numbers

Formatted: Font: Times New Roman, 12 pt

Formatted: Font: Times New Roman, 12 pt

Formatted: Font: Times New Roman, 12 pt

Formatted: Normal, Space Before: 12 pt, No widow/orphan control, Don't adjust space between Latin and Asian text, Don't adjust space between Asian text and numbers

Formatted: Font: Times New Roman, 12 pt

Formatted: Font: Times New Roman, 12 pt

Formatted: Normal, Space Before: 12 pt, No widow/orphan control, Don't adjust space between Latin and Asian text, Don't adjust space between Asian text and numbers

Formatted: Font: Times New Roman, 12 pt

Formatted: Font: Times New Roman, 12 pt

Formatted: Font: Times New Roman, 12 pt

Formatted: Font: Times New Roman, 12 pt

Formatted: Font: Times New Roman, 12 pt

Formatted: Font: Times New Roman, 12 pt

Formatted: Font: Times New Roman, 12 pt

Formatted: Font: Times New Roman, 12 pt

Formatted: Font: Times New Roman, 12 pt

Worsnop, D. R. and Robinson, A. L.: Photo-Oxidation of Low-Volatility Organics Found in Motor Vehicle Emissions: Production and Chemical Evolution of Organic Aerosol Mass, Environ. Sci. Technol., 44, 1638–1643, doi:10.1021/es902635c, 2010.

Misztal, P. K., Hewitt, C. N., Wildt, J., Blande, J. D., Eller, A. S. D., Fares, S., Gentner, D. R., Gilman, J. B., Graus, M., Greenberg, J., Guenther, A. B., Hansel, A., Harley, P., Huang, M., Jardine, K., Karl, T., Kaser, L., Keutsch, F. N., Kiendler-Scharr, A., Kleist, E., Lerner, B. M., Li, T., Mak, J., Nölscher, A. C., Schnitzhofer, R., Sinha, V., Thornton, B., Warneke, C., Wegener, F., Werner, C., Williams, J., Worton, D. R., Yassaa, N. and Goldstein, A. H.: Atmospheric benzenoid emissions from plants rival those from fossil fuels, Sci. Rep., 5, 12064, doi:10.1038/srep12064, 2015.

Murphy, D. M., Cziczo, D. J., Froyd, K. D., Hudson, P. K., Matthew, B. M., Middlebrook, a. M., Peltier, R. E., Sullivan, A., Thomson, D. S. and Weber, R. J.: Single-particle mass spectrometry of tropospheric aerosol particles, J. Geophys. Res., 111, D23S32, doi:10.1029/2006jd007340, 2006.

Myhre, G., Shindell, D., Bréon, F.-M., Collins, W., Fuglestad, J., Huang, J., Koch, D., Lamarque, J.-F., Lee, D., Mendoza, B., Nakajima, T., Robock, A., Stephens, G., Takemura, T. and Zhang, H.: Anthropogenic and Natural Radiative Forcing, in Climate Change 2013: The Physical Science Basis. Contribution of Working Group I to the Fifth Assessment Report of the Intergovernmental Panel on Climate Change, edited by ~~T. F. V. B. and P. M. M.~~ Stocker, ~~T. F.~~ D. Qin, G.-K. Plattner, M. Tignor, ~~S. K.~~ Allen, J. Boschung, A. Nauels, Y. Xia, ~~V. Bex, and P. M.~~ ~~Midgley~~, Cambridge University Press, Cambridge, United Kingdom and New York, NY, USA., 2013.

Nakashima, Y., Kato, S., Greenberg, J., Harley, P., Karl, T., Turnipseed, A., Apel, E., Guenther, A., Smith, J. and Kajii, Y.: Total OH reactivity measurements in ambient air in a southern Rocky mountain ponderosa pine forest during BEACHON-SRM08 summer campaign, Atmos. Environ., 85, 1–8, doi:10.1016/j.atmosenv.2013.11.042, 2014.

Ng, N. L., Chhabra, P. S., Chan, A. W. H., Surratt, J. D., Kroll, J. H., Kwan, ~~a~~ A. J., McCabe, D. C., Wennberg, P. O., Sorooshian, A., Murphy, S. M., Dalleska, N. F., Flagan, R. C. and Seinfeld, J. H.: Effect of NO<sub>x</sub> level on secondary organic aerosol (SOA) formation from the photooxidation of terpenes, Atmos. Chem. Phys., 7, 5159–5174, doi:10.5194/acp-7-5159-2007, 2007.

Nguyen, T. B., Crounse, J. D., Teng, A. P., St. Clair, J. M., Paulot, F., Wolfe, G. M. and Wennberg, P. O.: Rapid deposition of oxidized biogenic compounds to a temperate forest, ~~Proc~~ P. Natl. Acad. Sci. ~~USA~~, 112, E392–E401, doi:10.1073/pnas.1418702112, 2015.

Ortega, A. M., Day, D. A., Cubison, M. J., Brune, W. H., Bon, D., de Gouw, J. A. and Jimenez, J. L.: Secondary organic aerosol formation and primary organic aerosol oxidation from biomass-burning smoke in a flow reactor during FLAME-3, Atmos. Chem. Phys., 13, 11551–11571, doi:10.5194/acp-13-11551-2013, 2013.

Ortega, A. M., Hayes, P. L., Peng, Z., Palm, B. B., Hu, W., Day, D. A., Li, R., Cubison, M. J.,

Formatted: Font: Times New Roman, 12 pt

Formatted: Font: Times New Roman, 12 pt

Formatted: Font: Times New Roman, 12 pt

Formatted: Font: Times New Roman, 12 pt

Formatted: Font: Times New Roman, 12 pt

Formatted: Font: Times New Roman, 12 pt

Formatted: Font: Times New Roman, 12 pt

Formatted: Normal, Space Before: 12 pt, No widow/orphan control, Don't adjust space between Latin and Asian text, Don't adjust space between Asian text and numbers

Formatted: Font: Times New Roman, 12 pt, Subscript

Formatted: Font: Times New Roman, 12 pt

Formatted: Font: Times New Roman, 12 pt

Formatted: Font: Times New Roman, 12 pt

Formatted: Font: Times New Roman, 12 pt



1601 Brune, W. H., Graus, M., Warneke, C., Gilman, J. B., Kuster, W. C., de Gouw, J. A. and  
1602 Jimenez, J. L.: Real-time measurements of secondary organic aerosol formation and aging from  
1603 ambient air in an oxidation flow reactor in the Los Angeles area, *Atmos. Chem. Phys. Discuss.*,  
1604 15, 21907–21958, doi:10.5194/acpd-15-21907-2015, 2015.

1605 Ortega, J., Turnipseed, A., Guenther, A. B., Karl, T. G., Day, D. A., Gochis, D., Huffman, J. A.,  
1606 Prenni, ~~a~~A., J., Levin, E. J. T., Kreidenweis, S. M., DeMott, P. J., Tobo, Y., Patton, E. G.,  
1607 Hodzic, ~~a~~A., Cui, Y. Y., Harley, P. C., Hornbrook, R. S., Apel, E. C., Monson, R. K., Eller, A. S.  
1608 D., Greenberg, J. P., Barth, M. C., Campuzano-Jost, P., Palm, B. B., Jimenez, J. L., Aiken, ~~a~~A.,  
1609 C., Dubey, M. K., Geron, C., Offenberg, J., Ryan, M. G., Fornwalt, P. J., Pryor, S. C., Keutsch,  
1610 F. N., DiGangi, J. P., Chan, A. W. H., Goldstein, A. H., Wolfe, G. M., Kim, S., Kaser, L.,  
1611 Schnitzhofer, R., Hansel, ~~a~~A., Cantrell, C. ~~a~~A., Mauldin, R. L. and Smith, J. N.: Overview of the  
1612 Manitou Experimental Forest Observatory: site description and selected science results from  
1613 2008 to 2013, *Atmos. Chem. Phys.*, 14, 6345–6367, doi:10.5194/acp-14-6345-2014, 2014.

1614 Pankow, J. F.: An ~~absorption model~~Absorption-Model of ~~gas/particle partitioning~~Gas-Particle  
1615 Partitioning of organic compoundsOrganic-Compounds in the ~~atmosphere~~Atmosphere, *Atmos.*  
1616 *Environ.*, 28, 185–188, doi:~~Doi~~10.1016/1352-2310(94)90093-0, 1994.

1617 Paulot, F., Crounse, J. D., Kjaergaard, H. G., Kürten, A., St Clair, J. M., Seinfeld, J. H.,  
1618 Wennberg, P. O., Kurten, A., St Clair, J. M., Seinfeld, J. H., Wennberg, P. O., Kürten, A., St  
1619 Clair, J. M., Seinfeld, J. H. and Wennberg, P. O.: Unexpected epoxide formation in the gas-phase  
1620 photooxidation of isoprene., *Science*, 325, 730–3, doi:10.1126/science.1172910, 2009.

1621 Peng, Z., Day, D. A., Stark, H., Li, R., ~~Lee-Taylor, J.~~Lee-Taylor, J., Palm, B. ~~B.~~B., Brune, W. H. ~~H.~~H. and  
1622 Jimenez, J. ~~L.~~L.: HO<sub>2</sub> radical chemistry in oxidation flow reactors with low-pressure mercury  
1623 lamps systematically examined by modeling, *Atmos. Meas. Tech. Discuss.*, 8, ~~3883–3932~~3883–  
1624 4890, doi:10.5194/~~amt~~amt-8-~~3883~~4863-2015, 2015a.

1625 Peng, Z., Day, D. A., Ortega, A. M., Palm, B. B., Hu, ~~W.~~W., Stark, H., Li, R., Tsigaridis, K.,  
1626 Brune, W. H. and Jimenez, J. L.: Non-OH chemistry in oxidation flow reactors for the study of  
1627 atmospheric chemistry systematically examined by modeling, *Atmos. Chem. Phys. Discuss.*, 15,  
1628 23543–23586, doi:~~doi~~10.5194/acpd-15-23543-2015, 2015b.

1629 Petters, M. D. and Kreidenweis, S. M.: A single parameter representation of hygroscopic growth  
1630 and cloud condensation nucleus activity. Atmos. Chem. Phys., 7, 1961–1971, doi:10.5194/acp-7-  
1631 1961-2007, 2007.

1632 Pierce, J. R., Engelhart, G. J., Hildebrandt, L., Weitkamp, E. ~~a~~A., Pathak, R. K., Donahue, N. M.,  
1633 Robinson, ~~a~~A., L., Adams, P. J. and Pandis, S. N.: Constraining Particle Evolution from Wall  
1634 Losses, Coagulation, and Condensation-Evaporation in Smog-Chamber Experiments: Optimal  
1635 Estimation Based on Size Distribution Measurements, *Aerosol Sci. Technol.*, 42, 1001–1015,  
1636 doi:10.1080/02786820802389251, 2008.

1637 Pirjola, L., Kulmala, M., Wilck, M., Bischoff, A., Stratmann, F. and Otto, E.: Formation ~~of~~  
1638 ~~sulphuric acid aerosols and cloud condensation nuclei~~Of Sulphuric Acid Aerosols And Cloud  
1639 Condensation Nuclei; An ~~expression for significant nucleation and model comparison~~Expression For

Formatted: Font: Times New Roman, 12 pt

Formatted: Font: Times New Roman, 12 pt

Formatted: Font: Times New Roman, 12 pt

Formatted: Font: Times New Roman, 12 pt

Formatted: Font: Times New Roman, 12 pt

Formatted: Font: Times New Roman, 12 pt

Formatted: Font: Times New Roman, 12 pt

Formatted: Font: Times New Roman, 12 pt

Formatted: Font: Times New Roman, 12 pt

Formatted: Font: Times New Roman, 12 pt

Formatted: Font: Times New Roman, 12 pt

Formatted: Font: Times New Roman, 12 pt

Formatted: Font: Times New Roman, 12 pt

Formatted: Font: Times New Roman, 12 pt

Formatted: Font: Times New Roman, 12 pt

Formatted: Font: Times New Roman, 12 pt

Formatted: Font: Times New Roman, 12 pt, Subscript

Formatted: Font: Times New Roman, 12 pt

Formatted: Font: Times New Roman, 12 pt

Formatted: Font: Times New Roman, 12 pt

Formatted: Font: Times New Roman, 12 pt

Formatted: Font: Times New Roman, 12 pt

Formatted: Font: Times New Roman, 12 pt

Formatted: Font: Times New Roman, 12 pt

Formatted: Normal, Space Before: 12 pt, No widow/orphan control, Don't adjust space between Latin and Asian text, Don't adjust space between Asian text and numbers

Formatted: Font: Times New Roman, 12 pt

Formatted: Font: Times New Roman, 12 pt

1640 Significant Nucleation And Model Comparison, J. Aerosol Sci., 30, 1079–1094,  
 1641 doi:10.1016/S0021-8502(98)00776-9, 1999.

1642 Pope, C. A. and Dockery, D. W.: Health Effects of Fine Particulate Air Pollution: Lines that  
 1643 Connect, J. Air Waste Manage. Assoc., 56, 709–742, doi:10.1080/10473289.2006.10464485,  
 1644 2006.

1645 Pöschl, U., Canagaratna, M., Jayne, J. T., Molina, L. T., Worsnop, D. R., Kolb, C. E. and  
 1646 Molina, M. J.: Mass Accommodation Coefficient of H<sub>2</sub>SO<sub>4</sub> Vapor on Aqueous Sulfuric Acid  
 1647 Surfaces and Gaseous Diffusion Coefficient of H<sub>2</sub>SO<sub>4</sub> in N<sub>2</sub>/H<sub>2</sub>O, J. Phys. Chem. A, 102, 10082–  
 1648 10089, doi:10.1021/jp982809s, 1998.

1649 Presto, A. A., Miracolo, M. A., Donahue, N. M. and Robinson, A. L.: Secondary ~~organic aerosol~~  
 1650 ~~formation~~Organic Aerosol Formation from ~~high-NO(x)-photo-oxidation~~High-NOx Photo-Oxidation  
 1651 of ~~low-volatility precursors: n-alkanes~~,Low Volatility Precursors: N-Alkanes, Environ. Sci.  
 1652 Technol., 44, 2029–~~34~~2034, doi:10.1021/es903712r, 2010.

1653 Robinson, A. L., Donahue, N. M., Shrivastava, M. K., Weitkamp, E. A., Sage, A. M., Grieshop,  
 1654 A. P., Lane, T. E., Pierce, J. R. and Pandis, S. N.: Rethinking Organic Aerosols: Semivolatile  
 1655 Emissions and Photochemical Aging, Science, 315, 1259–1262, doi:10.1126/science.1133061,  
 1656 2007.

1657 Salcedo, D., Onasch, T. B., Dzepina, K., Canagaratna, M. R., Zhang, Q., Huffman, J. A.,  
 1658 DeCarlo, P. F., Jayne, J. T., Mortimer, P., Worsnop, D. R., Kolb, C. E., Johnson, K. S., Zuberi,  
 1659 B., Marr, L. C., Volkamer, R., Molina, L. T., Molina, M. J., Cardenas, B., Bernabé, R. M.,  
 1660 Márquez, C., Gaffney, J. S., Marley, N. A., Laskin, A., Shutthanandan, V., Xie, Y., Brune, W.,  
 1661 Leshner, R., Shirley, T. and Jimenez, J. L.: Characterization of ambient aerosols in Mexico City  
 1662 during the MCMA-2003 campaign with Aerosol Mass Spectrometry: results from the CENICA  
 1663 Supersite, Atmos. Chem. Phys., 6, 925–946, doi:10.5194/acp-6-925-2006, 2006.

1664 Sander, S. P., Friedl, R. R., Barker, J. R., Golden, D. M., Kurylo, M. J., Sciences, G. E., Wine, P. H.,  
 1665 Abbatt, J. P. D., Burkholder, J. B., Kolb, C. E., Moortgat, G. K., Huie, R. E., Orkin, V. L., Barker, J. R.,  
 1666 Burkholder, J. B., Friedl, R. R., Golden, D. M., Huie, R. E., Kolb, C. E., Kurylo, M. J., Moortgat,  
 1667 G. K., Orkin, V. L. and Wine, P. H.: Chemical Kinetics and Photochemical Data for Use in  
 1668 Atmospheric Studies Evaluation Number 17-NASA Panel for Data Evaluation, JPL Publ. 10-6, 2011.

1669 Seinfeld, J. H. and Pandis, S. N.: Atmospheric ~~Chemistry~~chemistry and ~~Physics~~physics: from air  
 1670 ~~pollution to climate change~~, 2nd ed., John Wiley & Sons, Inc., Hoboken, New York, Jersey, USA,  
 1671 2006.

1672 Slowik, J. G., Stroud, C., Bottenheim, J. W., Brickell, P. C., Chang, R. Y.-W., Liggio, J., Makar,  
 1673 P. A., Martin, R. V., Moran, M. D., Shantz, N. C., Sjostedt, S. J., van Donkelaar, A., Vlasenko,  
 1674 A., Wiebe, H. A., Xia, A. G., Zhang, J., Leaitch, W. R. and Abbatt, J. P. D.: Characterization of a  
 1675 large biogenic secondary organic aerosol event from eastern Canadian forests, Atmos. Chem.  
 1676 Phys., 10, 2825–2845, doi:10.5194/acp-10-2825-2010, 2010.

1677 Smith, J. D., Kroll, J. H., Cappa, C. D., Che, D. L., Liu, C. L., Ahmed, M., Leone, S. R.,

Formatted: Font: Times New Roman, 12 pt

Formatted: Font: Times New Roman, 12 pt, Subscript

Formatted: Font: Times New Roman, 12 pt

Formatted: Font: Times New Roman, 12 pt, Subscript

Formatted: Font: Times New Roman, 12 pt

Formatted: Font: Times New Roman, 12 pt, Subscript

Formatted: Font: Times New Roman, 12 pt

Formatted: Font: Times New Roman, 12 pt, Subscript

Formatted: Font: Times New Roman, 12 pt

Formatted: Font: Times New Roman, 12 pt, Subscript

Formatted: Font: Times New Roman, 12 pt

Formatted: Font: Times New Roman, 12 pt, Subscript

Formatted: Font: Times New Roman, 12 pt

Formatted: Font: Times New Roman, 12 pt, Subscript

Formatted: Font: Times New Roman, 12 pt

Formatted: Font: Times New Roman, 12 pt, Subscript

Formatted: Font: Times New Roman, 12 pt

Formatted: Font: Times New Roman, 12 pt, Subscript

Formatted: Font: Times New Roman, 12 pt

Formatted: Font: Times New Roman, 12 pt

Formatted: Normal, Space Before: 12 pt, No widow/orphan control, Don't adjust space between Latin and Asian text, Don't adjust space between Asian text and numbers

Formatted: Font: Times New Roman, 12 pt

Formatted: Font: Times New Roman, 12 pt

Formatted: Font: Times New Roman, 12 pt

Formatted: Font: Times New Roman, 12 pt

Formatted: Font: Times New Roman, 12 pt

Formatted: Font: Times New Roman, 12 pt

Formatted: Font: Times New Roman, 12 pt

Formatted: Font: Times New Roman, 12 pt

Formatted: Normal, Space Before: 12 pt, No widow/orphan control, Don't adjust space between Latin and Asian text, Don't adjust space between Asian text and numbers

Worsnop, D. R. and Wilson, K. R.: The heterogeneous reaction of hydroxyl radicals with sub-micron squalane particles: a model system for understanding the oxidative aging of ambient aerosols, *Atmos. Chem. Phys.*, 9, 3209–3222, doi:10.5194/acpd-9-3209-2009, 2009.

Surratt, J. D., Chan, A. W. H., Eddingsaas, N. C., Chan, M., Loza, C. L., Kwan, A. J., Hersey, S. P., Flagan, R. C., Wennberg, P. O. and Seinfeld, J. H.: Reactive intermediates revealed in secondary organic aerosol formation from isoprene., *Proc. Natl. Acad. Sci. U.S.A.*, 107, 6640–5, doi:10.1073/pnas.0911114107, 2010.

Tanaka, P. L., Allen, D. T. and Mullins, C. B.: An environmental chamber investigation of chlorine-enhanced ozone formation in Houston, Texas, *J. Geophys. Res.*, 108, 4576, doi:10.1029/2002JD003314, 2003.

Tang, M. J., Shiraiwa, M., Pöschl, U., Cox, R. A. and Kalberer, M.: Compilation and evaluation of gas phase diffusion coefficients of reactive trace gases in the atmosphere: Volume 2. Diffusivities of organic compounds, pressure-normalised mean free paths, and average Knudsen numbers for gas uptake calculations, *Atmos. Chem. Phys.*, 15, 5585–5598, doi:10.5194/acp-15-5585-2015, 2015.

Tkacik, D. S., Lambe, A. T., Jathar, S., Li, X., Presto, A. A., Zhao, Y., Blake, D., Meinardi, S., Jayne, J. T., Croteau, P. L. and Robinson, A. L.: Secondary Organic Aerosol Formation from in Use Motor Vehicle Emissions Using a Potential Aerosol Mass Reactor., *Environ. Sci. Technol.*, 48, 11235–42, doi:10.1021/es502239v, 2014.

Tkacik, D. S., Presto, A. A., Donahue, N. M. and Robinson, A. L.: Secondary organic aerosol formation from intermediate-volatility organic compounds: cyclic, linear, and branched alkanes., *Environ. Sci. Technol.*, 46, 8773–81, doi:10.1021/es301112c, 2012.

Tkacik, D. S., Lambe, A. T., Jathar, S., Li, X., Presto, A. A., Zhao, Y., Blake, D., Meinardi, S., Jayne, J. T., Croteau, P. L. and Robinson, A. L.: Secondary Organic Aerosol Formation from in Use Motor Vehicle Emissions Using a Potential Aerosol Mass Reactor, *Environ. Sci. Technol.*, 48, 11235–11242, doi:10.1021/es502239v, 2014.

Tsigaridis, K., Daskalakis, N., Kanakidou, M., Adams, P. J., Artaxo, P., Bahadur, R., Balkanski, Y., Bauer, S. E., Bellouin, N., Benedetti, A., Bergman, T., Berntsen, T. K., Beukes, J. P., Bian, H., Carslaw, K. S., Chin, M., Curci, G., Diehl, T., Easter, R. C., Ghan, S. J., Gong, S. L., Hodzic, A., Hoyle, C. R., Iversen, T., Jathar, S., Jimenez, J. L., Kaiser, J. W., Kirkevåg, A., Koch, D., Kokkola, H., Lee, Y. H., Lin, G., Liu, X., Luo, G., Ma, X., Mann, G. W., Mihalopoulos, N., Morcrette, J.-J., Müller, J.-F., Myhre, G., Myriokefalitakis, S., Ng, N. L., O'Donnell, D., Penner, J. E., Pozzoli, L., Pringle, K. J., Russell, L. M., Schulz, M., Sciare, J., Seland, Ø., Shindell, D. T., Sillman, S., Skeie, R. B., Spracklen, D., Stavrou, T., Steenrod, S. D., Takemura, T., Tiitta, P., Tilmes, S., Tost, H., van Noije, T., van Zyl, P. G., von Salzen, K., Yu, F., Wang, Z., Wang, Z., Zaveri, R. A., Zhang, H., Zhang, K., Zhang, Q. and Zhang, X.: The AeroCom evaluation and intercomparison of organic aerosol in global models, *Atmos. Chem. Phys.*, 14, 10845–10895, doi:10.5194/acp-14-10845-2014, 2014.

Tsimpidi, A. P., Karydis, V. A., Zavala, M., Lei, W., Molina, L., Ulbrich, I. M., Jimenez, J. L.

Formatted: Font: Times New Roman, 12 pt

Formatted: Font: Times New Roman, 12 pt

Formatted: Font: Times New Roman, 12 pt

Formatted: Font: Times New Roman, 12 pt

Formatted: Font: Times New Roman, 12 pt

Formatted: Font: Times New Roman, 12 pt

Formatted: Font: Times New Roman, 12 pt

Formatted: Normal, Space Before: 12 pt, No widow/orphan control, Don't adjust space between Latin and Asian text, Don't adjust space between Asian text and numbers

Formatted: Font: Times New Roman, 12 pt

Formatted: Font: Times New Roman, 12 pt

Formatted: Normal, Space Before: 12 pt, No widow/orphan control, Don't adjust space between Latin and Asian text, Don't adjust space between Asian text and numbers

Formatted: Font: Times New Roman, 12 pt

and Pandis, S. N.: Evaluation of the volatility basis-set approach for the simulation of organic aerosol formation in the Mexico City metropolitan area, *Atmos. Chem. Phys.*, 10, 525–546, doi:10.5194/acp-10-525-2010, 2010.

Tunved, P., Hansson, H.-C., Kerminen, V.-M., Ström, J., Maso, M. D., Lihavainen, H., Viisanen, Y., Aalto, P. P., Komppula, M. and Kulmala, M.: High natural aerosol loading over boreal forests., *Science*, 312, 261–3, doi:10.1126/science.1123052, 2006.

Vaden, T. D., Imre, D., Beranek, J., Shrivastava, M., Zelenyuk, A., Beranek, J., Shrivastava, M., and Zelenyuk, A.: Evaporation kinetics and phase of laboratory and ambient secondary organic aerosol., *Proc. Natl. Acad. Sci. U.S.A., USA*, 108, 2190–2195, doi:10.1073/pnas.1013391108, 2011.

Volkamer, R., Jimenez, J. L., San Martini, F., Dzepina, K., Zhang, Q., Salcedo, D., Molina, L. T., Worsnop, D. R. and Molina, M. J.: Secondary organic aerosol formation from anthropogenic air pollution: Rapid and higher than expected, *Geophys. Res. Lett.*, 33, L17811, doi:10.1029/2006GL026899, 2006.

Wolfe, G. M., Cantrell, C., Kim, S., Mauldin III, R. L., Karl, T., Harley, P., Turnipseed, A., Zheng, W., Flocke, F., Apel, E. C., Hornbrook, R. S., Hall, S. R., Ullmann, K., Henry, S. B., DiGangi, J. P., Boyle, E. S., Kaser, L., Schnitzhofer, R., Hansel, A., Graus, M., Nakashima, Y., Kajii, Y., Guenther, A., and Keutsch, F. N.: Missing peroxy radical sources within a summertime ponderosa pine forest, *Atmos. Chem. Phys.*, 14, 4715–4732, doi:10.5194/acp-14-4715-2014, 2014.

Wyche, K. P., Ryan, A. C., Hewitt, C. N., Alfarra, M. R., McFiggans, G., Carr, T., Monks, P. S., Smallbone, K. L., Capes, G., Hamilton, J. F., Pugh, T. A. M. and MacKenzie, A. R.: Emissions of biogenic volatile organic compounds and subsequent photochemical production of secondary organic aerosol in mesocosm studies of temperate and tropical plant species, *Atmos. Chem. Phys.*, 14, 12781–12801, doi:10.5194/acp-14-12781-2014, 2014.

Yatavelli, R. L. N., Stark, H., Thompson, S. L., Kimmel, J. R., Cubison, M. J., Day, D. A., Campuzano-Jost, P., Palm, B. B., Hodzic, A., Thornton, J. a., Jayne, J. T., Worsnop, D. R. and Jimenez, J. L.: Semicontinuous measurements of gas–particle partitioning of organic acids in a ponderosa pine forest using a MOVI-HRToF-CIMS, *Atmos. Chem. Phys.*, 14, 1527–1546, doi:10.5194/acp-14-1527-2014, 2014.

Zhang, H., Worton, D. R., Lewandowski, M., Ortega, J., Rubitschun, C. L., Park, J.-H., Kristensen, K., Campuzano-Jost, P., Day, D., Jimenez, J. L., Jaoui, M., Offenberg, J. H., Kleindienst, T. E., Gilman, J., Kuster, W. C., de Gouw, J., Park, C., Schade, G. W., Frossard, A., Russell, L., Kaser, L., Jud, W., Hansel, A., Cappellin, L., Karl, T., Glasius, M., Guenther, A., Goldstein, A. H., Seinfeld, J. H., Gold, A., Kamens, R. M. and Surratt, J. D.: Organosulfates as Tracers for Secondary Organic Aerosol (SOA) Formation from 2-Methyl-3-Buten-2-ol (MBO) in the Atmosphere, *Environ. Sci. Technol.*, 46, 9437–9446, doi:10.1021/es301648z, 2012.

Zhang, Q., Jimenez, J. L., Canagaratna, M. R., Allan, J. D., Coe, H., Ulbrich, I., Alfarra, M. R.,

Formatted: Font: Times New Roman, 12 pt

Formatted: Normal, Space Before: 12 pt, No widow/orphan control, Don't adjust space between Latin and Asian text, Don't adjust space between Asian text and numbers

Formatted: Font: Times New Roman, 12 pt

Formatted: Font: Times New Roman, 12 pt

Formatted: Font: Times New Roman, 12 pt

Formatted: Font: Times New Roman, 12 pt

Formatted: Font: Times New Roman, 12 pt

Formatted: Font: Times New Roman, 12 pt

Formatted: Font: Times New Roman, 12 pt

Formatted: Font: Times New Roman, 12 pt

Formatted: Font: Times New Roman, 12 pt

Formatted: Font: Times New Roman, 12 pt

Formatted: Font: Times New Roman, 12 pt

Formatted: Normal, Space Before: 12 pt, No widow/orphan control, Don't adjust space between Latin and Asian text, Don't adjust space between Asian text and numbers

Formatted: Font: Times New Roman, 12 pt

Formatted: Font: Times New Roman, 12 pt

1756 Takami, A., Middlebrook, ~~a~~A., M., Sun, Y. L., Dzepina, K., Dunlea, E., Docherty, K., DeCarlo,  
1757 P. F., Salcedo, D., Onasch, T., Jayne, J. T., Miyoshi, T., Shimon, A., Hatakeyama, S.,  
1758 Takegawa, N., Kondo, Y., Schneider, J., Drewnick, F., Borrmann, S., Weimer, S., Demerjian, K.,  
1759 Williams, P., Bower, K., Bahreini, R., Cottrell, L., Griffin, R. J., Rautiainen, J., Sun, J. Y.,  
1760 Zhang, Y. M. and Worsnop, D. R.: Ubiquity and dominance of oxygenated species in organic  
1761 aerosols in anthropogenically-influenced Northern Hemisphere midlatitudes, Geophys. Res.  
1762 Lett., 34, L13801, doi:10.1029/~~2007gl029979~~2007GL029979, 2007.

Formatted: Font: Times New Roman, 12 pt

1763 Zhang, X., Cappa, C. D., Jathar, S. H., McVay, R. C., Ensberg, J. J., Kleeman, M. J., ~~and~~  
1764 Seinfeld, J. H. ~~and Christopher D. Cappa~~: Influence of vapor wall loss in laboratory chambers on  
1765 yields of secondary organic aerosol., ~~Proc~~P. Natl. Acad. Sci. ~~U. S. A., USA~~, 111, ~~1-6~~5802-7,  
1766 doi:10.1073/pnas.1404727111, 2014.

Formatted: Font: Times New Roman, 12 pt

Formatted: Font: Times New Roman, 12 pt

Formatted: Font: Times New Roman, 12 pt

Formatted: Font: Times New Roman, 12 pt

Formatted: Font: Times New Roman, 12 pt

1767 Zhao, Y., Hennigan, C. J., May, A. A., Tkacik, D. S., ~~Gouw, J. A. De, Gilman, J. B., Kuster, W. C.,~~  
1768 ~~Borbon, A., Robinson, A. L., Daniel, S., Gouw, J. A. De, Gilman, J. B., Kuster, W. C., Robinson, A. L., Tkacik,~~  
1769 ~~D. S., Gouw, J. A. De, Gilman, J. B., Kuster, W. C., Borbon, A., Robinson, A. L., Daniel, S., Gouw, J. A. De,~~  
1770 ~~Gilman, J. B., Kuster, W. C., Robinson, A. L., Tkacik, D. S., de Gouw, J. A., Gilman, J. B., Kuster, W. C.,~~  
1771 ~~Borbon, A., Robinson, A. L., Daniel, S., Gouw, J. A. De, Gilman, J. B., Kuster, W. C.~~de Gouw, J. A.,  
1772 Gilman, J. B., Kuster, W. C., Borbon, A., and Robinson, A. L.: Intermediate-volatility organic  
1773 compounds: a large source of secondary organic aerosol., Environ. Sci. Technol., 48, 13743–50,  
1774 doi:10.1021/es5035188, 2014.

Formatted: Font: Times New Roman, 12 pt

1775 Ziemann, P. J. ~~P. J.~~ and Atkinson, R.: Kinetics, products, and mechanisms of secondary organic  
1776 aerosol formation., ~~Chem. Soc. Rev.~~, 41, 6582–~~605~~, doi:10.1039/c2cs35122f, 2012.

Formatted: Font: Times New Roman, 12 pt

Formatted: Font: Times New Roman, 12 pt

Formatted: Font: Times New Roman, 12 pt

Formatted: Font: Times New Roman, 12 pt

1778 ~~Table 1. List of prominent compounds detected by PTR-TOF-MS in the OFR. Likely compound~~  
1779 ~~identifications are taken from previous measurements at the same research site, described in Kim et al.~~  
1780 ~~(2010) and Kaser et al. (2013a).~~  
1781

1782 Table 1. List of prominent compounds detected by PTR-TOF-MS in the OFR. Likely compound  
 1783 identifications are taken from previous measurements at the same research site, described in Kim et al.  
 1784 (2010) and Kaser et al. (2013b).

Protonated molecular formula	Likely compound(s)	Exact mass ( <i>m/z</i> )
CH <sub>2</sub> O-H <sup>+</sup>	formaldehyde	31.02
CH <sub>4</sub> O-H <sup>+</sup>	methanol	33.03
C <sub>2</sub> H <sub>4</sub> O-H <sup>+</sup>	acetaldehyde	45.03
CH <sub>2</sub> O <sub>2</sub> -H <sup>+</sup>	formic acid	47.01
C <sub>3</sub> H <sub>6</sub> O-H <sup>+</sup>	acetone	59.05
C <sub>2</sub> H <sub>4</sub> O <sub>2</sub> -H <sup>+</sup>	acetic acid	61.03
C <sub>5</sub> H <sub>8</sub> -H <sup>+</sup>	MBO(~80%)+isoprene(~20%) <sup>a</sup>	69.07
C <sub>7</sub> H <sub>8</sub> -H <sup>+</sup>	toluene(74%)+p-cymene(26%) <sup>b</sup>	93.07
C <sub>10</sub> H <sub>14</sub> -H <sup>+</sup>	p-cymene	135.12
C <sub>10</sub> H <sub>16</sub> -H <sup>+</sup>	MT	137.13, 81.07
C <sub>9</sub> H <sub>14</sub> O-H <sup>+</sup>	nopinone	139.11
C <sub>10</sub> H <sub>14</sub> O-H <sup>+</sup>	pinonaldehyde(-H <sub>2</sub> O),caronaldehyde(-H <sub>2</sub> O)	151.11
C <sub>10</sub> H <sub>16</sub> O-H <sup>+</sup>	camphor+α-pinene oxide	153.13
C <sub>15</sub> H <sub>24</sub> -H <sup>+</sup>	SQT	205.20

1785 <sup>a</sup>{Karl et al., 2012, Kaser et al., 2013b}

1786 <sup>b</sup>{Kaser et al., 2013b}

1787

1788

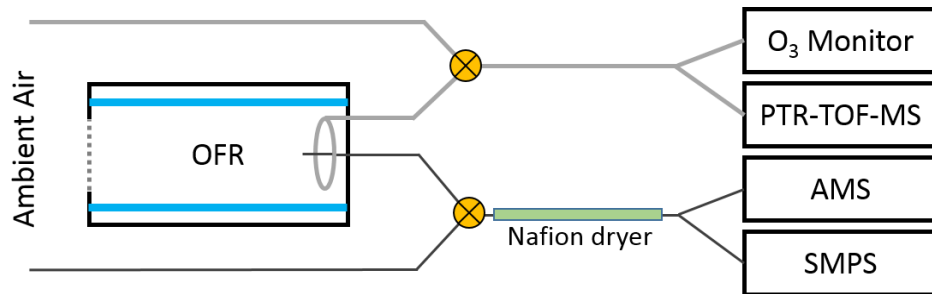
1789

1790

1791

1792

1793



<sup>a</sup>(Karl et al., 2012; Kaser et al., 2013a)

<sup>b</sup>(Kaser et al., 2013a)



1797 **Table 2.** Low-NO<sub>x</sub> SOA yield parameters using basis sets, used to estimate SOA yields from VOCs in the  
 1798 OFR (Sect. 3.6.1).

<u>SOA precursor</u>	<u>C* saturation vapor concentrations (<math>\mu\text{g m}^{-3}</math> at 298K)</u>			
	<u>1</u>	<u>10</u>	<u>100</u>	<u>1000</u>
<u>MT<sup>a</sup></u>	<u>0.107</u>	<u>0.092</u>	<u>0.359</u>	<u>0.600</u>
<u>SQT<sup>a</sup></u>	<u>0.075</u>	<u>0.150</u>	<u>0.750</u>	<u>0.900</u>
<u>Toluene<sup>a</sup></u>	<u>0.075</u>	<u>0.225</u>	<u>0.375</u>	<u>0.525</u>
	<u>C* saturation vapor concentrations (<math>\mu\text{g m}^{-3}</math> at 295K)</u>			
	<u>0.6</u>		<u>116</u>	
<u>Isoprene<sup>b</sup></u>	<u>0.0288</u>		<u>0.232</u>	

1799 <sup>a</sup>(Tsimpidi et al., 2010), not including the chemical “aging” parameterization

1800 <sup>b</sup>(Henze and Seinfeld, 2006)

1801

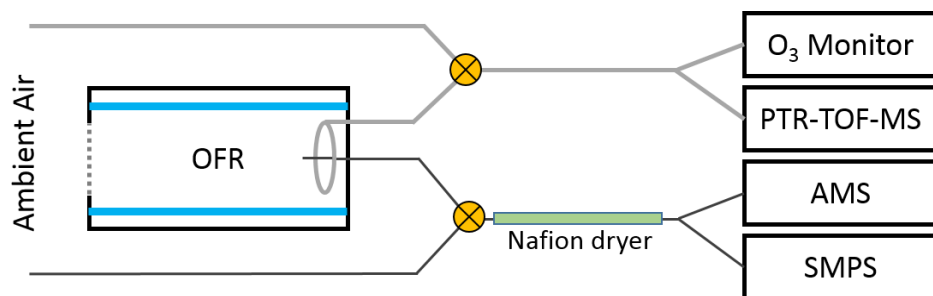
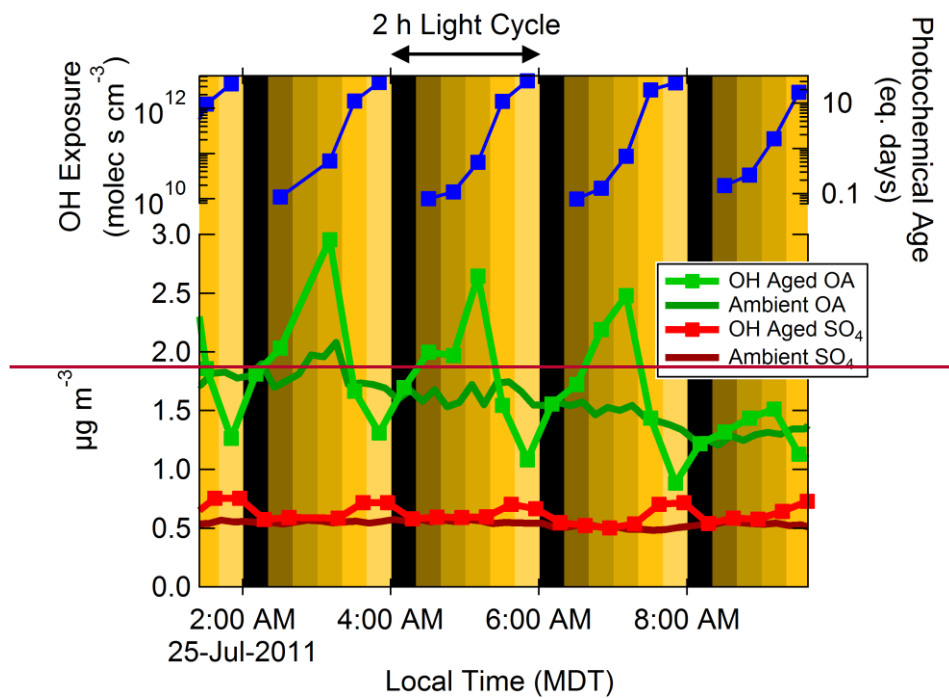


Fig. 1. Simplified schematic of the experimental setup. Ambient air was alternately sampled either directly or through the oxidation flow reactor (OFR). In the OFR, the concentration of OH was increased to simulate atmospheric aging from hours up to several weeks.



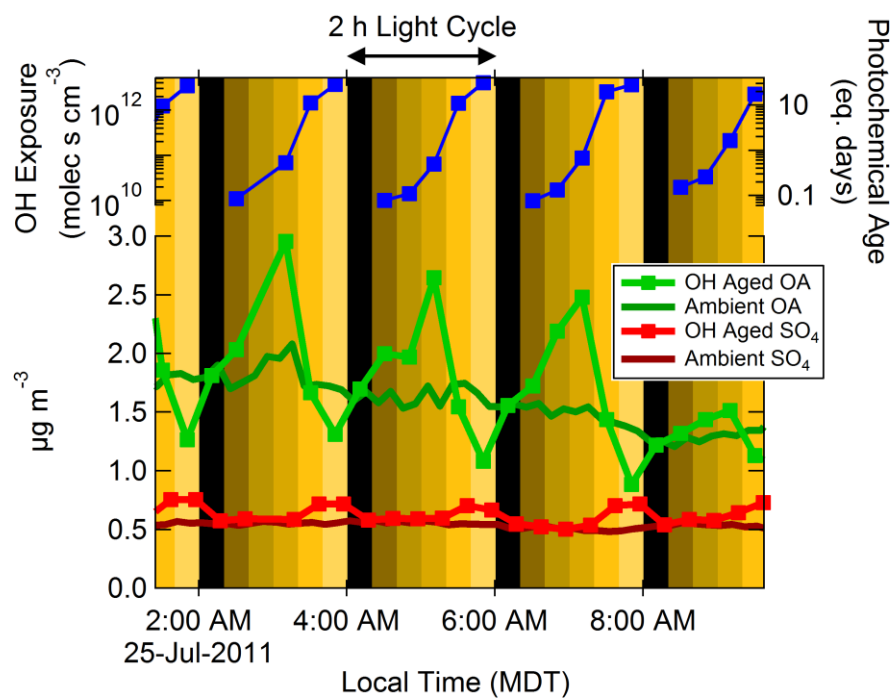
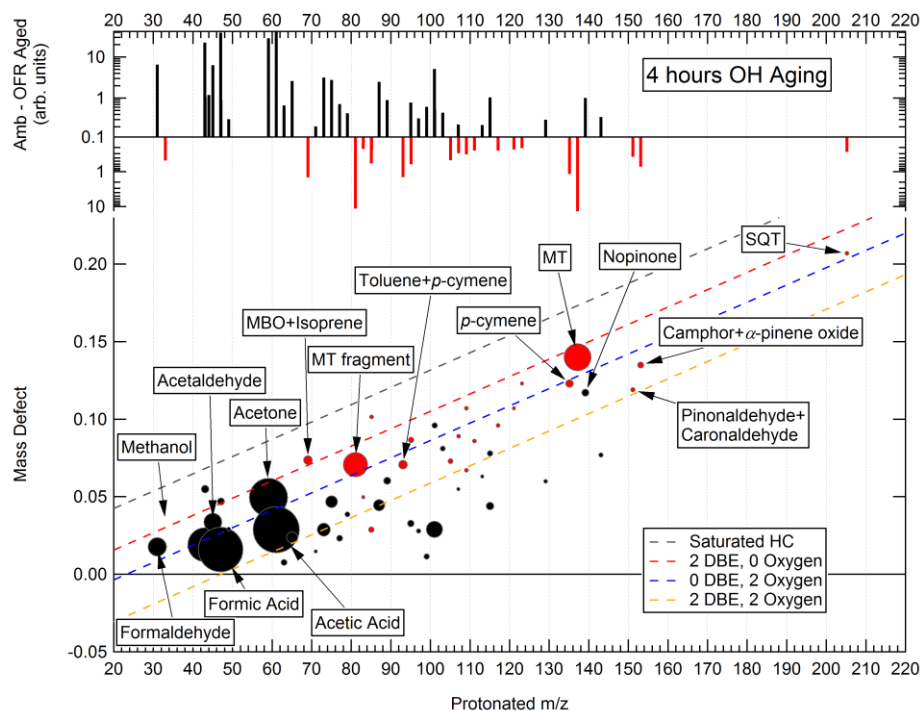


Fig. 2. Continuous cycling of OH oxidation using the OFR185 method, compared to concurrent ambient measurements. The sawtooth pattern in the OFR results from OA mass enhancement at low–intermediate OH exposure ( $\text{OH}_{\text{exp}}$ ) and decreases at the highest photochemical ages.  $\text{SO}_4$  mass increased monotonically with  $\text{OH}_{\text{exp}}$  and at higher exposures, as expected from relatively slow  $\text{SO}_2 + \text{OH}$  oxidation and lack of OH destruction of  $\text{SO}_4$ .

1820



Formatted: Space Before: 12 pt, After: 0 pt, Line spacing: 1.5 lines

1821

1822 Fig. 3. The absolute changes (signal after OH oxidation in the reactor minus ambient signal) of  
 1823 molecules measured by the PTR-TOF-MS after 4 hours of eq. aging using the OFR185 method, shown as  
 1824 a difference mass spectrum and in a mass defect diagram. The mass spectra are 10-min averages (5 min  
 1825 from each of the two sample cycles used). The background-subtracted signals are shown in arbitrary  
 1826 units, not corrected for differences in sensitivity of each compound due to the large number of  
 1827 compounds and the inability to positively identify all of them. Prominent molecules are labeled by name  
 1828 or elemental formula assignments. Dashed lines representing molecules with varying double bond  
 1829 equivalents (DBE) or number of oxygen atoms are shown for reference. A red marker signifies that the  
 1830 signal decreased due to oxidation, while a black marker indicates where signal was greater after  
 1831 oxidation. The markers are sized by the square root of the absolute change in signal at each peak after  
 1832 oxidation (i.e., marker area is proportional to signal). Minor signals with absolute change of <0.2 arb.  
 1833 units or change of <20% of total ambient signal were removed.

1834

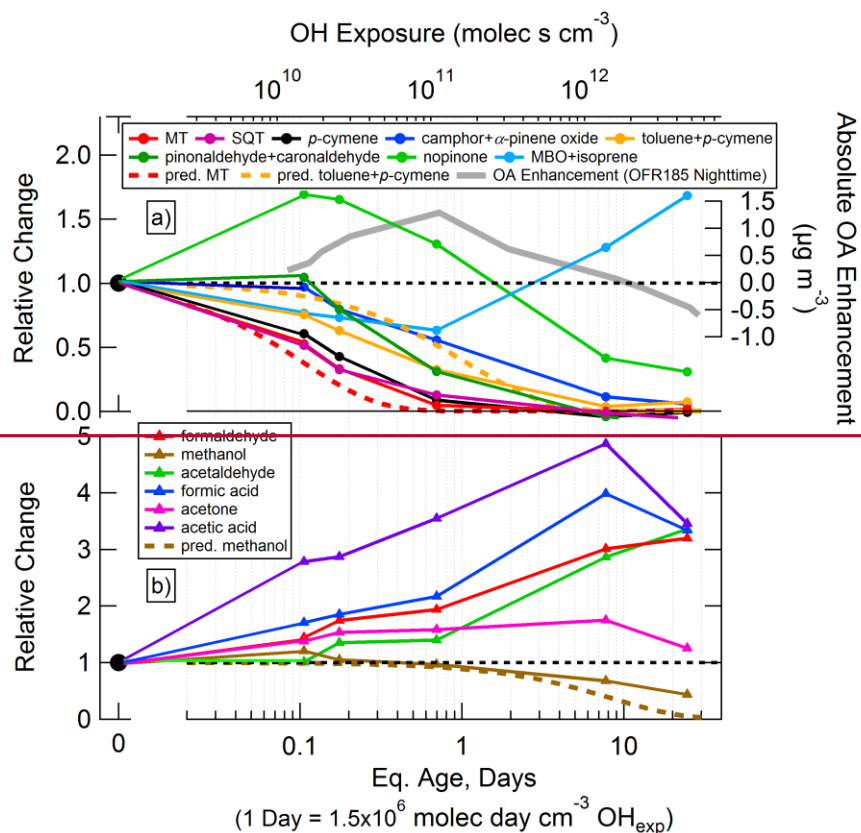
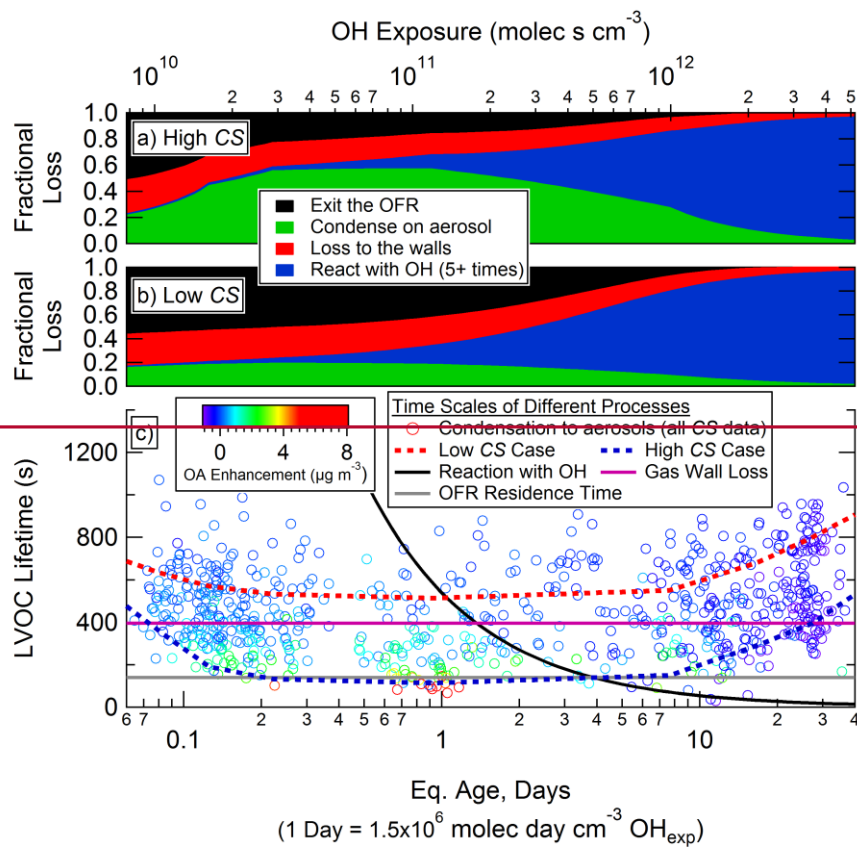


Fig. 4. Relative changes in prominent PTR-TOF MS compounds as a function of photochemical age using the OFR185 method: a) toluene+*p*-cymene and terpene-related signals compared to nighttime OA enhancement using the OFR185 method (not LVOC fate corrected), and b) oxidation products formed in the OFR. For comparison, dashed lines indicate theoretical depletion of an equal mix of  $\alpha$ -pinene,  $\beta$ -pinene, and 3-carene (the three major MT at this site; Kim et al., 2010; Ortega et al., 2014), a 74:26 mix of toluene+*p*-cymene (Kaser et al., 2013b), and methanol.





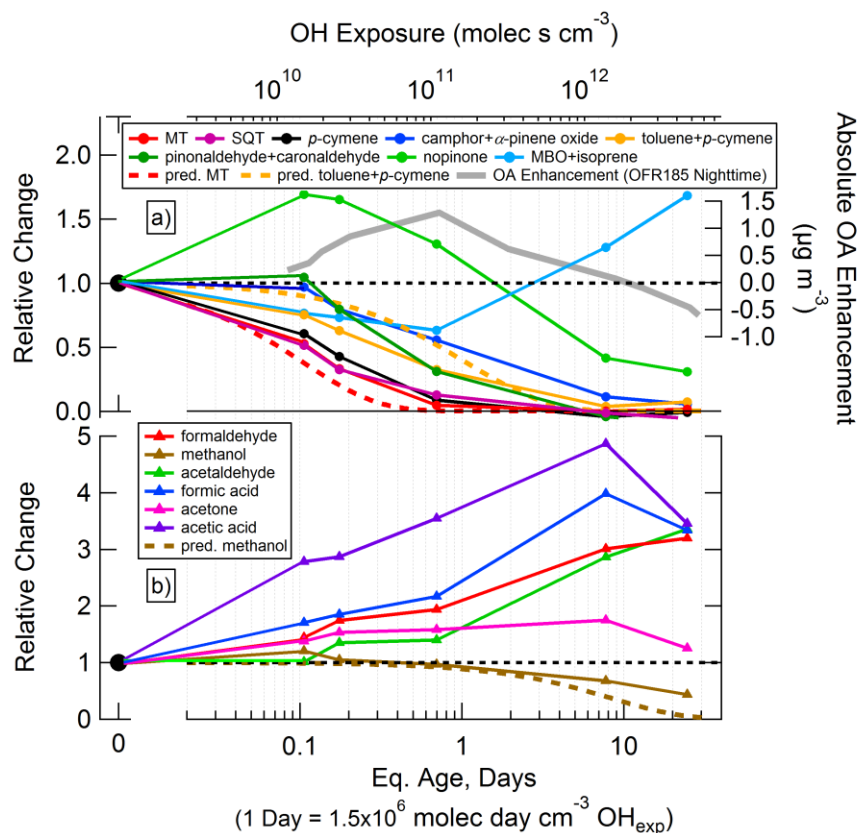
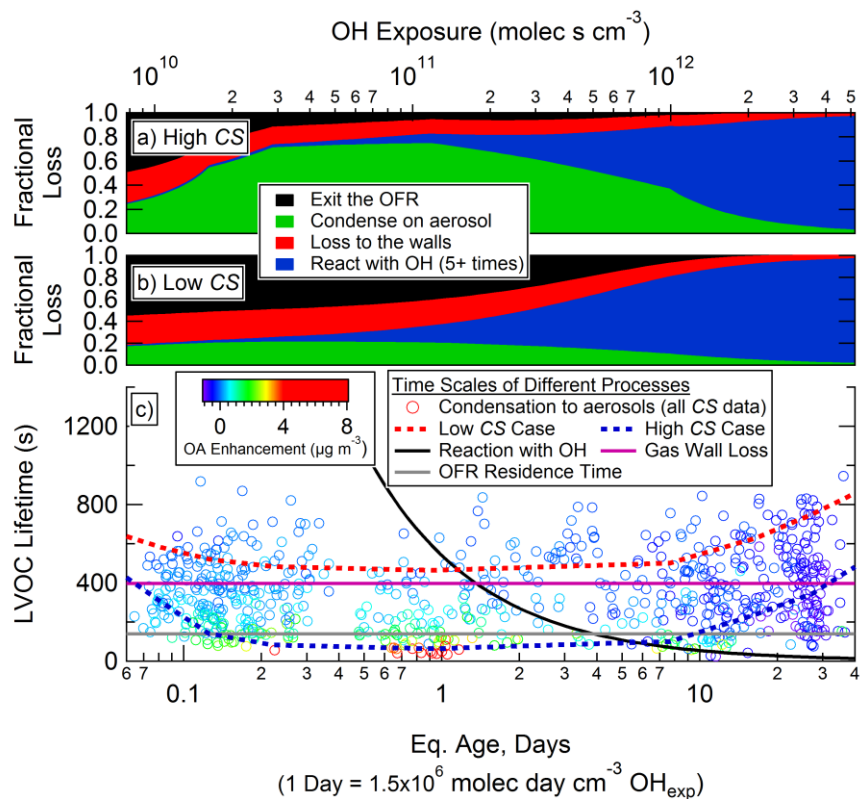


Fig. 4. Relative changes in prominent PTR-TOF-MS compounds as a function of photochemical age using the OFR185 method: a) toluene+*p*-cymene and terpene-related signals compared to nighttime OA enhancement using the OFR185 method (not LVOC fate corrected), and b) oxidation products formed in the OFR. For comparison, dashed lines indicate theoretical depletion of an equal mix of  $\alpha$ -pinene,  $\beta$ -pinene, and 3-carene (the three major MT at this site; Kim et al., 2010; Ortega et al., 2014), a 74:26 mix of toluene+*p*-cymene (Kaser et al., 2013a), and methanol.



1853

1854

1855

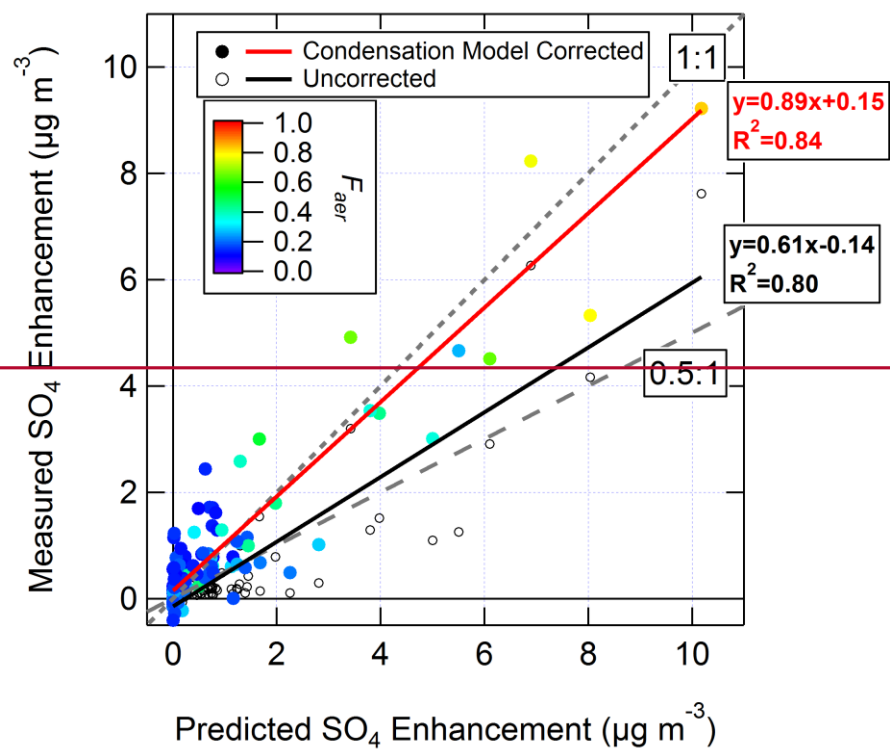
1856

1857

1858

1859

Fig. 5. Fractional fates of loss of LVOCs to OFR walls, condensation to aerosols, reaction with OH to produce volatile products, or exiting the OFR to be lost on sampling line walls as a function of photochemical age for a) high CS and b) low CS cases; c) LVOC lifetimes for each of these pathways. Lifetime for condensation to aerosols is shown for all data points (colored by OA enhancement after oxidation) using CS calculated from SMPS measurements.



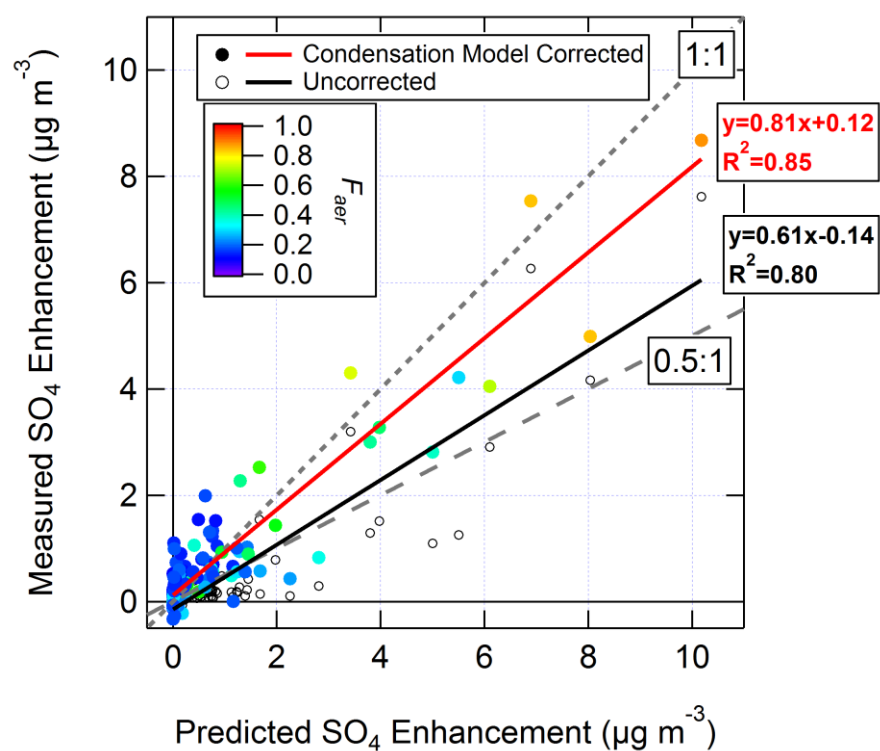
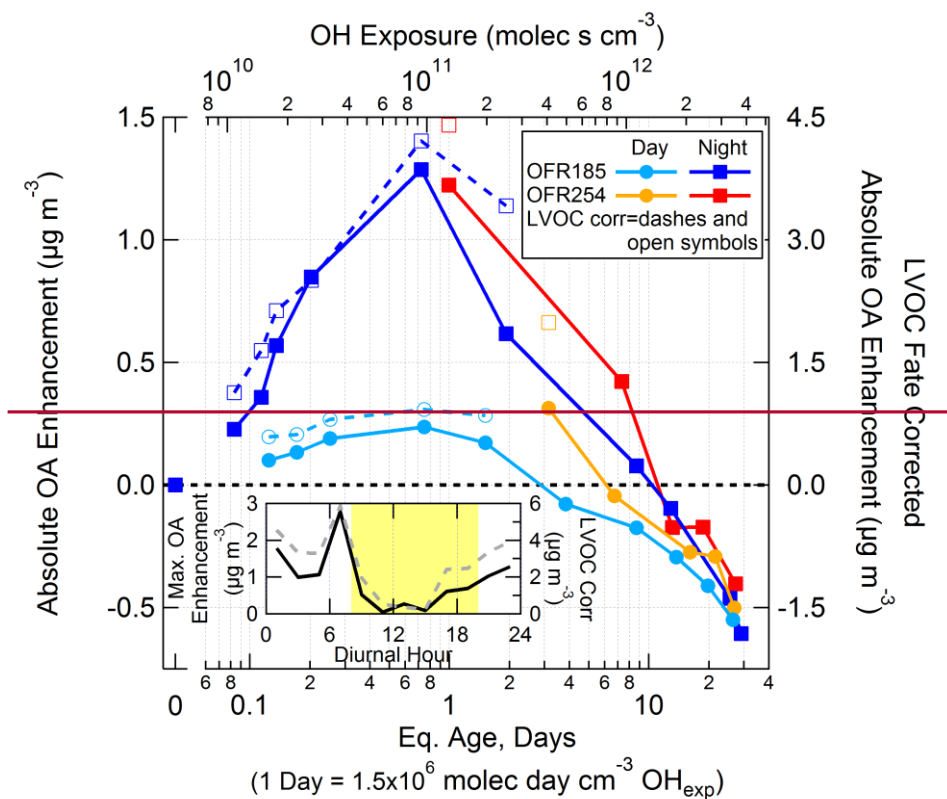


Fig. 6. Measured vs. predicted  $\text{SO}_4$  formation after OH oxidation in an OFR. The data points are colored by the fraction of  $\text{H}_2\text{SO}_4$  predicted to condense on aerosols, calculated using  $\alpha = 0.65$  and the average of the SMPS size distributions measured before and after oxidation. Data are shown with the LVOC fate correction applied, along with linear fits to the corrected (red) and uncorrected (blue) data. Ambient  $\text{SO}_2$  concentrations  $< 0.2$  ppb have been excluded from this analysis.



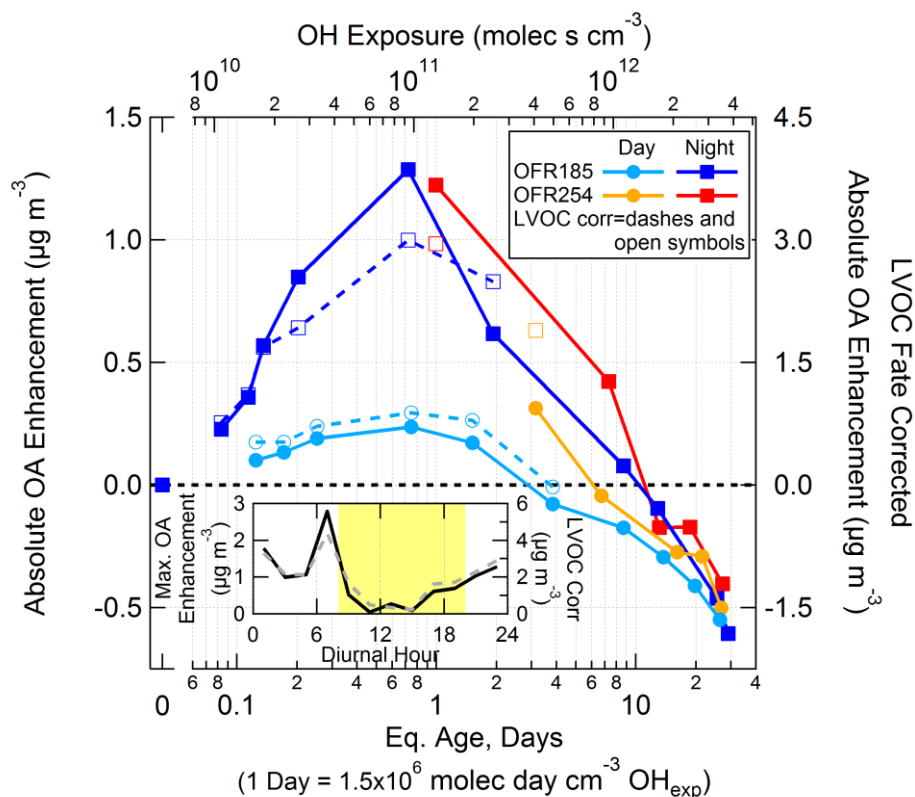
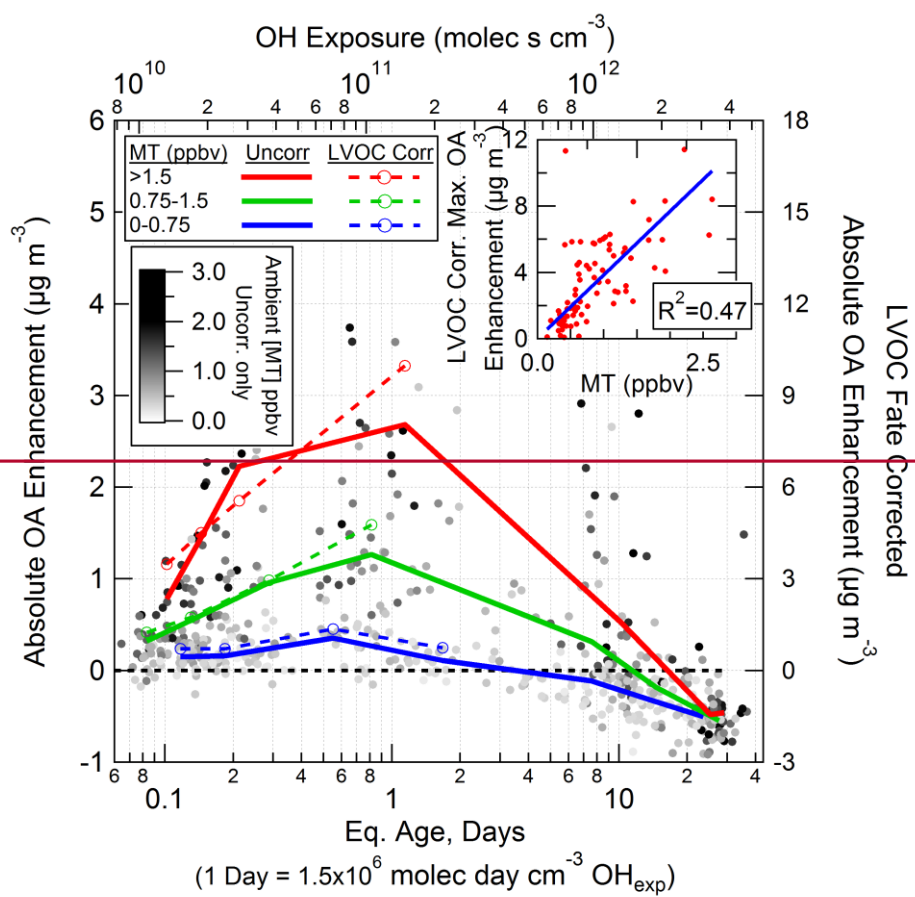


Fig. 7. Comparison of absolute OA enhancement from OH oxidation using the OFR185 and OFR254-70 methods, binned by photochemical age and separated into daytime (08:00–20:00 local time) and nighttime (20:00–08:00 local time) to reflect the changes in ambient SOA precursors between day and night. Data are shown with (right axis, open symbols, and dashed lines) and without (left axis, closed symbols and solid lines) the LVOC fate correction described in Sect. 3.3. Inset: the maximum OA enhancement (all data 0.4–1.5 days eq. age) as a function of time of day, with (dashed) and without (solid) the LVOC fate correction. OFR254-70 measurements with positive OA enhancement were multiplied by the ratio of ambient MT concentrations measured during OFR185 vs. OFR254-70 sampling periods (ratio = 1.8). Negative OA enhancements were not normalized in this way since the amount of mass lost due to heterogeneous oxidation would not necessarily correlate with ambient MT concentrations.

1885





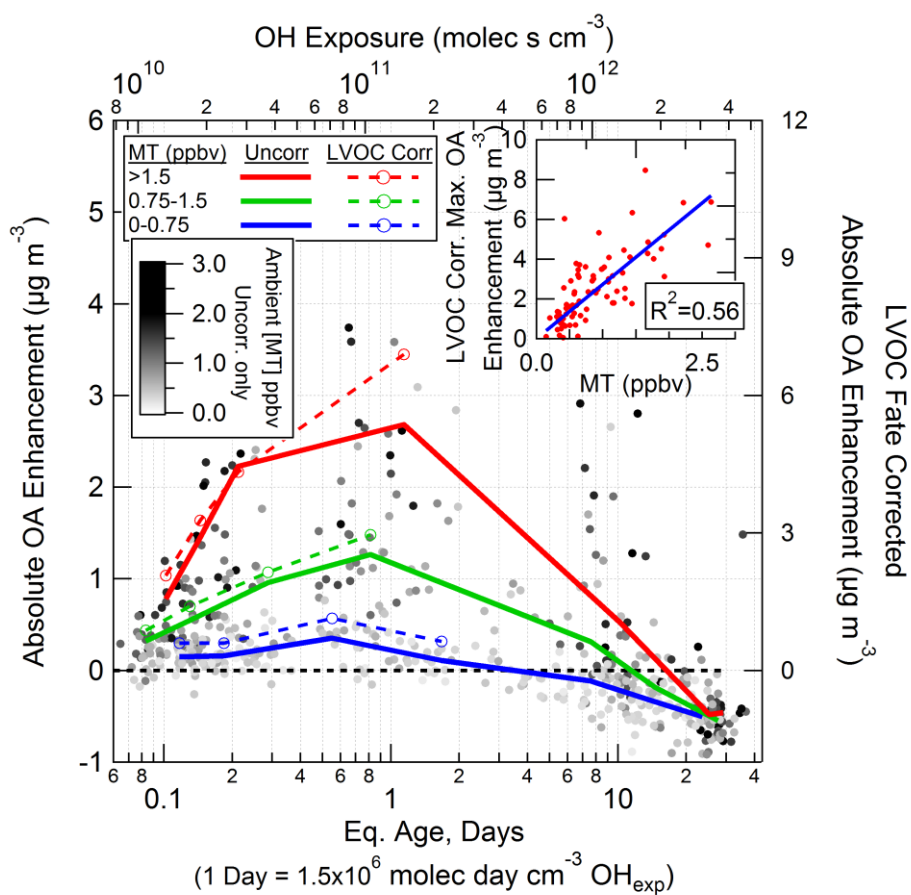
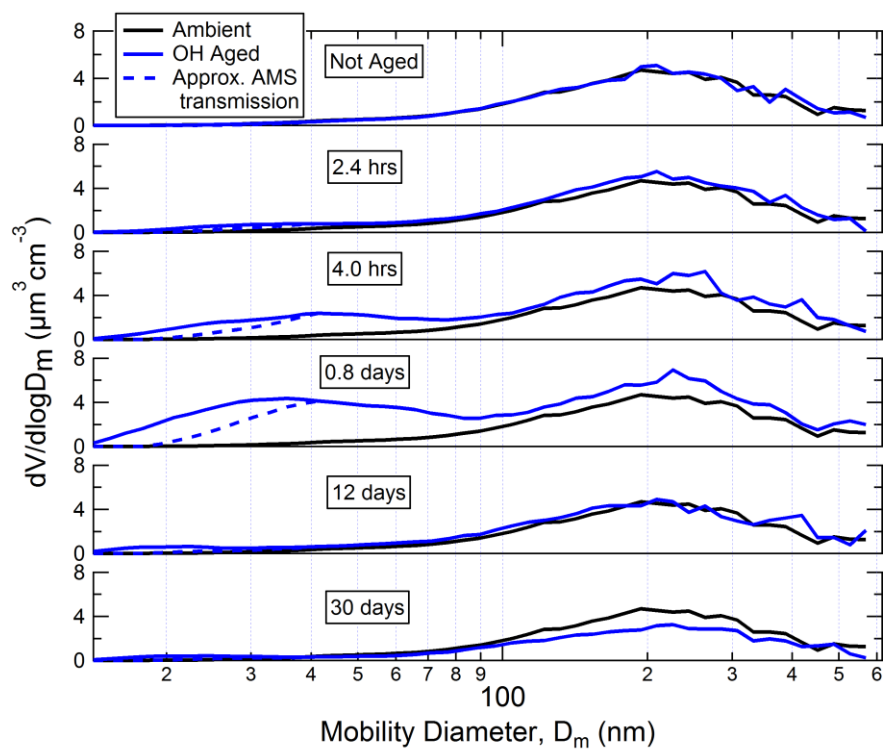


Fig. 8. OA enhancement from OH oxidation of ambient air using the OFR185 method as a function of photochemical age. All data points (uncorrected only) are shown, shaded by in-canopy monoterpene (MT) concentrations. Average OA enhancements of age quantiles with equal number of data points with (right axis, dashed lines) and without (left axis, solid lines) the LVOC fate correction are also shown, separated into low (0 to 0.75 ppbv), medium (0.75 to 1.5 ppbv), and high (>1.5 ppbv) ambient MT concentration ranges. The inset shows the correlation ( $R^2=0.4756$ ) between the LVOC fate corrected maximum OA enhancement (0.4–1.5 eq. days aging) and in-canopy MT concentrations.

Formatted: Space Before: 12 pt, After: 0 pt, Line spacing: 1.5 lines



1896

1897 Fig. 9. SMPS volume size distributions after OH oxidation using the OFR185 method, labeled by  
 1898 photochemical age and compared to concurrent ambient measurements. Each of the 6 OH-aged size  
 1899 distributions is an average of 6 SMPS scans from the night of 28–29 July, when relatively large OA  
 1900 enhancement was observed and the ambient aerosol dry surface area was in the range of 80–100  
 1901  $\mu\text{m}^2 \text{cm}^{-3}$ . Dashed lines represent the approximate size distributions that were transmitted through  
 1902 the AMS aerodynamic lens (for which a correction was applied to reported OA values as discussed in  
 1903 Sect. S3). Scans with large OA enhancement were used in order to more clearly illustrate the  
 1904 condensation vs. nucleation behavior in the OFR, so the AMS lens transmission correction in this figure  
 1905 appears larger than average. All scans have been corrected for small particle losses to sampling lines  
 1906 (Sect. S1).

1907

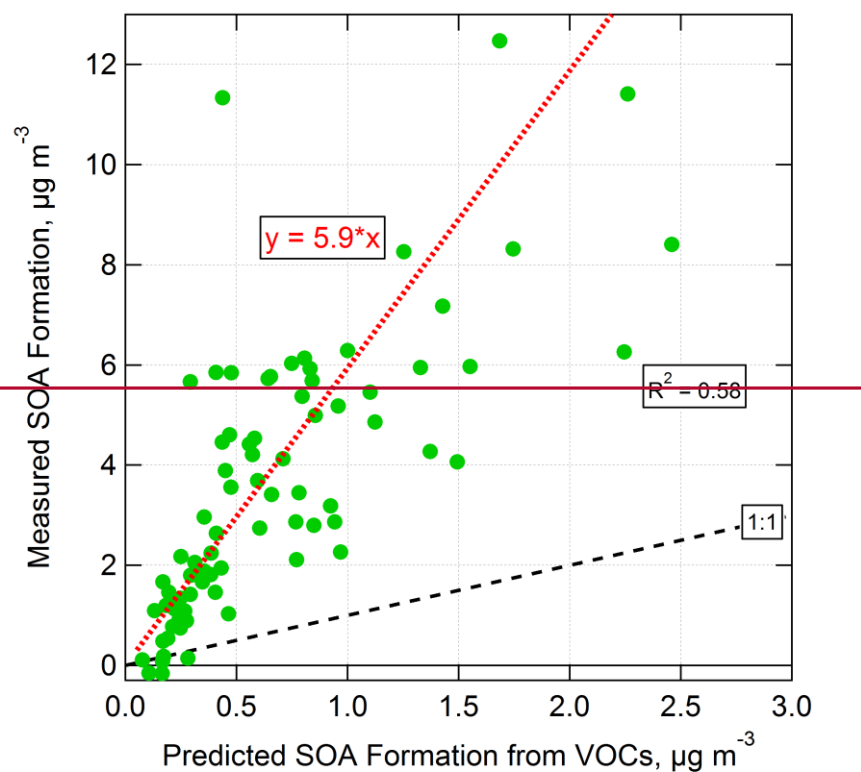
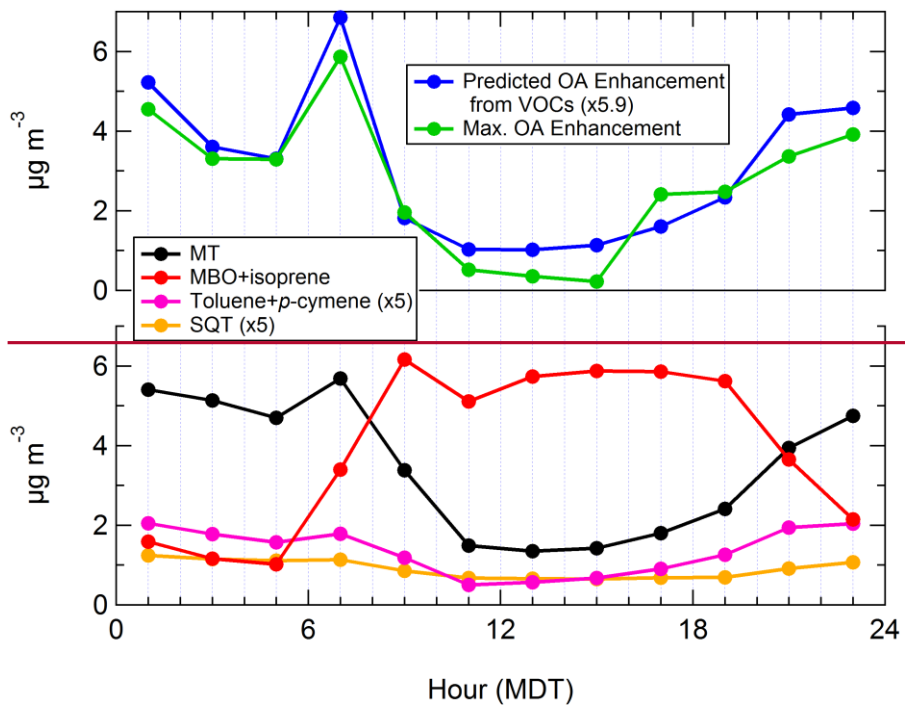


Fig. 10. Measured vs. predicted SOA formation from OH oxidation of ambient air in an OFR using the OFR185 method. Only the range of photochemical ages with the highest SOA formation (0.4–1.5 eq. days) was used, and the LVOC fate correction was applied. Predicted SOA formation was calculated by applying OA concentration-dependent yields (average of 13.3%, 14.9%, 15.9%, and 1.8% for MT, SQT, toluene+*p*-cymene, and isoprene, respectively, with average OA concentration of  $5.1 \mu\text{g m}^{-3}$ ) to VOCs reacted in the OFR (Tsimpidi et al., 2010). The amount of reacted VOCs was estimated using  $\text{OH}_{\text{exp}}$  and ambient VOC concentrations. If a non-zero y-intercept is allowed, the regression line becomes  $y = 7.0x - 1.0$ .

1918  
1919



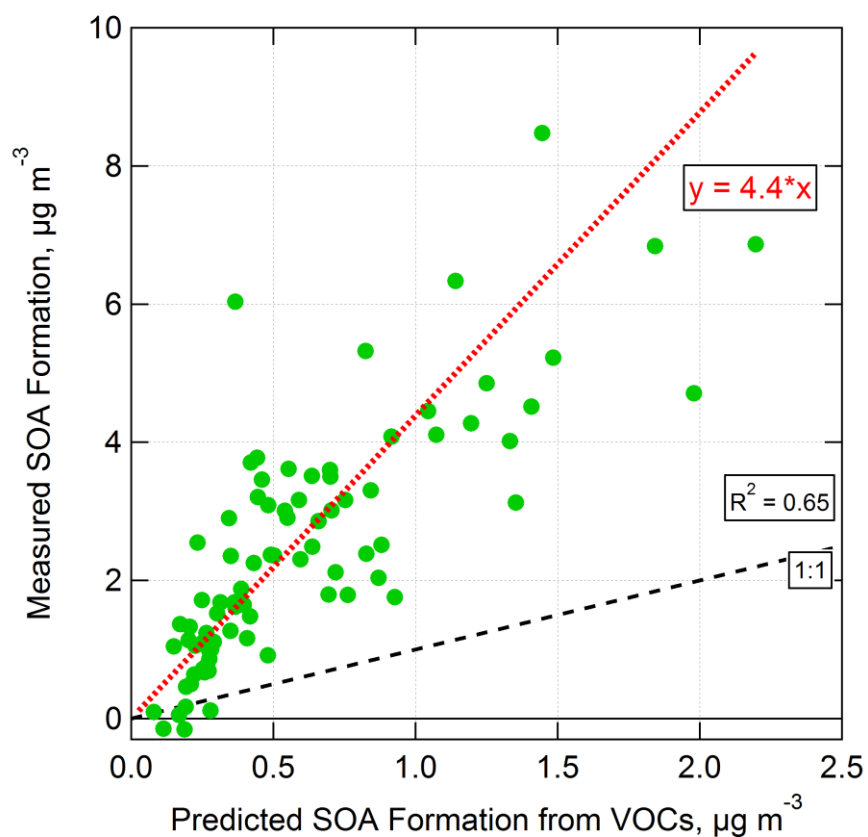


Fig. 10. Measured vs. predicted SOA formation from OH oxidation of ambient air in an OFR using the OFR185 method. Only the range of photochemical ages with the highest SOA formation (0.4–1.5 eq. days) was used, and the LVOC fate correction was applied. Predicted SOA formation was calculated by applying OA concentration-dependent yields (average of 12.5%, 13.2%, 13.8%, and 3.2% for MT, SQT, toluene+*p*-cymene, and isoprene, respectively, with average OA concentration of  $4.1 \mu\text{g m}^{-3}$ ) to VOCs reacted in the OFR (Tsimpidi et al., 2010). The amount of reacted VOCs was estimated using  $\text{OH}_{\text{exp}}$  and ambient VOC concentrations. If a non-zero y-intercept is allowed, the regression line becomes  $y = 5.0x - 0.5$ .

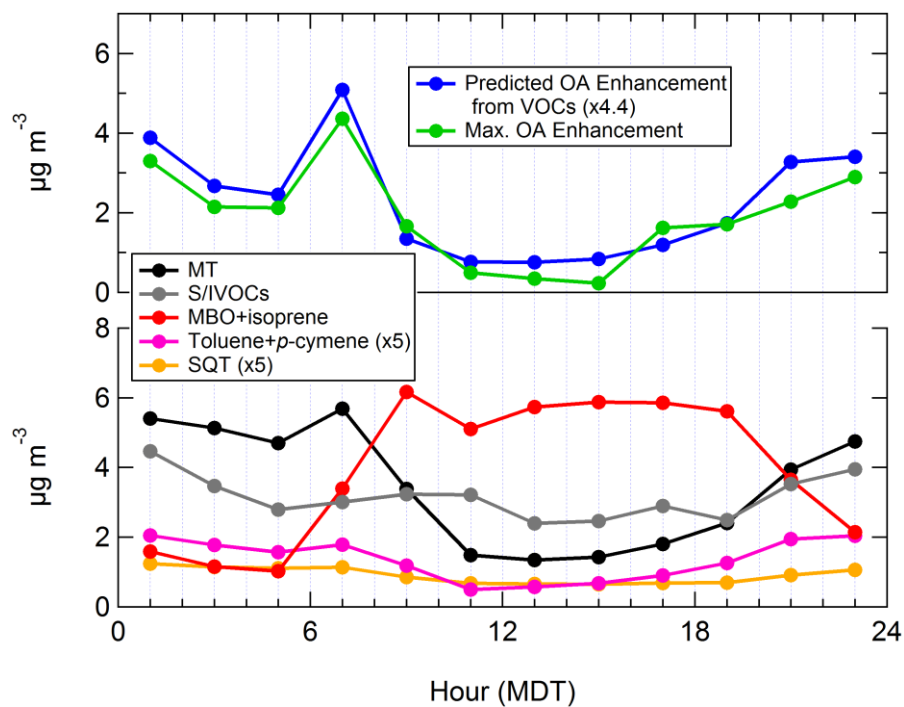
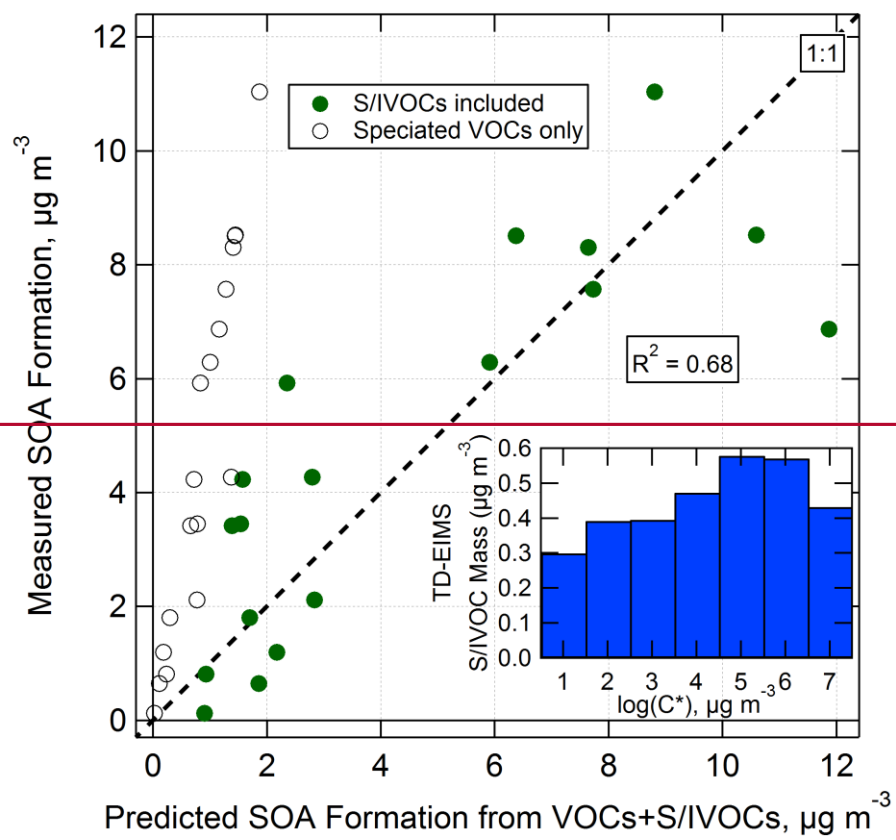


Fig. 11. Top: diurnal maximum measured OA enhancement (all data from 0.4–1.5 eq. days aging, LVOC fate corrected) in the OFR from OH oxidation using the OFR185 method, and predicted OA formation from measured VOCs (x5.9x4.4). Bottom: ambient MT, SQT (x5), toluene+p-cymene (x5), and MBO+isoprene, and S/IVOC mass concentrations vs. time of day.



1936

1937

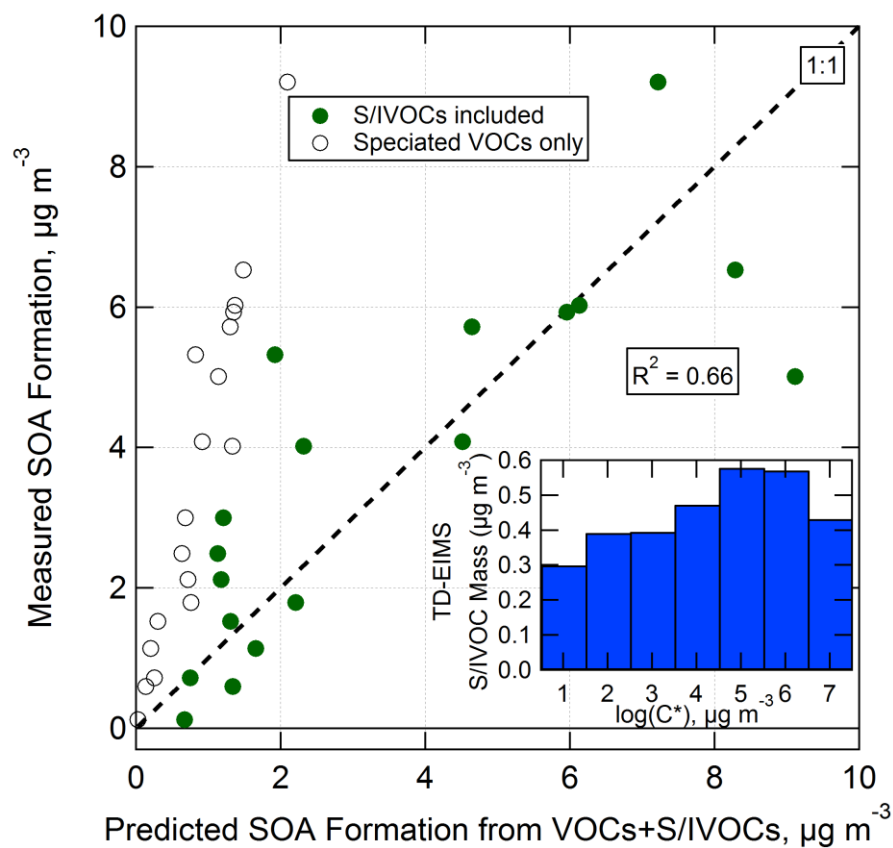
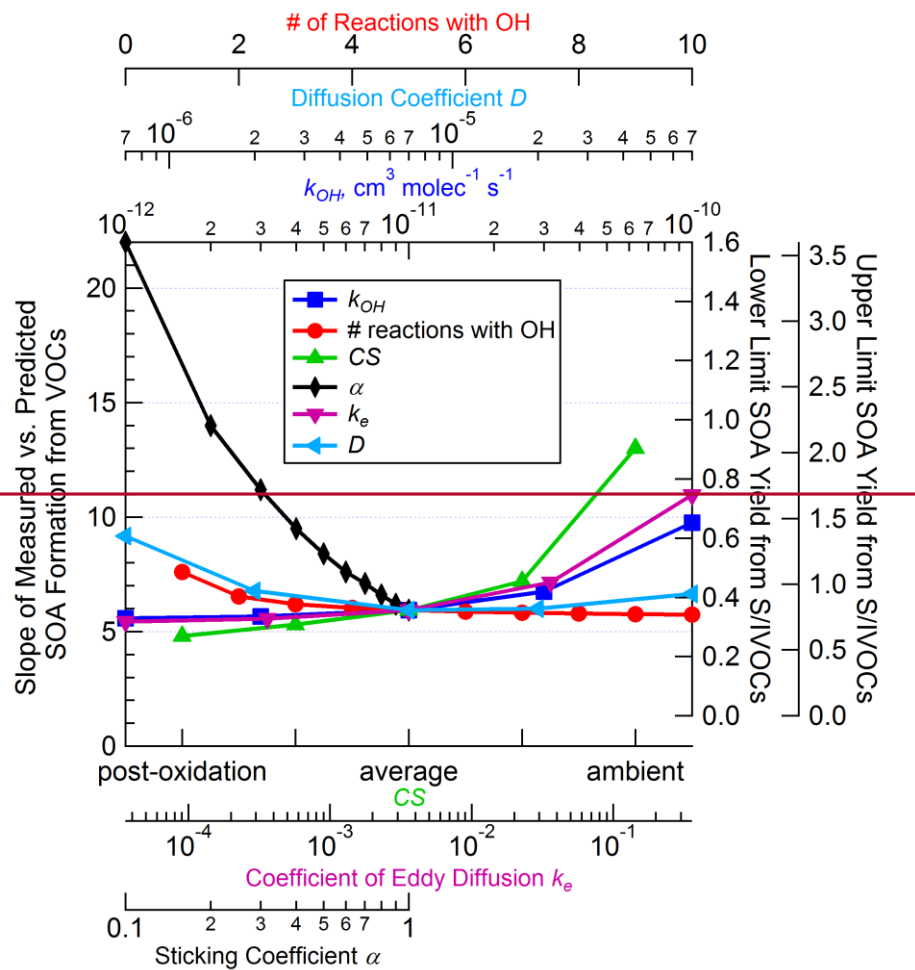
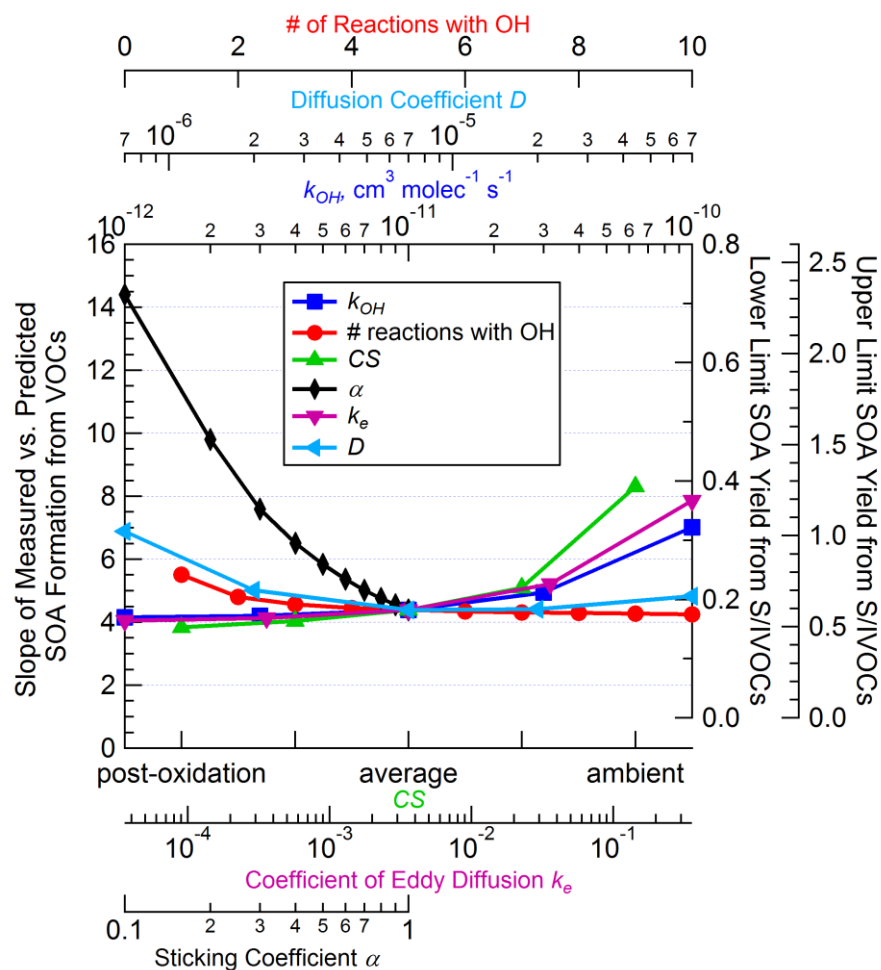


Fig. 12. Measured vs. predicted SOA formation from OH oxidation of ambient air in an OFR using the OFR185 method. Only the range of photochemical ages with the highest SOA formation (0.4–1.5 eq. days) was used, and the LVOC fate correction was applied. Predicted SOA formation is estimated using VOCs (described in Sect. 3.6.1) with and without including an empirical 89.58% SOA yield from S/IVOCs measured by the TD-EIMS (a lower limit of total S/IVOCs). Inset: average S/IVOC concentrations as a function of the log of the saturation vapor concentration  $C^*$ . This comparison includes all data for which S/IVOCs and SOA formation in the OFR were concurrently measured (26, 28–29 July, and 9–10, 12–13 August). For some data points, PTR-TOF-MS data was not available, so the VOC contribution was estimated using the linear fit in Fig. 10.







1949  
1950 Fig. 13. Sensitivity of the slope of measured vs. predicted SOA formation from VOCs, and of the range of  
1951 SOA yields estimated for bulk S/IVOCs (same curves, different Y axes), to parameters in the LVOC fate  
1952 model. The change in slope and yields is calculated by changing only one parameter at a time while  
1953 keeping the rest at the base case values of 5 reactions with OH,  $k_{OH} = 1 \times 10^{-11} \text{ cm}^3 \text{ molec}^{-1} \text{ s}^{-1}$ , average  
1954 CS,  $\alpha = 1$ ,  $k_e = 0.0036 \text{ s}^{-1}$ , and  $D = 7 \times 10^{-6} \text{ m}^2 \text{ s}^{-1}$ .

## Supplementary Information for:

### In-situ secondary organic aerosol formation from ambient pine forest air using an oxidation-flow reactor

Brett B. Palm<sup>1,2</sup>, Pedro Campuzano-Jost<sup>1,2</sup>, Amber M. Ortega<sup>1,2</sup>, Douglas A. Day<sup>1,2</sup>, Lisa Kaser<sup>4,5</sup>, Werner Jud<sup>5</sup>, Thomas Karl<sup>6</sup>, Armin Hansel<sup>5</sup>, James F. Hunter<sup>7</sup>, Eben S. Cross<sup>7</sup>, Jesse H. Kroll<sup>7,8</sup>, Zhe Peng<sup>1,2</sup>, William H. Brune<sup>9</sup>, and Jose L. Jimenez<sup>1,2</sup>

<sup>1</sup>Cooperative Institute for Research in Environmental Sciences, University of Colorado, Boulder, USA;

<sup>2</sup>Department of Chemistry and Biochemistry, University of Colorado, Boulder, USA;

<sup>3</sup>Department of Atmospheric and Oceanic Science, University of Colorado, Boulder, USA;

<sup>4</sup>National Center for Atmospheric Research, Boulder, CO, USA;

<sup>5</sup>Institute of Ion Physics and Applied Physics, University of Innsbruck, Innsbruck, Austria;

<sup>6</sup>Institute of Meteorology and Geophysics, University of Innsbruck, Innsbruck, Austria;

<sup>7</sup>Department of Civil and Environmental Engineering, Massachusetts Institute of Technology, Cambridge, MA, USA

<sup>8</sup>Department of Chemical Engineering, Massachusetts Institute of Technology, Cambridge, MA, USA

<sup>9</sup>Department of Meteorology, Pennsylvania State University, State College, PA, USA

Correspondence to: J.L. Jimenez (jose.jimenez@colorado.edu)

#### S1 — Correction for particle diffusion to sampling line walls

AMS and SMPS particle concentrations were corrected for diffusion losses to the walls of the inlet sampling lines, estimated using the Max Planck Institute for Chemistry's Particle Loss Calculator (von der Weiden et al., 2009). The sampling lines were constructed from a mixture of 3/8" and 1/4" OD copper tubing. The ambient air sampling line contained a PM<sub>2.5</sub> cyclone impactor at the inlet. The total length of tubing between the cyclone/OFR and AMS/SMPS was approximately 8 m, with a total residence time of about 9 s. The transmission curve used to correct for line losses is shown in Fig. S1. Estimates for particle losses in the ambient sampling line and in the OFR sampling line were similar, so a single transmission curve is applied to all data. The transmission curve was applied to SMPS size distributions to determine particle volume lost to the inlet walls. This volume was added to the AMS species in the same ratio that the species volumes were measured by the AMS. Mass was estimated from volume using densities of 1.52 g cm<sup>-3</sup> for chloride and 1.75 g cm<sup>-3</sup> for sulfate, ammonium, and nitrate AMS aerosol species (DeCarlo et al., 2004; Salcedo et al., 2006; Lide, 2013), and a parameterization using elemental composition to estimate the density of OA (Kuwata et al., 2012). The combination of the sampling line particle loss correction and the AMS lens transmission correction (discussed in Sect. S3) added an average of 4% to

the ambient OA, and an average of 12% to the OA measured after 0.4–1.5 days of aging (when the corrections were largest).

## **S2 — Determination of AMS collection efficiency (CE)**

CE is typically variable between 0.5 and 1, depending on composition, as detailed in Middlebrook et al. (2012). **S1 — Correction for particle diffusion to sampling line walls**

AMS and SMPS particle concentrations were corrected for diffusion losses to the walls of the inlet sampling lines, estimated using the Max Planck Institute for Chemistry's Particle Loss Calculator (von der Weiden et al., 2009). The sampling lines were constructed from a mixture of 3/8" and 1/4" OD copper tubing. The ambient air sampling line contained a PM<sub>2.5</sub> cyclone impactor at the inlet. The total length of tubing between the cyclone/OFR and AMS/SMPS was approximately 8 m, with a total residence time of about 9 s. The transmission curve used to correct for line losses is shown in Fig. S1. Estimates for particle losses in the ambient sampling line and in the OFR sampling line were similar, so a single transmission curve is applied to all data. The transmission curve was applied to SMPS size distributions to determine particle volume lost to the inlet walls. This volume was added to the AMS species in the same ratio that the species volumes were measured by the AMS. As seen in Fig. S1, there was on average only a slight size dependence to the species mass fractions of ambient aerosol. The mass fractions are also particularly noisy at smaller particle sizes due to small mass concentrations. Ideally, the species size distributions measured at each point in time could be used to allocate the sampling line particle losses to each species. In practice, the AMS size-distribution measurement mode is not sensitive enough at these concentrations to do such a correction at high time-resolution. Ambient AMS size distribution data could be averaged over long periods of time to increase the signal-to-noise, but this would not be possible for OFR measurements, since the OH exposure is changed between each successive data point. Thus, we have applied the best correction possible and expect that it should improve quantification. Regardless, the small size dependence of species mass fractions would have a minimal impact on this analysis since the correction is at most 20% at the smallest sizes. Mass was estimated from volume using densities of 1.52 g cm<sup>-3</sup> for chloride and 1.75 g cm<sup>-3</sup> for sulfate, ammonium, and nitrate AMS aerosol species (DeCarlo et al., 2004; Salcedo et al., 2006; Lide, 2013), and a parameterization using elemental composition to estimate the density of OA (Kuwata et al., 2012). The combination of the sampling line particle loss correction and the AMS lens transmission correction (discussed in Sect. S3) added an average of 4% to the ambient OA, and an average of 12% to the OA measured after 0.4–1.5 days of aging (when the corrections were largest).

## **S2 Determination of AMS collection efficiency (CE)**

CE is typically variable between 0.5 and 1, depending on composition, as detailed in Middlebrook et al. (2012). To our knowledge, ambient AMS measurements with a constant CE of ~1 have been reported in two prior studies in forested environments: during the wet season in the remote Amazon forest at the Amazonian Aerosol Characterization Experiment 2008 (Chen et al., 2015)(Chen et al., 2015), and South American Biomass Burning Analysis (SAMBBA) experiment during the dry season and dry-to-wet transition period in the southwestern Amazon rainforest in 2012 (Brito et al., 2014)(Brito et al., 2014). Here, we assessed CE by comparing AMS measurements with an SMPS that sampled from the same inlet. This SMPS measurement was validated by an intercomparison with four other calibrated and independently-operated SMPS instruments, as well as three CPC total particle number measurements, that sampled concurrently at the same research site. Fig. S2 shows that CE = 1 was required to match the AMS and SMPS measurements.

One concern was that the CE would change after oxidation in the OFR, due to changes in the aerosol composition and properties. A change in CE would result in a change in the slope of AMS vs. SMPS volume. However, we did not observe such a change, as seen in the comparison of total aerosol volume measured after the OFR in the left panel of Fig. S3. Occasionally, high concentrations of  $\text{NH}_4\text{NO}_3$  were produced in the OFR from OH oxidation. During those times, the AMS measured up to several times more volume than the SMPS (implying a  $\text{CE} \gg 1$ ). This is likely due to evaporation of the  $\text{NH}_4\text{NO}_3$  in the SMPS, as the SMPS sample flow was diluted inside the DMA column, as well as between the DMA and the CPC. For this reason, these data are not included in the analysis of CE.

Fig. S4 shows total particle volume enhancements as quantified by both the AMS and the SMPS for the OFR185 method vs. photochemical age, split into daytime and nighttime, showing that the two instruments measured similar enhancements within the errors at all ages. Data in Figs. S2, S3, and S4 were corrected using the sampling inlet line particle transmission efficiency curve in Fig. S1 as well as a correction for the transmission of the AMS aerodynamic lens, discussed in Sect. S3.

## **S3 Determination of AMS aerodynamic lens transmission efficiency**

As discussed in Sect. 3.5 and Fig. 9, OH oxidation of ambient air in the OFR often led to substantial new particle formation. The AMS aerodynamic lens is known to have less than 100% transmission at small sizes (Liu et al., 2007)(Liu et al., 2007). A standard transmission curve has been suggested for correcting AMS data when lacking a determination of the transmission for the particular operating conditions of

the AMS, referred to as case 0 here (Knote et al., 2011)(Knote et al., 2011). However, it is preferable to use data from a specific experiment when available to make such a determination for specific operating conditions. The lens transmission curve was estimated for the conditions in which the AMS was operated at the BEACHON-RoMBAS campaign by empirically finding the low particle size cutoff that resulted in the highest  $R^2$  correlation of the AMS and SMPS total volume sampled through an OFR (including all data from unperturbed to the highest  $OH_{exp}$ ). We tested a range of corrections, shown in Fig. S5. The results are shown in Table S1. Scatterplots of total volume and ~~change in volume-added~~ for the base case (no correction) and the chosen case 2 correction are shown in Figs. S6 and S3, respectively. The combination of the sampling line particle loss correction and the AMS lens transmission correction added an average of 4% to the ambient OA, and an average of 12% to the total OA measured after 0.4–1.5 days of aging in the reactor (when the corrections were largest).

Finally, to account for any particle losses on the surfaces inside the OFR, the aerosol mass measured in the OFR when no oxidant was added was adjusted to be equal to the concurrent ambient aerosol data, which was interpolated from the measurements immediately before and after the OFR data. Aerosol was sampled through the OFR with no added oxidant approximately every 2 hours. The OFR data for which oxidant concentrations were increased were corrected by multiplying by the average ratio of ambient aerosol mass to aerosol mass measured through the OFR without added oxidant. This correction was small, increasing the mass of OFR data by 4%, similar in magnitude to the loss of particles in the sampling lines and aerodynamic lens.

#### **S4 In-canopy vs. 25 m height PTR-TOF-MS measurements**

The primary PTR-TOF-MS dataset from BEACHON-RoMBAS was measured from an inlet located on a tower at 25 m, above the average canopy height of 16 m (Ortega et al., 2014). The OFR was located within the canopy at approximately 4 m height. Occasionally, concurrent PTR-TOF-MS measurements were available from the 25 m height and either through the OFR (1–6 and 8–10 August) or from a 1 m high inlet (19–21 August). Scatterplots of in-canopy (OFR or 1 m) vs. 25 m inlet MT, SQT, MBO+isoprene, and toluene+p-cymene concentrations are shown in Fig. S8. In-canopy concentrations were observed to be 1.9, 5.9, 1.4, and 1.2 times higher than at 25 m for those four compounds, respectively, and these ratios were used to estimate a campaign-long time series of in-canopy concentrations using the 25 m measurements. The correlations are high for MT, toluene, and MBO+isoprene ( $R^2=0.80-0.82$ ), but the correlation for SQT is  $R^2=0.12$ . This low correlation adds uncertainty to the estimation of in-canopy SQT

Field Code Changed

125 concentrations. However, this will have only a minor effect on the predicted SOA formation from VOCs  
126 (Sect. 3.6.1) since on average only 5% of the predicted SOA formation came from SQT.

127

## 128 References

- 129 Brito, J., Rizzo, L. V., Morgan, W. T., Coe, H., Johnson, B., Haywood, J., Longo, K., Freitas, S., Andreae, M.  
 130 O. and Artaxo, P.: Ground-based ~~aerosol characterization during the~~Aerosol Characterization During The  
 131 South American Biomass Burning Analysis (SAMBBA) ~~field experiment~~Field Experiment, Atmos. Chem.  
 132 Phys., 14, 12069–12083, [doi:10.5194/acp-14-12069-2014](https://doi.org/10.5194/acp-14-12069-2014), 2014.
- 133 Chen, Q., Farmer, D. K., Rizzo, L. V., Pauliquevis, T., Kuwata, M., Karl, T. G., Guenther, A., Allan, J. D., Coe,  
 134 H., Andreae, M. O., Pöschl, U., Jimenez, J. L., Artaxo, P. and Martin, S. T.: ~~Fine-mode organic mass~~  
 135 ~~concentrations and sources in the~~Submicron Particle Mass Concentrations And Sources In The  
 136 Amazonian ~~wet season~~Wet Season (AMAZE-08), Atmos. Chem. Phys., 15, 3687–3701, [doi:10.5194/acp-](https://doi.org/10.5194/acp-15-3687-2015)  
 137 15-3687-2015, 2015.
- 138 DeCarlo, P. F., Slowik, J. G., Worsnop, D. R., Davidovits, P. and Jimenez, J. L.: Particle Morphology ~~and~~And  
 139 Density Characterization ~~by~~By Combined Mobility ~~and~~And Aerodynamic Diameter Measurements. Part  
 140 1: Theory, Aerosol Sci. Technol., 38, 1185–1205, [doi:10.1080/027868290903907](https://doi.org/10.1080/027868290903907), 2004.
- 141 Knote, C., Brunner, D., Vogel, H., Allan, J., Asmi, A., Äijälä, M., Carbone, S., van der Gon, H. D., Jimenez, J.  
 142 L., Kiendler-Scharr, A., Mohr, C., Poulain, L., Prévôt, A. S. H., Swietlicki, E. and Vogel, B.: Towards ~~an~~  
 143 ~~online~~An Online-coupled ~~chemistry~~Chemistry-climate ~~model: evaluation of trace gases and aerosols~~  
 144 ~~in~~Model: Evaluation Of Trace Gases And Aerosols In COSMO-ART, Geosci. Model Dev., 4, 1077–1102,  
 145 [doi:10.5194/gmd-4-1077-2011](https://doi.org/10.5194/gmd-4-1077-2011), 2011.
- 146 Kuwata, M., Zorn, S. R. and Martin, S. T.: Using ~~elemental ratios to predict the density of organic~~  
 147 ~~material composed of carbon, hydrogen, and oxygen~~Elemental Ratios To Predict The Density Of Organic  
 148 Material Composed Of Carbon, Hydrogen, And Oxygen, Environ. Sci. Technol., 46, 787–94,  
 149 [doi:10.1021/es202525q](https://doi.org/10.1021/es202525q), 2012.
- 150 Lide, D. R.: CRC Handbook ~~of~~Of Chemistry ~~and~~And Physics, 94th Edition, 2013–2014–~~7~~, 2013.
- 151 Liu, P. S. K., Deng, R., Smith, K. a., Williams, L. R., Jayne, J. T., Canagaratna, M. R., Moore, K., Onasch, T.  
 152 B., Worsnop, D. R. and Deshler, T.: Transmission ~~efficiency of an aerodynamic focusing lens system:~~  
 153 ~~Comparison of model calculations and laboratory measurements for the~~Efficiency Of An Aerodynamic  
 154 Focusing Lens System: Comparison Of Model Calculations And Laboratory Measurements For The  
 155 Aerodyne Aerosol Mass Spectrometer, Aerosol Sci. Technol., 41, 721–733,  
 156 [doi:10.1080/02786820701422278](https://doi.org/10.1080/02786820701422278), 2007.
- 157 Middlebrook, A. M., Bahreini, R., Jimenez, J. L. and Canagaratna, M. R.: Evaluation ~~of~~Of Composition-  
 158 Dependent Collection Efficiencies ~~for the~~For The Aerodyne Aerosol Mass Spectrometer ~~using~~Using Field  
 159 Data, Aerosol Sci. Technol., 46, 258–271, [doi:10.1080/02786826.2011.620041](https://doi.org/10.1080/02786826.2011.620041), 2012.
- 160 Ortega, J., Turnipseed, A., Guenther, A. B., Karl, T. G., Day, D. A., Gochis, D., Huffman, J. A., Prenni, ~~a~~A. J.,  
 161 Levin, E. J. T., Kreidenweis, S. M., DeMott, P. J., Tobo, Y., Patton, E. G., Hodzic, ~~a~~A, Cui, Y. Y., Harley, P.  
 162 C., Hornbrook, R. S., Apel, E. C., Monson, R. K., Eller, A. S. D., Greenberg, J. P., Barth, M. C., Campuzano-  
 163 Jost, P., Palm, B. B., Jimenez, J. L., Aiken, ~~a~~A. C., Dubey, M. K., Geron, C., Offenberg, J., Ryan, M. G.,  
 164 Fornwalt, P. J., Pryor, S. C., Keutsch, F. N., DiGangi, J. P., Chan, A. W. H., Goldstein, A. H., Wolfe, G. M.,  
 165 Kim, S., Kaser, L., Schnitzhofer, R., Hansel, ~~a~~A, Cantrell, C. ~~a~~A, Mauldin, R. L. and Smith, J. N.: Overview  
 166 ~~of the~~Of The Manitou Experimental Forest Observatory: ~~site description and selected science results~~  
 167 ~~from~~Site Description And Selected Science Results From 2008 ~~to~~To 2013, Atmos. Chem. Phys., 14, 6345–  
 168 6367, [doi:10.5194/acp-14-6345-2014](https://doi.org/10.5194/acp-14-6345-2014), 2014.
- 169 Salcedo, D., Onasch, T. B., Dzepina, K., Canagaratna, M. R., Zhang, Q., Huffman, J. A., DeCarlo, P. F.,  
 170 Jayne, J. T., Mortimer, P., Worsnop, D. R., Kolb, C. E., Johnson, K. S., Zuberi, B., Marr, L. C., Volkamer, R.,

**Formatted:** Font: Times New Roman, 12 pt

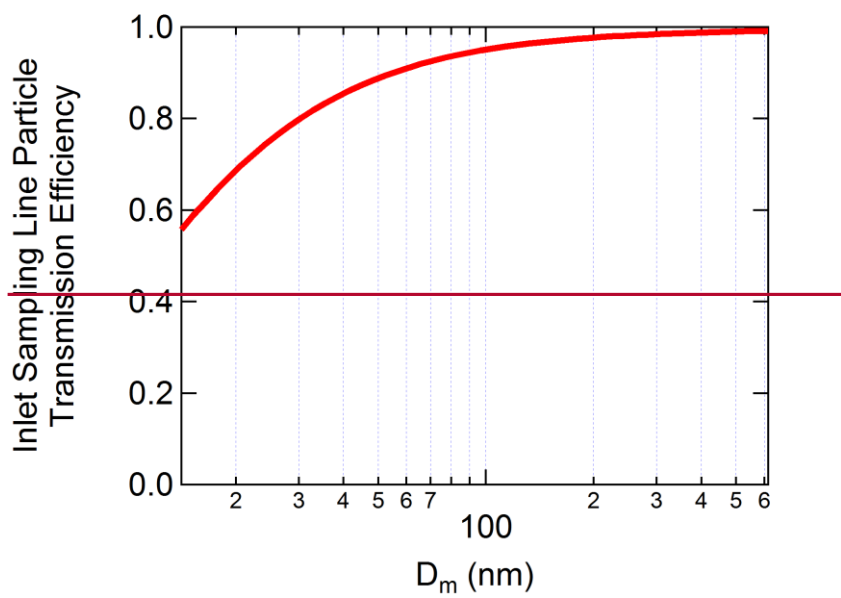
**Formatted:** Normal, Space Before: 5 pt, After: 5 pt,  
No widow/orphan control, Don't adjust space between  
Latin and Asian text, Don't adjust space between Asian  
text and numbers



171 Molina, L. T., Molina, M. J., Cardenas, B., ~~Bernabe, R. M., Marquez, C., Gaffney, J. S., Marley, N. A.,~~  
 172 ~~Laskin, A., Shutthanandan, V., Xie, Y., Brune, W., Leshner, R., Shirley, T., Jimenez, J. L., Salcedo, D., Onasch,~~  
 173 ~~T. B., Dzepina, K., Canagaratna, M. R., Zhang, Q., Huffman, J. A., DeCarlo, P. F., Jayne, J. T., Mortimer, P.,~~  
 174 ~~Worsnop, D. R., Kolb, C. E., Johnson, K. S., Zuberi, B., Marr, L. C., Volkamer, R., Molina, L. T., Molina, M.~~  
 175 ~~J., Cardenas, B., Bernabe, R. M., Marquez, C., Gaffney, J. S., Marley, N. A., Laskin, A., Shutthanandan, V.,~~  
 176 ~~Xie, Y., Brune, W., Leshner, R., Shirley, T., Jimenez, J. L., Salcedo, D., Onasch, T. B., Dzepina, K.,~~  
 177 ~~Canagaratna, M. R., Zhang, Q., Huffman, J. A., DeCarlo, P. F., Jayne, J. T., Mortimer, P., Worsnop, D. R.,~~  
 178 ~~Kolb, C. E., Johnson, K. S., Zuberi, B., Marr, L. C., Volkamer, R., Molina, L. T., Molina, M. J., Cardenas, B.,~~  
 179 ~~Bernabe, R. M., Marquez, C., Gaffney, J. S., Marley, N. A., Laskin, A., Shutthanandan, V., Xie, Y., Brune,~~  
 180 ~~W., Leshner, R., Shirley, T., Bernabé, R. M., Márquez, C., Gaffney, J. S., Marley, N. A., Laskin, A.,~~  
 181 ~~Shutthanandan, V., Xie, Y., Brune, W., Leshner, R., Shirley, T., and Jimenez, J. L., Bernabe, R. M., Marquez,~~  
 182 ~~C., et al.: Characterization of ambient aerosols in~~Of Ambient Aerosols In Mexico City ~~during the~~During  
 183 The MCMA-2003 campaign with Campaign With Aerosol Mass Spectrometry: ~~results from the~~Results  
 184 From The CENICA Supersite, Atmos. Chem. Phys., 6, 925–946, doi:10.5194/acp-6-925-2006, 2006.  
 185 Tsimpidi, A. P., Karydis, V. A., Zavala, M., Lei, W., Molina, L., Ulbrich, I. M., Jimenez, J. L. and Pandis, S. N.:  
 186 ~~of the volatility basis~~Of The Volatility Basis-set ~~approach for the simulation of organic aerosol~~  
 187 ~~formation in the~~Approach For The Simulation Of Organic Aerosol Formation In The Mexico City  
 188 ~~metropolitan area~~Metropolitan Area, Atmos. Chem. Phys., 10, 525–546, doi:10.5194/acp-10-525-2010,  
 189 2010.  
 190 ~~Von~~ der Weiden, S.-L., Drewnick, F. and Borrmann, S.: Particle Loss Calculator – ~~a new software tool~~  
 191 ~~for the assessment of the performance of aerosol inlet systems~~A New Software Tool For The Assessment  
 192 Of The Performance Of Aerosol Inlet Systems, Atmos. Meas. Tech., 2, 479–494, doi:10.5194/amt-2-479-  
 193 2009, 2009.

205 Table S1. Slope and correlation values for a comparison of AMS vs. SMPS volume, when applying  
206 aerodynamic lens transmission correction curves 0-5 (shown in Fig. S5) or no correction (base case).

Total Volume			<del>Added</del> Change in Volume		
Case	Slope	R^2	Case	Slope	R^2
0	1.056	0.85	0	1.446	0.77
1	1.036	0.85	1	1.341	0.77
2	1.017	0.86	2	1.219	0.75
3	1.001	0.85	3	1.107	0.70
4	0.989	0.84	4	1.032	0.65
5	0.983	0.82	5	0.997	0.61
base	0.981	0.81	base	0.986	0.58



213

214

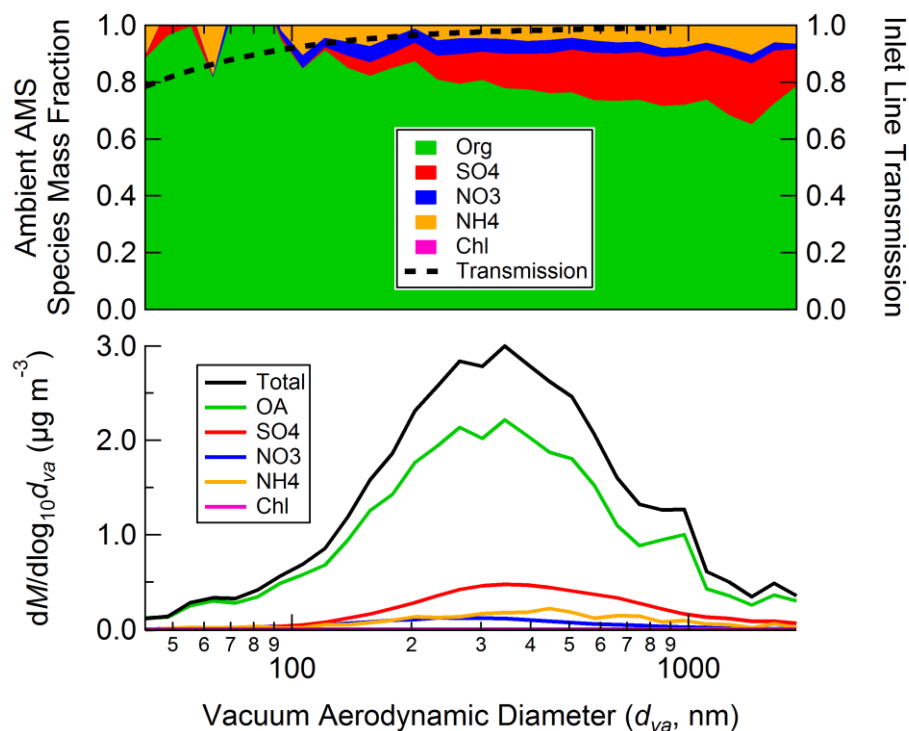


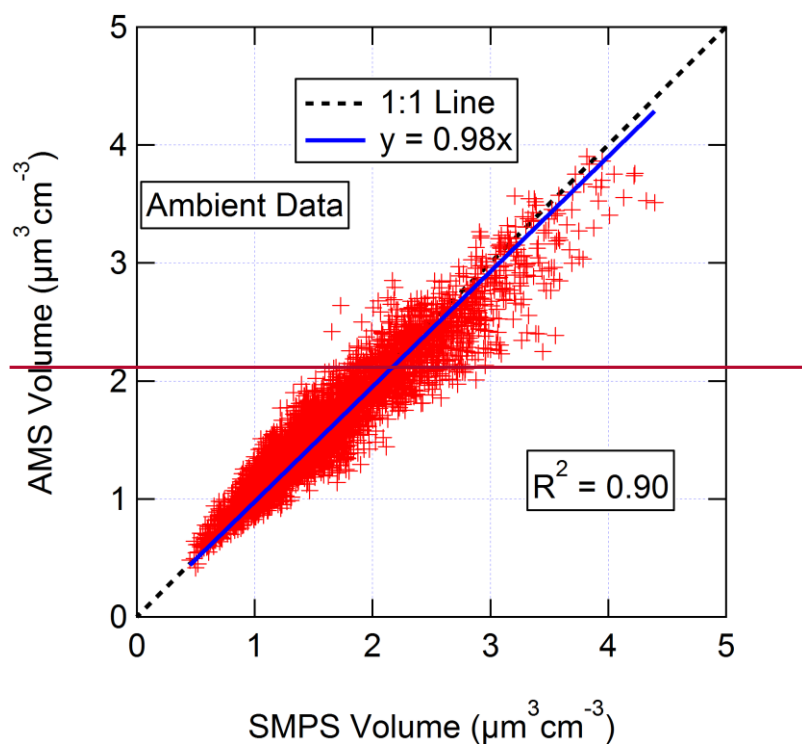
**Fig. S1. OFR and Top: Average species mass fraction of ambient aerosol measured by the AMS, and inlet sampling line particle transmission efficiency. The transmission efficiency was estimated using the Max Planck Institute for Chemistry Particle Loss Calculator (von der Weiden et al., 2009)(von der Weiden et al., 2009). This transmission curve was used to correct SMPS size distributions for particle losses in the ambient and OFR sampling lines. Particle losses to surfaces inside the OFR are discussed in Sect. S3.**

**Bottom: Average species mass size distribution of ambient aerosol measured by the AMS.**

Formatted: Font: Bold

Formatted: Font: Bold

222



223

224 Fig. S2. Scatter plot of ambient aerosol volume measurements from AMS vs. SMPS with regression line.  
 225 AMS data was calculated using CE=1. AMS volume was estimated using densities of  $1.52 \text{ g cm}^{-3}$  for  
 226 chloride,  $1.75 \text{ g cm}^{-3}$  for sulfate, ammonium, and nitrate (DeCarlo et al., 2004; Salcedo et al., 2006; Lide,  
 227 2013), and a parameterization using elemental composition to estimate the density of OA (Kuwata et al.,  
 228 2012). All data is shown without the LVOC fate correction.

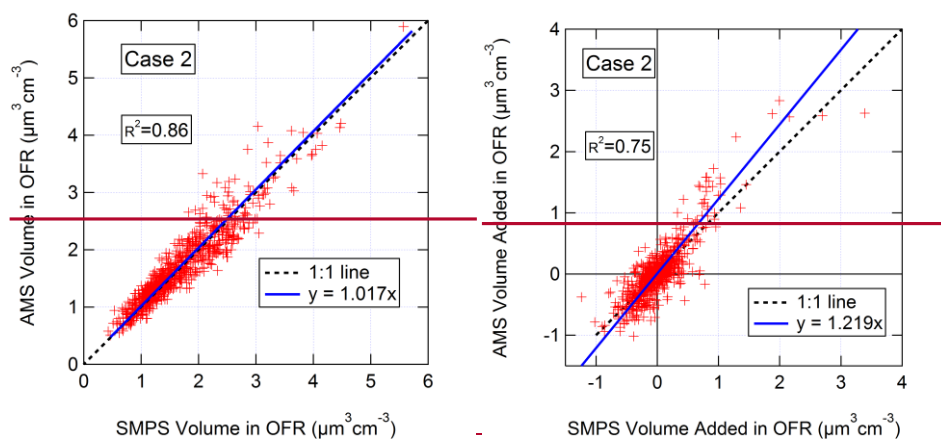


Fig. S3. Scatter plot of aerosol volume and volume added after OH aging from AMS vs. SMPS. AMS volume was estimated using densities of 1.52 for chloride, 1.75 for sulfate, ammonium, and nitrate (DeCarlo et al., 2004; Salcedo et al., 2006; Lide, 2013), and a parameterization using elemental composition to estimate the density of OA (Kuwata et al., 2012). Data is shown after correction for particle transmission losses in the AMS aerodynamic lens according to the case 2 correction in Fig. S5. All data is shown without the LVOC fate correction.

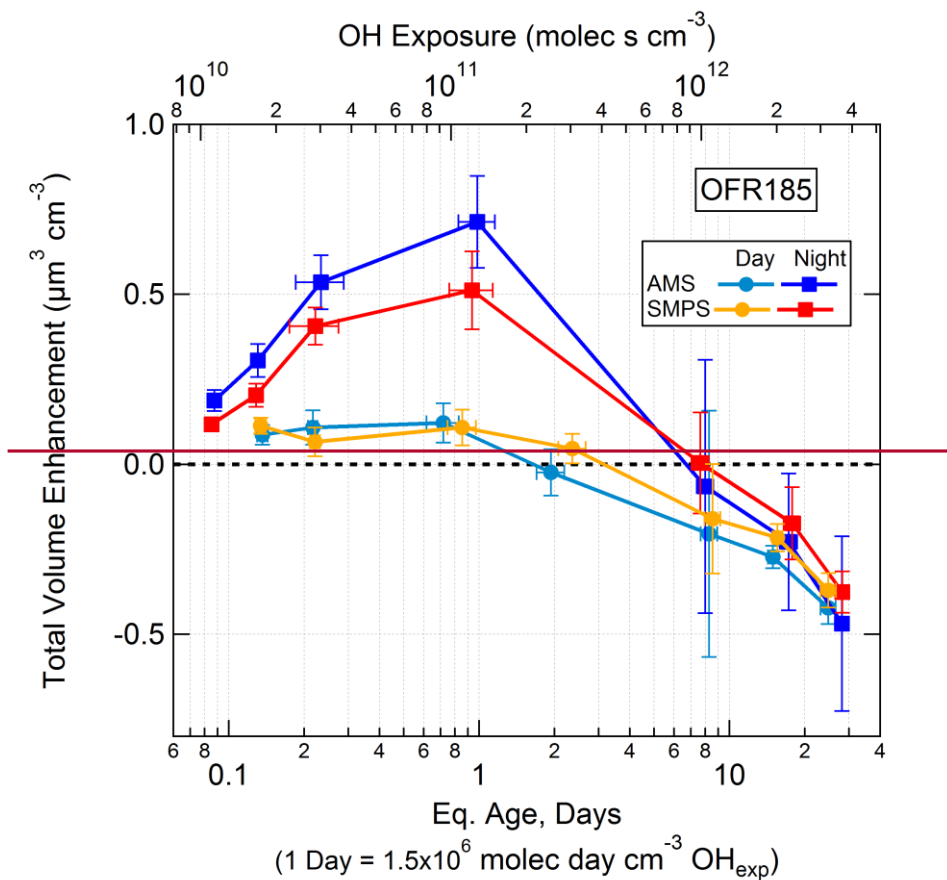


Fig. S4. Total particle volume enhancement as measured by the AMS and SMPS as a function of photochemical age, split into daytime (08:00–20:00 local time) and nighttime (20:00–08:00 local time) data. AMS volume was estimated using densities of  $1.52 \text{ g cm}^{-3}$  for chloride,  $1.75 \text{ g cm}^{-3}$  for sulfate, ammonium, and nitrate (DeCarlo et al., 2004; Salcedo et al., 2006; Lide, 2013), and a parameterization using elemental composition to estimate the density of OA (Kuwata et al., 2012). All data is shown without the LVOC fate correction. Error bars represent the standard error of the mean of each quantile of data.

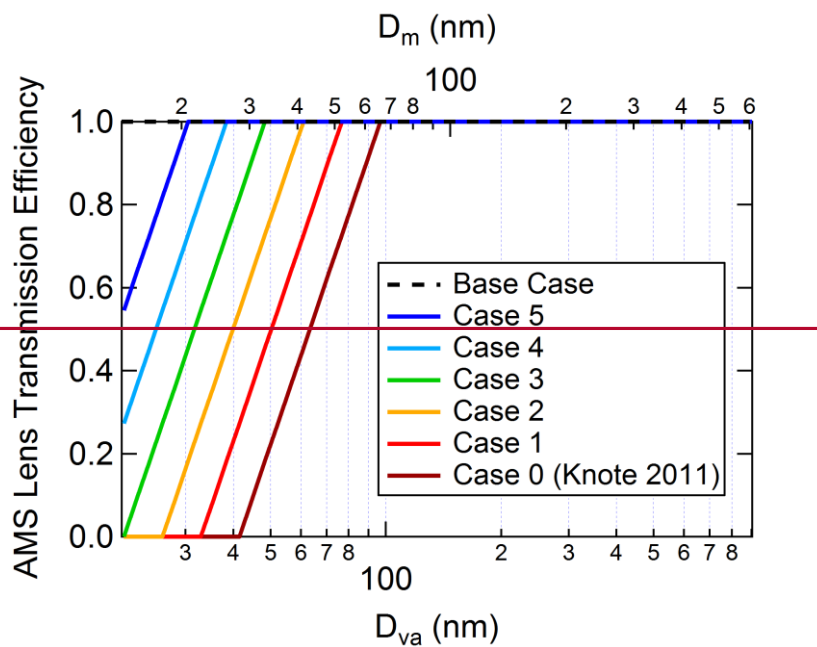


Fig. S5. Potential AMS aerodynamic lens transmission efficiency curves used to evaluate small particle losses in the lens, as a function of vacuum aerodynamic diameter  $D_{va}$  and mobility diameter  $D_m$ .  $D_{va}$  was converted to  $D_m$ , assuming a density of  $1.45 \text{ g cm}^{-3}$  (the campaign average). Case 0 is the recommended AMS lens transmission efficiency when no campaign specific determination is possible (Knote et al., 2011). Case 2 was chosen as the best fit for the data under the conditions during BEACHON-RoMBAS.



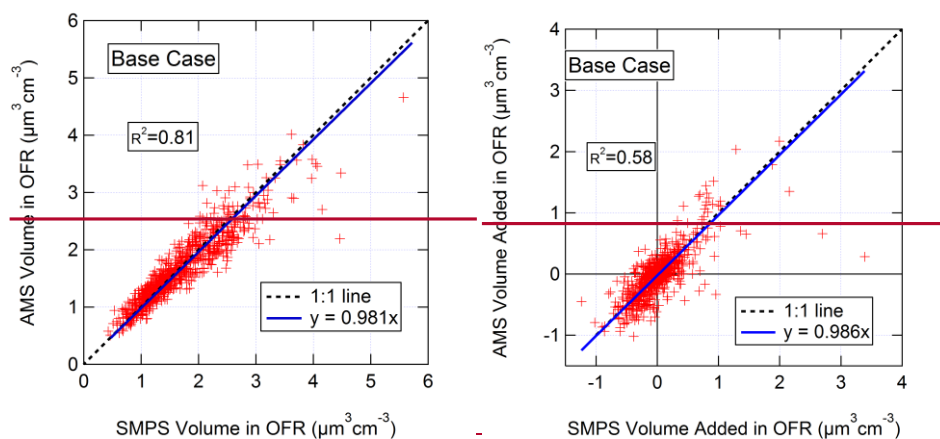
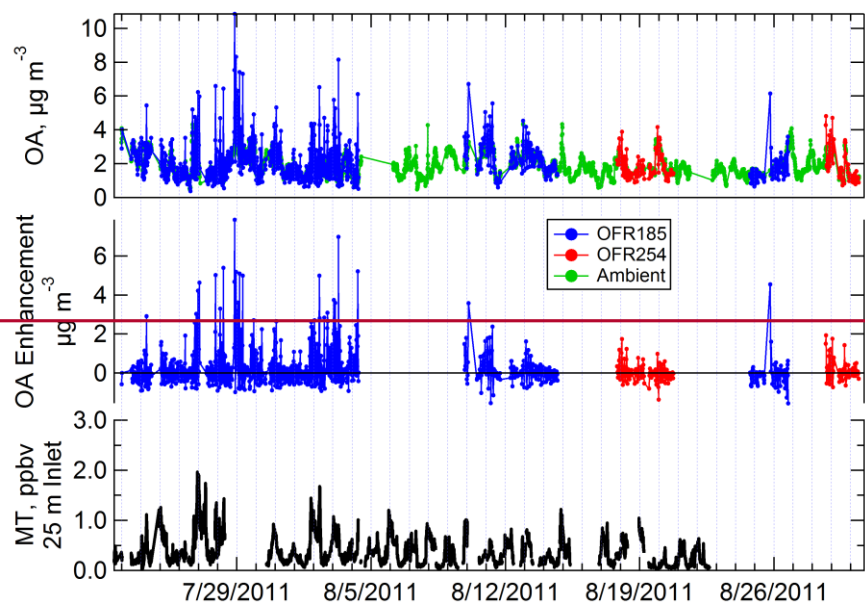


Fig. S6. Scatter plot of aerosol volume and volume added after OH aging from AMS vs. SMPS. AMS volume was estimated using densities of  $1.52 \text{ g cm}^{-3}$  for chloride,  $1.75 \text{ g cm}^{-3}$  for sulfate, ammonium, and nitrate (DeCarlo et al., 2004; Salcedo et al., 2006; Lide, 2013), and a parameterization using elemental composition to estimate the density of OA (Kuwata et al., 2012). Data is shown for base case (uncorrected) for particle transmission losses in the AMS aerodynamic lens according to Fig. S5. All data is shown without the LVOC fate correction.



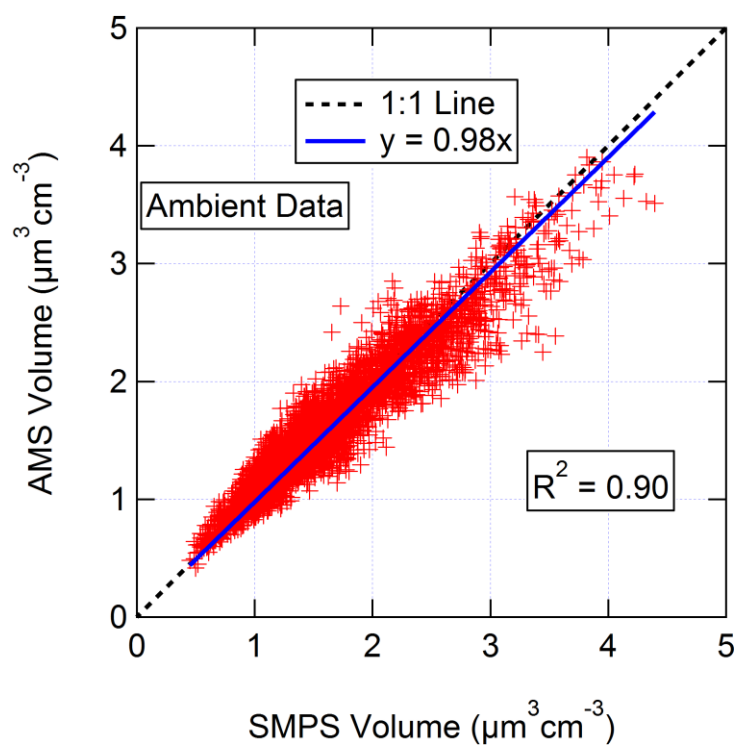


Fig. S2. Scatter plot of ambient aerosol volume measurements from AMS vs. SMPS with regression line. AMS data was calculated using CE=1. AMS volume was estimated using densities of  $1.52 \text{ g cm}^{-3}$  for chloride,  $1.75 \text{ g cm}^{-3}$  for sulfate, ammonium, and nitrate (DeCarlo et al., 2004; Salcedo et al., 2006; Lide, 2013), and a parameterization using elemental composition to estimate the density of OA (Kuwata et al., 2012). All data is shown without the LVOC fate correction.

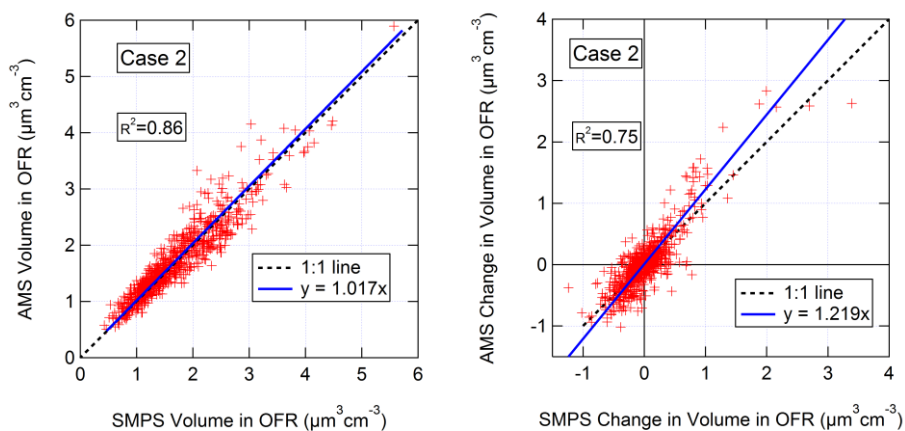


Fig. S3. Scatter plot of aerosol volume and change in volume after OH aging from AMS vs. SMPS. AMS volume was estimated using densities of 1.52 for chloride, 1.75 for sulfate, ammonium, and nitrate (DeCarlo et al., 2004; Salcedo et al., 2006; Lide, 2013), and a parameterization using elemental composition to estimate the density of OA (Kuwata et al., 2012). Data is shown after correction for particle transmission losses in the AMS aerodynamic lens according to the case 2 correction in Fig. S5. All data is shown without the LVOC fate correction. At the highest ages, heterogeneous oxidation led to fragmentation/volatilization of preexisting OA, resulting in a net loss of OA.

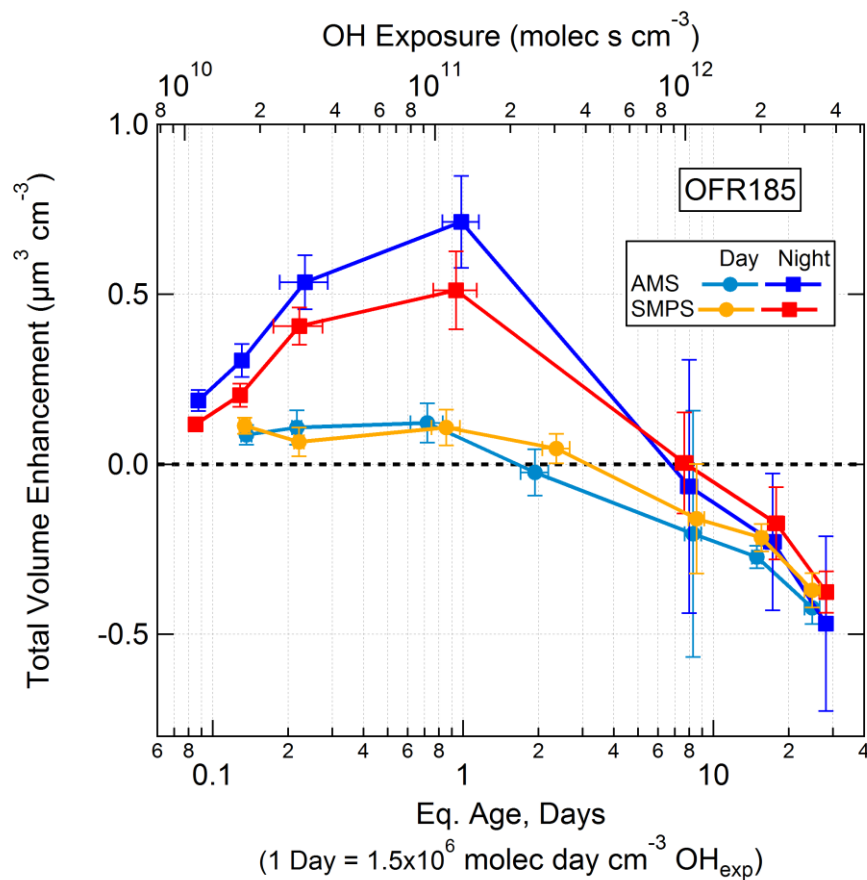


Fig. S4. Total particle volume enhancement as measured by the AMS and SMPS as a function of photochemical age, split into daytime (08:00–20:00 local time) and nighttime (20:00–08:00 local time) data. AMS volume was estimated using densities of  $1.52 \text{ g cm}^{-3}$  for chloride,  $1.75 \text{ g cm}^{-3}$  for sulfate, ammonium, and nitrate (DeCarlo et al., 2004; Salcedo et al., 2006; Lide, 2013), and a parameterization using elemental composition to estimate the density of OA (Kuwata et al., 2012). All data is shown without the LVOC fate correction. Error bars represent the standard error of the mean of each quantile of data.

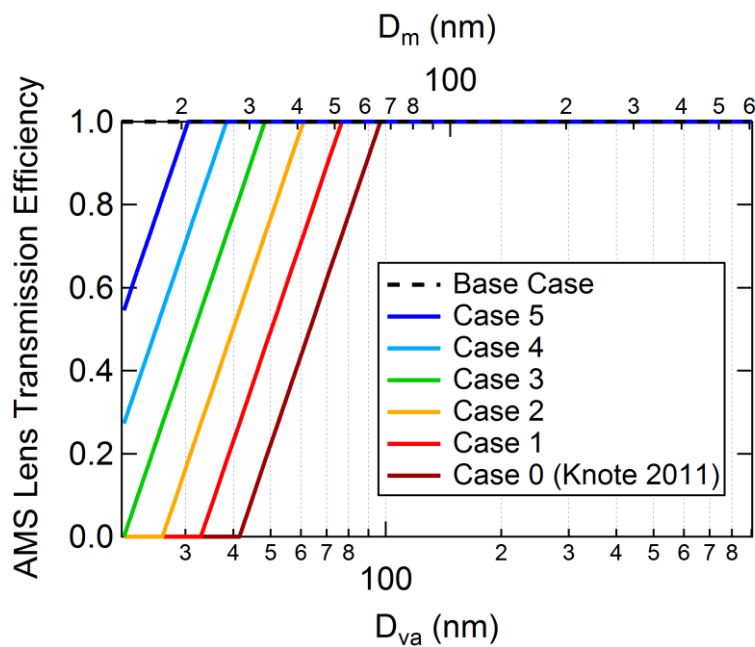


Fig. S5. Potential AMS aerodynamic lens transmission efficiency curves used to evaluate small particle losses in the lens, as a function of vacuum aerodynamic diameter  $D_{va}$  and mobility diameter  $D_m$ .  $D_{va}$  was converted to  $D_m$  assuming a density of  $1.45 \text{ g cm}^{-3}$  (the campaign average). Case 0 is the recommended AMS lens transmission efficiency when no campaign-specific determination is possible (Knote et al., 2011). Case 2 was chosen as the best fit for the data under the conditions during BEACHON-RoMBAS.

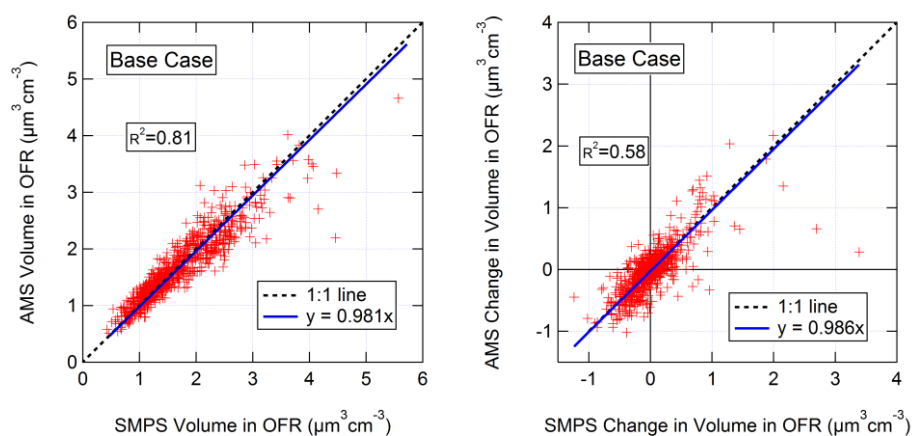


Fig. S6. Scatter plot of aerosol volume and change in volume after OH aging from AMS vs. SMPS. AMS volume was estimated using densities of  $1.52 \text{ g cm}^{-3}$  for chloride,  $1.75 \text{ g cm}^{-3}$  for sulfate, ammonium, and nitrate (DeCarlo et al., 2004; Salcedo et al., 2006; Lide, 2013), and a parameterization using elemental composition to estimate the density of OA (Kuwata et al., 2012). Data is shown for base case (uncorrected) for particle transmission losses in the AMS aerodynamic lens according to Fig. S5. All data is shown without the LVOC fate correction. At the highest ages, heterogeneous oxidation led to fragmentation/volatilization of preexisting OA, resulting in a net loss of OA.

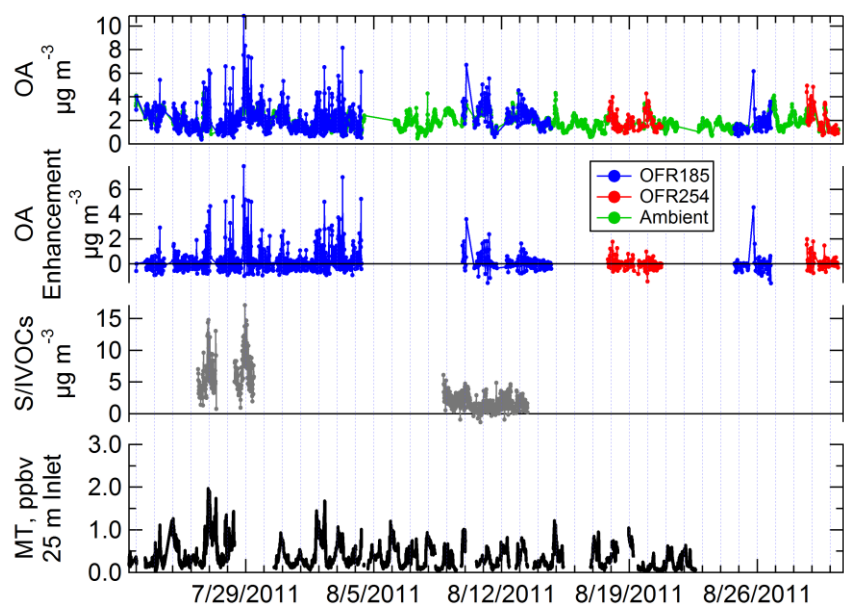


Fig. S7. Time series of ambient OA, total OA<sub>t</sub> and OA enhancement for OFR185 and OFR254 methods, ~~and ambient MT (25 m inlet), and ambient S/IVOC mass concentrations measured by the TD-EIMS.~~ The OA enhancements are not LVOC fate corrected here, and include all ages.



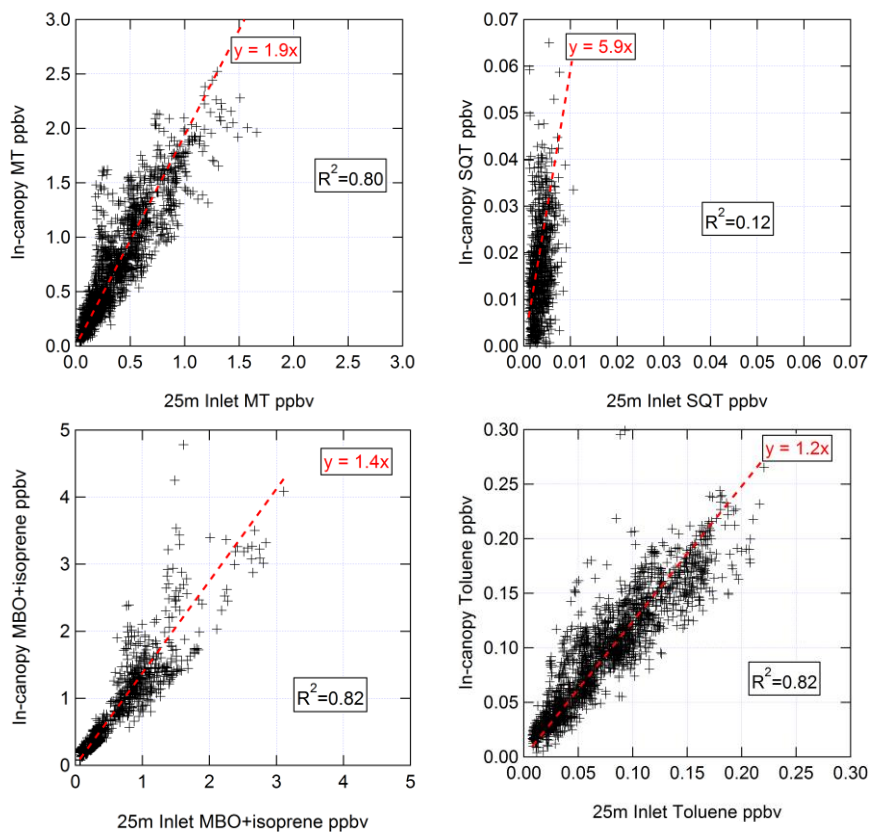
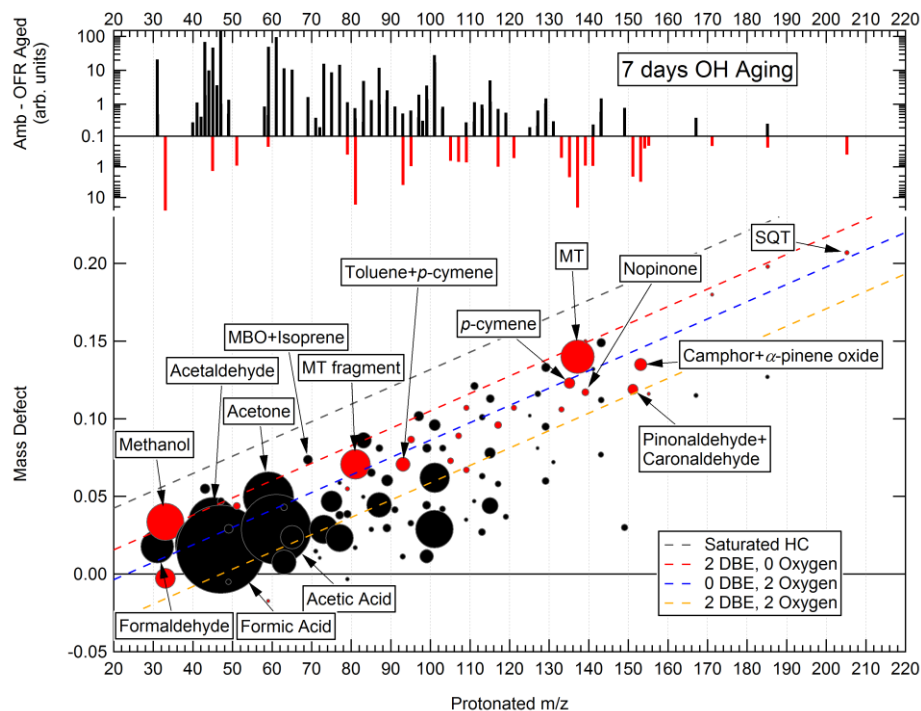


Fig. S8. Scatterplots of in-canopy (through OFR or 1 m inlet) vs. 25 m inlet for PTR-TOF-MS measurements of MT, SQT, MBO+isoprene, and toluene. In-canopy concentrations were 1.9, 5.9, 1.4, and 1.2 times higher than at 25 m, respectively.



308

309 Fig. S9. The absolute changes of ions (signal after OH oxidation in the reactor minus ambient signal)

310 measured by the PTR-TOF-MS after 7 days of aging using the OFR185 method, shown as a difference

311 mass spectrum and in a mass defect diagram. The mass spectra are 10-min averages (5 min from each of

312 the two sample cycles used). The background-subtracted signals are shown in arbitrary units, not

313 corrected for differences in sensitivity of each compound due to the large number of compounds and

314 the inability to positively identify all of them. Prominent ions are labeled by name or elemental formula

315 assignments. Dashed lines representing molecules with varying double bond equivalents (DBE) or

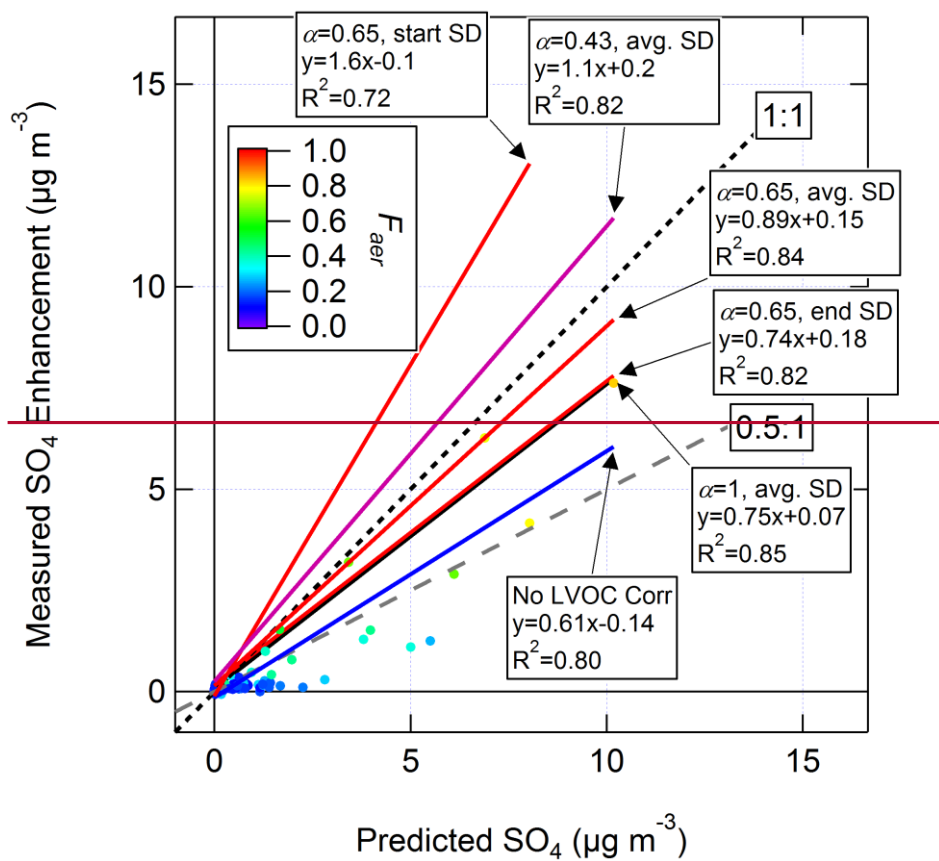
316 number of oxygen atoms are shown for reference. A red marker signifies that the signal decreased due

317 to oxidation, while a black marker indicates where signal was greater after oxidation. The markers are

318 sized by the square root of the absolute change in signal at each peak after oxidation (i.e., marker area is

319 proportional to signal). Minor signals with absolute change of <0.2 arb. units or change of <20% of total

320 ambient signal are removed.



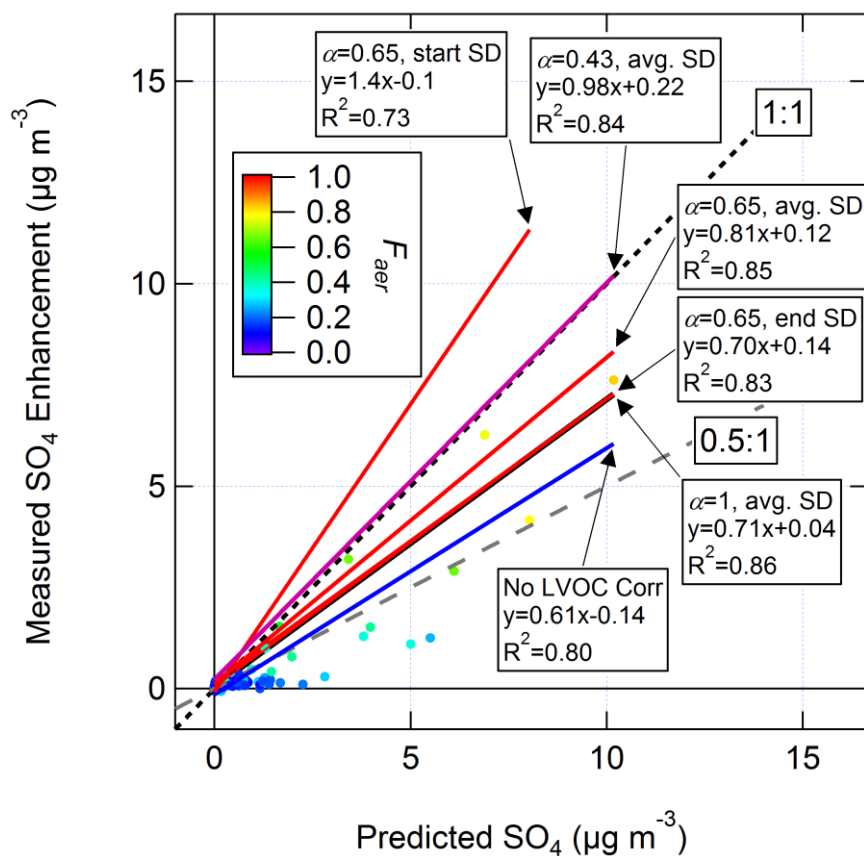
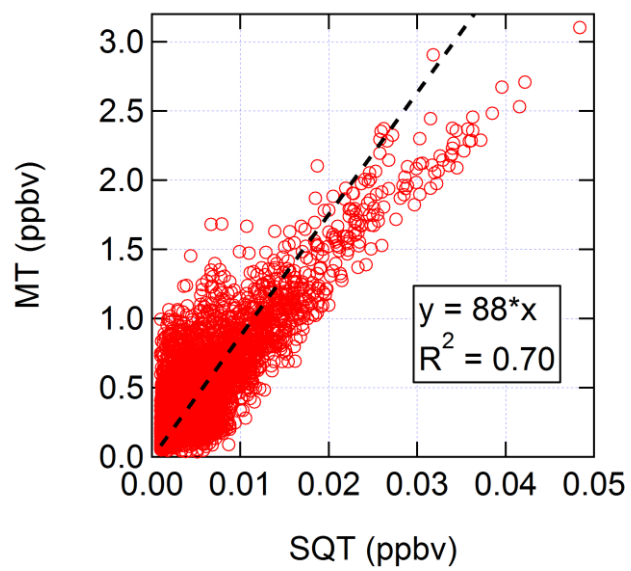


Fig. S10. Sensitivity study of the measured vs. predicted  $\text{SO}_4$  formation after OH oxidation in the OFR vs. key uncertain parameters. The data points are colored by the fraction of  $\text{H}_2\text{SO}_4$  predicted to condense on aerosols, calculated using  $\alpha = 0.65$  and the average of the SMPS size distributions (SD) measured before and after oxidation. Data are shown without applying the LVOC fate correction, along with linear fits that result from applying various sets of corrections including  $\alpha = 0.43$ -1 and using the ambient (start), post-oxidation (end), or average SD to calculate the CS. [Ambient  \$\text{SO}\_2\$  concentrations <0.2 ppb have been excluded from this analysis.](#)



330  
331 Fig. S11. Scatterplot of ambient MT vs. SQT concentrations measured by the PTR-TOF-MS at the 25 m  
332 inlet above the canopy.

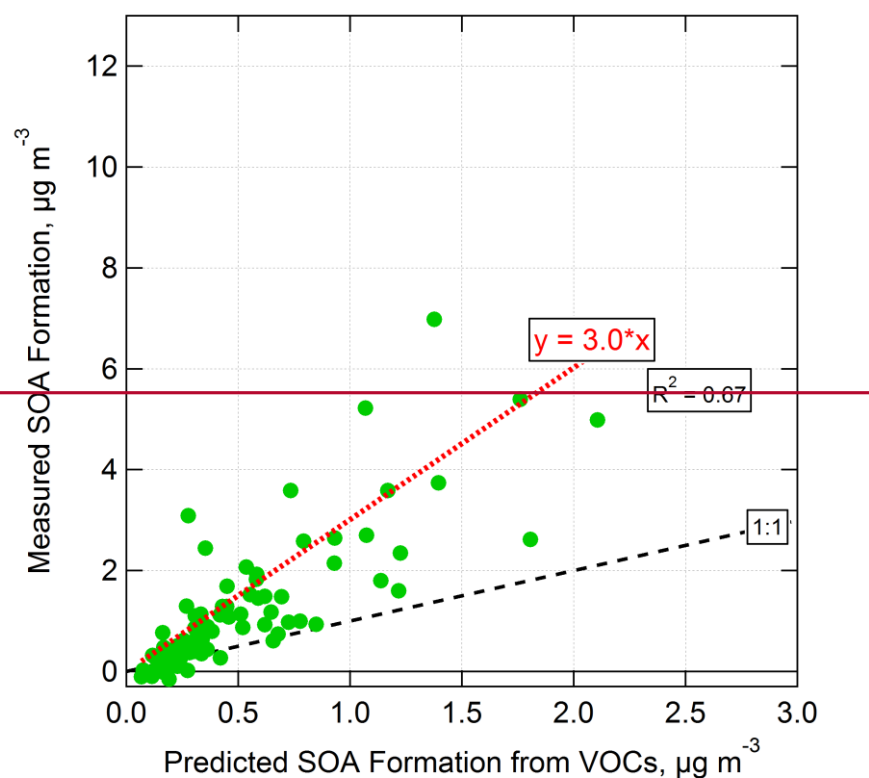
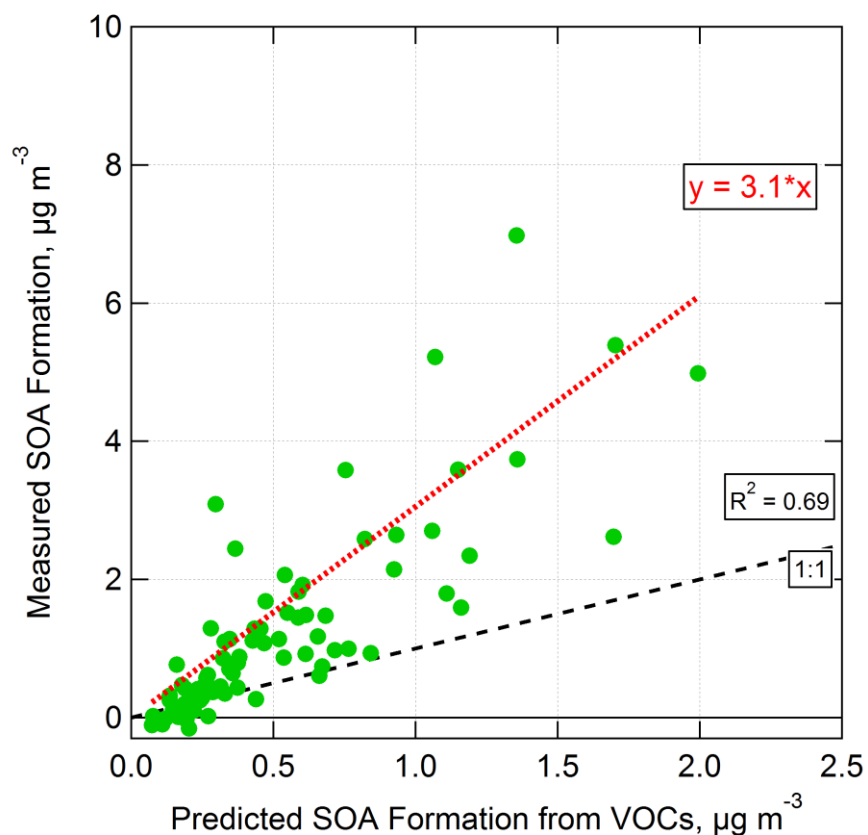
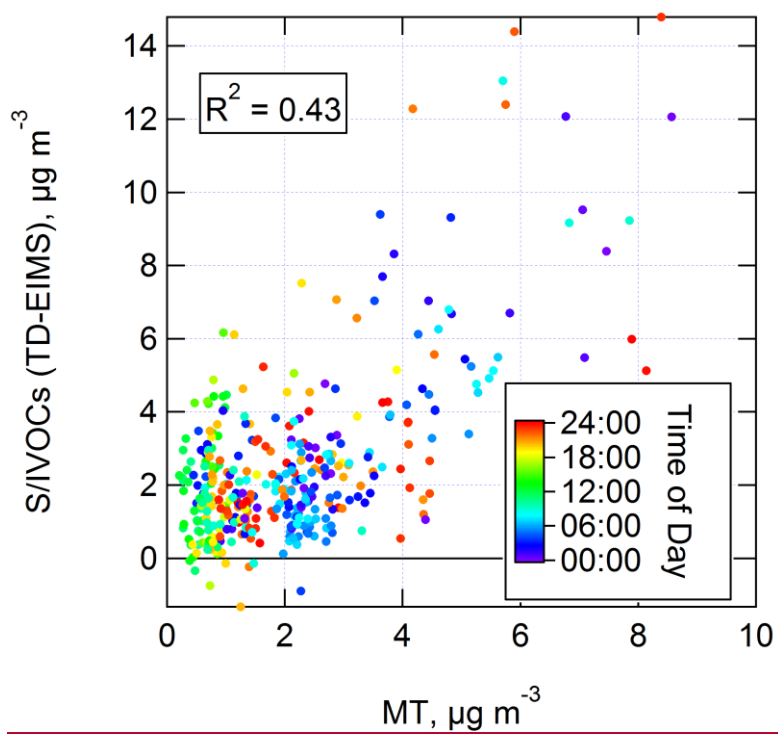


Fig. S12. Measured vs. predicted SOA formation from OH oxidation of ambient air in an OFR using the OFR185 method. Only the range of photochemical ages with the highest SOA formation (0.4–1.5 eq. days) was used. The LVOC fate correction was not applied. Predicted SOA formation was calculated by applying OA concentration dependent yields (average of 10.9%, 10.6%, 12.3%, and 1.4% for MT, SQT, toluene, and isoprene, respectively, with average OA concentration of  $2.9 \mu\text{g m}^{-3}$ ) to VOCs reacted in the OFR (Tsimpidi et al., 2010). The amount of reacted VOCs was estimated using  $\text{OH}_{\text{exp}}$  and ambient VOC



concentrations. If a non-zero y-intercept is allowed, the regression line becomes  $y = 3.9x - 0.7$ .

Fig. S12. Measured vs. predicted SOA formation from OH oxidation of ambient air in an OFR using the OFR185 method. Only the range of photochemical ages with the highest SOA formation (0.4-1.5 eq. days) was used. The LVOC fate correction was not applied. Predicted SOA formation was calculated by applying OA concentration-dependent yields (average of 10.9%, 11.1%, 11.5%, and 2.9% for MT, SQT, toluene, and isoprene, respectively, with average OA concentration of  $2.9 \mu\text{g m}^{-3}$ ) to VOCs reacted in the OFR (Tsimpidi et al., 2010). The amount of reacted VOCs was estimated using  $\text{OH}_{\text{exp}}$  and ambient VOC concentrations. If a non-zero y-intercept is allowed, the regression line becomes  $y = 4.0x - 0.8$ .



**Fig. S13.** Scatterplot of mass concentration of ambient S/IVOCs (lower limit measured by TD-EIMS) vs. ambient MT measured by PTR-TOF-MS. Data are shown colored by local time of day.

Formatted: Space Before: 12 pt

Formatted: Font: Not Bold